Synthesis of Eco-Friendly and Reusable Heterogeneous Acid Catalysts From Coal Fly Ash and Volcanic Ash for Catalyzing Conventional and Microwave Assisted Organic Reactions

A Thesis

Submitted to

University of Kota, Kota

for the Award of the Degree of

Doctor of Philosophy

in Chemistry
(Faculty of Science)

Supervised by	Submitted by
Prof. Ashu Rani	**Sakshi Kabra**

Department of Pure and Applied Chemistry
University of Kota, Kota

2015

UNIVERSITY OF KOTA, KOTA

M.B.S. Marg, Near Kabir Circle, Kota (Raj.) – 324005.

Prof. Ashu Rani
Head,
Dept. of Pure & Applied Chemistry
University of Kota, Kota

Residence
2-m-1, Rangbari Scheme
Kota-324005 (Raj.) India
Ph: +91-9352619059
e-mail: ashu.uok@gmail.com

Date*:……………..*

CERTIFICATE

It is to certify that the

i. Thesis entitled *"Synthesis of Eco-Friendly and Reusable Heterogeneous Acid Catalysts From Coal Fly Ash and Volcanic Ash for Catalyzing Conventional and Microwave Assisted Organic Reactions"* submitted by *Sakshi Kabra* is an original piece of research work carried out by the candidate under my supervision.

ii. Literary presentation is satisfactory and the thesis is in a form suitable for publication.

iii. Work evidences the capacity of the candidate for critical examination and independent judgment.

iv. Candidate has put in at least 200 days of attendance every year.

Prof. Ashu Rani
Head,
Department of Pure and Applied Chemistry
University of Kota, Kota

Dedicated

to

My Beloved

Parents

and

Husband

"Chemistry without catalysis, would be a sword without a handle, a light without brilliance, a bell without sound."

-Alwin Mittasch.

ACKNOWLEDGEMENT

To the people who propelled, dragged and accompanied me on the way:

One of the glorious moments of completion is to look over the footsteps past and remember all the friends and family who have helped and came hand in hand with me to accomplish this long journey.

*It has been my great pleasure to acknowledge all with the deep sense of gratitude who helped and encouraged me for the successful completion of the work. First and foremost, praises and thanks to the **God, The Almighty**, for his showers of blessings, for leading me in the right path and for giving me strength to cross the toughest situations.*

*I avail myself of this pleasant opportunity in expressing profound gratitude to my research supervisor with respect and appreciation, **Prof. Ashu Rani**, Head, Department of Pure and Applied Chemistry, University of Kota, for her constructive criticism, invaluable and stimulating suggestions. Her remarkable scientific abilities, hardworking, affectionate and amicable nature are always an inspiration for me towards achieving a good career. Without her untiring patience, constant encouragement, guidance, and knowledge, this work would not have been possible. Not only did she direct my learning and research as a student, but she also played the very important role of a mentor. I want to thank her for the support, she has provided me, and for all the opportunities she has created during the last five years for me to grow as a professional and as a person. She has proved herself as a successful woman chemist and professor. I am sure that I will pass on the research values and the dreams that she had given to me.*

*I am grateful to **Sh. Onkar Singh**, Vice Chancellor and **Prof. Madhusudan Sharma**, former Vice Chancellor, University of Kota, for providing necessary facilities to carry on my research work.*

*They are always being there when I needed them most. Completion of this Ph.D. would have been impossible without their support. The encouragement and support of my loving brother and mentor, **Sanket** has always been a powerful source of inspiration and energy. I am extremely indebted towards my respected Nanaji and Naniji, **Mr. M.L. Sharda** and **Mrs. C.D. Sharda** for their endless love and blessings.*

*I consider myself to be fortunate enough to have a caring and understanding husband **Aditya**, who always stood by my decisions, realize my dreams, encourage me to achieve my goals and helped me in resolving technical difficulties during thesis preparation. I also extend my thanks to my in-laws, **Mr. Dilip Malpani**, **Mrs. Kalpana Malpani**, Brother-in-laws, **Mayur** and **Vaibhav**, uncle-in-law, **Dr. Basant Malpani** (Scientist, BARC, Mumbai) for their moral support, constant encouragement and patience throughout the work. Last but not the least, I would also like to thank all members of **Kabra** (paternal) and **Sharda** (maternal) families for their support, love and wishes.*

Sakshi Kabra

INDEX

Introduction

Abstract

This chapter deals with the introduction of catalysis, its types, homogeneous and heterogeneous catalysis, drawbacks of classical homogeneous catalysts, examples of supported heterogeneous catalysts, their industrial applications. Herein, generation of acidic sites in solid acid catalysts and the measurement techniques to characterize and quantify acidic sites are also reported. An overview on catalytic applications of fly ash and volcanic ash, also known as perlite in area of heterogeneous catalysis is presented. It also figures out advantages of solid acid catalysts, synthesized from waste ashes over other reported catalysts, reasons behind selection of these wastes and requirement of substitution of classical, expensive heterogeneous acid catalysts by innovative, cost-effective materials and presents scope of the thesis.

1.1   Introduction

Catalyst, term coined by **J.J. Berzelius** is defined as "a substance that increases the rate of a reaction without modifying the overall standard Gibbs energy change in the reaction". Catalysts are responsible for the production of over 60 % of all chemicals and are used in about 90 % of all chemical processes worldwide [1]. Catalyst manufacturing alone accounts for over 10 billion dollar sales globally in major sectors namely: refining, fine chemicals, polymerization, exhaust emission catalysts, pharmaceuticals [2] etc. Modern catalysis is centred on the development of more efficient catalysts, which must be used under both sustainable and eco-friendly conditions, hence envisaging all possible principles of green chemistry, with special attention to strategies to approach a renewable chemical industry. Catalysis can be broadly divided into acid and base catalysis. Acid catalysis facilitates the rate of reaction by transfer of proton to reactants while during base catalysis, proton is abstracted from reactants. Acid and base catalysis are economically and ecologically important in various industrial applications including alkylation, isomerization, dehydration, condensation, amination, cracking, etherification, aromatization, hydration, hydrocracking, oligomerization, polymerization as well as esterification [3–14] etc. Further, acid catalysis can also be classified according to their phase composition: homogeneous and heterogeneous catalysis. Homogeneous catalysts act in same phase as reaction mixture, whereas heterogeneous catalysts act in a different phase from reaction mixture. Few reports on homogeneous and heterogeneous catalysts are as follows-

1.2   Homogeneous acid catalysis

Besides several environmentally hazardous features of homogeneous acid catalysis, this concept is still popular in industrial applications because of its ease of operation and low cost. Use of sulphuric acid is common in various reactions such as benzylation of phenol with benzyl alcohol to produce benzyl phenol, esterification of acetic acid with methanol, esterification reaction of oleic acid and oleyl alcohol to produce oleyl oleate, a wax ester, transesterification of Nigerian *Jatropha curcas* oil into Biodiesel [15–17] etc. The scope of homogeneous Lewis

acid-catalyzed benzo [*N*,*N*]-heterocyclic condensation has been expanded to include the use of **SnCl$_2$·2H$_2$O** [18]. Esterification of acetic, propanoic and pentanoic acids with methanol, ethanol, 1-propanol, 2-propanol, butanol and 2-butanol is studied in the presence of **liquid HCl** [19]. The synthesis of cyclic carbonates by CO$_2$ insertion into epoxides catalysed by homogeneous **MTBD (7-methyl-1,5,7-triazabicyclo[4.4.0]dec-5-ene)** is reported [20]. Homogeneous **hydrogen iodide** has also been utilized in esterification of acetic acid with methanol [21]. But these catalysts cannot be regenerated and their application can cause unavoidable problems like corrosion of reactor, environmental hazards, separation and recycling of catalysts, higher cost for waste disposal and waste water treatment etc. Therefore, the replacement of the homogeneous catalysts with the heterogeneous ones is becoming more important in chemical and life science industry. Heterogeneous catalysts are noncorrosive and environmentally benign, presenting fewer disposal problems. Their repeated use is possible and their separation from liquid products is much easier. Furthermore, they can be designed to give higher activity, selectivity, and longer catalyst life.

1.3   Heterogeneous acid catalysis

One of the classes of heterogeneous catalysts that have generated a particular interest is supported homogeneous catalysts, that combine the potential versatility and selectivity of homogeneous catalysts with the practical advantages of solid materials, such as easier catalyst separation from the reaction medium, recovery and use of a large variety of reaction conditions [22]. The term supported material has been used to describe a wide range of materials involving an inorganic or organic support onto which a reagent species has been chemically or physically adsorbed. Supports tend to disperse the active promoter uniformly, provide a larger surface area for catalytic activity [23]. There are numerous inorganic and organic support materials that are potentially suitable for conversion into supported catalysts and widely used in the organic transformations. These include silica, alumina, activated carbon, clay, biomass derivatives, zeolite, polymeric resins and other aluminosilicates.

In contrast to extensive studies of heterogeneous catalysts, fewer efforts have been done for the study of different supported solid acid catalysts and their uses in organic transformation reactions. This review is a survey of supported solid acid catalysts and is not comprehensive but leads to the conclusion that, although many catalysts and catalyst supports have already been discovered over the past century, many opportunities nevertheless exist for new developments, new processes and new catalytic materials.

1.3.1 Silica supported solid acid catalysts

In recent years, silica supported reagents are gaining considerable attention because of higher activity of the catalyst due to the larger surface area and better selectivity, low toxicity, chemical inertness, unique pore system and numerous possibilities to modify their composition, morphology, and sorption properties. **Silica supported perchloric acid** as a highly efficient catalyst has been reported for *gem*-diacylation of aldehydes under solvent-free conditions [24] as shown in **Scheme 1.1.**

$$RCHO \xrightarrow[\text{rt, 2-10 min, 85-98\%}]{Ac_2O,\ HClO_4\text{-}SiO_2\ (0.5mol\%)} RCH(OAc)_2$$

R = aliphatic / aromatic
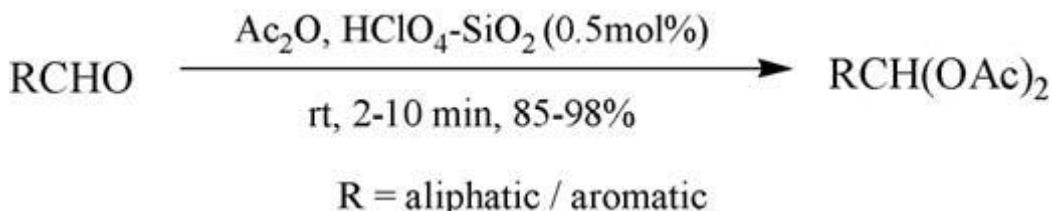
Scheme 1.1: Gem-diacylation of aldehydes in presence of silica supported perchloric acid as catalyst.

Raney Ni–Si catalysts are synthesized by treating Raney nickel with silane in a fluidized bed reactor and tested in the selective hydrogenation of 2-butyne-1,4-diol at high concentration [25]. Compared with the traditional Lindlar-type catalysts, such Raney Ni–Si materials can be used extensively in organic synthesis for selective hydrogenation of alkynes, avoiding the associated hazards of toxic additives. **MoO$_3$/SiO$_2$, silica supported 12-molybdophosphoric acid catalysts** have been proved to be a good catalyst for partial oxidation of methane to formaldehyde [26]. **Silica-supported sulfonic acid** has been reported as efficient catalyst in the dihydroxylation of 1-methylcyclohexene with aqueous hydrogen

peroxide, without the use of additional solvents, under mild conditions [27]. **Silica-bonded S-sulfonic acid** has been employed as a recyclable catalyst for the synthesis of coumarins from phenols and -ketoesters at 80°C under solvent-free conditions [28] as shown in **Scheme 1.2.**
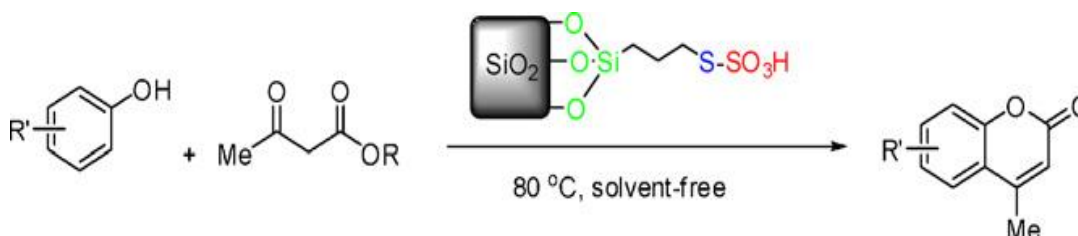
Scheme 1.2: **Silica-bonded S-sulfonic acid catalyzed condensation of phenols with ethyl or methyl acetoacetates.**

An efficient and direct protocol for the preparation of amidoalkyl naphthols employing a multi-component and one-pot condensation reaction of 2-naphthol, aromatic aldehydes, and acetonitrile or acetamide in the presence of silica supported perchloric acid under solvent, solvent-free, and microwave irradiation conditions [29] is described in **Scheme 1.3**. o-QMs formed as intermediate is o-quinone methides.
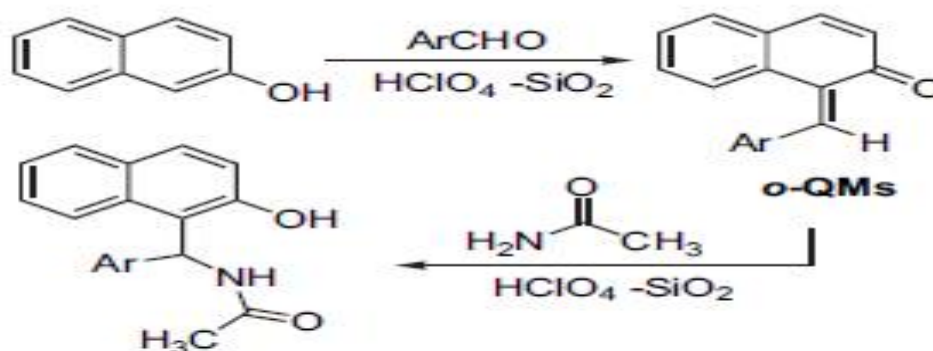
Scheme 1.3: **Multicomponent reaction over silica supported perchloric acid catalyst.**

Indoles undergo smooth alkylation with benzylic alcohols on the surface of 10 mol% of **phosphomolybdic acid supported on silica gel (PMA/SiO$_2$)** under mild conditions to produce C-3 benzylated-indoles in high yields and with high selectivity [30] as shown in **Scheme 1.4.**
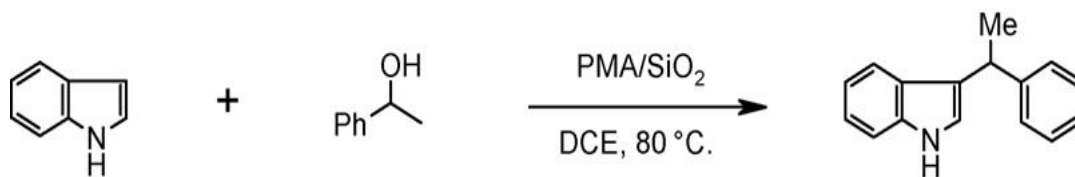
Scheme 1.4: **Alkylation of indole with benzylic alcohols over PMA/SiO$_2$.**

      Silica gel supported aluminium trichloride (SiO$_2$-AlCl$_3$) has been shown to be a mild, efficient, and chemoselective heterogeneous Lewis acid catalyst for the acylation of aromatic compounds with acid chlorides [31] (**Scheme 1.5**).

Scheme 1.5: **Acylation of aromatic compounds with acid chlorides over SiO$_2$/AlCl$_3$.**

      Silica-supported sulphuric acid catalysts are used for the esterification of long-chain aliphatic acids with alcohol to produce the corresponding esters having a wide range of end use applications such as cosmetic materials, topical medicines, and polyolefin catalyst components [32]. A direct approach has been developed for the preparation of pyrazole derivatives in the presence of **nano-silica sulfuric acid** [33] by condensation of 1,3-diketones and hydrazines as shown on **Scheme 1.6**.
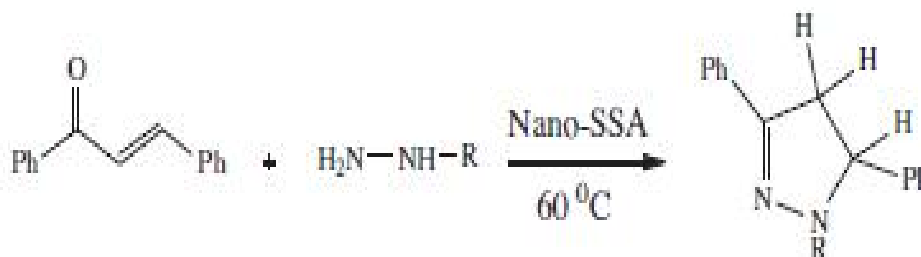
Scheme 1.6: **Synthesis of pyrazole derivatives using nano-silica sulphuric acid.**

      Nickel metal nanoparticles supported on low surface area silica, prepared by reduction of nickel acetate with hydrazine in aqueous medium are

evaluated in the gas-phase hydrogenation of benzene [34]. **Tungstophosphoric acid supported on SiO₂** has shown high activity, good selectivity of producing linear alkylbenzene and 2-phenyl isomer and sufficient catalytic stability [35]. An efficient and environmentally benign procedure for the catalytic esterification of salicylic acid with aliphatic alcohols and benzylic alcohols has been developed using **Nano-SiO₂-supported Preyssler heteropolyacid** both under thermal conditions and microwave irradiations [36]. Aliphatic and aromatic amines undergo smooth nucleophilic Michael addition to , -unsaturated compounds in the presence of a catalytic amount of **silica supported aluminum chloride** at 60°C and under solvent-free conditions to produce the corresponding -amino compounds in excellent yields [37] **(Scheme 1.7).**
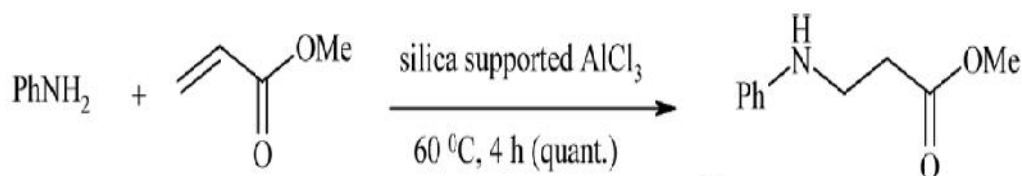
Scheme 1.7: **Michael addition of aromatic amines with methyl acrylate over AlCl₃/SiO₂.**

Under solvent free conditions between 40-50°C, **BF₃.SiO₂**, a mild solid acid catalyst, is applied to regio-chemo and stereoselective Claisen-Schmidt condensation [38] as described in **Scheme 1.8**.
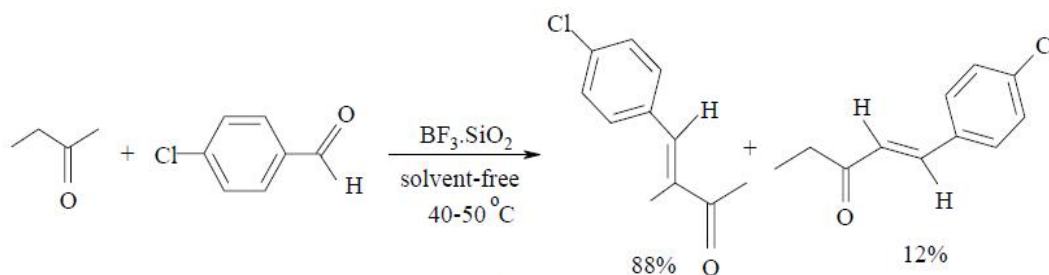
Scheme 1.8: **Crossed aldol condensation of 2-butanone with 4-chloro benzaldehyde over BF₃.SiO₂.**

1.3.2 Alumina/silica-alumina supported solid acid catalysts

Unlike silica, which is a natural compound, alumina does not occur in nature. - and -alumina having high degree of porosity and surface area are widely used in catalysis as inert supports for active metals [39]. **Alumina supported 12-tungstophosphoric acid (TPA/Al₂O₃)** catalyzes efficiently the

reaction of *o*-phenylenediamine with ketones under solvent-free conditions to afford the corresponding 1,5-benzodiazepines in excellent yields [40] (**Scheme 1.9**).
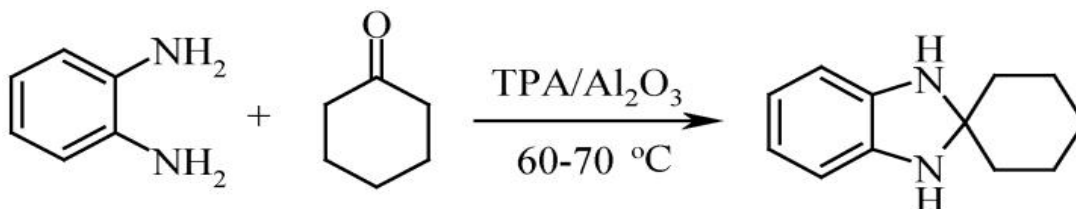
Scheme 1.9: **Reaction between cyclohexanone and o-phenylene diamine to give 2,3-dihydrobenzimidazole-2-spirocyclohexane over TPA/Al₂O₃.**

Mesoporous Zn– and Fe–Al-MCM-41 molecular sieves with different metal contents are synthesised hydrothermally. *t*-Butylation of phenol with *t*-butyl acetate, is carried out in vapour phase over these mesoporous materials [41]. Catalytic activity of **phosphotungstic acid supported on Al-MCM-41** is evaluated in the esterification of succinic anhydride with ethanol [42]. **Phosphoric acid supported on alumina (H₃PO₄/Al₂O₃)** is found to be an efficient catalyst for the three-component condensation reaction of -naphthol, aromatic aldehydes and amides or carbamates to afford the corresponding -amidoalkyl- -naphthols, -carbamato-alkyl- -naphthols under solvent-free conditions [43] as shown in **Scheme 1.10**.

R= CH₃, Ph, CH₃O, CH₃CH₂O, PhCH₂O
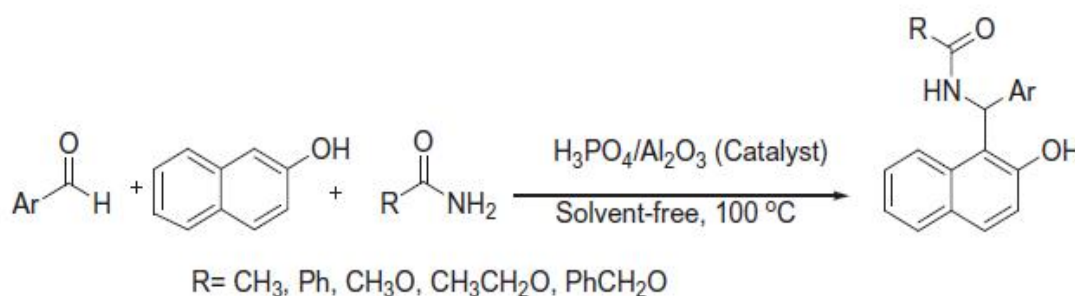
Scheme 1.10: Synthesis of -amidoalkyl- - naphthols and -carbamato-alkyl- –naphthols over H₃PO₄/Al₂O₃.

The acidic properties of **alumina-supported molybdenum oxide (MoO₃/Al₂O₃)** calcined at high temperatures, with MoO₃ loadings of 5–30 wt%, are investigated for benzylation of anisole and isomerization of -pinene [44]. A

series of solid strong acid catalysts are synthesized from fibrous **ZrO₂/Al₂O₃** core and shell nanocomposites. The acidity of the obtained solid acids is tested by using them as catalysts for the benzoylation of toluene [45]. Friedel–Crafts alkylation reactions such as tert-butylation, iso-propylation and sec-butylation of phenol have been carried out over **12-tungstophosphoric acid supported onto neutral alumina** under mild conditions by varying different parameters [46].

1.3.3 Activated carbon supported solid acid catalysts

Activated carbon is defined as a wide range of amorphous carbon based materials prepared to exhibit chemical inertness, good mechanical and pH stability and an extended interparticulate surface area [47] . It can be produced from a wide variety of carbon-rich raw materials of animal, mineral or agricultural wastes origins [48]. These materials are characterized by their extraordinary large specific surface areas, well-developed porosity and tunable surface-containing functional groups [49] thus they are favourable for application as catalyst support material. **Sulfonated (SO₃H-bearing) activated carbon (AC-SO₃H)** has been synthesized by an aryl diazonium salt reduction process. The catalytic activity of AC-SO₃H has been assessed in the esterification of aliphatic acids with longer carbon chains such as hexanoic acid and decanoic acid [50]. **Carbon-based solid acid (CBSA)**, prepared by sulfation of naphthalene proved to be an effective and reusable catalyst [51] for the synthesis of -amino carbonyl compounds by one-pot three-component Mannich reaction of acetophenone, aromatic aldehydes and aromatic amines, as described in **Scheme 1.11**.
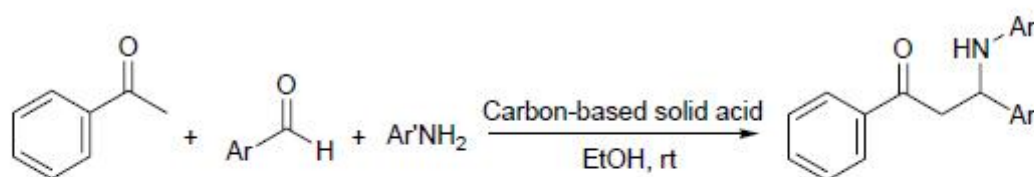
Scheme 1.11: Mannich reaction of acetophenone, aromatic aldehydes and aromatic amines using CBSA.

Tungstophosphoric and tungstosilicic acid catalysts supported on carbon are prepared by equilibrium and incipient wetness impregnation techniques for isopropanol dehydration [52]. The esterification of free fatty acids

with methanol is studied using **Sulfonated Porous Carbon** as catalyst [53]. The prepared catalyst is reused at least three times without loss of activity. **Carbon-based sulfonated catalyst (CBSC)** has become a research hot-spot in recent years. Biomass derived CBSC has shown high catalytic activities in many chemical reactions, including hydrolysis, esterification, alkylation, condensation, benzylation [54] etc. Michael-type Friedel-Crafts reaction is shown in **Scheme 1.12**.
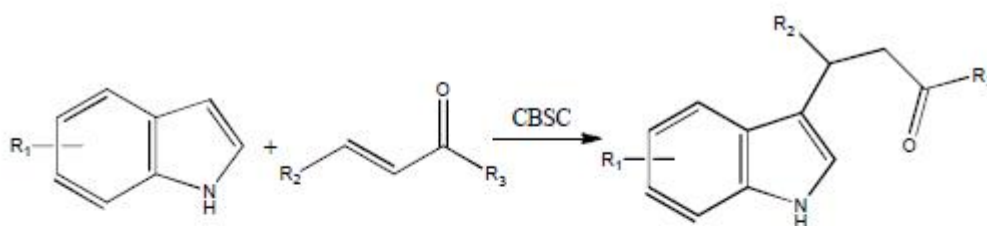
Scheme 1.12: Catalytic Michael-type Friedel–Crafts of indoles with , - unsaturated carbonyl compounds over CBSC.

A solid acid catalyst, prepared by **sulfonating carbonized corn straw**, has proved to be an efficient and environmental benign catalyst for the esterification of oleic acid and methanol [55]. An efficient and selective acylation of alcohols and amines employing carboxylic acids as acylating agents is developed using **iron oxide containing activated carbon catalyst** [56] as shown in **Scheme 1.13**.
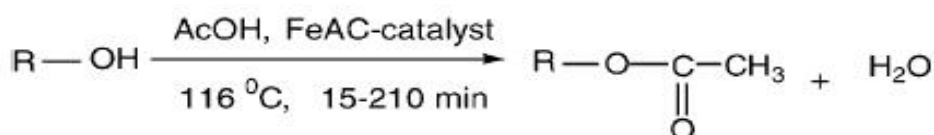
Scheme 1.13: Acylation of alcohols with carboxylic acids over FeO/activated carbon catalyst.

A highly **sulfonated carbon** is used in one pot three-component condensation reaction of various aromatic aldehydes with -ketoester and urea under solvent-free conditions to afford the corresponding dihydropyrimidinones (DHPMs) [57] as shown in **Scheme 1.14.**
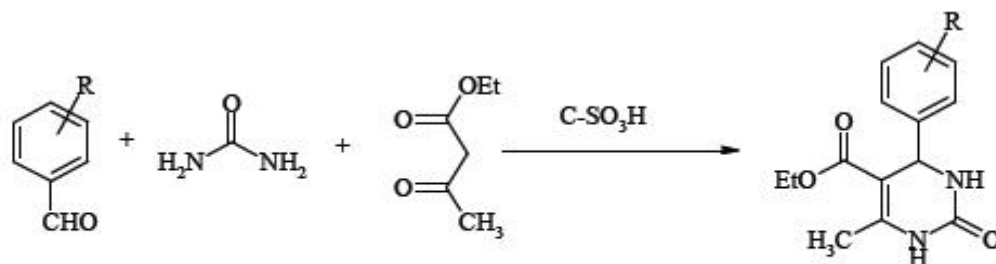
Scheme 1.14: Preparation of dihydropyrimidinones in the Biginelli-type reactions of ethyl acetoacetate, aromatic aldehydes and urea over sulfonated carbon catalyst.

1.3.4 *Polymer supported solid acid catalysts*

Porous polymer particles, especially the ones that are spherical in shape, have been utilized in numerous applications for decades. The different characteristics of polymers such as high surface area, ability to uptake various solvents with different polarity and increased brittleness are utilized in heterogeneous catalysis. In general, polymer particles are produced by heterogeneous polymerizations using the immiscibility of two or more liquids through suspension, dispersion, precipitation, multistage, membrane/micro channel emulsification and micro fluidic polymerizations [58]. **Polystyrene-supported sulphonic acid (NKC-9)** efficiently catalyzed the cross-aldol condensation of benzaldehyde and cyclopentanone to afford , '-bis(benzylidene) cyclopentanones [59] in good yields (**Scheme 1.15**).
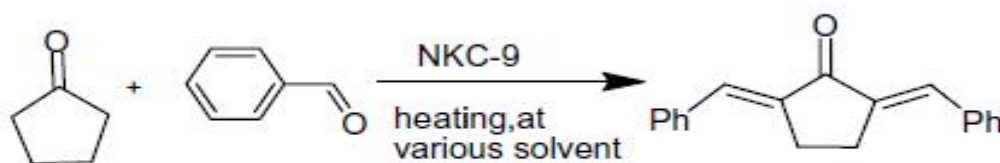
Scheme 1.15: Reaction of cyclopentanone with benzaldehyde over NKC-9.

New materials have been obtained from **aluminium or copper salts of tungstophosphoric and tungstosilicic acids immobilized in a PVA-PEG** (Polyvinyl alcohol and polyethyl glycol) polymeric blend by the freezing-thawing method. Their catalytic activities are tested for acylation of anisole [60]. A new **SO₃H-functionalized HPA-based acidic polymeric hybrid** has prepared by

coupling task-specifically designed SO₃H-functionalized polymeric ionic liquids with Keggin-structured heteropolyanions [61]. Its catalytic performance for esterification of alcohols with carboxylic acids is studied under solvent-free conditions. The synthesis of catalyst is given in **Scheme 1.16.**
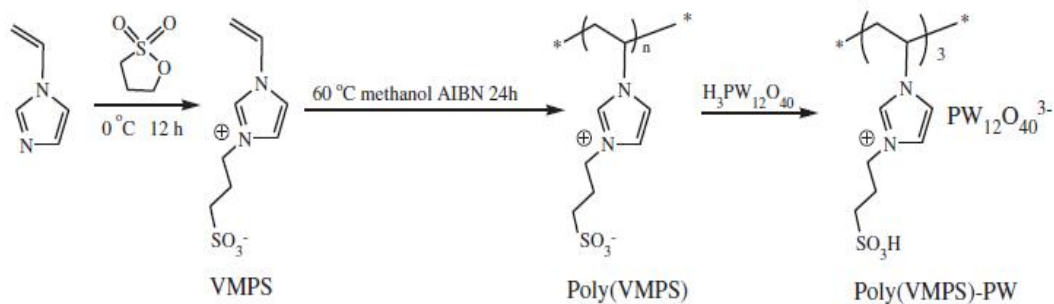
Scheme 1.16: Synthesis of the acidic polymeric hybrid Poly (VMPS)-PW.

A **polymer-supported gadolinium triflate (CMPS-IM-Gd) catalyst** is used as an efficient Lewis acid catalyst for the acetylation of various alcohols and phenols with acetic anhydride [62], affording high yields under mild conditions as shown in **Scheme 1.17**.
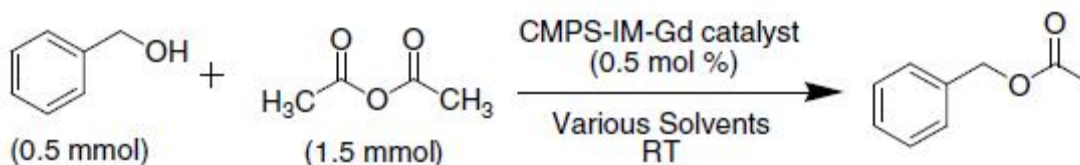
Scheme 1.17: Acetylation of benzyl alcohol with acetic anhydride over CMPS-IM-Gd catalyst.

HPA-polymer composite film catalysts prepared by membrane preparation technique are cut into small pieces, and applied as heterogeneous catalysts to the liquid-phase *tert*-butyl alcohol synthesis, vapor-phase ethyl *tert*-butyl ether synthesis, and vapor-phase ethanol conversion [63]. Chitosan is an optically active biopolymer that can be used as a support for the preparation of heterogeneous catalysts in the form of colloids, flakes, gel beads, fibers (including hollow fibers), or immobilized on inorganic supports (alumina, silica, or other metal oxides) [64]. Examples of reactions catalyzed with **chitosan-supported materials** are oxidation, hydrogenation, Suzuki and Heck reactions, cyclopropanation of olefins, asymmetric dihydroxylation of olefins, carbonylation etc.

1.3.5 Ion-exchange resin supported solid acid catalysts

An ion exchange material may be defined as an insoluble matrix containing labile ions capable of exchanging with ions in the surrounding medium without any major physical change in structure. In 1940s **I.G. Farbenindustrie** developed the first commercial esterification process over **Wofatit phenolsulphonic acid-formaldehyde resins** [65]. Ion-exchange resins, especially the cation-exchange resins such as Dowex, Amberlyst series are manufactured mainly by sulfonation of ethylbenzene first, followed by a cross-link with divinylbenzene. Because of their selective adsorption of reactants, surface acid site features, and swelling nature, these resins not only catalyze the esterification reaction but also affect the equilibrium conversion. The esterification of acrylic acid and n-butanol catalyzed by three different ion exchange resins, Amberlyst 15, Amberlyst 131 and Dowex 50Wx-400 has been studied [66]. **Amberlyst 131** has found to be more efficient catalyst giving the maximum conversion of acrylic acid. **Nafion (tetrafluoroethylene-perfluoro-3,6-dioxa-4-methyl-7-octensulfonic acid) catalyst**, a perfluroalkanesulfonic acid resin was developed by **DuPont** chemists in early 1960. It is a recyclable Brønsted acid catalyst and hence is able to catalyze a variety of organic reactions such as transalkylation, ether synthesis, esterification, condensation of ketones, Friedel-Crafts alkylation [67], acylation of anisole, toluene **(Scheme 1.18)** [68].
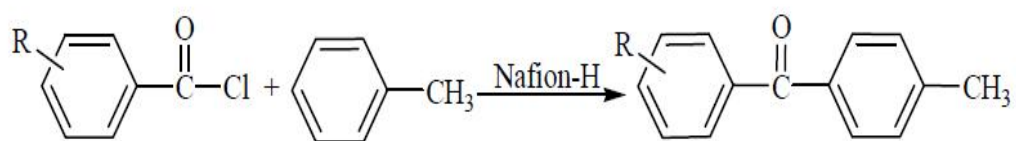
Scheme 1.18: Friedel-Crafts acylation of aroyl chlorides with toluene to give substituted methylbenzophenones over Nafion-H.

Amberlyst, acidic cation-exchange resin bead, is widely used as excellent heterogeneous acid catalysts for a wide variety of organic reactions including esterification, transesterification, Friedel-Crafts alkylation, acylation, benzylation of arenes as shown in **Scheme 1.19** [69], hydroalkylation, halogenation, protection of carbonyls, crossed-aldol condensation, synthesis of quinolines, xanthenes, coumarins, furans, and substituted phosphonates [70].
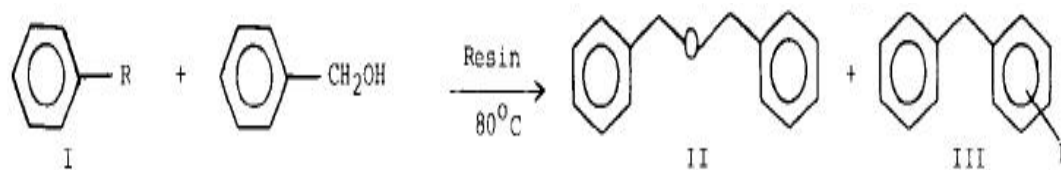
Scheme 1.19: Benzylation of arenes by benzyl alcohol over Amberlyst-15.

Dowex50Wx8-400 has been utilized in esterification of propionic acid with 1-propanol [71].

1.3.6 *Zeolite supported solid acid catalysts*

Since 1960s, zeolites catalysts have conquered the petroleum refining and petrochemical industries. Zeolites are three-dimensional crystalline aluminosilicates consisting of a framework of SiO_4 and AlO_4 tetrahedra, each with a silicon or aluminum in the center [72]. The oxygen atoms are shared between adjacent tetrahedra. Zeolites provide great thermal and chemical stability as well as acid strength, which are comparable to homogeneous acid catalysts. The most important of these processes are hydrocracking of heavy petroleum distillates, octane number enhancement of light gasoline by isomerization, the isomerization of xylenes, n-hexane etc. [73]. The Friedel–Crafts acylation of 2-methoxynaphthalene has carried out in the liquid-phase batch conditions using **H-mordenite, H-beta and H-Y zeolite** as catalysts [74] as shown in **Scheme 1.20**.
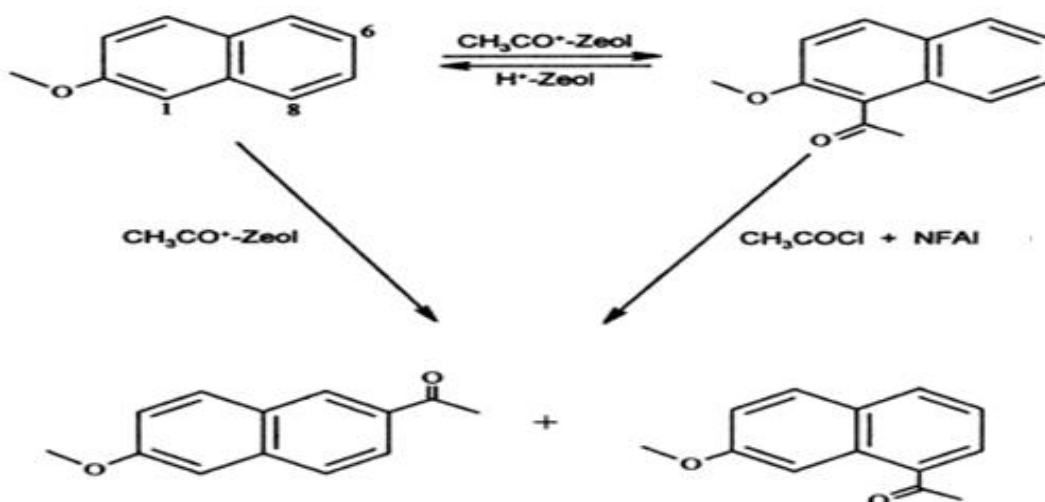
Scheme 1.20: Acylation of 2-methoxynaphthalene over zeolites.

The esterification of acetic acid with ethanol on **zeolites- BEA, FER, MFI, and MOR** has been evaluated [75]. The acetylation of 1,2-, 1,3- and 1,4-dimethoxybenzenes with acetic anhydride [76] has been investigated in the liquid phase using chlorobenzene as solvent over the **H-forms of various zeolites (Scheme 1.21)**. **H-Y and H-Beta** have been shown to be efficient catalysts in such a reaction, and led to the selective formation of the corresponding dimethoxyacetophenones.
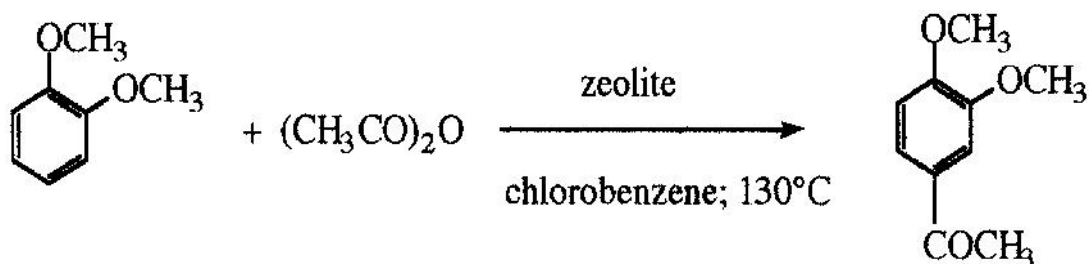
Scheme 1.21: Synthesis of 3,4-dimethoxyacetophenone from the acylation of 1,2-dimethoxybenzene with acetic anhydrides over zeolites.

Direct synthesis of microporous-mesoporous **zeolite-SBA-15 (ZBS-15)** composite catalyst under acidic hydrothermal conditions through the simultaneous self-assembly of mesoporous silica SBA-15 and zeolite. The activity of ZBS-15 composite catalyst for the nitration of benzenes under solvent-free conditions has been investigated [77] **(Scheme 1.22)**.
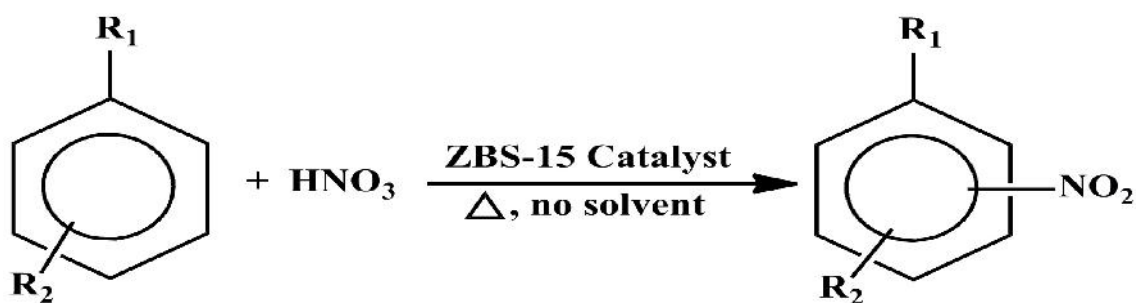
Scheme 1.22: The nitration of substituted benzenes over ZBS-15 catalyst.

The catalytic liquid phase benzylation of benzene to diphenylmethane with benzyl chloride is investigated over a number of zeolite catalysts at 358 K and under atmospheric pressure **(Scheme 1.23)**. **Zeolite H-beta** is found to be more selective but less active compared to HY and H-ZSM-5 zeolites in the benzylation of benzene [78].
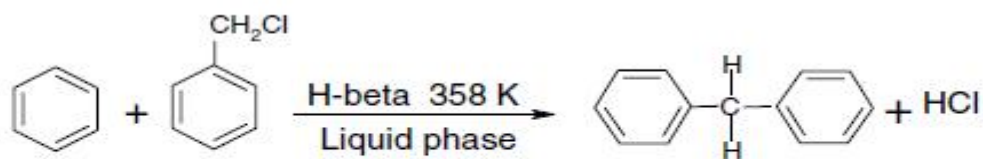
Scheme 1.23: Benzylation of benzene to diphenylmethane with benzyl chloride over H-beta catalyst.

The liquid phase benzoylation of *o*-xylene with benzoyl chloride over various zeolite catalysts is studied in a batch reactor at atmospheric pressure and temperature, 411 K [79]. The protonic form of **zeolite beta** is found to be an efficient catalyst compared to other zeolites in the benzoylation of *o*-xylene as shown in **Scheme 1.24**.
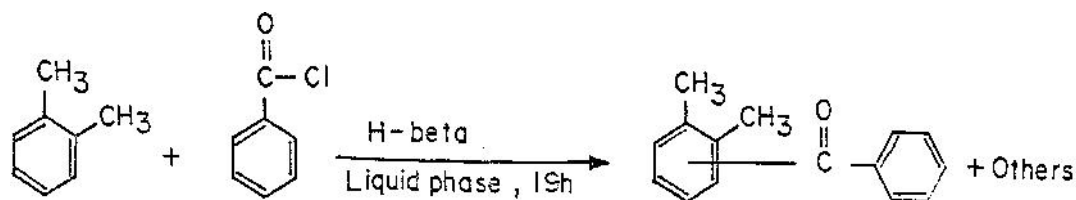
Scheme 1.24: Benzoylation of o-xylene to 3,4-dimethylbenzophenone with benzoyl chloride over H-beta zeolite.

1.3.7 *Rice husk ash supported solid acid catalysts*

Rice husk is a biomass by-product from rice mill that has been used as an energy source in many industries, containing ca. 92–95% silica [80]. Burning rice husk generates rice husk ash (RHA) which is rich in silica and can be an economically valuable raw material for production of natural silica [81] and at the same time help to solve rice husk disposal problem faced by rice milling industries. Recently, much research has been done on the potential use of the silica from rice husk as a support for heterogeneous catalysts in many industrially important reactions such as in the oxidation, esterification and benzylation [82,83]. **Nickel catalysts supported on RHA-alumina** are prepared by the incipient wetness impregnation method. The catalytic activities of nickel catalysts are tested by CO_2 hydrogenation [84]. Al, Ga and Fe catalysts supported on silica obtained from RHA are synthesized using the sol–gel technique at room temperature [85]. The benzylation of benzene and substituted benzenes with

benzyl chloride are studied over the prepared catalysts. RHA–Fe showed excellent activity for the benzylation of benzene, whereas, RHA–Ga gave good selectivity towards diphenylmethane. 7-Amino-1-naphthalene sulfonic acid (ANSA) has immobilized onto silica via a simple sol–gel technique to form catalyst with strong Brønsted acid site, **RHANPSO₃H**. The catalytic performance of RHANPSO₃H is tested in the esterification of n-butyl alcohol with different mono and di-acids [86]. The proposed catalytic cycle is given in **Scheme 1.25**.
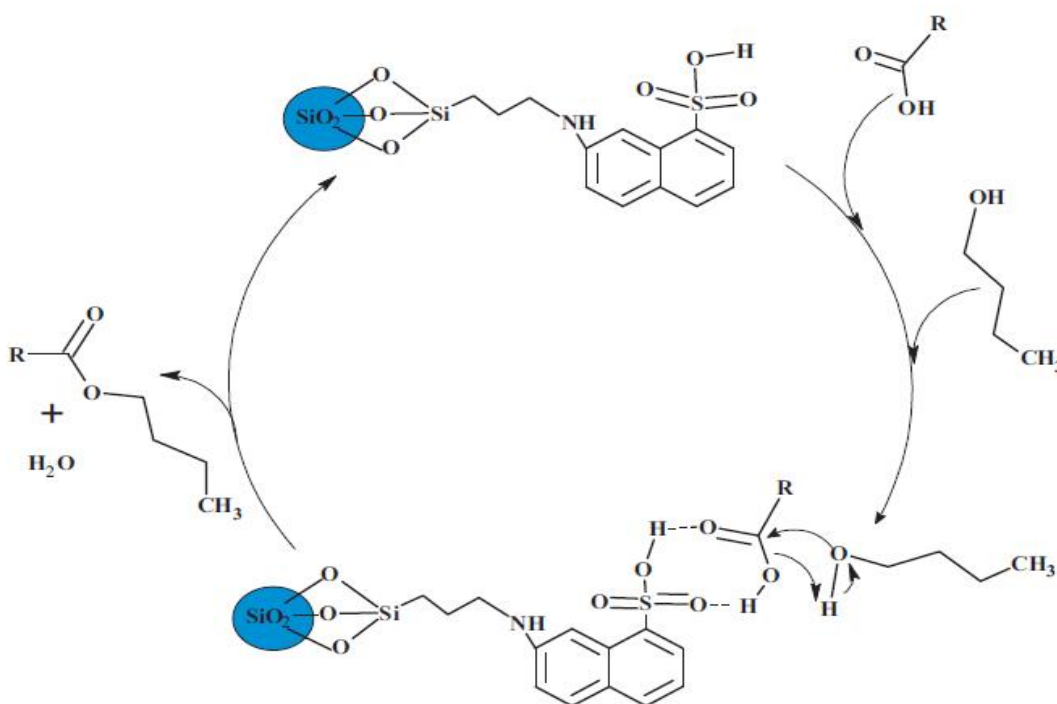
Scheme 1.25: **The proposed catalytic cycle for the esterification reaction over RHANPSO₃H.**

Iron and 4-(methylamino) benzoic acid/RH-silica** has been successfully tested for Friedel–Crafts benzylation reaction with toluene [87]. Sulfanilic acid is immobilized onto rice husk ash via 3-(chloropropyl)triethoxy-silane to form an acidic solid catalyst denoted as **RHAPhSO₃H**. Brønsted acid sites of catalyst have been utilized in t-butylation of phenol [88] as shown in **Scheme 1.26**.
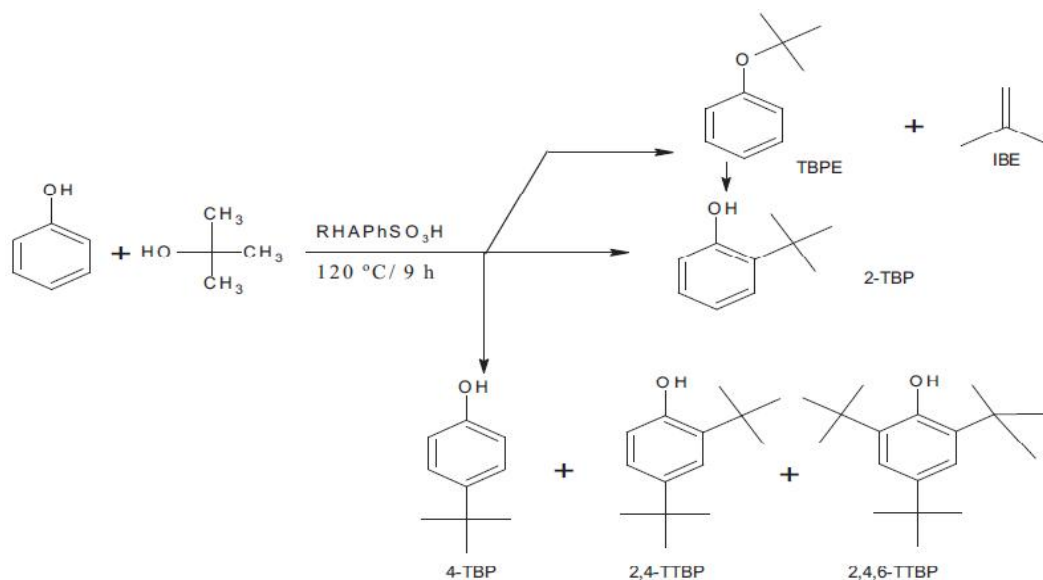
Scheme 1.26: Tert-butylation of phenol over RHAPhSO₃H.

RHA-MCM-41 is prepared from rice husk silica using cetyltrimethylammonium bromide as a structure directing agent via a simple sol–gel method and utilized to study styrene oxide ring opening with aniline to form -amino alcohols via aminolysis reaction [89] **(Scheme 1.27)**.
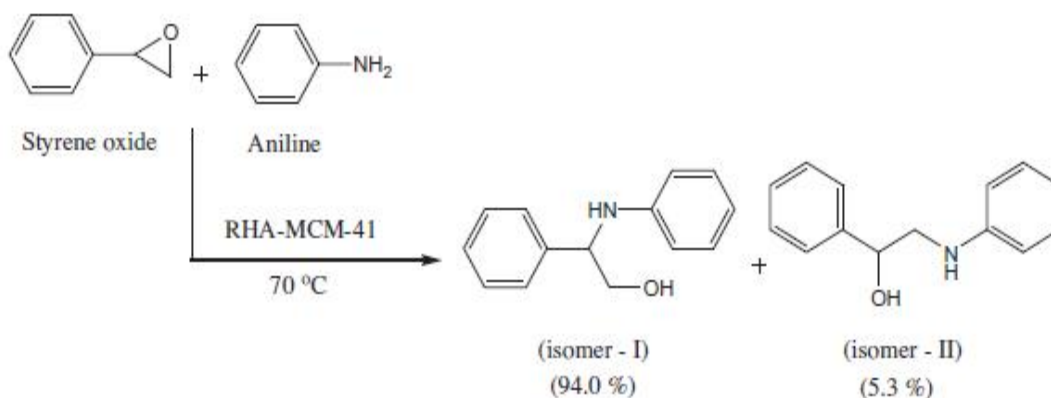
Scheme 1.27: Ring opening of styrene oxide over RHA-MCM-41.

1,1-Diacetates are produced from a variety of aromatic aldehydes using **rice husk supported FeCl₃** nanoparticles as catalyst. The procedure generally resulted in good yields (98%) of aromatic aldehydes [90].

1.3.8 *Clay supported solid acid catalysts*

The term 'clay' refers to widespread, naturally occurring materials composed primarily of fine-grained minerals, which generally display both Lewis and Brønsted acidity. The strong Brønsted acidity is caused by the Si-OH…Al structure generated by the protonation at the Si-O-Al linkage in the tetrahedral sheet. The layers possess net negative charge that is neutralized by cations such as Na^+, K^+, Ca^{2+} etc., which occupy the interlamellar space. This provides tremendous scope for altering the properties of clays like acidity, pore size, surface area, polarity and other characteristics that govern their performance as catalysts. To date, there are numerous reports on the catalytic activity of clays and clay-based materials, in a large variety of organic transformations including benzylation, dehydration, addition, Diels Alder reaction, hydrocracking, isomerisation etc. [91]. Tailor made catalysts can be prepared from montmorillonite clays by suitably adjusting their acidity and surface area by acid activation and their catalytic performance has been assessed in a test Friedel–Craft alkylation reaction of benzyl chloride with toluene. **Activated montmorillonite K10 clay** has found to catalyze the reaction of allyl trimethylsilane with aromatic aldehydes to give homoallylic silyl ethers **(Scheme 1.28).**
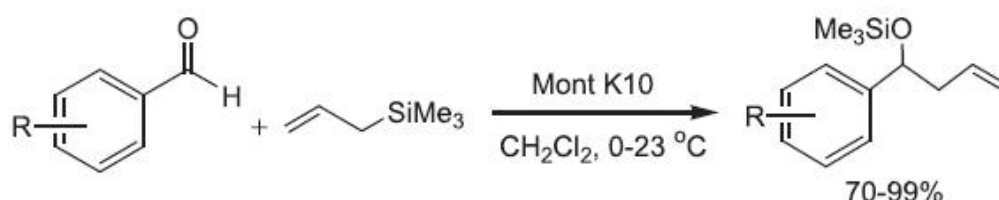
Scheme 1.28: Reaction of allyl trimethylsilane with aromatic aldehydes over activated montmorillonite K 10 clay.

Sulphuric acid-treated montmorillonite clay is a highly active catalyst for bringing out addition of methanol to 2,3-dimethyl-1-butene **(Scheme 1.29)**. The activity of the catalyst depends on the sulphuric acid content in the clay.
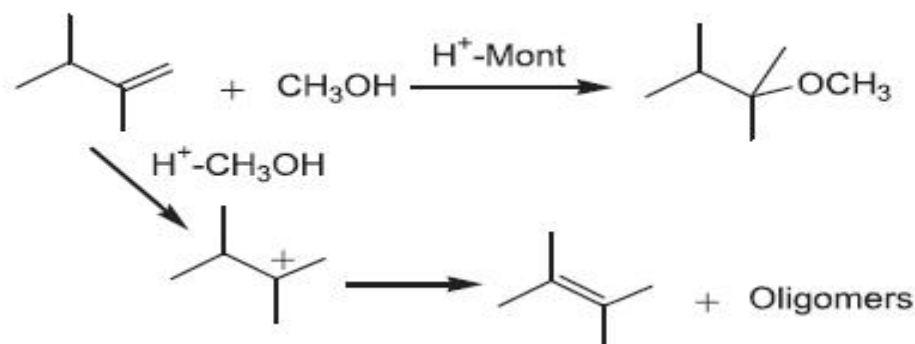
Scheme 1.29: **Synthesis of ethers by the addition of methanol to 2,3-dimethyl-1-butene over acid treated montmorillonite.**

Acid activated Indian bentonite has reported to be a good catalyst for the preparation of aryl and alkyl esters of different aromatic and aliphatic carboxylic acids as shown in **Scheme 1.30**.
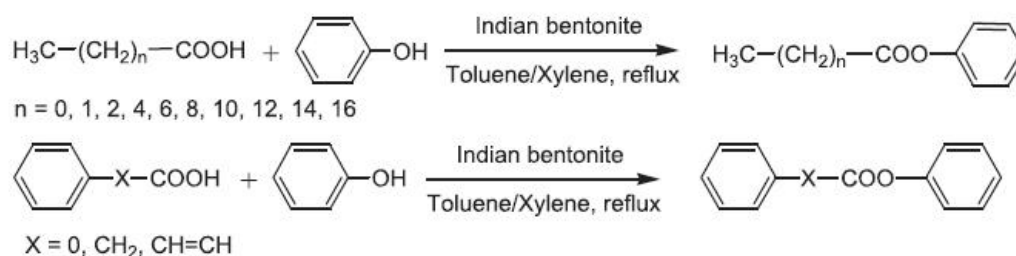
Scheme 1.30: **Synthesis of aryl and alkyl esters over Indian bentonite.**

Methyl mandelate, used in flavouring and perfumery, has been prepared by esterification of mandelic acid with methyl alcohol in the presence of **montmorillonite K10 supported dodecatungstophosphoric acid (DTP/K10)** and its cesium salt **(Cs-DTP/K10)** as shown in **Scheme 1.31**.
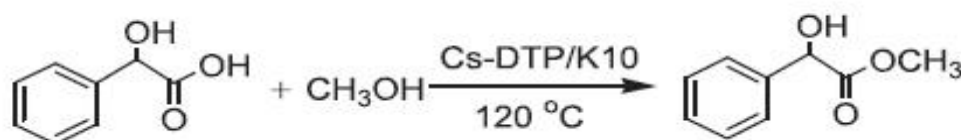
Scheme 1.31: **Esterification of mandelic acid with methanol giving methyl mandelate over Cs-DTP/K10.**

An interesting case of **Fe–Mg–hydrotalcite anionic clay** being used for the Friedel–Crafts alkylation [92] has been described in **Scheme 1.32**. They have benzylated anisole, mesitylene, p-xylene, toluene and naphthalene with high degree of conversions, using benzyl choride.
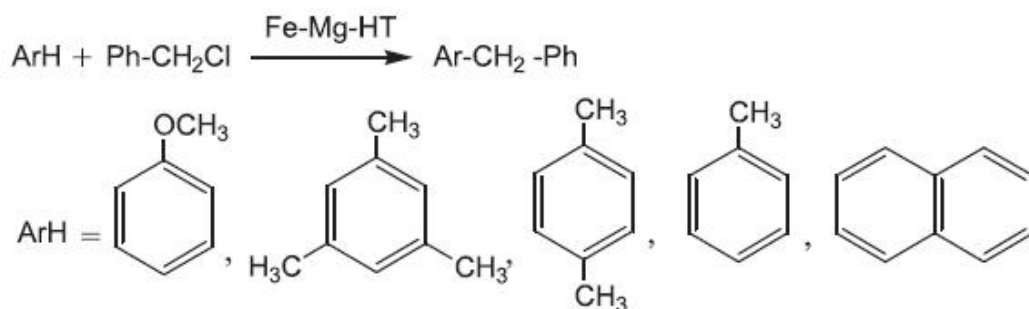
Scheme 1.32: Friedel-Crafts alkylation by benzyl chloride over anioinic clays.

Phenol has been benzoylated by benzoic acid to 4-hydroxybenzophenone via the formation of phenyl benzoate as intermediate which underwent Fries rearrangement, a variant of Friedel–Crafts acylation over **Cs-DTP/K10 catalyst** as shown in **Scheme 1.33**.
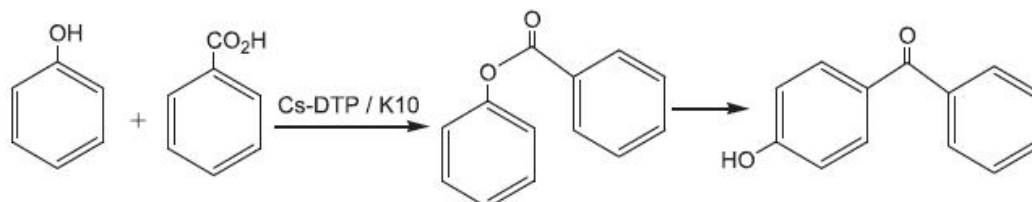
Scheme 1.33: Benzoylation of phenol by benzoic acid to give 4-hydroxy benzophenone over Cs-DTP/K10 catalyst.

The diastereomeric (R)-(+)-limonene diepoxides underwent isomerisation at room temperature on **synthetic K10 clay** calcined at 100°C to give various isomers in a ratio of ~4:3:7:2 as shown in **Scheme 1.34**.
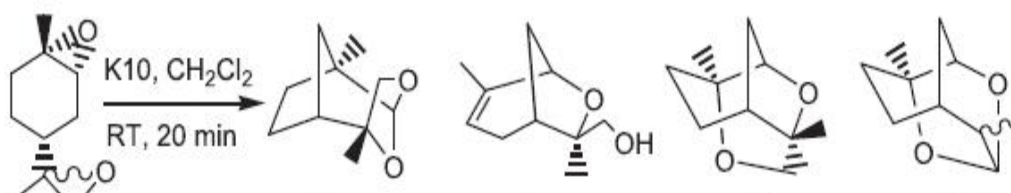
Scheme 1.34: Isomerization of diastereomeric (R)-(+)-limonene diepoxides over K10 clay.

1.4 Microwave assisted heterogeneous acid catalyzed organic reactions

Microwave synthesis represents a major break-through in synthetic methodology, first reported by the group of **Gedye and Gigure Majetich** [93] in 1986. Microwave absorbing materials are of utmost importance for microwave chemistry and three main different mechanisms are involved for their heating namely: Dipolar polarization, Conduction mechanism and Interfacial polarization. Microwave-assisted organic synthesis uses both less energy and solvent, and it enables difficult compound synthesis. Conventional organic synthesis is carried out by conductive heating with an external heat source (for example, an oil bath). This is a comparatively slow and less efficient method for transferring energy into the system, since it depends on the thermal conductivity of the various materials that must be penetrated, and results in the temperature of the reaction vessel being higher than that of the reaction mixture. In contrast, microwave irradiation produces efficient internal heating (in-core volumetric heating) by direct coupling of microwave energy with the molecules (solvents, reagents, catalysts) that are present in the reaction mixture. Microwave include following advantages, over the conventional heating - uniform heating throughout the material, increase in process speed, high efficiency of heating, enhanced product yield and purity, reduction in unwanted side reactions, rapid reaction optimization, purity in final product, improvement in reproducibility, minimization of environmental heat loss, lowering of operating cost etc. Coupling of microwave irradiations with the use of mineral-supported catalysts, under solvent-free conditions, provides clean chemical processes with the advantage of enhanced reaction rates, higher yields and greater selectivity [94]. Avoiding organic solvents during the reactions in organic synthesis, use of non-conventional microwave source of energy, less generation of wastes during the whole procedure leads to a clean, efficient, and economical technology as per the principles of green chemistry. Some industrially important microwave assisted heterogeneous acid catalyzed organic transformations are summarized in **Table 1.1.**

Table 1.1:   **Some microwave assisted heterogeneous acid catalyzed organic transformations.**

S.No.	Reactions	Catalysts	Reaction Conditions	Product	Ref.
1.	Formylation Reaction	HCOOH/SiO$_2$	35-95 sec	Formamides	[95]
2.	Pechmann Reaction (Resorcinol + ethyl acetoacetate	Sulfated Zirconia	150°C, 15 minutes	7-hydroxy 4-methyl coumarin	[96]
3.	Three component aza-Diels-Alder cyclization (Aniline + cyclohexene-2-one + 4-bromo benzaldehyde	Silicotungstic acid	100°C, 5 minutes	Aza bicyclo [2.2.2] octan-5-ones	[97]
4.	Trans-esterification Reactions				
(i)	Castor bean oil + methanol/ethanol	Acidic silica gel	60°C, 3 h	Esters	[98]
(ii)	Stearic acid + ethanol	Aminophosphonic acid resin D418	80°C, 7 h	Esters	[99]
5.	Friedel-Crafts Acylation Reactions				
(i)	Methyl salicylate + acetyl chloride	Cu(OTf)$_2$-silica	120-180°C, 0.13 h	o-acyl methyl salicylate	[100]
(ii)	Indole + acetic anhydride	Phosphotungstic acid modified Hβ zeolite	120°C, 8 minutes	3-acetyl indole	[101]

6.	Alkylation Reactions				
(i)	Anisole + hexanoic acid	HY-zeolite	190°C, 30 minutes	1-(4-methoxy phenyl)-1- hexanone	[102]
(ii)	Naphthalene + t-butyl alcohol	HM-zeolite	150°C, 30 minutes	2,6-di-tert-butyl naphthalene	[103]
7.	Biginelli Reaction (Benzaldehyde + methyl acetoacetate + urea)	Molybdophosphoric acid	80°C, 5 minutes	5-ethoxy carbonyl-6-methyl-4- phenyl-3,4-dihydro pyrimidin-2 (1H)-one	[104]
8.	Claisen-Schmidt Condensation Reaction (Cyclohexanone + benzaldehyde)	Sulfated zirconia	140°C, 20 minutes	α,α' bis (benzylidine) cyclohexanone	[105]
9.	Benzoylation (Anisole + benzoyl chloride)	BEA zeolite on β-SiC	80°C, 0.5 h	p-methoxy benzophenone	[106]
10.	Benzylation Reaction (Benzene + Benzyl chloride)	Mesoporous zirconium phosphate	110°C, 30 min	Diphenyl methane	[107]
11.	One pot cyclo- condensation of benzil, aldehydes, ammonium acetate	$SbCl_3/SiO_2$	120°C, 15 minutes	Substituted imidazole derivatives	[108]
12.	Triple self- condensation of acetophenone	Nano-silica supported tungstophosphoric acid	90°C, 18-30 minutes	1,3,5 triaryl benzenes	[109]

1.5   Generation of acidic sites

Two distinct types of surface acidity have been identified in the literature. Brønsted acidity is attributed to acidic protons on surface hydroxyl groups, while Lewis acidity is attributed to surface cations which can accept electronic charge from a donor (Lewis base) molecule. Generation of Brønsted and Lewis acidic sites are provided in **Figure 1.1** and **Figure 1.2**. Concentration, strength, and accessibility of acid sites on a solid acid catalyst are important and these features need to be controlled when a solid acid catalyst is designed and optimized for a specific catalytic reaction [110]. A high concentration of acid sites is vital in controlling catalytic activity and, activity might be expected to be proportional to the concentration of surface acid sites. However, it is not always the case that increased acid strength will lead to increased activity. One reason for this is that the rate of a reaction will depend on the rate of desorption of products from the acid sites, and in some cases this will be reduced if acid strength is increased.
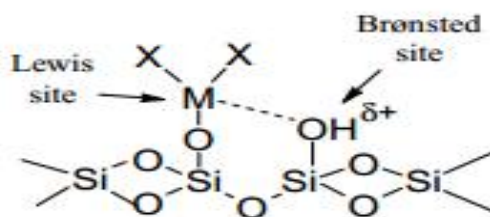
Figure 1.1: Brønsted acidity arising from inductive effect of Lewis acid center coordinated to a silica support.
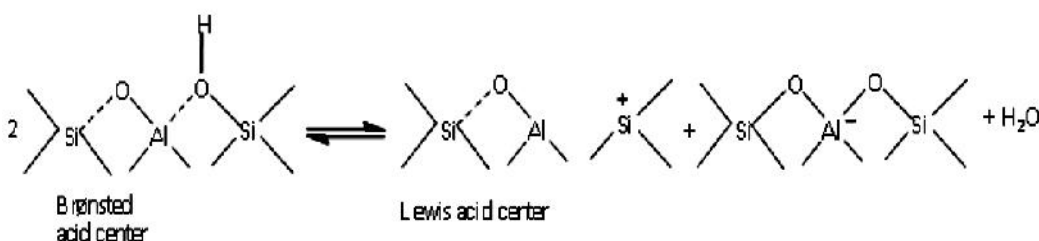
Figure 1.2: Formation of Lewis acid centres on silica-alumina surface.

The concepts of Lewis acid-base theory and Brønsted-Lowry acid-base theory may be applied to solid surfaces; however there is no general theory that serves to determine surface acidity or basicity [111]. All the properties of acidic sites cannot be measured by any single method. Integration of the results obtained

by different characterizations leads us to understand the structures, reactivity, strengths, and amounts of the acidic sites on the surfaces. The understanding of the acidic nature of a solid surface is of great importance in the field of ion exchange and catalysis.

1.6   Measurement of acidity in solid acid catalysts

Different techniques have been used to study the surface acidity of solid acid catalysts which are as follows:

1.6.1 Titration methods – Hammett indicators and acidity function

One of the oldest techniques for measuring acidity is based on a proposal by **Hammet and Deyrup** [110] for ordering strengths of solid acids on the basis of amine titrations. Unfortunately, this method is strictly applicable only to protonic (Brønsted) acids. The Hammett acidity function (H_o) is related to the degree of transformation of a weakly basic indicator B to its conjugate acid form BH^+ and defines Brønsted acid strength. It is important that this base is stronger than the indicator; n-butylamine (pKa   10) which is often used [110]. As the base is added it adsorbs on the acid sites and displaces the indicator from the solid acid, and as Hammett indicators exhibit distinctly different colours in the protonated and unprotonated forms, an end point can be determined. According to Hammett, the strength of a Brønsted surface site can be determined by the Hammett acidity function-

$$H_o = pK_{BH^+} - log\frac{[BH^+]}{[B]}$$

where B is the basic indicator molecule. A series of Hammett indicators covers the range of $-18 < H_o < 4$, where $H_o = -12$ corresponds to 100% H_2SO_4 [112]. As these titration and indicator methods can yield erroneous results, they are used less frequently. This method gives the sum of the amount of Brønsted and Lewis acid sites, and only if arylcarbinols are used as indicators Brønsted acid sites can be measured separately.

1.6.2 Vibrational spectroscopy methods

Both Raman and Infrared (IR) spectroscopy have been used to investigate the acidity of solid acids, with and without adsorbed probe molecules. IR is

especially useful as this identifies the hydroxyl groups present in solids through adsorbed probe molecules. **Mapes and Eischens** were the first to demonstrate the power and utility of IR studies of chemisorbed ammonia and provide direct experimental evidence for the existence of Lewis and Brønsted acidity on surfaces. In principle, the concentration of hydroxyl groups and therefore the concentration of potential Brønsted acid sites can be determined from the corresponding IR bands [110]. An important feature is that distinct bands occur for pyridine at Lewis acid and Brønsted acid sites in the region 1400 – 1700 cm^{-1} **(Table 1.2)** [113]. When IR is combined with temperature programmed desorption (TPD), it provides an estimate of the acid strength distribution profile. Parry pioneered the use of pyridine as probe molecule alike ammonia. A problem associated with use of pyridine is that owing to its strong basicity it adsorbs strongly so will not distinguish between strong and weak sites. Because of this, weaker bases such as carbon monoxide (CO) have also been used. It specifically interacts with hydroxyl acid groups via hydrogen bonding and with cationic Lewis acid sites. Recently, trichloromethane, acetylene and substituted acetylenes and even methane are proposed and successfully tested as acidic probe molecules. The interaction of pyridine molecules with Brønsted and Lewis acidic sites is also explained through **Figure 1.3**.

Laser Raman spectroscopy can also be used for detection of pyridine adsorption on Brønsted and Lewis sites. As Raman bands arise from polarizability changes which accompany skeletal and stretching vibrations, the protonation of pyridine is difficult to detect [110]. This means that it has low sensitivity towards measuring Brønsted acidity. Quinoline is a larger, more basic molecule than pyridine, which can distinguish between Brønsted and Lewis acidity simultaneously, and due to its large size has been used to measure the external number of acid sites in microporous acid materials [110].

Figure 1.3: **Interacrion of pyridine with Brønsted and Lewis acidic sites.**

Table 1.2: **IR bands for Brønsted and Lewis acidic sites characterized by pyridine adsorption.**

Hydrogen-bonded pyridine	Co-ordinately bonded pyridine	Pyridinium ion
1400-1447 (vs)*	1447-1460 (vs)	-
1485-1490 (w)	1488-1503 (v)	1485-1500 (vs)
		1540 (s)
1580-1600 (s)	1580 (v)	1620(s)
	1600-1633 (s)	1640

Band intensities: vs, very strong; s, strong; w, weak; v, variable.

1.6.3 *Nuclear Magnetic Resonance (NMR) methods*

NMR is a powerful technique, and advanced methods such as cross-polarization, magic angle spinning (MAS) of solids, high resolution magnetic resonance etc. have increased the capabilities of this technique to study the acidity of solid acid catalysts [110]. Total numbers of acid sites and strengths have been identified by using MAS NMR techniques. Solid-state ^{1}H magic-angle spinning (MAS) NMR spectroscopy measures proton chemical shifts, which are thought to reflect the deprotonation energies of surface OH groups [112]. Dissociative chemisorption of CH_3I has proposed for characterization of surface basicity by ^{13}C NMR spectroscopy. The number and strength of OH acidic groups can be directly determined by ^{13}C shifts of the adsorbed molecules. ^{31}P NMR has also been used to study trimethylphosphine oxide on solid acids [114] whose mechanism is shown in **Scheme 1.35**.
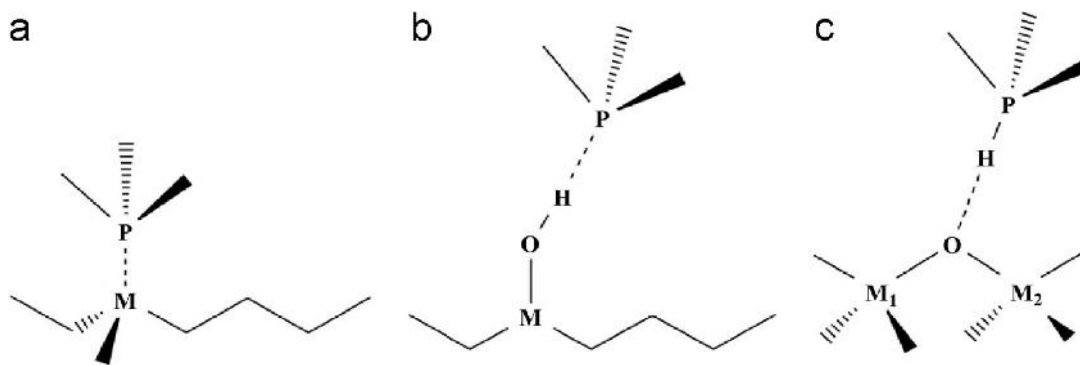
Scheme 1.35: **TMP adsorption: (a) chemisorbed on Lewis acid centers, (b) physisorbed on hydroxyls (weak H-bonding interaction), and (c) chemisorbed on Brønsted acid sites.**

1.6.4 Photoelectron Spectroscopy methods

Photoelectron spectroscopy methods such as X-Ray Photoelectron Spectroscopy (XPS) measure the kinetic energy of photoelectrons emitted from the core of surface atoms upon X-ray irradiation of the uppermost atomic layers of a solid. Therefore they can be used to characterize surface acid sites again through the use of basic probe molecules [110]. It is especially useful for monitoring the acidity of solid acids which are opaque to IR irradiations. Problems with this technique are that due to contamination and charging it is very difficult to obtain accurate measurements and moreover, it cannot be used to determine total acidity of microporous solid acids.

1.6.5 UV-Visible Spectroscopy

UV-visible spectroscopy was first used in the characterization of the strengths of solid acids by **Walling** [115]. In this method, indicator bases that change colour on protonation are used to probe the Brønsted acid characteristics of solid surfaces. Nevertheless, the difficulties in this approach have also been well documented, and it appears that most investigators who have examined the method in detail as a general approach for quantitative scaling of solid acids have suggested either significant experimental modifications, or have abandoned the UV-Vis analysis entirely.

1.6.6 Temperature-programmed desorption of base molecules

Temperature-programmed desorption is based on the adsorption of volatile amines such as pyridine, alkyl amines including n-butylamine, methylamine, ethylamine, n-propylamine etc. [115]. The principle behind this method is that the higher the temperature required to desorb the base, the stronger the acid site. An excess of base is added, and physically adsorbed base is removed by evacuation at 100-150°C. Whatever is left is chemically adsorbed and is used to measure the total number of acid sites. Acidity values are determined by desorbing the pre-adsorbed base by heating the sample at a controlled constant rate and measuring the concentration of probes desorbing as a function of temperature. Limitations of this technique include the restriction to certain basic probe compounds. Use of ammonia may be misleading as it can dissociate to give NH^{2-} and H^+ especially at high temperatures, so can be adsorbed onto both acidic and basic sites. Thus, amines have been recommended as more appropriate adsorbates.

1.6.7 Microcalorimetric methods

Base adsorption microcalorimetry allows an insight into both the overall heats of adsorption and any distribution of values of the heat exhibited by a solid acid, and this has been taken as an indicative way of characterizing the surface of acid catalysts. The variation of the differential heats of adsorption as a function of coverage is an indication of the homogeneity or heterogeneity of the adsorption sites, and has been achieved by measuring differential heats of adsorption vs. gas uptake using a basic probe molecule such as ammonia with high accuracy by heat-flow calorimetry and differential scanning calorimetry [112]. The amount of probe gas is usually determined by gravimetry or more commonly by volumetric glassware attached to the calorimeter cell [110]. Calorimetric methods can be considered to give a measure of the total acidity or basicity as it do not discriminate between Lewis and Brønsted sites. In particular, differential heats of adsorption can distinguish between sites of different strength, hence providing a measure of the number of energetically different sites as well as a thermodynamic measure of their acidity.

1.7 Fly ash supported solid acid catalysts

Fly ash (FA) is a predominantly inorganic residue obtained from the flue gases of high temperature furnaces at pulverized coal thermal power plants. It is a most commonly used cementitious or artificial pozzolanic material. According to the **American Society for Testing Materials (ASTM C618)** [116], the ash normally produced from bituminous coals containing more than 70 wt% SiO_2, Al_2O_3, Fe_2O_3 and being low in lime is defined as **Class F**, while those produced from lignite or sub-bituminous coal possessing SiO_2, Al_2O_3, Fe_2O_3 content between 50 and 70 wt% and high in lime are defined as **Class C**. In our work, we have focussed on **Class F fly ash** from a pulverized power plant. The conventional application areas of fly ash utilization includes, geo-polymer formation, zeolite synthesis, cement industries, adsorption of dyes and heavy metals, waste water treatment, agriculture etc. [117–121].

FA cenospheres supported CuO-BiVO₄ prepared by modified metal-organic decomposition (MOD) method is used for photocatalytic activity for methylene blue degradation [122]. **FA impregnated with iron nitrate** used as a substrate to produce industrial grade multiwalled carbon naotubes (MWNTs). **TiO₂ nanoparticles in situ coated on FA** have been utilized for water vapor adsorption, decolourization and degradation of methyl orange under UV irradiations [123]. **FA modified with CuBr₂, CuCl₂ and FeCl₃** are promising materials for mercury adsorption and can be a potential alternative to activated carbon [124]. **Raw and modified coal FA** effectively adsorb Cu^{+2} ions from waste water [125]. FA has been used for adsorption of NO_x, SO_x, organic compounds and mercury in air and cations, anions, dyes and other organic matters in water [116]. **Nitric acid activated FA** act as heterogeneous Fenton-like catalyst for p-nitrophenol removal from water [126]. **FA catalysts activated with microwave irradiations** have been applied in efficient and rapid synthesis of an array of naphthyl-substituted cyclohexanone, carboxylates, indazolonols and nitrohydrazones in dry medium [127]. **Ru-based FA catalysts** are employed for H_2 generation from NH_3 decomposition [128]. The results revealed that the surface area of FA could be enhanced and thus improved the dispersion of Ru particles, resulting in higher catalytic activity. **Acid treated FA** having Brønsted

acidic sites act as low cost, effective and stable catalyst, highly suited for DME production by dehydration reaction of methanol under vapor phase conditions [129] as shown in **Scheme 1.36**.
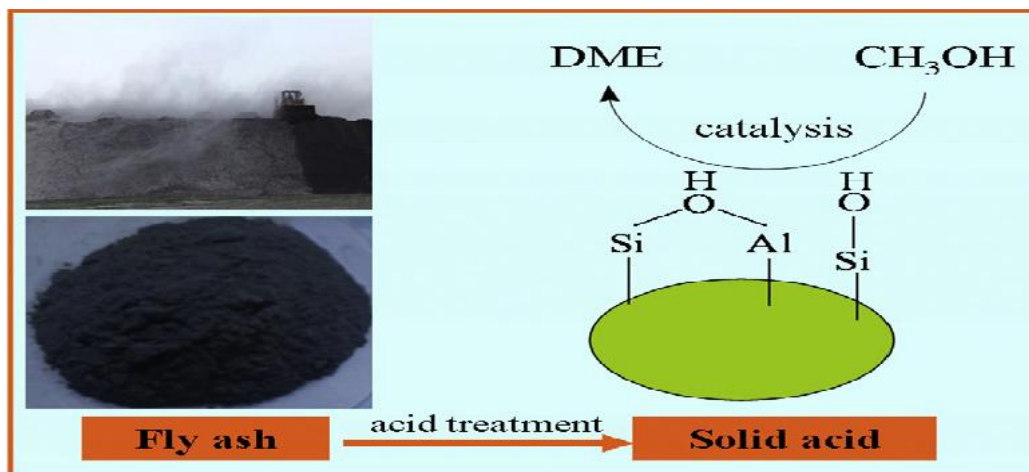
Scheme 1.36: Dehydration of methanol over acid activated FA.

Catalytic activity of **cobalt-FA catalysts** are tested in oxone activation for phenol degradation during waste water treatment [130]. Some 2E aryl chalcones have been synthesized using greener catalyst **Fly ash: H$_2$SO$_4$** assisted solvent-free environmentally benign crossed Aldol reaction [131] as shown in **Scheme 1.37**.
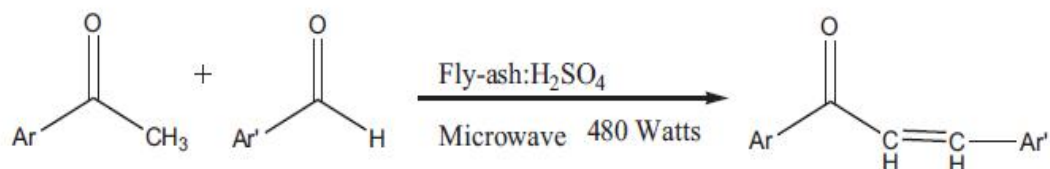
Scheme 1.37: Synthesis of chalcones over Fly ash:H$_2$SO$_4$ catalyst.

Green catalyst **Fly ash:PTS**, formed by mixing of appropriate quantity of FA and p-toluene sulfonic acid possess vigorous catalytic activity for microwave assisted aldol condensation of methyl ketones and substituted aldehydes [132] as shown in **Scheme 1.38**.
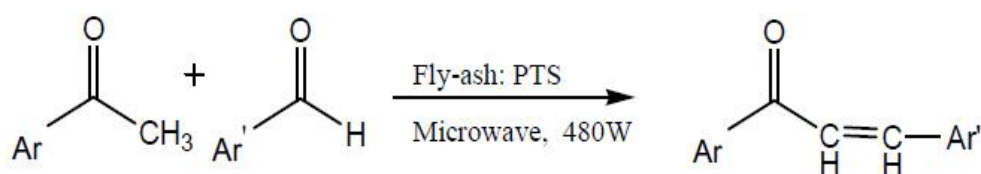
Scheme 1.38: Synthesis of aryl chalcones by arl methyl ketones and benzaldehyde over Fly ash:PTS catalyst.

FA has also been used as a solid support for microwave assisted solvent-free O-alkylation and acylation of thymol and geraniol [133]. A series of 6-substituted 2-naphthacyl esters have been synthesized by greener synthetic method using **Fly ash: water** catalyzed aqueous phase reactions [134] as shown in **Scheme 1.39**.

Scheme 1.39: Synthesis of esters over FA:water catalyst.

Coal FA has been used as a support material for nickel in the application of CO_2 methane reforming [135]. The catalytic role of activated FA for different reactions such as oxidation, oxychlorination and hydrogenolysis [136,137] is well documented in the literature. Recently FA has been used for developing several solid acid catalysts by loading various acids, super acids etc. **FA supported scandium triflate** has been utilized for catalyzing Friedel-Crafts acylation of 2-methoxy naphthalene by acetic anhydride to give 2-acetyl-6-methoxynaphthanlene [138]. The proposed model structure of FA supported scandium triflate is shown in **Scheme 1.40**.

Scheme 1.40: The proposed model structure of FA supported scandium triflate catalyst showing Lewis and Brønsted acidic sites.

Sulfated zirconia/FA (SZF-12) catalyst has been developed for catalyzing liquid phase benzylation of benzene and toluene with benzyl chloride to produce diphenylmethane and p-benzyl toluene [139] as shown in **Scheme 1.41**.
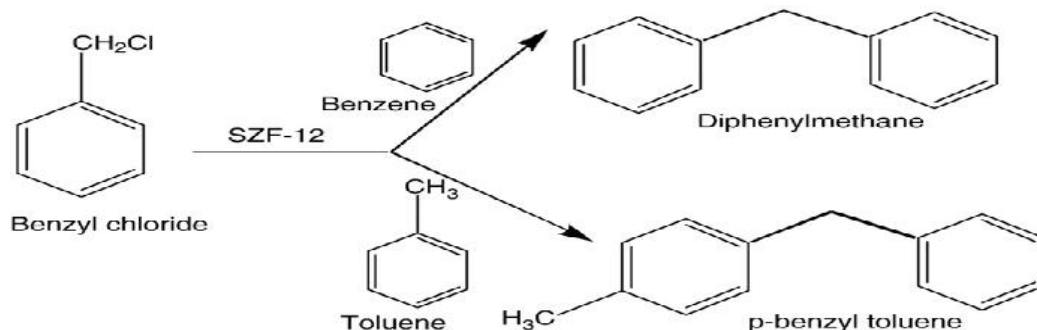
Scheme 1.41: Benzylation of benzene and toluene with benzyl chloride over SZF-12 catalyst.

Cerium triflate/FA catalyst (CFT) has been used for the synthesis of 3, 4-dimethoxyacetophenone (anti neoplastic) by Friedel-Crafts acylation of veratrole [140] as shown in **Scheme 1.42**.
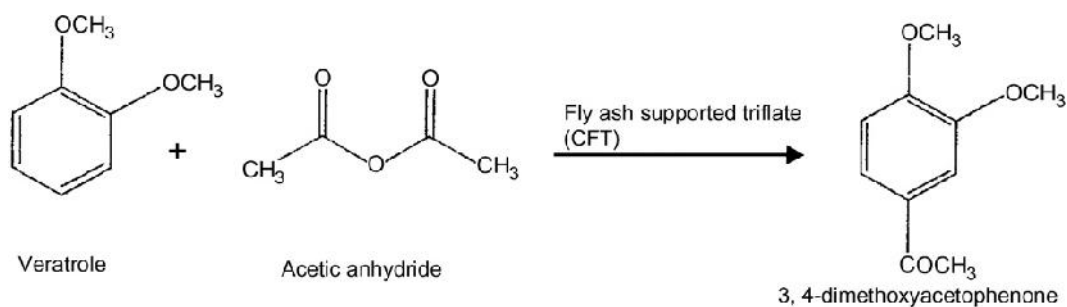
Scheme 1.42: Acylation of veratrole with acetic anhydride over CFT.

FA supported concentrated sulphuric acid, hydrochloric acid, perchloric acid has been synthesized by refluxing and used as solid acid catalyst for the synthesis of aspirin **(Scheme 1.43)**, oil of wintergreen, a series of acetates, important chemical intermediates [141]. The attractive features of these procedures are the mild reaction conditions, high conversions, operational simplicity, regeneration and reuse of the catalyst.
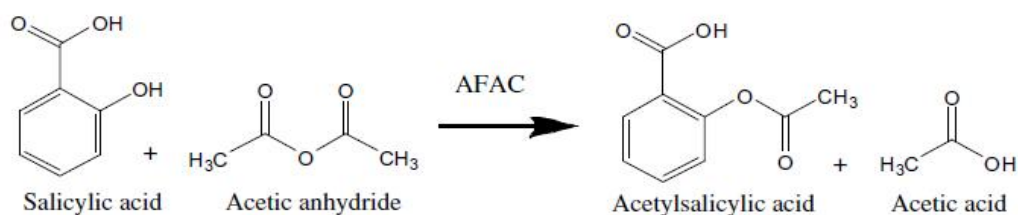
Scheme 1.43: Esterification of salicylic acid with acetic anhydride to acetylsalicylic acid (aspirin) by AFAC.

1.8 Perlite as catalyst support

Perlite is a glassy, amorphous, hydrated volcanic ryholitic rock. Most of perlite has produced from flows associated with thick accumulations of tuffs and lava flows, and from domes. The perlite is a natural, vitreous substance that contains 2–6% water [142] and is easily accessible in the most parts of the world. It exists in gray, silver gray, dark brown and black colours. The density of the perlite decreases as its volume increases, and it can be described as a lightweight material. Total worldwide annual production of perlite is 700 million tons [143] while in Turkey, 8 billion tons of perlite exist, corresponding to 70% of the total world reserves [144]. In this work, **Turkish Perlite** has been employed. The types of perlite found in Turkey are - **Granular Perlite, Pumicite Perlite, Concentric Structured Perlite, Devitrified Perlite, Phenicrystalline Perlite and Sandy Perlite**. Its average chemical composition is approximately 75% SiO_2 with oxides of Al_2O_3 (14.8%), K_2O (4.8%), Na_2O (2.9%), CaO (0.9%), MgO (0.1%), Fe_2O_3 (1.5%), and water (4.0%) [145]. Perlite can be unusually expanded up to 10–20 times of its original volume when heated rapidly at 850–1150°C [146] in a manner similar to popcorn, due to the large volume change of trapped water during its liquid–vapour phase transition in the softened structure [147]. The resulting expanded perlite (EP) particles are spherical in shape, usually fluffy, highly porous due to a foam-like cellular internal structure. Perlite is generally chemically inert and has a pH of approximately 7 [148]. The silicon atoms at the surface tend to maintain their tetrahedral coordination with oxygen. They complete their coordination at room temperature by attachment to monovalent hydroxyl groups, forming different types of silanol groups [149] as shown in **Figure 1.4**. However, silanol groups form on the perlite surface provide various adsorption properties.

Hydroxyl or silanol groups   Silanediol groups   Silanetriol groups
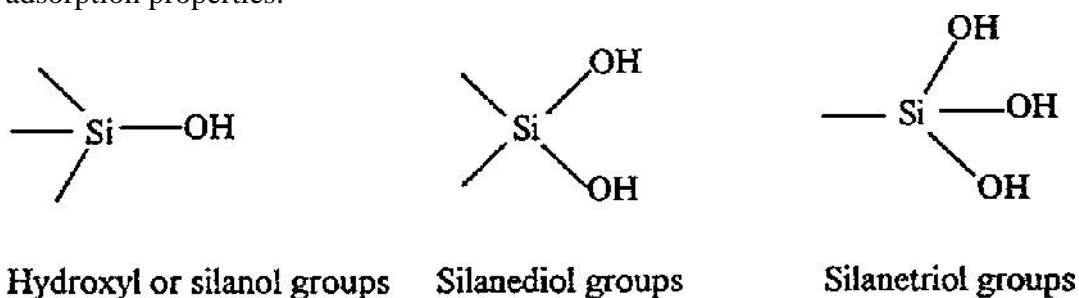
Figure 1.4:   Types of silanol groups on perlite surface.

Most expanded perlite used by industry is in fillers, concrete and plasters, roof insulation board, pipe insulation, refrigerator insulation, acoustical ceiling tiles, filtration aids, oil absorbents, horticultural applications, animal feedstuff, and crop farming [142,150–155]. The advantage of perlite is that this micro porous and chemically inert silica support except than other benefits is more inexpensive than the other supports. This could make it a viable candidate as an economical adsorbent as well as good catalyst support. **TiO$_2$ immobilized on perlite granules** can be utilized in photocatalytical degradation of ammonia, photo-catalytic decomposition of phenol, photocatalytic activity in NO oxidation [145,156,157]. In the literature, adsorption of various dyes such as methylene blue, victoria blue and methyl violet, oil, metal ions such as Cu(II) and Cd(II), onto perlite samples have been investigated [150,158]. Perlite is essentially a metastable amorphous aluminum silicate, and has recently been used as an aflatoxin binder and adsorbent for controlling of wet litter and also decrease level of chloride in blood serum [159]. Perlite due to its unique characteristic from the processing point of view, enables it to get wetted with the polluted solution and simultaneously be exposed to the radiation source when coated with the photocatalyst makes it an ideal support for the immobilization of photocatalysts [160]. Photocatalytic activity of the **In–TiO$_2$/perlite materials** has been evaluated by the decomposition of ethylbenzene in moist air [161]. A composite material, prepared by crosslinking perlite with polyacrylamide (PAAm) and named as **P(AAm–EP)**, appeared to have much improved adsorptive features [162]. The feasibility of preparing **nickel boride catalyst supporting on perlite** and its catalytic aptitude for potential use in industrial processes has also been evaluated [163]. Catalytic pyrolysis of tire waste using expanded perlite as an additive material has also studied [164]. Novel composite adsorbents for As(V) removal from aqueous solution are synthesized by successfully incorporating **MnO$_2$ nanorods and Fe$_2$O$_3$ nanoparticles onto ball-milled expanded perlite** carrier material [165]. **Silver coated perlite** produced through spray pyrolysis technique has been utilized for studying ozone decomposition [166]. The potential use of expanded perlite, a metastable amorphous hydrated aluminum silicate, as a permanent medium for the long-term confinement of caesium has been reported.

This simple method seems to be a good way to permanently confine caesium discharged from recycled nuclear waste [167]. The conversion of perlite to zeolitic materials and geolpolymers [168] under humid atmosphere and low to medium temperatures (75–250°C) has been reported [169] and hence revealed a novel way in enhancing the commercial value of the mineral. Various types of zeolites have been synthesized from perlite, for example, ZSM-5, epistilbite, gismondine, heulandite, tobermorite, zeolite-Pc, zeolite-V, zeolite-A, phillipsite, analcime, Na-P1, sodalite octahydrate and faujasite [170–173] having widespread applications in FCC naphtha aromatization, FCC gasoline aromatization etc.

1.9   Scope of the work

The present thesis proposed the modification of properties of fly ash and perlite through appropriate activation techniques in order to convert them into potential solid acid catalysts having similar catalytic activity as other commercial supported solid acid catalysts. The solid acid catalysts reported in this work are synthesized by loading of metal oxides, super acids as well as various mineral acids on fly ash and perlite through adopting various methodologies viz. precipitation, sol-gel, refluxing, incipient wetness impregnation etc. The prepared catalysts from fly ash and perlite are characterized by different analytical techniques like N_2 adsorption-desorption, XRD, FT-IR, Pyridine adsorbed FT-IR, SEM, SEM-EDX, TEM, TGA, UV-Vis DRS, NMR to evaluate their physico-chemical properties. Adequate physico-chemical characterization of perlite is lacking and little systematic work has been carried out on the compositional analysis, chemical and physical nature of this material. The catalytic activity of as prepared catalysts has been tested by industrially important acid catalyzed reactions such as condensation, Friedel- Craft acylation, esterification, benzoylation etc. via conventional and microwave assisted methods. The foremost advantages of using microwave technique in this work are the very short time periods involved in the synthesis, higher yields of products, enhanced reaction kinetics and simplification of many reactions. All the prepared catalysts are found to be recyclable up to many reaction cycles with analogous efficiency through simple thermal activation suggesting that the prepared catalysts could not get

deactivated during reactions. While extensive studies have been made on the adsorption and other applications of perlite and fly ash, limited information is available with regard to their use in catalysis. This catalytic study also explores the wide applications of fly ash and perlite as solid acid catalysts in pharmaceutical, petrochemical, fine chemical industries etc. To the best of our knowledge, there has been no report related to the solid acid catalytic activity of expanded perlite until now. Our research work is important as it has developed novel type of solid acid catalysts from waste materials, fly ash and perlite to catalyze many industrially important organic transformations, thus recommends an innovative pathway to utilize huge reserves of such solid wastes and finds possibilities of their valorization. This work is aimed to act as a stepping-stone for the prospective researchers into the rewarding field of utilization of waste materials.

1.10 References

[1]   R.J.F. C.H. Bartholomew, Fundamentals of Industrial Catalytic Processes, 2005.

[2]   N.R. Shiju, V. V Guliants, Appl. Catal. A Gen. 356 (2009) 1.

[3]   S. Sahebdelfar, M. Kazemeini, F. Khorasheh, A. Badakhshan, Chem. Eng. Sci. 57 (2002) 3611.

[4]   A. Alsalme, E.F. Kozhevnikova, I. V Kozhevnikov, "Applied Catal. A, Gen. 390 (2010) 219.

[5]   N. Khan Abedin, D. Mishra Kumar, I. Ahmed, J. YoonWoong, J. Hwang, S. Jhung Hwa, "Applied Catal. A, Gen. 452 (2013) 34.

[6]   S. Bhagat, R. Sharma, A.K. Chakraborti, J. Mol. Catal. A Chem. 260 (2006) 235.

[7]   I. Fatimah, K. Wijaya, K.H. Setyawan, Bull. Chem. React. Engg. Catal. 3 (2008) 9.

[8]   M. Zhu, Catal. Letters 144 (2014) 1568.

[9]   W. Yu, M. Wen, G.Y. Zhao, L. Yang, Z.L. Liu, Chinese Chem. Lett. 17 (2006) 15.

[10]   M.C. Avila, N.A. Comelli, N.H. Firpo, E.N. Ponzi, M.I. Ponzi, J. Chil. Chem. Soc. 53 (2008) 1449.

[11]   C. Nicolaides, M.S. Scurell, P.M. Semano, Appl. Catal. A Gen. 245 (2003) 43.

[12]   M.A. Ali, T. Kimura, Y. Suzuki, M.A. Al-saleh, H. Hamid, T. Inui, Appl. Catal. A Gen. 277 (2002) 63.

[13]   D. Chen, Z. Xue, Z. Su, J. Mol. Catal. A Chem. 203 (2003) 307.

[14]   A. Patel, V. Brahmkhatri, Fuel Process. Technol. 113 (2013) 141.

[15]   Y. Liu, E. Lotero, J. Goodwinjr, J. Catal. 242 (2006) 278.

[16]   N. Al-arafi, J. Salimon, E-Journal Chem. 9 (2012) 99.

[17]   E.F. Aransiola, M.O. Daramola, T.V. Ojumu, B.O. Solomon, S.K. Layokun, Mod. Res. Catal. 2 (2013) 83.

[18]   H.R. Darabi, K. Aghapoor, F. Mohsenzadeh, M.R. Jalali, S. Talebian, L. Ebadi-Nia, E. Khatamifar, A. Aghaee, Bull. Korean Chem. Soc. 32 (2011) 213.

[19]   J. Lilja, D.Y. Murzin, T. Salmi, J. Aumo, P. Mäki-arvela, M. Sundell, J. Mol. Catal. A Chem. 182-183 (2002) 555.

[20]   A. Barbarini, R. Maggi, A. Mazzacani, G. Mori, Tetrahedron Lett. 44 (2003) 2931.

[21]   R. Ronnback, T. Salmi, A. Vuori, H.H. Juha, A. Sundqvist, E. Tirronen, Chem. Eng. Sci. 52 (1997) 3369.

[22]   C.M.A. Parlett, K. Wilson, A.F. Lee, Chem. Soc. Rev. 42 (2013) 3876.

[23]   H. Juntgen, Fuel 65 (1986) 1436.

[24]   A.T. Khan, L.H. Choudhury, S. Ghosh, J. Mol. Catal. A Chem. 255 (2006) 230.

[25]   X. Chen, M. Zhang, K. Yang, W.T. Christopher, C. Liang, Catal. Letters 144 (2014) 1118.

[26]   L. Zhong, J. Feng, F.-L. Qiu, J. Nat. Gas Chem. 6 (1997) 322.

[27]   R. Maggi, G. Martra, C. Giancarlo, G. Alberto, G. Sartori, J. Catal. 294 (2012) 19.

[28] K. Niknam, D. Saberi, M. Baghernejad, Chinese Chem. Lett. 20 (2009) 1444.

[29] H.R. Shaterian, H. Yarahmadi, M. Ghashang, Tetrahedron 64 (2008) 1263.

[30] J.S. Yadav, B.V.S. Reddy, A.S. Reddy, J. Mol. Catal. A Chem. 280 (2008) 219.

[31] K.P. Boroujeni, Chinese Chem. Lett. 21 (2010) 1395.

[32] M.K. Yadav, A.V. Kothari, D.G. Naik, V.K. Gupta, Green Chem. Lett. Rev. 2 (2009) 181.

[33] H. Emtiazi, M.A. Amrollahi, B. Bi, F. Mirjalili, Arab. J. Chem. (2013) 6.

[34]   a. G. Boudjahem, S. Monteverdi, M. Mercy, M.M. Bettahar, J. Catal. 221 (2004) 325.

[35] J. Zhang, Z. Zhu, C. Li, L. Wen, E. Min, J. Mol. Catal. A Chem. 198 (2003) 359.

[36] F.F. Bamoharram, M.M. Heravi, J. Ebrahimi, A. Ahmadpour, M. Zebarjad, Chinese J. Catal. 32 (2011) 782.

[37] M.R. Saidi, Y. Pourshojaei, F. Aryanasab, Synth. Commun. (2009) 1109.

[38] B. Sadeghi, B.F. Mirjalili, M.M. Hashemi, J. Iran. Chem. Soc. 5 (2008) 694.

[39] S.N. Rashkeev, K. Sohlberg, M. V Glazoff, J. Novak, S.J. Pennycook, S.T. Pantelides, Phys. Rev. 67 (2003) 1.

[40] M. Abdollahi-alibeik, Z. Zaghaghi, I. Mohammadpoor-baltork, J. Chinese Chem. Soc. 55 (2008) 1.

[41] R. Savidha, A. Pandurangan, M. Palanichamy, V. Murugesan, J. Mol. Catal. A Chem. 211 (2004) 165.

[42] K.U. Nandhini, B. Arabindoo, M. Palanichamy, V. Murugesan, J. Mol. Catal. A Chem. 243 (2006) 183.

[43] H.R. Shaterian, K. Azizi, N. Fahimi, Arab. J. Chem. (2012).

[44] T. Kitano, S. Okazaki, T. Shishido, K. Teramura, T. Tanaka, "Journal Mol. Catal. A, Chem. 371 (2013) 21.

[45] E. Liu, A.J. Locke, R.L. Frost, W.N. Martens, "Journal Mol. Catal. A, Chem. 353-354 (2012) 95.

[46] N. Bhatt, A. Patel, J. Taiwan Inst. Chem. Eng. 42 (2011) 356.

[47] A. H.I., A. F.A., Adv. Nat. Appl. Sci. 4 (2010) 293.

[48] O.K. Austin, Commercial Manufacture of Carbon Black in Reinforcement of Elastomers, 1987.

[49] S. Pradhan, Production and Characterization of Activated Carbon Produced from a Suitable Industrial Sludge Department of Chemical Engineering, 2011.

[50] X. Liu, M. Huang, H. Ma, Z. Zhang, J. Gao, Y. Zhu, X. Han, X. Guo, Molecules 15 (2010) 7188.

[51] A. Davoodnia, A. Tavakoli-nishaburi, N. Tavakoli-hoseini, Bull. Korean Chem. Soc. 32 (2011) 10.

[52] M.E. Chimienti, L.R. Pizzio, C. V Cáceres, M.N. Blanco, Appl. Catal. A Gen. 208 (2001) 7.

[53] A. Shokrolahi, A. Zali, H.R. Pouretedal, Iran. J. Catal. 1 (2011) 37.

[54] S. Kang, J. Ye, J. Chang, Int. Rev. Chem. Eng. 5 (2013) 133.

[55] T. Liu, Z. Li, W. Li, C. Shi, Y. Wang, Bioresour. Technol. 133 (2013) 618.

[56] B. Sreedhar, V. Bhaskar, C. Sridhar, T. Srinivas, L. Kótai, K. Szentmihályi, J. Mol. Catal. A Chem. 191 (2003) 141.

[57] V. Mirkhani, M. Moghadam, S. Tangestaninejad, M. Mahdavi, J. Iran. Chem. Soc. 8 (2011) 608.

[58] M.T. Gokmen, F.E. Du Prez, Prog. Polym. Sci. 37 (2012) 365.

[59] L.-T. An, J.-P. Zou, L.-L. Zhang, Catal. Commun. 9 (2008) 349.

[60] V.M. Fuchs, L.R. Pizzio, N.B. Mirta, Sci. Bases Prep. Heterog. Catal. (2006) 793.

[61] Y. Leng, P. Jiang, J. Wang, CATCOM 25 (2012) 41.

[62] H.-J. Yoon, S.-M. Lee, J.-H. Kim, H.-J. Cho, J.-W. Choi, S.-H. Lee, Y.-S. Lee, Tetrahedron Lett. 49 (2008) 3165.

[63] W.Y.L. In Kyu Songa, Appl. Catal. A Gen. 256 (2003) 77.

[64] E. Guibal, Prog. Polym. Sci. 30 (2005) 71.

[65]   A. Chakrabarti, M.M. Sharma, React. Polym. 20 (1993) 1.

[66]   E. Sert, A.D. Buluklu, S. Karakus, F.S. Atalay, Chem. Eng. Process. Process Intensif. 73 (2013) 23.

[67]   J.K. and J.B. G. A. Olah, J. Org 42 (1977) 4187.

[68]   R.M. and S.C.N. G. A. Olah, Synthesis (Stuttg). (1978) 672.

[69]   M. de M.P. Maria Sol Marques da Silva, Claudia Lucas da Costa, E.R. Lachte, React. Polym. 25 (1995) 55.

[70]   R. Pal, T. Sarkar, S. Khasnobis, ARKIVOC 1 (2012) 570.

[71]   S.H. Ali, A. Tarakmah, S.Q. Merchant, T. Al-sahhaf, Chem. Eng. Sci. 62 (2007) 3197.

[72]   I. Fechete, Y. Wang, J.C. Védrine, Catal. Today 189 (2012) 2.

[73]   A.M.G. Pedrosa, M.J.B. Souza, A.O.S. Silva, D.M.A. Melo, A.S. Araujo, Catal. Commun. 7 (2006) 791.

[74]   D. Das, S. Cheng, Appl. Catal. A Gen. 201 (2000) 159.

[75]   J. Bedard, H. Chiang, A. Bhan, J. Catal. 290 (2012) 210.

[76]   P. Moreau, A. Finiels, P. Meric, J. Mol. Catal. A Chem. 154 (2000) 185.

[77]   V. Siva, P. Ganjala, C. Krishna, P. Neeli, C.V. Promod, M. Khagga, K. Seetha, R. Rao, D.R. Burri, CATCOM In Press (2014).

[78]   V.D. Chaube, Catal. Commun. 5 (2004) 321.

[79]   B. Jacob, S. Sugunan, A.P. Singh, J. Mol. Catal. A Chem. 139 (1999) 43.

[80]   T. Radhika, S. Sugunan, J. Mol. Catal. A Chem. 250 (2006) 169.

[81]   C. Siriluk, S. Yuttapong, in:, 8th Asian Symp. Vis., 2005, pp. 23–27.

[82]   F. Adam, R. Thankappan, Chem. Eng. J. 160 (2010) 249.

[83]   F. Adam, A.E. Ahmed, Chem. Eng. J. 145 (2008) 328.

[84]   F. Chang, M. Kuo, M. Tsay, M. Hsieh, Appl. Catal. A Gen. 247 (2003) 309.

[85]   A.E. Ahmed, F. Adam, Microporous Mesoporous Mater. 118 (2009) 35.

[86] F. Adam, K. Mohammed, M. Ramadan, B. Aisha, J. Taiwan Inst. Chem. Eng. 42 (2011) 843.

[87] F. Adam, J. Andas, J. Colloid Interface Sci. 311 (2007) 135.

[88] F. Adam, K. Mohammed, T. Hussein, "Applied Catal. A, Gen. 399 (2011) 42.

[89] J.N. Appaturi, F. Adam, Z. Khanam, Microporous Mesoporous Mater. 156 (2012) 16.

[90] F. Shirini, S. Akbari-dadamahaleh, A. Mohammad-khah, "Journal Mol. Catal. A, Chem. 363-364 (2012) 10.

[91] G. Nagendrappa, Appl. Clay Sci. 53 (2011) 106.

[92] V.R. Choudhary, R. Jha, P.A. Choudhari, J. Chem. Sci. 117 (2005) 635.

[93] S. Mallakpour, Z. Rafiee, Iran. Polym. J. 17 (2008) 907.

[94] M. Gopalakrishnan, P. Sureshkumar, V. Kanagarajan, J. Thanusu, ARKIVOC 2006 (2006) 130.

[95] A. Khoramabadi-zad, H. Veisi, S. Akbari, A. Shiri, J. Chinese Chem. Soc. 54 (2007) 479.

[96] B. Tyagi, M.K. Mishra, R. V Jasra, J. Mol. Catal. A Chem. 286 (2008) 41.

[97] D. Borkin, E. Morzhina, S. Datta, A. Rudnitskaya, A. Sood, T. Marianna, Org. Biomol. Chem. 9 (2011) 1394.

[98] E. Westphal, L.H. Viana, R.G. Jacob, G. Perin, E.J. Lenarda, M.G.M.D. Oca, Fuel 87 (2008) 2838.

[99] W. Liu, P. Yin, X. Liu, W. Chen, H. Chen, C. Liu, R. Qu, Q. Xu, Energy Convers. Manag. 76 (2013) 1009.

[100] M.J. Gronnow, D.J. Macquarrie, J.H. Clark, P. Ravenscroft, J. Mol. Catal. A Chem. 231 (2005) 47.

[101] G. Bai, T. Li, Y. Yang, H. Zhang, X. Lan, F. Li, J. Han, Z. Ma, Q. Chen, G. Chen, CATCOM 29 (2012) 114.

[102] H. Yamashita, Y. Mitsukura, H. Kobashi, "Journal Mol. Catal. A, Chem. 327 (2010) 80.

[103] H. Yamashita, Y. Mitsukura, H. Kobashi, K. Hiroki, J. Sugiyama, K. Onishi, T. Sakamoto, "Applied Catal. A, Gen. 381 (2010) 145.

[104] H. Salehi, S. Kakaei, S.J. Ahmadi, M.A. Firooz Zareh, S.M. Sadat Kiai, H.R. Pakoyan, H. Tajik Ahmadi, J. Appl. Chem. Res. (2010).

[105] K. Rawal, M.K. Mishra, M. Dixit, M. Srinivasarao, J. Ind. Eng. Chem. 18 (2012) 1474.

[106] G. Winé, E. Vanhaecke, S. Ivanova, R. Ziessel, C. Pham-huu, Catal. Commun. 10 (2009) 477.

[107] A. Sinhamahapatra, N. Sutradhar, B. Roy, P. Pal, H.C. Bajaj, A.B. Panda, Appl. Catal. B Environ. 103 (2011) 378.

[108] J. Safari, S. Naseh, Z. Zarnegar, Z. Akbari, J. Taibah Univ. Sci. In Press (2014).

[109] R. Ghanbaripour, I. Mohammadpoor-baltork, M. Moghadam, A.R. Khosropour, S. Tangestaninejad, V. Mirkhani, Polyhedron 31 (2012) 721.

[110] C. Savill-Jowitt, Catalytic and Adsorbent Properties of Solid Acid Catalysts Studied by Ammonia Adsorption Microcalorimetry by Claire Savill-Jowitt M . Chem A Thesis Submitted to the University of Huddersfield in Partial Fulfilment of the Requirements for the Degree of Doc, 2007.

[111] H. Hattori, Chem. Rev. 95 (1995) 537.

[112] O. Deutschmann, H. Knozinger, K. Kochloefl, T. Turek, Heterogeneous Catalysis and Solid Catalysts, 2009.

[113] E.P. Parry, J. Catal. 2 (1963) 371.

[114] A. Zheng, S. Liu, F. Deng, Solid State Nucl. Magn. Reson. 55-56 (2013) 12.

[115] W.E. Farneth, R.J. Gorte, Chem. Rev. 95 (1995) 615.

[116] M. Ahmaruzzaman, Prog. Energy Combust. Sci. 36 (2010) 327.

[117] S.M. Shaheen, P.S. Hooda, C.D. Tsadilas, J. Environ. Manage. 145 (2014) 249.

[118] M. Visa, L. Isac, A. Duta, Appl. Surf. Sci. 258 (2012) 6345.

[119] O. Babajide, N. Musyoka, L. Petrik, F. Ameer, Catal. Today 190 (2012) 54.

[120] Y. Zhang, L. Liu, Particuology 11 (2013) 353.

[121] S. Wang, H. Wu, J. Hazard. Mater. 136 (2006) 482.

[122] J. Zhang, H. Cui, B. Wang, C. Li, J. Zhai, Q. Li, Chem. Eng. J. 223 (2013) 737.

[123] A.N. Ökte, D. Karamanis, D. Tuncel, Catal. Today In Press (2014) 1.

[124] W. Xu, H. Wang, T. Zhu, J. Kuang, P. Jing, J. Environ. Sci. 25 (2013) 393.

[125] T. Hsu, C. Yu, C. Yeh, Fuel 87 (2008) 1355.

[126] A. Zhang, N. Wang, J. Zhou, P. Jiang, G. Liu, J. Hazard. Mater. 201-202 (2012) 68.

[127] V. Kanagarajan, M.R. Ezhilarasi, J. Thanusu, M. Gopalakrishnan, Green Chem. Lett. Rev. (2011) 37.

[128] L. Li, S. Wang, Z. Zhu, X. Yao, Z. Yan, Fuel Process. Technol. 89 (2008) 1106.

[129] D. Zeng, S. Liu, W. Gong, J. Qiu, H. Chen, G. Wang, Fuel 119 (2014) 202.

[130] E. Saputra, S. Muhammad, H. Sun, H. Ming, M.O. Tadé, S. Wang, Catal. Today 190 (2012) 68.

[131] G. Thirunarayanan, P. Mayavel, K. Thirumurthy, Spectrochim. Acta Part A Mol. Biomol. Spectrosc. 91 (2012) 18.

[132] R. Sundararajan, R. Arulkumaran, D. Kamalakkannan, R. Suresh, K. Ranganathan, S.P. Sakthinathan, G. Vanangamudi, Int. J. Pharm. Chem. Sci. 1 (2012) 1657.

[133] D.H. More, D.G. Hundiwale, U.R. Kapadi, P.P. Mahulikar, J. Sci. Ind. Res. (India). 65 (2006) 817.

[134] G. Thirunarayanan, G. Vanangamudi, V. Sathiyendran, K. Ravi, Indian J. Chem. 50B (2011) 593.

[135] R.S. Blissett, N.A. Rowson, Fuel 97 (2012) 1.

[136] W. Jarmohamed, P. Mulder, Chemosphere 29 (1994) 1911.

[137] C. V Rode, R.B. Mane, A.S. Potdar, P.B. Patil, P.S. Niphadkar, P.N. Joshi, Catal. Today 190 (2012) 31.

[138] A. Rani, C. Khatri, R. Hada, Fuel Process. Technol. 116 (2013) 366.

[139] C. Khatri, M.K. Mishra, A. Rani, Fuel Process. Technol. 91 (2010) 1288.

[140] C. Khatri, D. Jain, A. Rani, Fuel 89 (2010) 3853.

[141] C. Khatri, A. Rani, Fuel 87 (2008) 2886.

[142] M. Gürtürk, H.F. Oztop, A. Hepbaslı, Energy Convers. Manag. 75 (2013) 488.

[143] S. Kabra, S. Katara, A. Rani, Int. J. Innov. Res. Sci. Eng. Technol. 2 (2013) 4319.

[144] M. Alkan, M. Karadas, M. Dogan, O. Demirbas, Colloids Surfaces A Physicochem. Eng. Asp. 259 (2005) 155.

[145] M. Giannouri, T. Kalampaliki, N. Todorova, T. Giannakopoulou, N. Boukos, D. Petrakis, T. Vaimakis, C. Trapalis, Int. J. Photoenergy 2013 (2013).

[146] A. Sarı, A. Karaipekli, C. Alkan, Chem. Eng. J. 155 (2009) 899.

[147] M. Taherishargh, I. V Belova, G.E. Murch, T. Fiedler, Mater. Sci. Eng. A 604 (2014) 127.

[148] S. Hasan, T.K. Ghosh, D.S. Viswanath, V.M. Boddu, J. Hazard. Mater. 152 (2008) 826.

[149] M. Dogan, M. Alkan, U. Cakir, J. Colloid Interface Sci. 118 (1997) 114.

[150] D. Bastani, a. a. Safekordi, a. Alihosseini, V. Taghikhani, Sep. Purif. Technol. 52 (2006) 295.

[151] M. Alkan, M. Do, J. Colloid Interface Sci. 243 (2001) 280.

[152] N. Zhang, Y. Yuan, Y. Yuan, T. Li, X. Cao, Energy Build. 82 (2014) 505.

[153] O. Sengul, S. Azizi, F. Karaosmanoglu, M. Ali, Energy Build. 43 (2011) 671.

[154] A. Silber, B.Y. B, S. Suryano, I. Levkovitch, Geoderma 170 (2012) 159.

[155] A.U.S. S.T. Erdogan, Cem. Concr. Compos. 38 (2013) 29.

[156] S.N. Hosseini, S.M. Borghei, M. Vossoughi, N. Taghavinia, Appl. Catal. B Environ. 74 (2007) 53.

[157] Y. Shavisi, S. Sharifnia, S.N. Hosseini, M.A. Khadivi, J. Ind. Eng. Chem. 20 (2014) 278.

[158] M. Alkan, M. Karadas, M. Dogan, O. Demirbas, J. Colloid Interface Sci. 291 (2005) 309.

[159] J.G. Ghalehkandi, H. Karamouz, N.M. Sis, Int. J. Anim. Vet. Adv. 3 (2011) 305.

[160] S.N. Hosseini, M. Borghei, M. Vossoughi, N. Taghavinia, in:, 3rd IASME/WSEAS Int. Conf. Energy Environ. Univ. Cambridge, UK, 2008, pp. 46–50.

[161] M. Hinojosa-reyes, S. Arriaga, L.A. Diaz-torres, V. Rodríguez-gonzález, Chem. Eng. J. 224 (2013) 106.

[162] R. Akkaya, Desalination 321 (2013) 3.

[163] D. Acosta, J. Martinez, C. Carrera, E. Erdmann, E. Gonzo, H. Destéfanis, Lat. Am. Appl. Res. 320 (2006) 317.

[164] Y. Kar, Waste Manag. 31 (2011) 1772.

[165] D.N. Thanh, M. Singh, P. Ulbrich, N. Strnadova, Sep. Purif. Technol. 82 (2011) 93.

[166] K. Genov, V. Georgiev, T. Batakliev, D.K. Sarker, World Acad. Sci. Eng. Technol. 80 (2011) 202.

[167] J. Rehspringer, J. Balencie, S. Vilminot, D. Burger, A. Boos, C. Estourn, J. Eur. Ceram. Soc. 27 (2007) 619.

[168] E.R. Vance, D.S. Perera, P. Imperia, D.J. Cassidy, J. Davis, J.T. Gourley, J. Aust. Ceram. Soc. 45 (2009) 44.

[169] P. Wang, B. Shen, J. Gao, Catal. Today 125 (2007) 155.

[170] P. Kongkachuichay, P. Kim-lohsoontorn, Sci. Asia 32 (2006) 13.

[171] A. Rujiwatra, Mater. Lett. 58 (2015) 2012.

[172] V. Psycharis, V. Perdikatsis, G. Christidis, Bull. Geol. Soc. Greeceeological Soc. Greece 36 (2004) 121.

[173] P. Wang, B. Shen, D. Shen, T. Peng, J. Gao, Catal. Commun. 8 (2007) 1452.

Extraction and Quantification of Silica from Perlite by Precipitation Using Four Different Mineral Acids

Abstract

The procedure of extraction of silica through precipitation from an innovative, naturally abundant silica enriched source- perlite has been discussed. Different extraction methodologies adopted in previous reports, their drawbacks, applications of commercial silica are reported here. Perlite formation, characterization by different analytical techniques is also included in this chapter. Structure, morphology, chemical bonding of extracted silica is discussed on the basis of results obtained from different characterization techniques. The results depict that the precipitated silica possesses higher surface area, spherical shape and its maximum yield can be achieved under optimized synthesis conditions. Effects of various acids and other extraction parameters on yield%, morphology, surface area of extracted silica are also illustrated here. In addition, comparable FT-IR and XRD results of the extracted silica with that of commercial silica gel indicate the superior quality of silica extracted by the optimized procedure. The study suggests a lesser energy consuming, eco-friendly path for production of highly pure amorphous silica from perlite. The chemicals used in this process can be recycled and reused, making the whole procedure environmentally benign, efficient, cost effective and thus finds a novel route to utilize huge reserves of natural waste- perlite. Development of economically viable processes for getting precipitated silica with specific properties assumes importance at this juncture.

2.1   Introduction

Silica or SiO_2 is one of the valuable inorganic multipurpose chemical compounds. It is the second most abundant material on earth's crust and accounts for approximately 32% of total weight of the earth crust [1]. Silica is a polymer of silicic acid comprising of interlinked tetrahedral SiO_4 units with general formula, SiO_2. Naturally, silica is found in form of sand, glass, quartz etc. and exists in gel, crystalline and amorphous forms. Silica gel can be classified into three different types, depending on process of preparation, namely, aquagel (water filled pores), xerogel (aqueous phase in pores is removed by evaporation method) and aerogel (supercritical drying is used to remove aqueous phase). Amorphous silica of fine particle size, high purity and surface area has tremendous potential as catalyst support and adsorbent in different chemical synthesis like pharmaceuticals, cosmetics, paints [2–5], fertilizers, as precursor in ceramic industry, reinforcing agent in rubber industry, cleansing agent in tooth pastes, anti-caking agent in food industries [2,6–8] etc. Silica also has been used as a major precursor for various inorganic and organometallic materials having wide applications in synthetic chemistry as catalysts and in thin films or coatings for electronic and optical materials [9,10]. Precipitated silica is used as a filling material in shoes and general rubber goods production [4,11]. In tires, it reduces rolling resistance, increases abrasion resistance and wet grip [11] while, it is also used as desiccant for moisture adsorption in various house-hold as well as electronic goods. Silica particles coated with organic modifiers are used in stationary chromatography phases, heterogeneous supported catalysts, in automotives, aerospace and sensor industries [4,12–15]. Ultrafine silica has substantial potential for wide range of applications including manufacturing of light-weight structural materials, colloidal damper in field of mechanical engineering and other fine precision equipments, zeolite synthesis etc. [4,16–20].

Silica used in various chemical applications is produced from either silicate solution or silane reagents such as TMOS (tetramethylorthosilicate), TEOS (tetraethylorthosilicate), PEDS (polyethoxydisiloxane) etc. [10,12,13,21]. Sodium silicate (commercially known as sodium water glass) is a complex mixture of silicate anions and polymer silicate particles [10] and is generally utilized as a

precursor for silica precipitation. Manufacturing of sodium silicate is expensive due to costly precursors and energy required to reach high temperature generally above 1300°C during calcination stages. This technique also produces environmental pollution by generating CO_2, waste water, sodium sulphate in huge quantities, so, it is a very costly and environmental hazardous process. Various synthetic procedures reported in literature for silica precipitation are- sol-gel, micro-emulsion processing, plasma synthesis, chemical vapour deposition, combustion synthesis, hydrothermal technique, fluidized bed, pressurized hot water treatment process, carbonization and combustion, non isothermal decomposition in oxidizing atmosphere [4,13,22,23] etc. Amongst, sol-gel process is common which involves hydrolysis and condensation of TEOS in a mixture of alcohol, water and NH_3. Hydrolysis reaction gives slightly hydrolyzed TEOS monomer intermediate which undergoes condensation to form silica [12]. Here, starting materials (alkoxides) are very expensive, hazardous and can cause blindness (with TMOS), therefore, their commercialization is prohibited [10]. Silica precipitation can also be carried out in open system under atmospheric pressure [24], but results are poor in terms of yield% of silica so precipitated, thus, closed systems under controlled temperature and pressure conditions is favoured. In recent years, one of the world's primary concerns is the "greenhouse" effect, especially relating with CO_2 [22]. The main disadvantages of the traditional techniques bring the high energy consumption and heavy pollution, production of large quantities of CO_2 and inorganic salts, which have limited their large-scale commercial applications and violated the principles of green chemistry. Therefore, it is our industrial demand to develop a simple, energy efficient, cost-effective method for producing silica which is very advantageous in our day-to-day life. Besides amorphous silica, ordered mesoporous silica can also be synthesized by TEOS and sodium silicate having wide catalytic applications in alkylation, isomerisation, trans-esterification, esterification, polymerisation reactions [25–29] etc. Ordered mesoporous silica such as MCM-41, MCM-48, SBA-15, SBA-3, SBA-16, MSU-X etc. are generally synthesized through various routes including, hydrothermal synthesis, surfactant-templated method, cationic-neutral templating, co-condensation of chiral organosilane precursors, sol-gel etc.

Perlite is a naturally occurring dense, glassy ryholitic volcanic rock mainly comprising of fused silicoaluminate (more than 85%) and 3-5 % water. It is a natural pozzolanic material, formed by cooling of volcanic eruptions with simultaneous gas dissolving, so, the resultant solidified matter acquires a porous structure. When rapidly heated at above 1000°C, perlite expands up to 10-20 times of its original volume [30]. Expanded perlite has fire resistance, sound insulation, low moisture retention and low density properties, hence, used in fillers, concrete and plaster, phase changing materials, insulators, acoustical ceiling tiles, filtration aids, oil adsorption, horticultural applications [31–37] etc. Particularly due to its silicoaluminate composition as well as high reactivity in alkaline environment, perlite is used in zeolite synthesis [38]. This property can also be utilized in silica precipitation. Perlite having amorphous silica is highly soluble in basic solution which helps in silica precipitation. Its chemically inert character and highly porous nature make it a good adsorbent and it has been rarely explored as a raw material for silica production.

This chapter describes the procedure of extraction of silica from a naturally abundant silica enriched source- perlite via precipitation. Basic characterization of perlite and precipitated silica by different analytical techniques is included in this chapter. The results depict that the precipitated silica is globular, fine and agglomerated possessing higher specific surface area and its maximum yield can be achieved in optimized synthesis conditions. The influences of extraction parameters including pre-washing procedure, effect of different acids, time, temperature, pH of precipitation, NaOH concentration on yield of extracted silica are also studied. In this chapter, FT-IR and XRD results of the extracted silica with that of commercial silica are compared which indicate the improved quality of silica extracted by the optimized procedure and also recommends the further utilization of extracted silica in various value-added applications like adsorption, catalyst support etc. A new, less energy consuming, eco-friendly and recyclable technique for the precipitation of silica is proposed in our present work. All the reactants and by-products are recyclable in this process, and no pollutants are released to the environment. Therefore, the recyclable technology is propitious to reduce polluting emission and also finds a novel route to utilize huge reserves of natural waste- perlite.

2.2   Experimental Procedure

2.2.1 *Materials*

Perlite is supplied by Indica Chem. Ind. Pvt. Ltd., India. Sodium hydroxide, sulphuric acid, nitric acid, hydrochloric acid, perchloric acid, ammonia solution are purchased from Merck.

2.2.2 *Methodology*

Dissolution-precipitation technique has been employed for silica extraction from perlite, involving alkali solubilisation and acid precipitation. First of all, perlite is thoroughly rinsed with 1 N HCl solution to remove dust and other metallic impurities. Then, it is successively washed with distilled water to remove acid from perlite. After washing, perlite is calcined at 800°C for 3 h, named as thermally activated perlite (TAP) and is utilized as a raw material to produce silica by adopting following procedure-

(i)   **Dissolution-** 10 gm of TAP is stirred with 80 ml of NaOH solution with varying concentration in a covered 250 ml Erlenmeyer flask at various temperatures ranging from 30-120°C for different time periods ranging from 1-24 h. The resultant sodium silicate solution is then filtered through Whatman No. 41 ashless filter paper and residue is washed with 50 ml of boiling distilled water. Washings and filtrate are allowed to cool at room temperature and used for subsequent steps.

(ii) **Precipitation-** Viscous, transparent, odourless filtrate containing sodium silicate is titrated with 5 N solutions of different acids (HCl, H_2SO_4, $HClO_4$ and HNO_3) under constant stirring up to varying pH, i.e., 2, 5, 7 and 8.5. In order to attain basic pH, NH_4OH is used after adding acidic solution to the filtrate. Acidic solution is added slowly with constant stirring to avoid local changes in pH during precipitation. On fast addition of acid, chemistry of reacting mass may change along with physical properties. The acidic conditions indicate approximately complete precipitation of silica from sodium silicate solution. A soft gel is formed after precipitation which is then aged for 12 h.

(iii) **Washing-** After ageing, precipitated silica so formed is filtered from mother liquor and successively washed by vacuum filtration using hot distilled water to remove respective metal salts like Na_2SO4, $NaCl$, $NaNO_3$, $NaClO_4$. The washings or clear supernatant liquid are tested qualitatively to determine the presence of Cl^-, SO_4^{-2}, ClO_4^- and NO_3^- ions. The filtrate is repeatedly washed up to negative results of above tests.

(iv) **Drying-** Thus obtained slurry is dried in vacuum oven at 110°C for 12 h. The dried material is then refluxed with 1 N HCl at 100°C for 2 h for removal of mineral impurities like Al, Na, K etc. from silica. Then, it is washed repeatedly to get rid of acidic contents with demineralised water. Now, the obtained precipitated silica is dried at 110°C for 12 h and designated as precipitated silica (S), (N), (ClO_4) and (Cl) precipitated by H_2SO_4, HNO_3, $HClO_4$ and HCl respectively.

(v) **Quantification-** Following formula is used to determine yield% of silica precipitated after adopting above steps-

$$\text{Silica extraction yield (\%)} = \frac{\text{mass of silica precipitated}}{\text{mass of perlite used}} \times 100$$

The steps of silica extraction from perlite are summarized in **Scheme 2.1**.

2.2.3 *Characterization of samples*

Physicochemical properties of all prepared samples and starting material (perlite) are studied by N_2 adsorption-desorption, XRD, FT-IR, SEM, SEM-EDX, TEM, TGA and UV-Vis DRS techniques, as described in **Annexure-I**.

2.3 Characterization of perlite and TAP

Thermal activation of perlite results in its colour change from light grey to light pink, due to removal of excess water and carbon. A colour change at 800-900°C corresponds to the crystallization of phases and reduction of glass content [39]. The major component of perlite is silica and untreated silica is totally hydroxylated, also covered with physically adsorbed water.

As received perlite

Thermal activation of perlite at 800°C for 3 h (TAP)

Dissolution of TAP in NaOH solution at different temperatures for different time periods to form sodium silicate solution

Precipitation of sodium silicate solution with different mineral acids

Filtration and washing with hot distilled water up to neutral pH

Qualitative chemical tests of washings

Drying of so-obtained pulp at 110°C for 12 h

Refluxing of dried material with 1 N HCl

Repeated washing of above material with distilled water up to neutral pH

Drying of precipitated silica at 110°C for 12 h

Precipitated silica is obtained

Scheme 2.1: Precipitation of silica from perlite using various mineral acids.

Thermal treatment of the support initially removes water (dehydration) and then combines adjacent hydroxyl groups to form water (dehydroxylation). This dehydroxylation leads to the formation of surface siloxane bridges [40] which helps in increasing surface hydroxyl groups. Loss on ignition (LOI) is determined experimentally by heating a certain weighed quantity of perlite in muffle furnace at 800°C for 3 h. The LOI amount is 4.1 wt % which corresponds to the removal of moisture and coexisting unburned carbon from sample [41].

2.3.1 BET analysis

BET specific surface area of samples indicates that on thermal activation, specific surface area of perlite decreases from 2.6 to 2.2 m^2/g.

2.3.2 X-ray diffraction analysis

The broad X-ray diffraction pattern of perlite **(Figure 2.1a)** confirmed the absence of crystalline structure [9] which is typical for amorphous solids. However, thermal treatment of perlite at higher temperature could convert less ordered structure to more ordered structure and a single, small crystalline peak appears in TAP at $2\theta = 27.642°$ **(Figure 2.1b)** which shows crystalline quartz formation in perlite [42] along with a broad hump at $2\theta = 22-23°$ confirming amorphous nature of silica [23]. Previous reports [43] reveal that burning temperature higher than 973 K induced production of crystalline structure in silica.

2.3.3 Fourier transform infra-red analysis (FT-IR)

FT-IR spectra of perlite and TAP **(Figure 2.2)** shows a broad band between 3600-3300 cm^{-1}, which is attributed to surface hydroxyl groups of –Si-OH and water molecules adsorbed on the surface [44]. The broadness of band indicates the presence of strong hydrogen bonding in the sample [45].
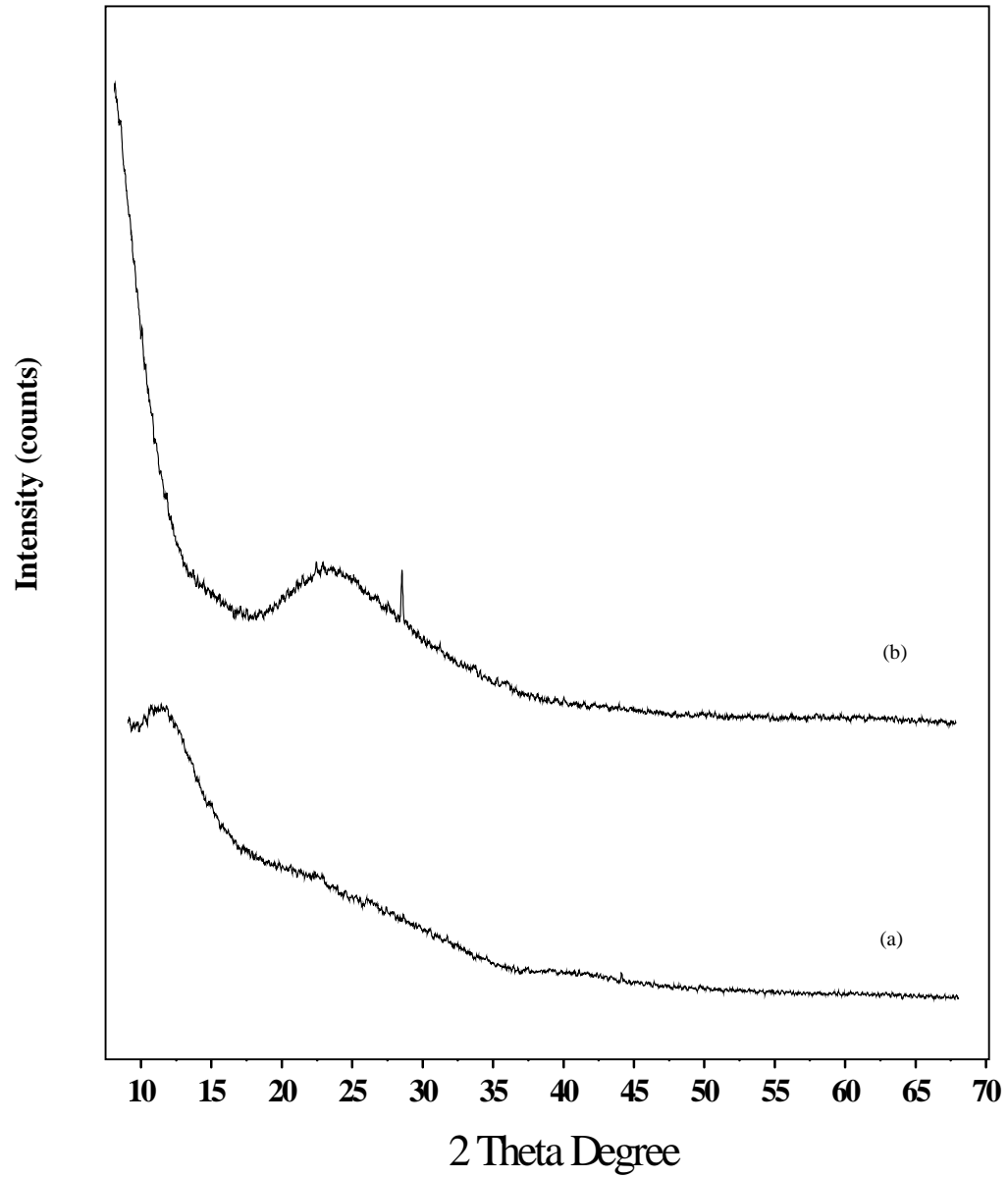
Figure 2.1: **X-ray diffraction pattern of (a) perlite and (b) TAP.**

In perlite, the hydroxyl groups exist in higher degree of association with each other which results in extensive hydrogen bonding, while in FT-IR spectrum of TAP **(Figure 2.2b)**, the intensity and broadness of band is decreased which confirms the loss of water. The strong band at 1178 cm^{-1}, due to the structural siloxane framework, attributes to the vibrational frequency of the Si-O-Si bond. The peak is shifted to higher wave number, i.e., 1227 cm^{-1} after thermal treatment, which is normally observed in amorphous silica samples [46]. An intense peak at 1632 cm^{-1} in the spectrum of perlite is attributed to bending mode ($_{O-H}$) of water molecule [47], which is again highly decreased in case of TAP.

2.3.4 Scanning electron microscopy (SEM and SEM-EDX analysis)

SEM micrograph of perlite **(Figure 2.3a)** revealed the irregular, crumbled morphology of perlite particles. Similar pattern is observed in other reported micrographs of perlite [31]. SEM image of TAP **(Figure 2.3b)** is mainly fragmatic and random as a result of thermal activation. But here, the morphology is less irregular which confirms the evaporation of water from the perlite sample on heating it at high temperature.

EDX analysis of perlite and TAP is given in **Table 2.1**.

Table 2.1:   **EDX analysis of perlite and TAP.**

Samples	SiO$_2$ (wt%)	Al$_2$O$_3$ (wt%)	K$_2$O (wt%)	Na$_2$O (wt%)	ZnO (wt%)	FeO (wt%)	TiO$_2$ (wt%)	LOI
Perlite	72.74	14.79	7.48	2.10	2.04	0.91	0.07	4.1
TAP	72.24	14.59	7.42	2.01	2.04	0.91	0.07	2.3

LOI- Loss on ignition

2.3.5 Transmission electron microscopy (TEM analysis)

A more realistic vision of irregular morphology of perlite can be furnished by TEM image **(Figure 2.4)**. In TEM micrograph, irregular plate-like particles and small aggregates are clearly observed due to hydrogen bonds between the surface hydroxyl groups of silica particles.
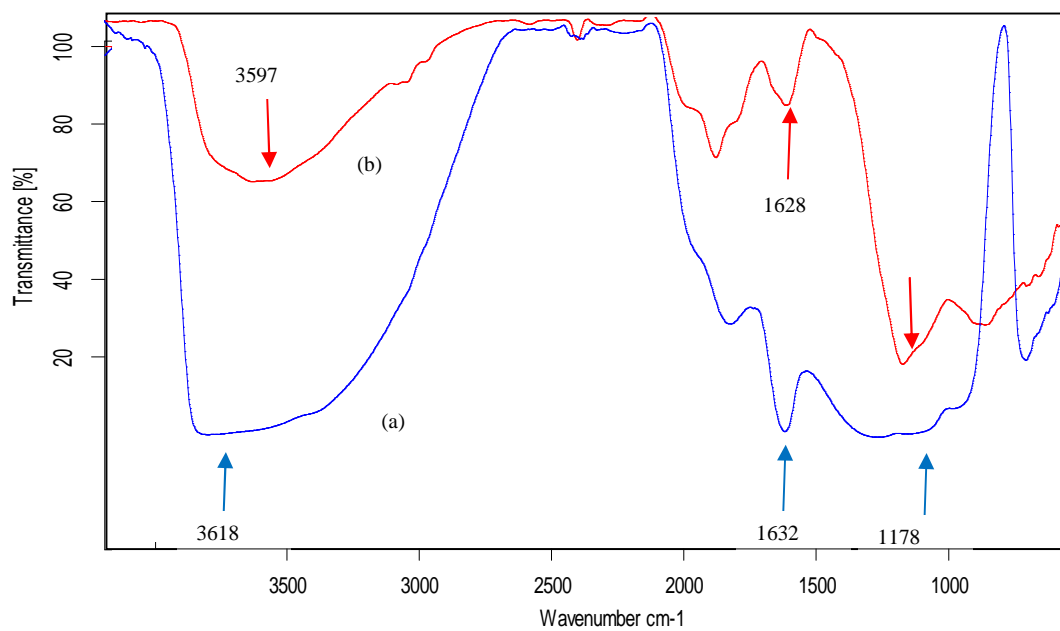
Figure 2.2: **FT-IR spectra of (a) perlite and (b) TAP.**
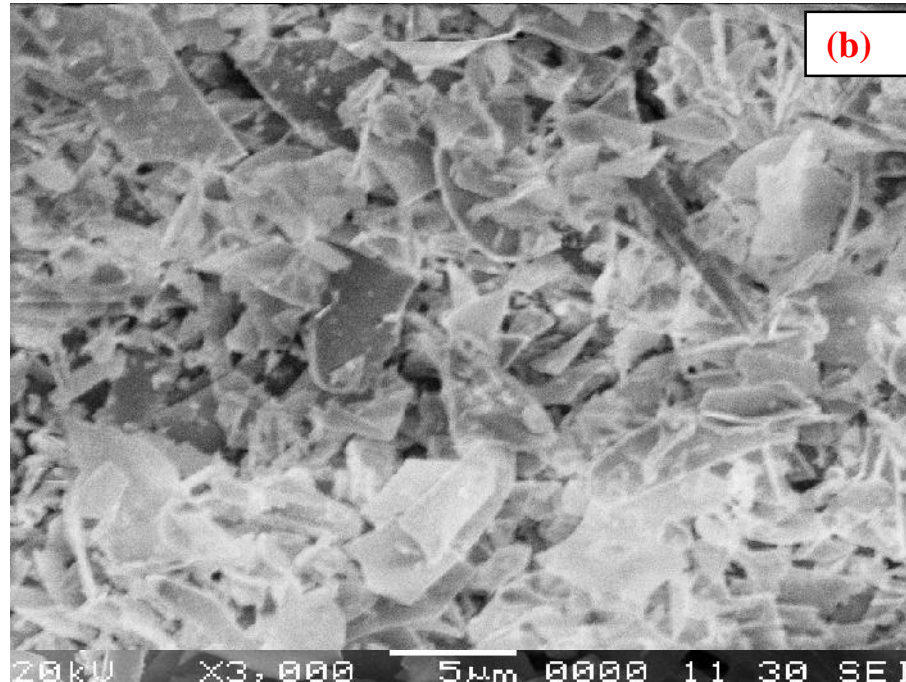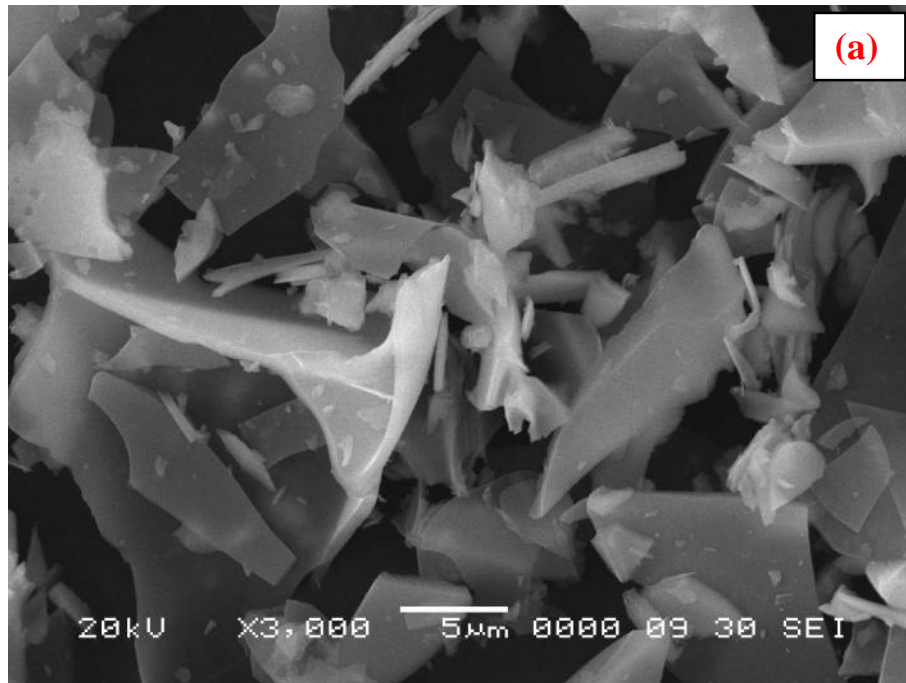
Figure 2.3: **SEM micrographs of (a) perlite and (b) TAP.**
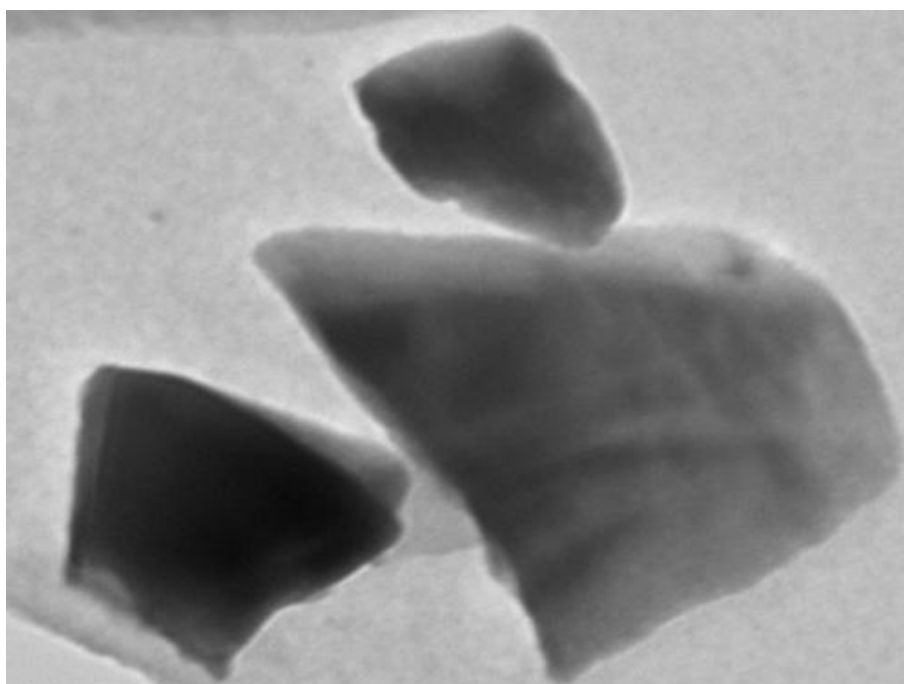
Figure 2.4: **TEM micrograph of perlite.**

2.3.6 Thermo-gravimmetric analysis (TGA)

The TGA curve of perlite, as shown in **Figure 2.5**, shows continuous decrease of 4.53 wt% from 50-1000°C which is in accordance with LOI value. Weight loss in lower temperature range (50-400°C) corresponds to the removal of moisture content of the sample or physically adsorbed water molecules together with some volatile materials. Total moisture content comprises of water entrapped in core, silanol hydroxyl groups and physically adsorbed water. While, the weight loss of sample within range of 400-1000°C corresponds to the burning of carbonaceous materials that were firmly adsorbed on the surface of the solid materials, removal of chemisorbed water and volatilization of some trace metal oxides [41].
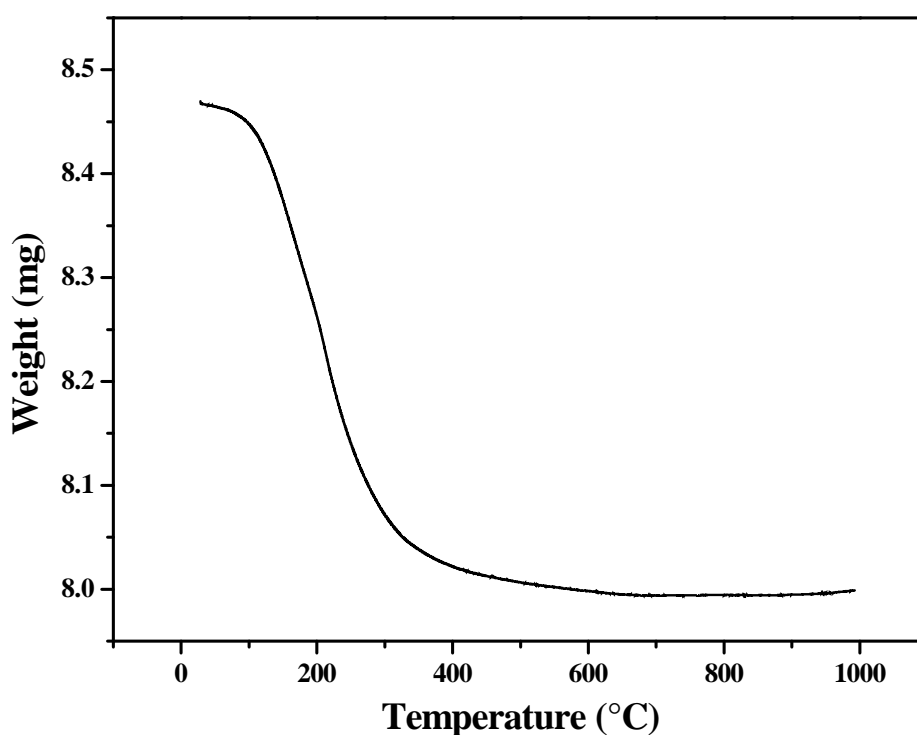
Figure 2.5:   TGA curve of perlite.

2.3.7 Ultra violet-Visible Diffuse Reflectance spectroscopy (UV-Vis analysis)

UV-Vis DRS spectrum of perlite (**Figure 2.6**) shows a broad band around 230 nm which is a common feature of aluminosilicate samples [48]. This band appears not only for amorphous systems, such as silica gels but also present in crystalline silica structures as well as in zeolites too.
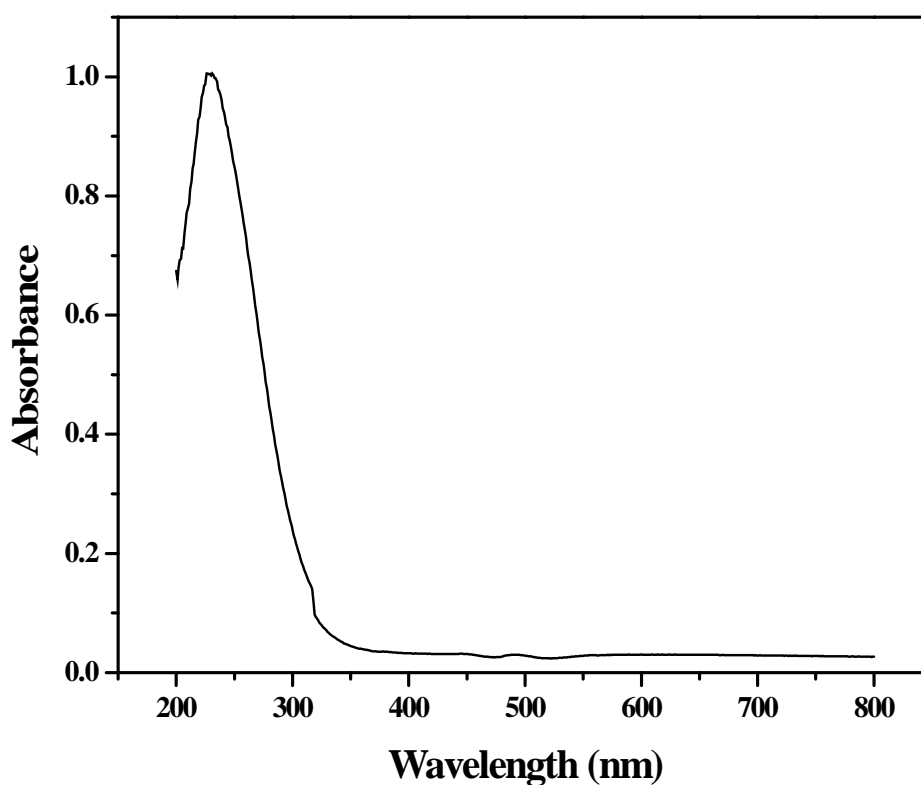
Figure 2.6: UV-Vis DRS spectrum of perlite.

2.4 Characterization of silica precipitated from perlite

2.4.1 BET analysis

Surface area of precipitated silica depends on several process parameters such as concentration of silicate solution used for precipitation, temperature of precipitation, duration of precipitation [49] etc. Precipitated silica possesses greater surface area than perlite and its value is highest for silica precipitated by HCl, as demonstrated in **Table 2.2**. It can be explained on the basis of sodium content present in all samples. The order of sodium content in all samples is – Perlite > Silica (N) > Silica (ClO$_4$) > Silica (S) > Silica (Cl). This is due to formation of various sizes of sodium salts during acid precipitation [50]. Residual metals and sodium salts adhere to silica matrix, block the pores [51] and thus decreases surface area. NaCl formed by HCl precipitation is smaller in size, thus gets removed by water washing and sodium content decreases while surface area of sample increases. According to BET calculation, average pore diameter of silica (Cl) particles is 4.97 nm suggesting mesoporous nature of silica precipitated.

Table 2.2:   BET specific surface area data of samples.

Samples	BET specific surface area (m^2/g)
Perlite	2.6
TAP	2.2
Silica (Cl)	114.14
Silica (S)	104.42
Silica (ClO$_4$)	98.02
Silica (N)	94.56

2.4.2 X-ray diffraction analysis

All precipitated silica samples **(Figure 2.7a-d)** show the amorphous nature as observed with absence of sharp defined peaks in XRD patterns [9]. The broad hump centred at 2 = 22-32° is characteristic of amorphous silica and indicate its disordered structure [23]. Absence of any peak attributed to metallic impurities or

any other metallic salts like NaCl, Na$_2$SO$_4$ etc. shows that acid washing of perlite before precipitation as well as acid washing of silica after drying is effective in removing metallic impurities which is confirmed later by SEM-EDX results. Precipitated silica (Cl) sample has most intense hump which confirms the higher amount of amorphous silica in it. The XRD patterns as observed for precipitated silica samples are found similar to that of commercial silica shown in **Figure 2.7e**. More intense hump shown in case of precipitated silica (Cl) **(Figure 2.7a)** indicates its finer quality.

2.4.3 *Fourier transform infra-red analysis (FT-IR)*

FT-IR spectra of all precipitated silica samples are shown in **Figure 2.8a-d**. Band between 3600-3300 cm^{-1} is attributed to surface –OH groups, adsorbed water molecules bound to silica surface and hydrogen bonding between them. Intensity of –OH band seems higher due to increased intermolecular hydrogen bonding as a result of agglomeration of silica particles [50]. Shoulder present at 3246 cm^{-1} could be assigned to stretching vibrations of Si-OH group in amorphous silica samples [52]. Bands appearing at 800, 1080 and 1200 cm^{-1} denotes Si-O-Si vibration modes of highly condensed gel network. Peak at 800 cm^{-1} is due to Si-O-Si symmetric stretching vibrations [21] while peak at 960 cm^{-1} appears due to stretching mode of Si-OH (silanol groups) typically present in amorphous silica gel structures [53]. Peak at 1098 cm^{-1} is due to Si-O-Si asymmetric stretching vibrations. IR band at 1111 cm^{-1} with a shoulder at 1188 cm^{-1} is generally ascribed to TO and LO modes of Si-O-Si asymmetric vibrations [52]. Band between 1400-1250 cm^{-1} is due to structural siloxane bonds (Si-O-Si). Band appearing at 3600-3300 cm^{-1}, and 1650 cm^{-1} responsible for –OH stretching and bending respectively are more pronounced in the spectrum of commercial silica gel **(Figure 2.8e)** indicating thes presence of intense hydrogen bonding. The bands at 800, 900, and 1,220 cm^{-1} which are more clearly visible in the commercial silica gel could be attributed to the network vibration modes indicating the existence of a highly condensed gel network [3]. The comparable chemical bonding with commercial silica confirms the finer quality of silica so produced by HCl precipitation.
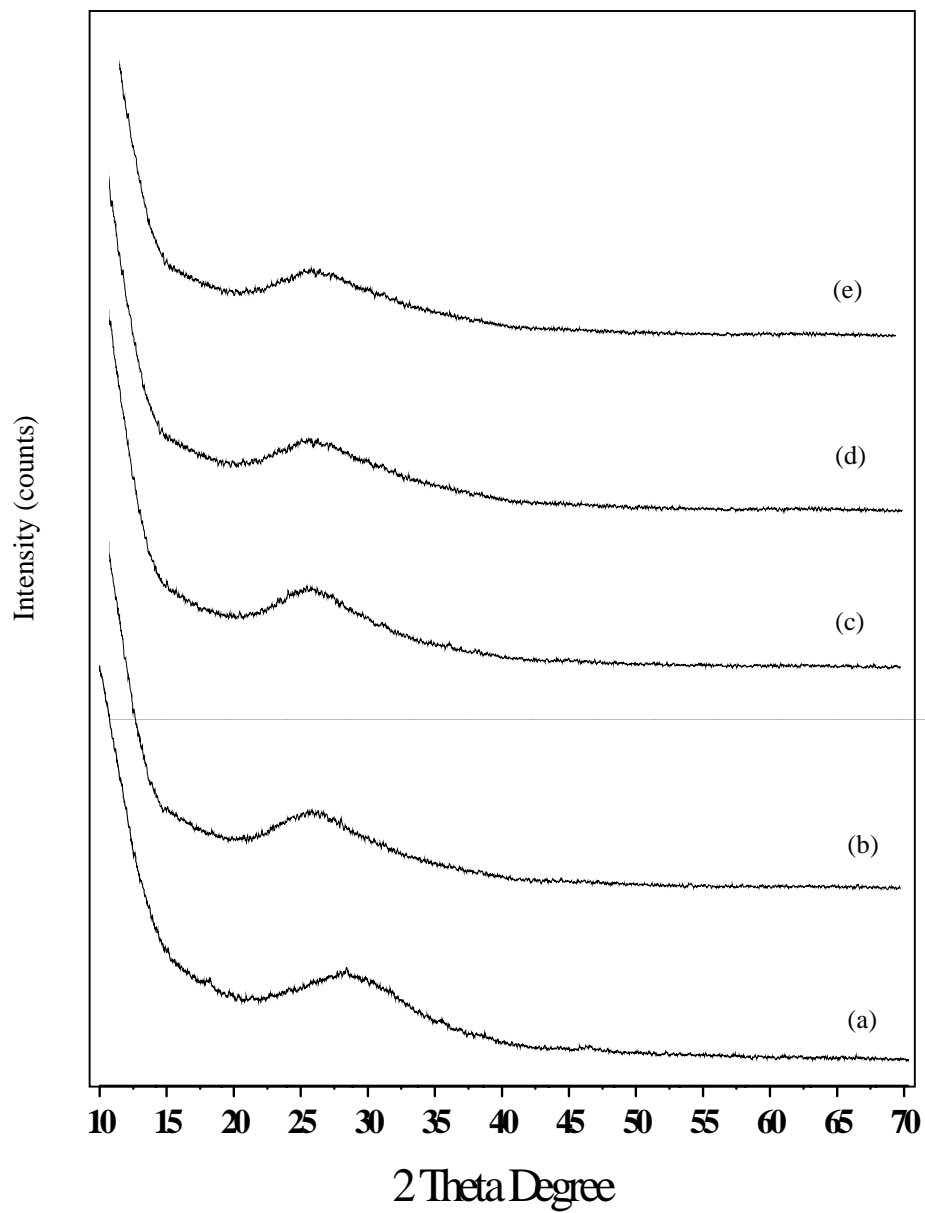
Figure 2.7: **X-ray diffraction pattern of (a) precipitated silica (Cl) (b) silica (S), (c) silica (ClO₄), (d) silica (N) and (e) commercial silica.**
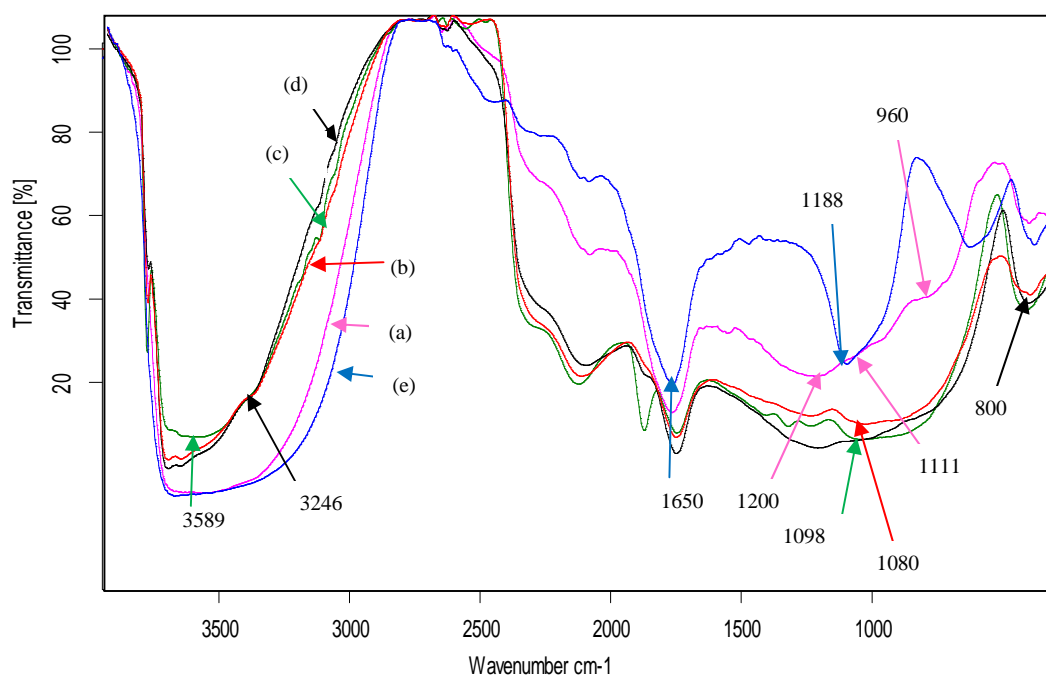
Figure 2.8: **FT-IR spectra of (a) precipitated silica (Cl) (b) silica (S), (c) silica (ClO₄), (d) silica (N) and (e) commercial silica.**

2.4.4 Scanning electron microscopy (SEM and SEM-EDX analysis)

SEM micrographs of silica precipitated by different acids are shown in **Figure 2.9**. They demonstrate that agglomeration occurs and particles tend to acquire spherical shape confering increase in amorphous silica content after precipitation [23]. Extracted silica particles are globular, highly porous and present in different shapes and sizes. Such type of gelatinous mass is due to the presence of amorphous silica gel skeleton. Most ultra fine, spherical and uniform particles are shown in case of precipitated silica (Cl), (**Figure 2.9a)** conferring that silica particles with superior and fine qualities are produced by HCl precipitation.

SEM-EDX analysis of silica precipitated by different acids is given in **Table 2.3** which does not show the presence of sulfate, chloride, chlorate, nitrate ions, thus indicating that these ions are well removed from the mother liquor by washing. Generally, sulfate ions specifically adsorb on (hydrous) oxide surfaces, similar to phosphates or chromates [54]. As evident from the table, silica precipitated by HCl possesses highest amount silica amongst all precipitated silica samples.

Table 2.3:   **EDX analysis of precipitated silica samples.**

Samples	SiO_2 (wt%)	Al_2O_3 (wt%)	Na_2O (wt%)	TiO_2 (wt%)	SO_4^{-2} (wt%)	Cl^- (wt%)	ClO_4^- (wt%)	NO_3^- (wt%)
Precipitated Silica (Cl)	90.02	9.41	0.48	0.09	-	-	-	-
Precipitated Silica (S)	88.13	10.86	0.87	0.14	-	-	-	-
Precipitated Silica (ClO_4)	84.36	14.02	1.36	0.39	-	-	-	-
Precipitated Silica (N)	81.36	16.44	2.05	0.14	-	-	-	-
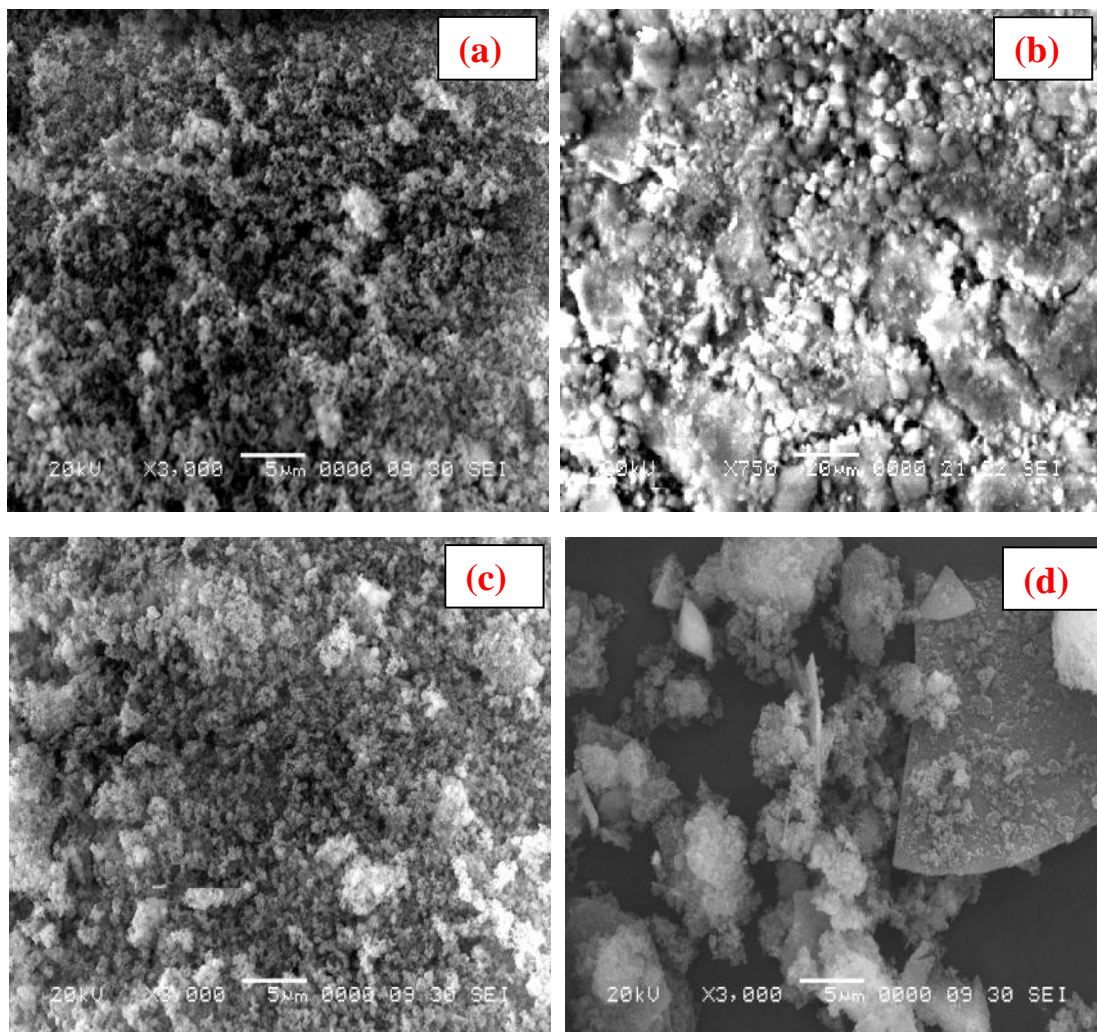
Figure 2.9:   **SEM micrographs of (a) Precipitated silica (Cl), (b) silica (S), (c) silica (ClO$_4$) and (d) silica (N).**

2.4.5 Thermo-gravimmetric analysis (TGA)

The difference in mass of sample before and after thermal treatment is referred as Loss on Ignition (LOI). The unburnt carbon, adsorbed moisture and CO_2 remain present as LOI in perlite. The pre-treatment of perlite with HCl before precipitation reduces carbon and mineral impurities present in the sample through leaching. The TGA curve of precipitated silica (Cl) sample having highest silica content is shown in **Figure 2.10**. A sharp weight loss seen up to 200°C could be ascribed to evaporation of physically adsorbed residual water [55]. Further considerable weight loss is observed between 300-1000°C which is due to progressive poly-condensation, dehydration of chemically adsorbed water molecules and decomposition of volatile metallic impurities. Silanol groups present on surface of precipitated silica condense to form siloxane bridges. In this region, residual sodium salt (NaCl) also gets decomposed [50].
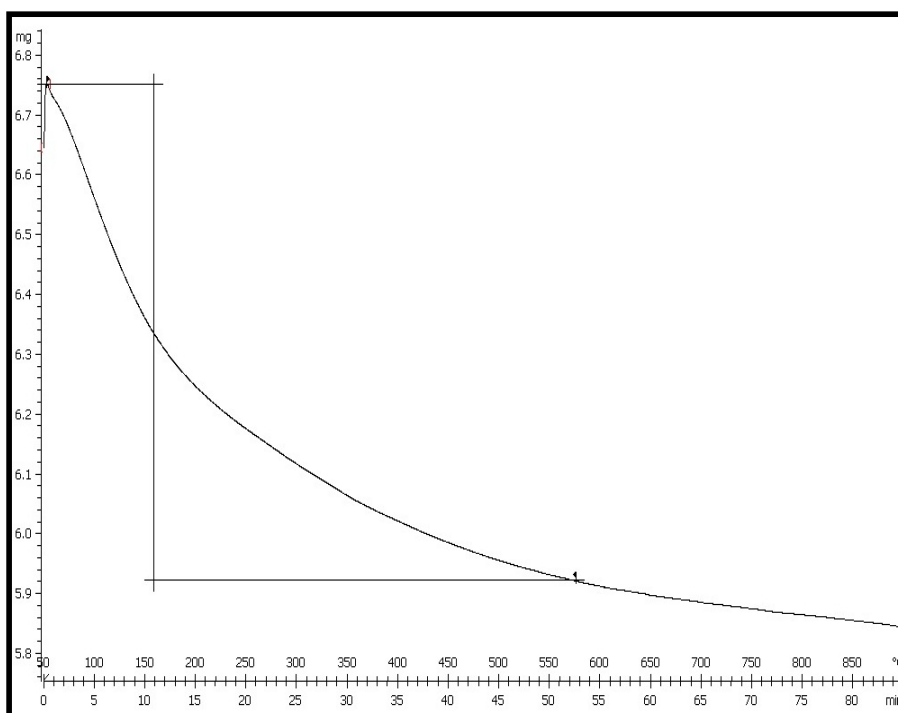
Figure 2.10:   TGA curve of precipitated silica (Cl).

2.4.6 *Ultra violet-Visible Diffuse Reflectance spectroscopy (UV-Vis analysis)*

A broad band centred at 230 nm is typically for aluminosilicates [48]. On comparing UV-Vis spectra of all precipitated silica samples as shown in **Figure 2.11**, it is demonstrated that highest absorbance is seen in case of precipitated silica (Cl) concluding highest silica content in it as compared to other samples. The intensity and absorbance of this band in precipitated silica (Cl) is even higher than that of perlite indicating higher percentage of silica in precipitated silica than perlite. This band appears not only for amorphous systems, such as silica gels but also present in crystalline silica materials as well as in zeolites.
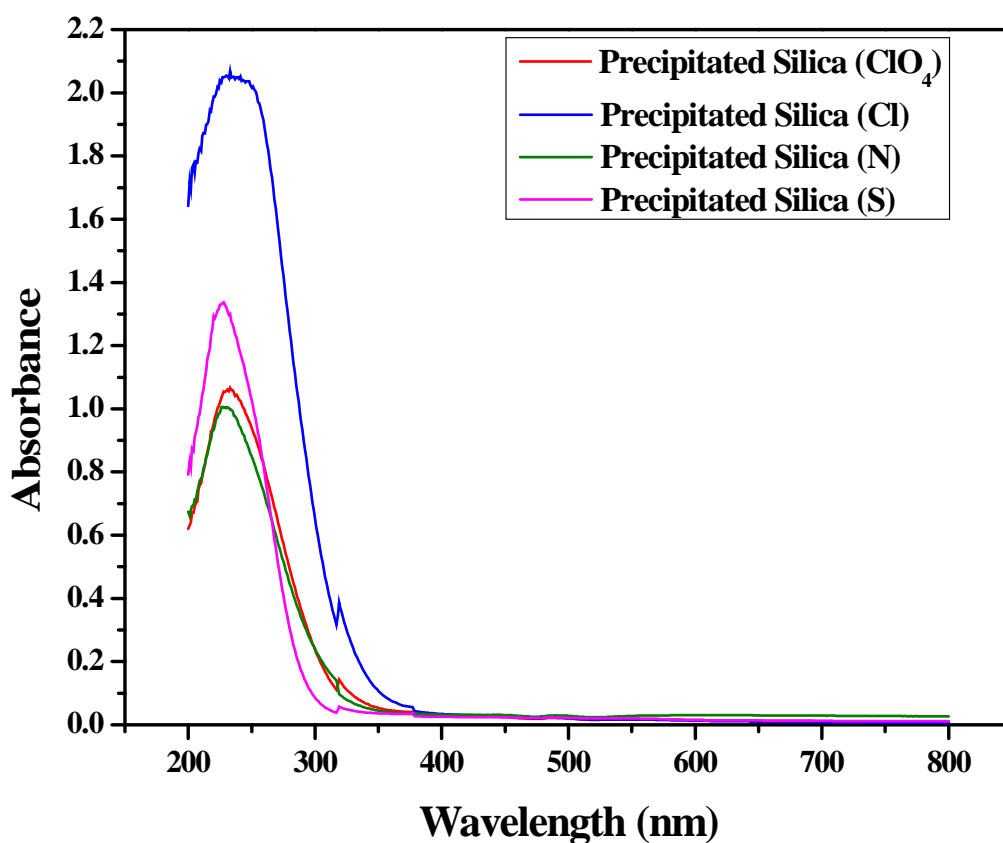
Figure 2.11:   UV-Vis DRS spectra of precipitated silica samples.

2.5   Parametric studies

Solubility of amorphous silica is lower in acidic pH and increases sharply at pH > 10. The properties of precipitated silica depend strongly on its synthesis conditions such as ageing time, temperature, pH, modes of washing, concentration of NaOH etc. These factors influence size of SiO_2 particles, their aggregation and specific surface area. The optimization of above synthesis factors is attained so that silica precipitated in this work can be further utilized for commercial applications.

2.5.1 Influence of different acids

Table 2.4 shows the influence of different acids on yield% of precipitated silica. On precipitation by acids, metallic and non-metallic impurities get leached off from the final product. By HCl precipitation, maximum metallic impurities removed as metallic salts with chloride ions are small in size, so they cannot entrap in amorphous silica structure and eliminated from the final silica product through washing and drying. Thus, highest yield% of precipitated silica is attained through HCl precipitation.

Table 2.4:   **A comparison of yield% of precipitated silica samples under optimized synthesis conditions.**

Samples	Yield%
Silica (Cl)	92.64
Silica (ClO$_4$)	88.26
Silica (S)	86.98
Silica (N)	78.86

Optimized synthesis conditions: Ageing time = 12 h; Ageing temperature = 90°C; NaOH concentration = 6M; pH = 5.

2.5.2 Influence of washing or pre-treatment

The metallic impurities of perlite like K, Na, Ca, Mg have a substantial effect on quality of silica precipitated from perlite as potassium causes surface melting, accelerates crystallization of amorphous silica [56]. All other impurities

can form respective salts with acids used for precipitation and block the pores of surface resulting in decrease in surface area. Therefore, acid washing of perlite prior to precipitation is preferable to obtain highly purified silica powder with lesser impurities. The chemical reaction between HCl and metal ions results in leaching of metallic impurities in form of salts which is later removed by filtration. After washing, perlite is thermally activated which helps in decomposition of remaining volatile metal impurities at higher temperature. Similar acid washing step is also applied after drying of precipitated silica powder to get rid of remaining metallic impurities. Washing of dried silica powder with deionized water is more effective than washing the silica gel before drying in terms of removal of metal ions from silica. During drying, metals entrapped in silica framework get free which then can be removed by acid washing. Divalent and trivalent ions like Ca, Mg, Fe are strongly adsorbed on silica surface and require lower pH washing for their removal. Thus, an initial acid washing of perlite before silica precipitation is essential. It does not cause any adverse effect on silica yield%. In fact, initial acid washing of substrate and final water washing of dried silica effectively enhances purity of the silica sample so precipitated [50].

2.5.3 Influence of ageing temperature

Figure 2.12 shows effect of ageing temperature on yield% of precipitated silica. On increasing ageing temperature from 30 to 90°C, yield% also increases due to accelerated growth of silica framework. However, on further increase in ageing temperature up to 120°C, gelation rate becomes faster thus forms thicker silica framework while, yield% decreases. These thicker and larger silica particles lead to pore shrinkage which ultimately reduces surface area of silica so precipitated.
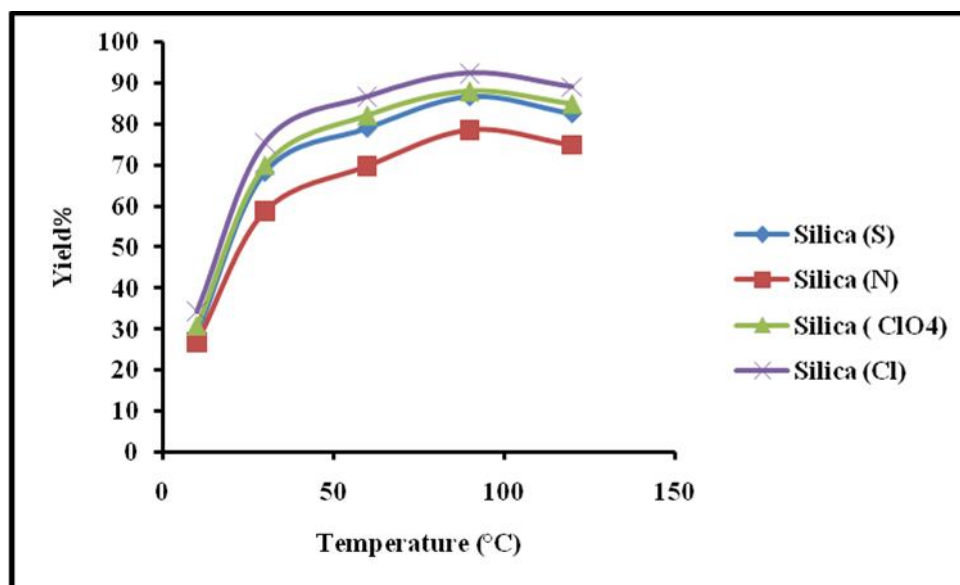
Figure 2.12: **Variation of yield% of silica precipitated by different acids with temperature.**

2.5.4 Influence of ageing time

Ageing time plays a significant role in silica yield% and particle size distribution. It is a process of dissolution and precipitation driven by solubility difference. During ageing, smaller silica particles are dissolved and then precipitated onto larger particles with increase in ageing time. **Figure 2.13** shows the yield% of silica obtained by hatching of sodium silicate solution at various ageing time periods during gel formation. On increasing ageing time from 1 to 12 hours, a remarkable increase in yield% is seen which is then decreased on increasing time period from 12 to 24 h. During ageing period, particle formation is controlled by nucleation and surface growth. In beginning, nucleation process is slow, so yield% is also less which is optimized at 12 h. When time exceeds 12 h, surface growth begins to control silica formation, thus particle size increases and yield% decreases. This increase in particle size also decreases surface area of silica so precipitated. At 12 h, silica gel reached dissolution equilibrium and thus yield% is maximum here. Between 0-6 h, yield% is very less as amorphous silica of perlite does not get dissolved initially. After acid precipitation, during ageing, 3-D silica framework continues to grow and become more rigid by contracting and expelling water present inside the pores [53].
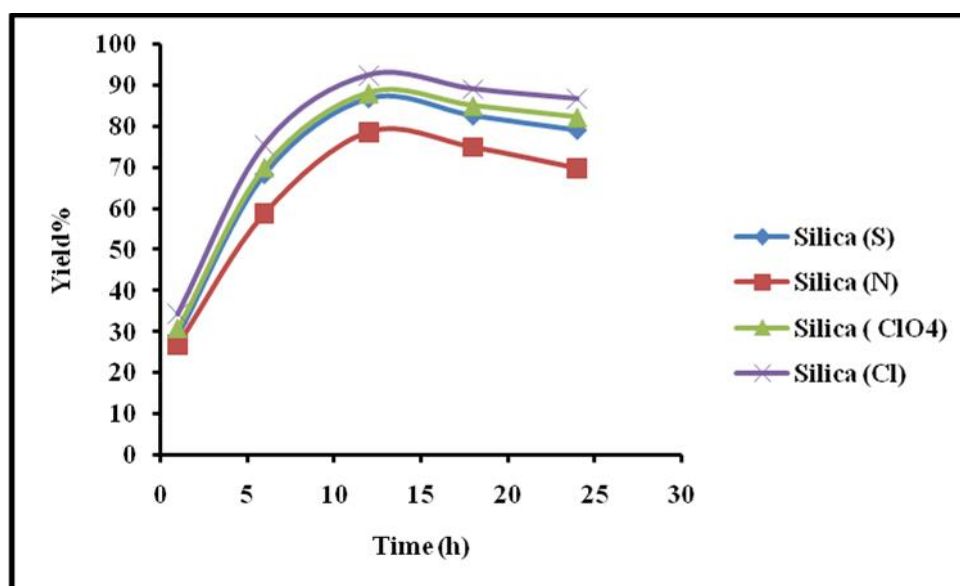
Figure 2.13: **Variation of yield% of silica precipitated by different acids with time.**

2.5.5 *Influence of NaOH concentration*

Figure 2.14 shows effect of NaOH concentration on yield% of silica precipitated. As NaOH concentration is increased from 2 M to 6 M, yield% also increases progressively which is then decreased at 8 M NaOH concentration. At lower NaOH concentration up to 6 M, gelation rate is slow hence yield% is less while above 6 M NaOH concentration, gelation rate is accelerated, forming thicker and bigger silica particles resulting in reduced yield% and surface area because of reduction in pore size. At 6 M NaOH concentration, gelation rate is optimum and an equilibrium has formed between nucleation and growth reaction and thus yield% is also maximum.
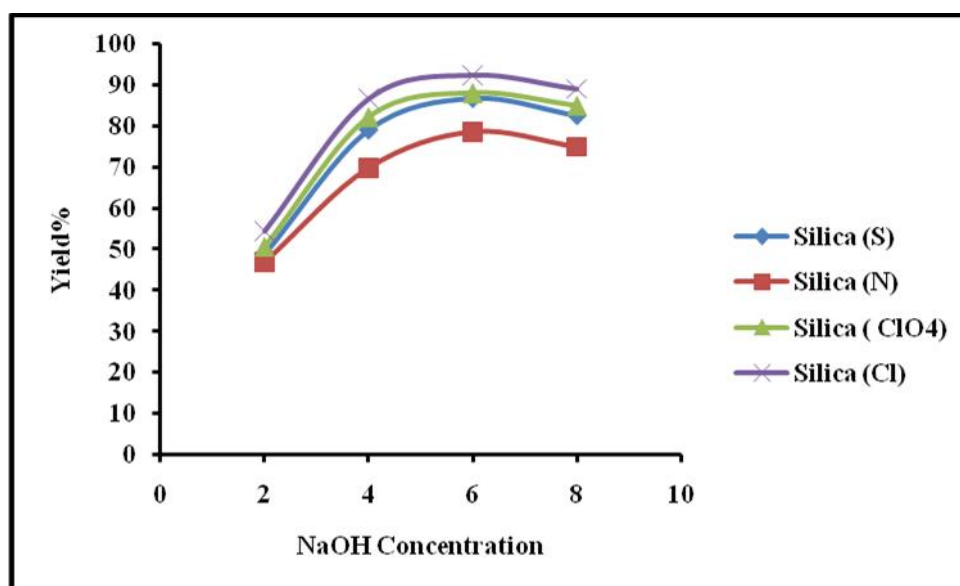
Figure 2.14: **Variation of yield% of silica precipitated by different acids with NaOH concentration.**

2.5.6 *Influence of pH*

Silica precipitation is observed over a wide range of pH, from acidic (pH = 2, 5), neutral (pH = 7) up to basic (pH = 8.5) which is summarised in **Figure 2.15**. Solubility of amorphous silica is very low at pH < 10 and increases sharply at pH > 10. Thus silica is extracted from perlite by solubilising under alkaline conditions and subsequently precipitation at low pH. At acidic pH, metallic impurities are easily leached off from the precipitated silica and thus purity of silica increases. Silica starts to precipitate as pH decreases to less than 10. At pH > 7 in the absence of salts, electrostatic interaction between charged particles limits the aggregation process to form a three-dimensional, porous silica network. Therefore, primary particles increase in size and decrease in number as a result of the Oswald ripening process and consequently yield% decreases. Impurities are higher at pH = 7 and 8.5, while at pH = 5, comparatively more pure silica is obtained with maximum yield%. Silica samples obtained at low pH comprises of fine particles with agglomeration due to H-bonding and Vaander Waals force of attraction [9] leading to enhancement in specific surface area. On the contrary, silica obtained at higher pH consists of coarse, large particles resulting in decrease in pore size, thus decrease in surface area due to pore blockage by metallic impurities. Gelation pH is a critical parameter in quality determination [57]. For

higher pH, two step procedure has been applied. NH$_4$OH is used to precipitate silica up to pH = 8.5 which is initially precipitated by HCl. It increases rate of condensation and rate of gelation, thus producing coarse, large silica particles with reduced surface area.
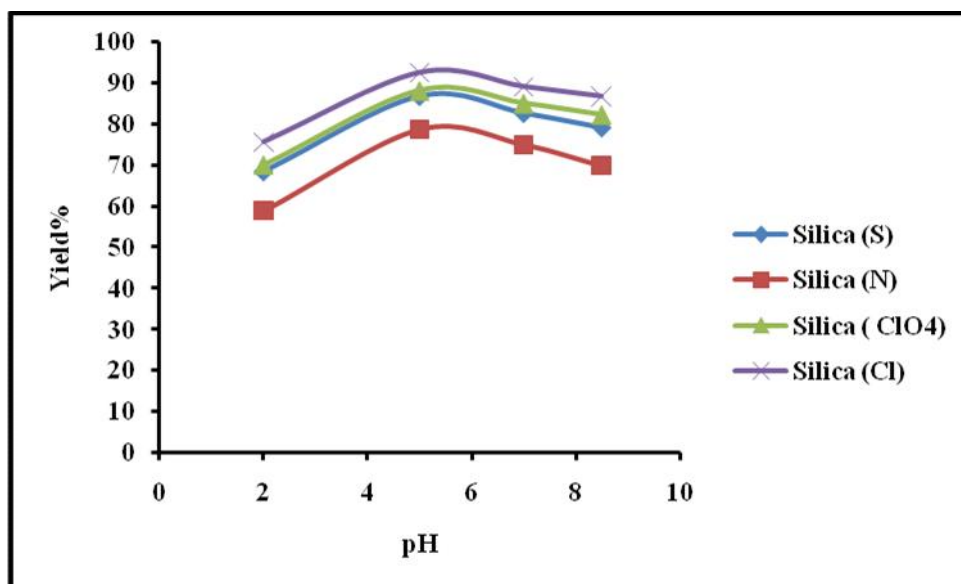
Figure 2.15: **Variation of yield% of silica precipitated by different acids with pH.**

2.6 Mechanism

In silica precipitation, two reactions take place simultaneously i.e., condensation and sodium silicate acidification. The condensation reaction is formation of siloxane linkage between surface silanol groups. In this step, sodium meta-silicate is formed as a result of solubilization of silica present in perlite in caustic soda and it can be written as-

$$SiO_2 + 2\,NaOH \longrightarrow Na_2SiO_3 + H_2O$$

| Silica of Perlite | Caustic soda | | Sodium meta-silicate | Water |
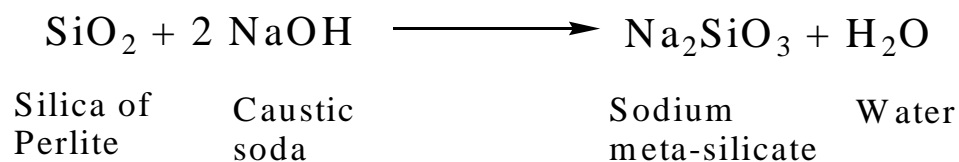
Reaction of sodium meta-silicate, so produced in above step with HX (different acids) solution during acidification process can be written as-

$$Na_2SiO_3 + HX \text{ or } 2HX \longrightarrow SiO_2 + 2\,NaX \text{ or } Na_2X + H_2O$$

Sodium   Acid   Silica   Sodium   Water
meta-silicate   precipitated   salts
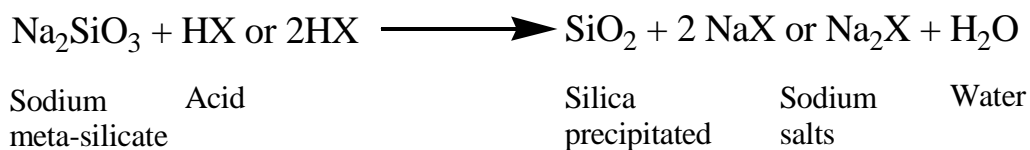
As a result of above two-step procedure, amorphous silica gets precipitated from perlite, along with sodium salts and water as by-products which can be recycled and reused further. During regeneration, calcium hydroxide reacts with residue containing insoluble metallic salts viz. Na_2SO_4, $NaCl$, $NaNO_3$, $NaClO_4$ to form $CaSO_4$, $CaCl_2$, $Ca(NO_3)_2$ and $Ca(ClO_4)_2$ respectively with sodium hydroxide. This NaOH can be regenerated up to 90% and utilized again for digestion of perlite [2]. The dried calcium salts can be either calcined to get CaO or can be as such sold for value added applications.

2.7   Conclusion

In the present work, a simple chemical process is described which uses a non-conventional raw material, perlite for extraction of silica. A rapid, environmentally benign, and low-energy method has been developed to precipitate silica from perlite by alkali solubilization and subsequent acid treatment. Prior to characterization of precipitated silica, physico-chemical characteristics of substrate (perlite) are also studied. The amorphous nature of perlite and precipitated silica are clearly visible via XRD, FT-IR, SEM and TEM results. UV-Vis DRS results also confirm the presence of amorphous silica skeleton in all samples. The properties of precipitated SiO_2 depend strongly on the conditions of its synthesis, such as the synthesis temperature, time of precipitation, pH, NaOH concentration and modes of pre-washing, washing and drying. These factors influence the yield%, size of the SiO_2 particles, their aggregation and specific surface area. The optimization of the synthesis factors is achieved, so that precipitated SiO_2 with higher specific surface area, produced as described in the present work can be used for further academic investigations, and also as a valuable commercial product. The comparison of precipitated silica with commercial silica gel demonstrates that certain physical and chemical properties

of precipitated silica are similar to commercial silica gel. This low energy method could be more cost effective compared to the conventional smelting method. Perlite can be a cost-effective raw material for silica production because amorphous silica content of perlite can easily be dissolved in sodium hydroxide solution. This process not only alleviates the problems associated with perlite waste disposal but also generates a higher profit margin, value-added product creating a profitable new industry in developing country like India.

2.8   References

[1]   F. Ghorbani, H. Younesi, Z. Mehraban, M.S. C, A.A. Ghoreyshi, M. Anbia, J. Taiwan Inst. Chem. Eng. 44 (2013) 821.

[2]   N.K.S.R. D.N. Subbukrishna, K.C. Suresh, P.J. Paul, S. Dasappa, in:, 15th Eur. Biomass Conf. Exhib., 2007, pp. 2091–2093.

[3]   S.R. Kamath, A. Proctor, Cereal Chem. 75 (1998) 3.

[4]   R. Prasad, M. Pandey, Bull. Chem. React. Engg. Catal. 7 (2012).

[5]   Y. Yaacob, S.Z. Saad, M.R. Othman, N.S.M. Noor, in:, Malaysia Polym. Int. Conf., 2009, pp. 395–401.

[6]   M. Mansha, S.H. Javed, M. Kazmi, N. Feroze, Adv. Chem. Eng. Sci. 1 (2011) 147.

[7]   D. Singh, R. Kumar, A. Kumar, K.N. Rai, M.S. Programme, M. Engineering, Ceramica 54 (2008) 203.

[8]   P. Lu, Y. Hsieh, Powder Technol. 225 (2012) 149.

[9]   U. Kalapathy, A. Proctor, J. Shultz, Bioresour. Technol. 73 (2000) 257.

[10]   A.S. Dorcheh, M.H. Abbasi, J. Mater. Process. Technol. 199 (2008) 10.

[11]   H. Sahabi, M. Kind, Polymers (Basel). 3 (2011) 2156.

[12]   R. Ranjan, Surface Modification of Silica Nanoparticles, 2008.

[13]   G. Gao, H. Zou, S. Gan, Z. Liu, B. An, J. Xu, G. Li, Powder Technol. 191 (2009) 47.

[14]   J. Andas, I.A.R. Adam, Farook, Appl. Surf. Sci. 284 (2013) 503.

[15]   M.K. Dongare, V. V Bhagwat, C. V Ramana, M.K. Gurjar, Tet. Lett. 45 (2004) 4759.

[16]   K. Kordatos, S. Gavela, A. Ntziouni, K.N. Pistiolas, A. Kyritsi, V.K. Rigopolou, Micropor. Mesopor. Mater. 115 (2008) 189.

[17] S.B. R. Ghosh, Chmeical Eng. Process Technol. 4 (2013).

[18] V.B. Carmona, R.M. Oliveira, W.T.L. Silva, L.H.C. Mattoso, J.M. Marconcini, Ind. Crop. Prod. 43 (2013) 291.

[19] H.J.H.B. G. Quercia, in:, 8th Fib PhD Symp. Kgs. Lyngby, Denmark, 2010.

[20] T. B. Kurck, Jesionowski, A. Krysztafkiewicz, Physicochem. Probl. Miner. Process. 42 (2008) 67.

[21] J.P. Nayak, J. Bera, Trans. Ind. Ceram. Soc. 68 (2009) 1.

[22] X. Ma, B. Zhou, W. Gao, Y. Qu, L. Wang, Z. Wang, Y. Zhu, Powder Technol. 217 (2012) 497.

[23] K. Amutha, R. Ravibaskar, G. Sivakumar, Int. J. Nanotechnol. Appl. 4 (2010) 61.

[24] E.L. Foletto, E. Gratieri, L.H. De Oliveira, S.L. Jahn, S.M. Rs, Mater. Res. 9 (2006) 335.

[25] J.S. Choi, D.J. Kim, S.H. Chang, W.S. Ahn, Appl. Catal. A: Gen. 254 (2003) 225.

[26] M. Alvaro, A. Corma, D. Das, V. Fornés, H. García, J. Catal. 231 (2005) 48.

[27] T. Jiang, J. Cheng, W. Liu, L. Fu, X. Zhou, Q. Zhao, H. Yin, J. Solid State Chem. 218 (2014) 71.

[28] Q. Zhao, Y. Shen, Q. Wang, J. Tian, X. Zhou, T. Jiang, Chem. Eng. J. 230 (2013) 124.

[29] D. Zuo, J. Lane, D. Culy, M. Schultz, A. Pullar, M. Waxman, Appl. Catal. B: Environ. 129 (2013) 342.

[30] A. Sarı, A. Karaipekli, C. Alkan, Chem. Eng. J. 155 (2009) 899.

[31] D. Bastani, a. a. Safekordi, a. Alihosseini, V. Taghikhani, Sep. Purif. Technol. 52 (2006) 295.

[32] M. Gürtürk, H.F. Oztop, A. Hepbaslı, Energy Convers. Manag. 75 (2013) 488.

[33] N. Zhang, Y. Yuan, Y. Yuan, T. Li, X. Cao, Energy Build. 82 (2014) 505.

[34] M. Alkan, M. Do, J. Colloid Interface Sci. 243 (2001) 280.

[35] O. Sengul, S. Azizi, F. Karaosmanoglu, M. Ali, Energy Build. 43 (2011) 671.

[36] A. Silber, B.Y. B, S. Suryano, I. Levkovitch, Geoderma 170 (2012) 159.

[37] A.U.S. S.T. Erdogan, Cem. Concr. Compos. 38 (2013) 29.

[38] P. Wang, B. Shen, J. Gao, Catal. Today 125 (2007) 155.

[39] J.M. Fox, in:, 2005 World Coal Ash, 2005.

[40] B.M. Reddy, G.K. Reddy, K.N. Rao, A. Khan, I. Ganesh, J. Mol. Catal. A: Chem. 265 (2007) 276.

[41] M.M. Abou-sekkina, Int. J. Chem. 2 (2010) 81.

[42] S. Kabra, S. Katara, A. Rani, Int. J. Innov. Res. Sci. Eng. Technol. 2 (2013) 4319.

[43] C.M. Ana Maria de Sousa, Leila Visconte, and C. Furtado, Chem. Chem. Technol. 3 (2009).

[44] R.H. and A.R. Sakshi Kabra, Anita Sharma, Stuti Katara, Indian J. Appl. Res. 3 (2013) 40.

[45] D. Jain, M. Mishra, A. Rani, Fuel Process. Technol. 95 (2012) 119.

[46] F. Adam, S. Balakrishnan, P. Wong, J. Phys. Sci. 17 (2006) 1.

[47] B.J. Saikia, G. Parthasarathy, J. Mod. Phys. 1 (2010) 206.

[48] K. Genov, V. Georgiev, T. Batakliev, D.K. Sarker, World Acad. Sci. Eng. Technol. 80 (2011) 202.

[49] A.W. Bhuiyan, R.R. Mojumdar, A.K.M.K. Hasan, Int. J. Environ. Sci. Dev. 2 (2011) 299.

[50] T. Liou, C. Yang, Mater. Sci. Eng. B 176 (2011) 521.

[51] C.R.P. C.H. Yun, Y.H. Park, G.H. Oh, Carbon N. Y. 41 (2003) 2009.

[52] L.S. S. Music, N.F. Vincekovic, Brazilian J. Chem. Eng. 28 (2011) 89.

[53] R.O.S. Enobong R. Essien, Oluyemi A. Olaniyi, Luqman A. Adams, J. Miner. Mater. Charact. Eng. 11 (2012) 976.

[54] M. Musi , S., Risti , M., Tonkovi , Z. Wasser, Abwasser-Forsh. 19 (1986) 186.

[55] C. Lin, S.A. Al-muhtaseb, J.A. Ritter, J. Sol-Gel Sci. Technol. 28 (2003) 133.

[56] E. Rafiee, S. Shahebrahimi, M. Feyzi, M. Shaterzadeh, Int. Nano Lett. 2 (2012) 1.

[57] S. Affandi, H. Setyawan, S. Winardi, A. Purwanto, R. Balgis, Adv. Powder Technol. 20 (2009) 468.

Synthesis of Perlite Supported Nickel Catalysts, their Characterization and Application in Claisen-Schmidt Condensation Reaction

Abstract

Potentially active, eco-friendly, innovative solid acid catalysts have been synthesized by loading various weight fractions of nickel on thermally activated perlite through deposition-precipitation method. The physico-chemical properties of prepared catalysts are analyzed using BET surface area analysis, XRD, FT-IR, SEM, SEM-EDX, TEM, TGA-DSC and UV-Vis DRS techniques. Brønsted acidic sites in catalysts as confirmed by pyridine adsorbed FT-IR analysis are utilized for catalyzing condensation of cyclohexanone and benzaldehyde giving higher conversion (92%), selectivity (99%) and yield (90%) of desired product 2, 6- bis (benzylidene) cyclohexanone, used in anti-tumor and cytotoxic activities. Effect of reaction parameters like reaction temperature and time, molar ratio of reactants and substrate/catalyst weight ratio on conversion, selectivity and yield% of product are also studied. The catalyst is regenerated and reused up to six reaction cycles with almost equal efficiency. This application recommends perlite as a novel siliceous support for generating solid acid catalysts.

3.1   Introduction

Acid catalysis is an important area of organic synthesis and of vital industrial significance predominantly in petrochemical, fine chemical and pharmaceutical industries [1]. Homogeneous acids such as H_2SO_4, CH_3SO_3H, $AlCl_3$, $SnCl_2$, etc. are commercially used as catalysts in various organic reactions including esterification [2], isomerisation [3], alkylation [4], benzylation [5], condensation [6], etc. However, the use of homogeneous acid catalysts has some intrinsic drawbacks such as their difficult separation, tedious washing, corrosive nature, lower selectivity of desired products etc. The principles of green chemistry and increasing concerns about environmental issues have stimulated the research for recyclable strong solid acids to replace conventional, toxic, homogeneous acid catalysts. Heterogeneous catalysts such as silicotungstic acid, H_2SO_4-SiO_2 [7], sulfamic acid [8], silica-sulfuric acid [9], ruthenium trichloride [10] are being used as a replacement of homogeneous acids in condensation reactions.

Nickel based catalysts supported on different substrates like silica, alumina, zirconia, zeolites have attracted research attentions because of their potential applications in many important reactions such as hydrogenation [11], diesel steam reforming [12], CO_2 reforming [13], dry reforming of methane [14] etc., while less records are found for its application in condensation reactions [15]. Catalyst support is vital as it facilitates higher dispersion of nickel oxide and prevents aggregation of its particles [16] which in turn enhances efficiency of catalyst and thus, maximum conversion and yield% of desired products is achieved. As a lucrative alternative to these expensive classical supports, coal generated solid waste, fly ash has been reported to synthesize many effective solid acid catalysts [17–21]. With the increasing social interests over environmental degradation and future resources, it is of great importance for chemists to come up with new approaches that are less hazardous to human health and environment. In this series, we have tried to explore stable surface active sites of a novel silica-alumina enriched natural waste- perlite and its efficiency as a catalyst support. Application of perlite as heterogeneous catalyst is not much explored in past except only few earlier reports [22,23].

The present chapter reports the synthesis, characterization and application of perlite supported nickel catalysts, prepared by loading of nickel on thermally activated perlite. The prepared NPC-15 catalyst has found to be effectively recyclable up to six reaction cycles giving higher conversion (92%) and yield (90%) with good selectivity (99%) of desired product, 2,6- bis (benzylidene) cyclohexanone, used for anti-tumor and cytotoxic activities [24] and also an important precursor for synthesis of potentially bioactive pyrimidine derivatives [25,26]. The product is also used as intermediates in perfumes, pharmaceuticals and agro-chemicals [27]. The reaction is carried out in single step, solvent free reaction conditions. Effect of various reaction parameters on yield of products are also studied during the course of the reaction. The study provides an innovative use of abundant waste, perlite in area of heterogeneous catalysis and also imparts an alternate cost-effective route for the substitution of corrosive homogeneous and expensive heterogeneous acid catalysts used in the synthesis of 2,6- bis (benzylidene) cyclohexanone.

3.2   Experimental

3.2.1 Materials

Nickel nitrate, sodium hydroxide, dimethyl glyoxime (DMG), cyclohexanone and benzaldehyde are purchased from Sigma Aldrich. Perlite is supplied by Indica Chem. Ind. Pvt. Ltd., India.

3.2.2 Catalyst preparation

As received perlite is initially activated thermally at 800°C for 3 h to remove excess water, carbon and other impurities [28] and converted into thermally activated perlite (TAP). All the catalysts investigated in this study (NPC-10, 15 and 50) are synthesized by loading 10, 15 and 50 wt% nickel on TAP by deposition-precipitation method. The requisite amounts (1.97 g for 10 wt%, 2.95 g for 15 wt%, 9.83 g for 50 wt%) of precursor salt (nickel nitrate) dissolved in distilled water are added to 5 g of TAP. The resultant slurry is stirred for 12 h at room temperature to obtain homogeneity. Subsequently, the homogenized slurry is titrated with aqueous NaOH solution until pH = 9-10 is

attained. Thus formed precipitated gel is filtered, washed several times up to neutral pH, dried at 110°C for 12 h and then calcined in static air at 450°C for 4 h. The negative results of DMG tests confirm that no nickel ions leached off from the catalysts during their synthesis [29]. The steps for synthesis of nickel perlite catalysts (NPC) are given in **Scheme 3.1**.

3.2.3 Catalyst characterization

Physicochemical properties of all catalytic materials are studied by N_2 adsorption-desorption, XRD, FT-IR and pyridine adsorbed FT-IR, SEM, SEM-EDX, TEM, TGA-DSC and UV-Vis DRS techniques, as described in **Annexure-I**.

3.2.4 Catalytic activity

Claisen-Schmidt condensation between cyclohexanone and benzaldehyde catalyzed by NPC-10, 15 and 50 to give 2,6- bis (benzylidene) cyclohexanone is performed in a liquid phase batch reactor comprising of 250 ml round bottom flask equipped with digital magnetic stirrer and spiral glass condenser, immersed in a constant temperature oil bath. In this procedure, a mixture of cyclohexanone and benzaldehyde (different molar ratios) is taken in round bottom flask. The varying amounts of catalyst activated at 450°C for 2 h, is then added to the reaction mixture. The reaction is carried out at different molar ratio of substrates at different temperatures ranging from 120-170°C for time in the range of 30 to 180 minutes. After completion of the reaction the catalyst is separated and the product is analyzed by Gas Chromatograph.

The conversion% of cyclohexanone is calculated by following method-

$$\text{Conversion (\%)} = 100 \text{ X } \frac{(\text{Initial wt \% - Final wt \%})}{\text{Initial wt \%}}$$

The yield% of 2, 6- bis (benzylidene) cyclohexanone is calculated by using following weight percent method-

$$\text{\% yield of product obtained} = 100 \text{ X } \frac{\text{g of product obtained experimentally}}{\text{g of product btained theoretically}}$$

As received perlirte → Thermal activation of perlite at 800°C for 3 h (TAP) → **Deposition-precipitation method**

Dissolution of requisite amount of nickel nitrate (10, 15 and 50 wt%) in distilled water

Stirring of resultant slurry at room temperature for 12 h

Titration of slurry with aqueous NaOH solution until pH = 9-10

Addition of above solution to 5 g TAP

Drying at 110°C for 12 h → Calcination in static air at 450°C for 4 h

Filtration of precipitated gel and washing with distilled water up to neutral pH

Nickel perlite catalyst (NPC-10, 15 and 50)

Scheme 3.1: Synthesis of nickel perlite catalysts (NPC).

Catalytic activities of catalysts are tested by Claisen-Schmidt condensation between cyclohexanone and benzaldehyde in solvent-free, liquid phase reaction conditions as shown in **Scheme 3.2**.
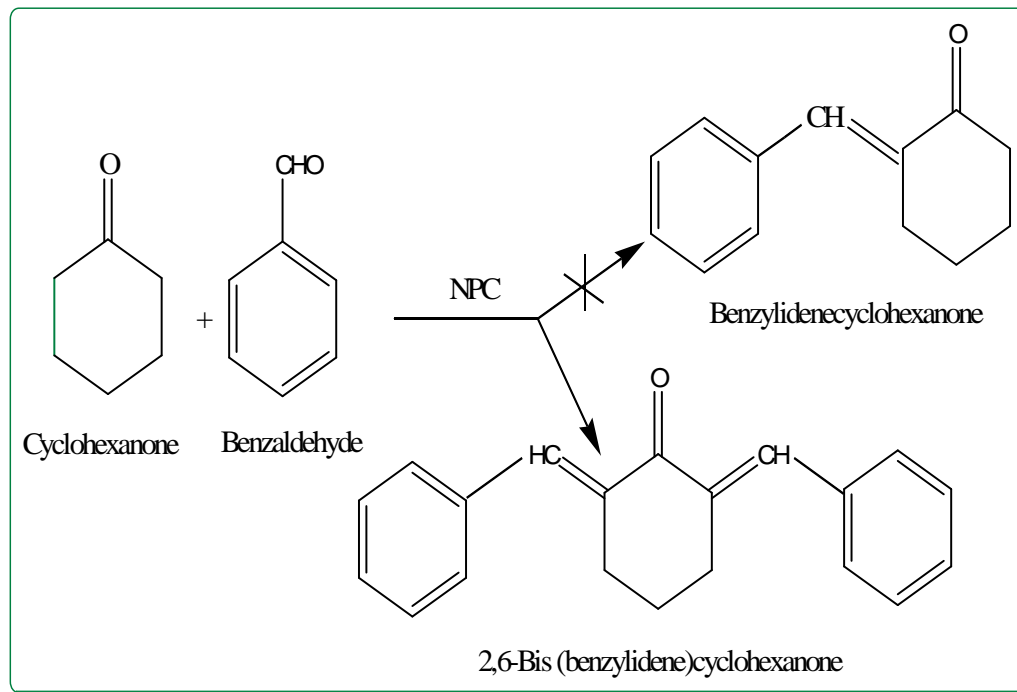
Scheme 3.2: **Simplified reaction pathway of condensation of cyclohexanone and benzaldehyde over NPC to give 2,6- bis (benzylidene) cyclohexanone.**

3.3   Results and discussion

3.3.1 BET analysis

BET specific surface area of samples as given in **Table 3.1** indicates that with increasing loading of nickel content from 10 to 50 wt%, the specific surface area of catalysts decreases, probably due to blockage of perlite pores by NiO particles [30,31].

Table 3.1: **BET specific surface area data of samples.**

Samples	BET specific surface area (m^2/g)
Perlite	2.3
NPC-10	2.2
NPC-15	1.9
NPC-50	1.1

3.3.2 X-ray diffraction analysis

The broad X-ray diffraction pattern of perlite **(Figure 3.1a)**, confirmed the absence of any ordered crystalline structure [32]. However, in TAP, a single, small crystalline peak appears at 2 = 27.642° **(Figure 3.1b)** which shows formation of quartz crystalline phase in the sample [33] along with a broad hump at 2 = 22-23° confirming amorphous nature of silica [34,35]. The absence of crystalline peaks in X-ray diffraction patterns of NPC-10 and 15 **(Figure 3.1c** and **d)** is due to the fact that in the lower weight fraction catalysts, nickel oxide particles remain dispersed on perlite surface in amorphous phase and more likely too small in size to give a XRD peak [36]. While, in case of NPC-50 **(Figure 3.1e)**, small humps begin to appear at 2 = 37.26, 43.29, 62.88° corresponding to Miller indices [003], [012] and a combination of the [104] and [110] reflections of NiO, respectively [37] which are evident of formation of Ni-O phase in the sample. However, because of the weak, broad, and partially overlapping peaks, the crystallite size determination of the Ni containing phase is difficult in NPC-50 [38].
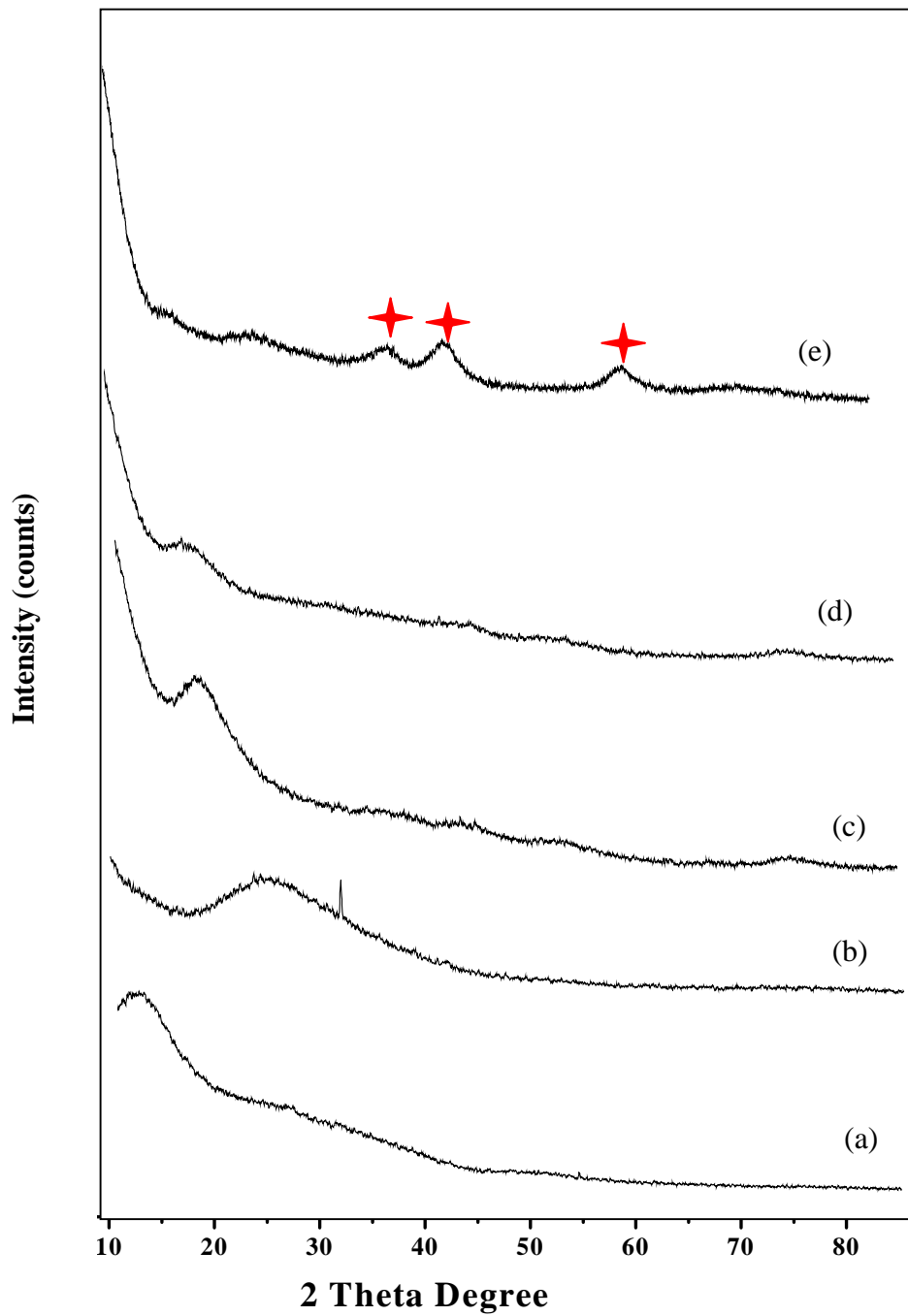
Figure 3.1: **X-ray diffraction pattern of (a) perlite, (b) TAP, (c) NPC-10, (d) NPC-15 and (e) NPC-50.**

3.3.3 *Fourier transform infra-red analysis (FT-IR)*

FT-IR spectrum of perlite **(Figure 3.2a)** shows a broad band between 3600-3300 cm^{-1}, which is attributed to surface hydroxyl groups of –Si-OH and water molecules adsorbed on the surface [39]. The broadness of band indicates the presence of strong hydrogen bonding [40] while in FT-IR spectrum of TAP **(Figure 3.2b)**, the intensity and broadness of band decreases which confirms the loss of water during thermal treatment. The strong band appearing at 1178 cm^{-1}, due to structural siloxane framework, is attributed to the asymmetric vibrational frequency of Si-O-Si bond. The peak gets shifted to 1227 cm^{-1} after thermal treatment, normally observed in amorphous silica samples [41]. An intense peak around 1630 cm^{-1} in perlite, characteristic of bending mode ($_{O-H}$) of water molecule [42,43] is again highly decreased in case of TAP.

While loading of nickel on perlite, the surface gets activated through hydroxyl groups as aqueous NaOH is used during catalyst preparation. The FT-IR spectra of NPC-10,15 and 50 **(Figure 3.3)** show increase in broadness and peak intensity of the band attributed to –OH groups. A new band appeared around 1050 cm^{-1} can be assigned to $\equiv$Si – O – Ni stretching vibration [11] which is normally observed in the range of 1000 – 1100 cm^{-1} but cannot be resolved because of its overlap with the absorbance of Si – O – Si stretching, appearing in 1300-1000 cm^{-1} range. The band at about 964 cm^{-1} may be attributed to the stretching vibrations of surface Si–O–Ni [44] and its intensity is slightly increased after increasing nickel incorporation. The results imply that the interactions between the surface silanols and nickel species are present in the catalysts.

3.3.4 *Pyridine adsorbed FT-IR analysis of catalysts*

The FT-IR spectra of NPC-10, 15 and 50, obtained after pyridine adsorption in the range of 1550-1400 cm^{-1} is shown in **Figure 3.4**. The band at 1538 cm^{-1} **(Figure 3.4a)** indicates the presence of few Brønsted acidic sites in NPC-10. In NPC-15 **(Figure 3.4b)**, broad bands appearing at 1438 and 1540 cm^{-1} respectively [45–47] show existence of some Lewis and optimal Brønsted acidic sites for suitable catalytic activity. NPC-50 has maximum Lewis acidic sites corroborated by appearance of intense bands at 1438 and 1450 cm^{-1} **(Figure 3.4c)**.
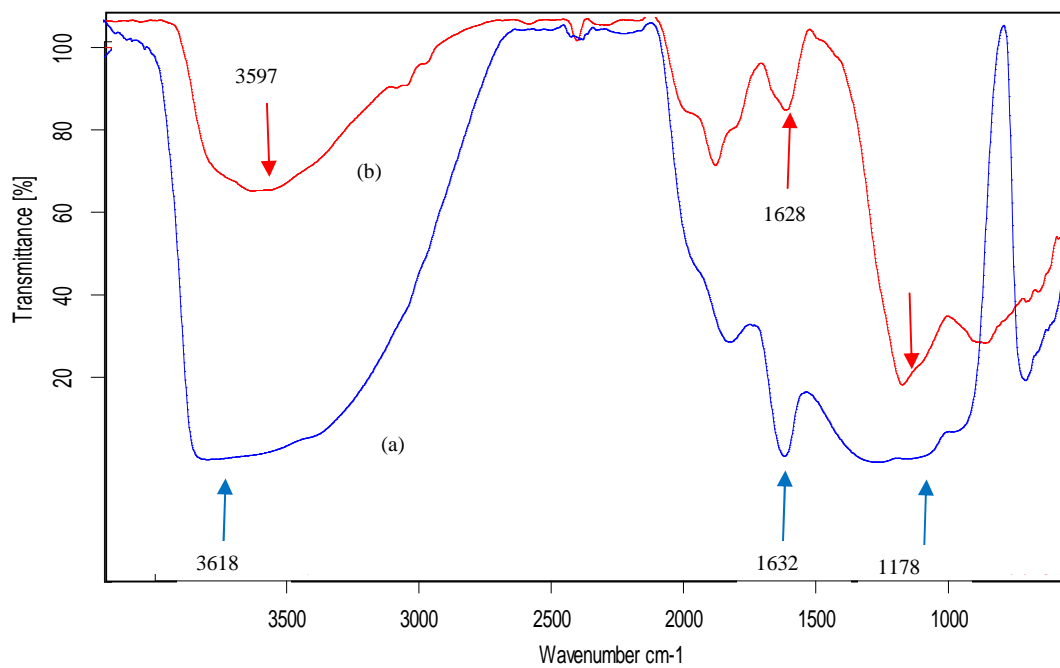
Figure 3.2: **FT-IR spectra of (a) perlite and (b) TAP.**
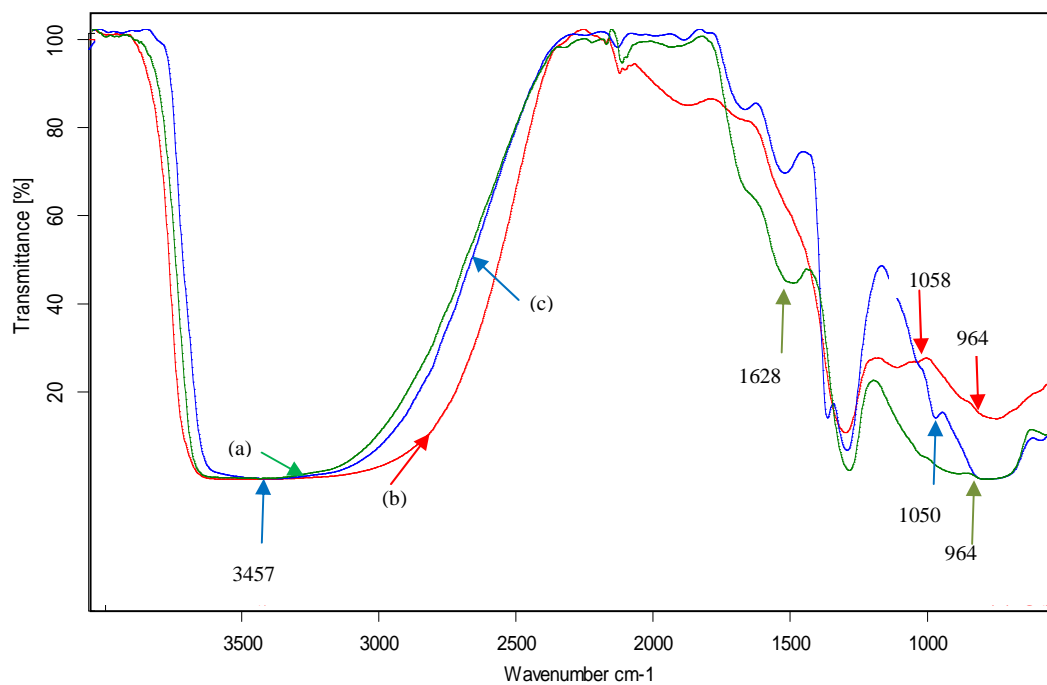
Figure 3.3: **FT-IR spectra of (a) NPC-10, (b) NPC-15 and (c) NPC-50.**
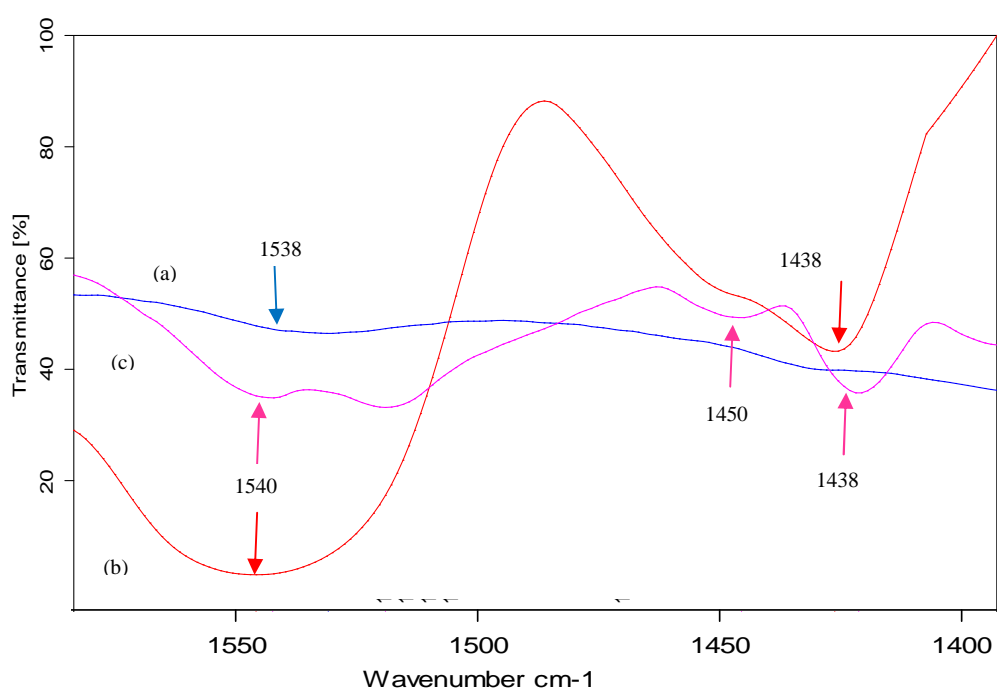
Figure 3.4: **Pyridine adsorbed FT-IR spectra of (a) NPC-10, (b) NPC-15 and (c) NPC-50.**

3.3.5 Scanning electron microscopy (SEM and SEM-EDX analysis)

SEM micrograph of perlite **(Figure 3.5a)** revealed irregular morphology of perlite particles with broken or ragged edges, also observed in other reported micrographs of perlite [48,49]. SEM image of TAP **(Figure 3.5b)** is mainly fragmatic and random [50] but the morphology is less irregular which suggests the evaporation of water from the sample on heating at high temperature. SEM images of NPC-10, 15 and 50 **(Figure 3.5c, d and e)** demonstrates dispersion of shiny, fine nickel oxide particles on surface of perlite.

EDX analysis of perlite, NPC-10, 15 and 50 **(Table 3.2)** shows the presence of SiO_2, Al_2O_3, K_2O, Na_2O and other minor metal oxides in the samples. However, the presence of nickel oxide in all NPC samples confirms its loading on perlite surface.

Table 3.2:   EDX analysis of perlite, NPC-10, 15 and 50.

Samples	SiO_2 (wt%)	Al_2O_3 (wt%)	K_2O (wt%)	Na_2O (wt%)	ZnO (wt%)	FeO (wt%)	NiO (wt%)	LOI
Perlite	72.74	14.79	7.48	2.10	2.04	0.91	-	4.1
NPC-10	71.09	12.14	5.68	1.86	-	-	8.42	1.2
NPC-15	67.40	11.69	5.24	1.78	-	-	13.89	0.8
NPC-50	40.28	9.47	-	1.54	-	-	48.69	0.24

LOI- Loss on ignition

3.3.5 Transmission electron microscopy (TEM analysis)

A more realistic vision of irregular morphology of perlite can be furnished by TEM image **(Figure 3.6a)**. The micrograph of NPC-15 **(Figure 3.6b)** shows fine dispersion of nickel oxide particles on perlite surface. The results are in agreement with SEM images. Particle size of nickel oxide could not be measured because of its finer dispersion on the support.
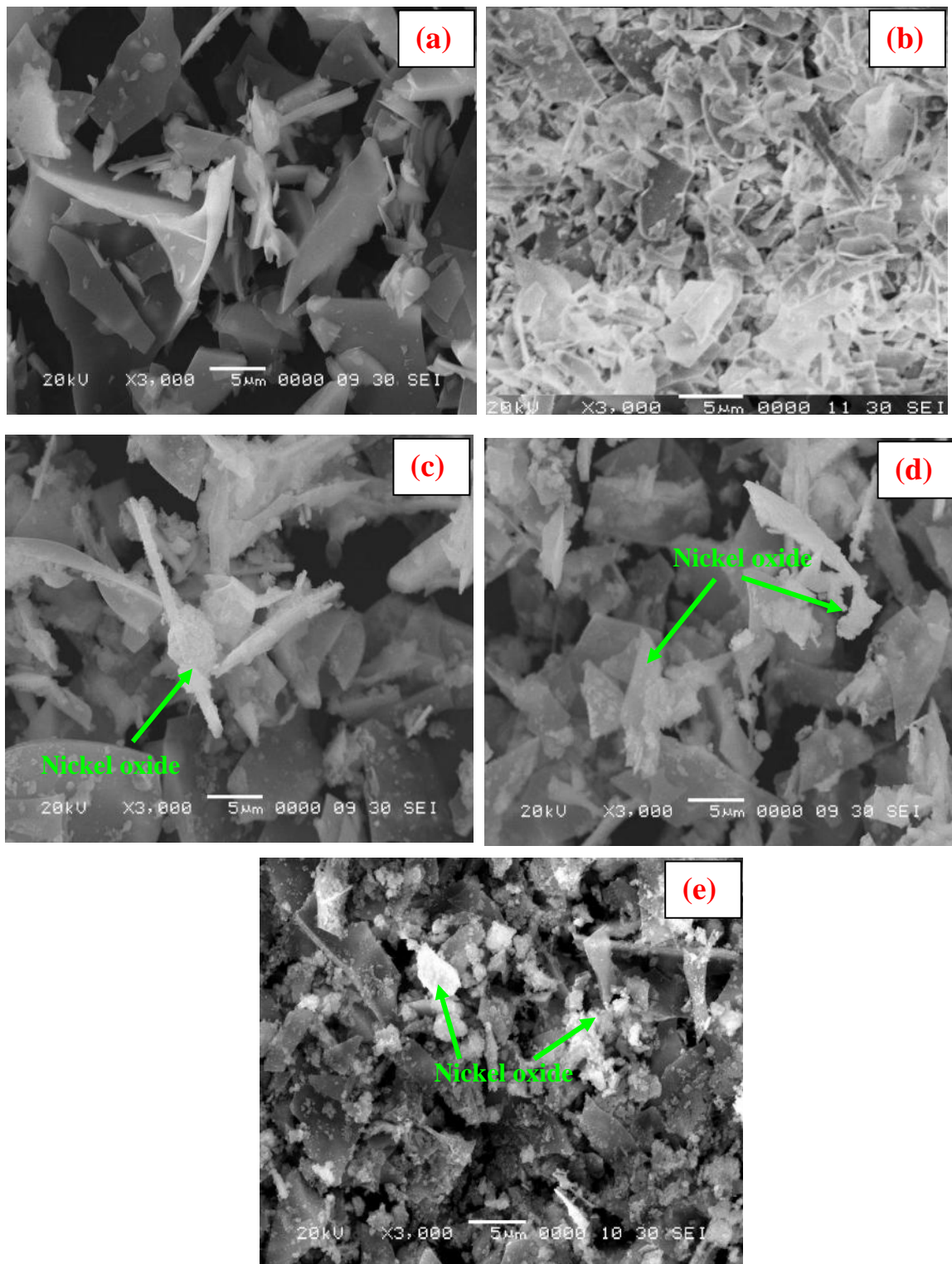
Figure 3.5: **SEM micrographs of (a) perlite, (b) TAP, (c) NPC-10, (d) NPC-15 and (e) NPC-50.**
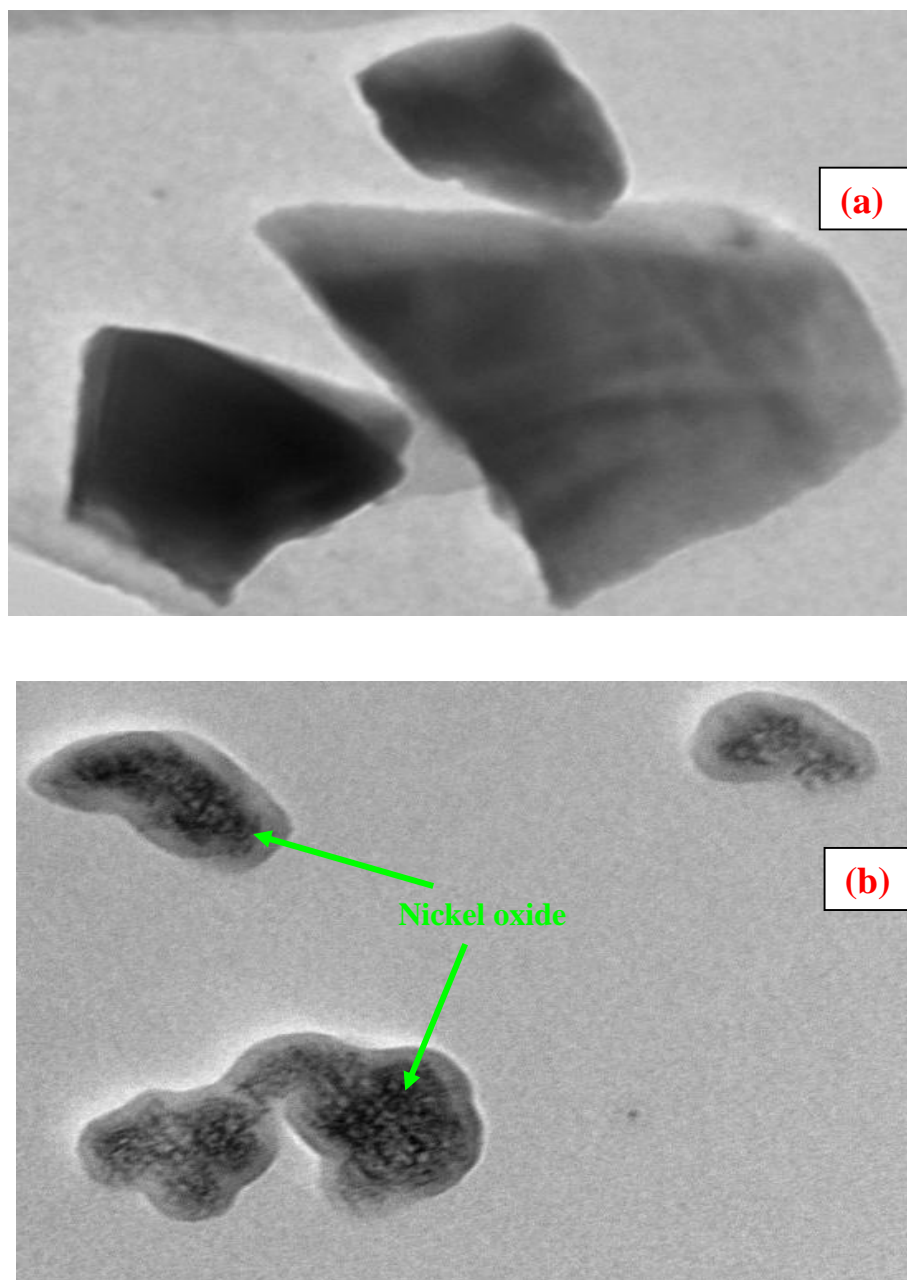
Figure 3.6: **TEM micrographs of (a) perlite and (b) NPC-15.**

3.3.6 Thermal analysis (TGA-DSC)

The TGA and DSC curve of NPC-15 **(Figure 3.7)** comprises of two main regions having a major weight loss of about 8.96% up to 643.83°C and a minor one of approximately 0.82% at higher temperature along with an exothermic DSC band. The weight loss in first region could be due to removal of bulk water, physisorbed water and loosely bound hydroxyl groups [51] and decomposition of nickel precursor entrapped in the pores of the support [52]. The second region exhibits only a slight weight loss probably due to further removal of chemisorbed water through decomposition of $Ni(OH)_2$ into NiO.
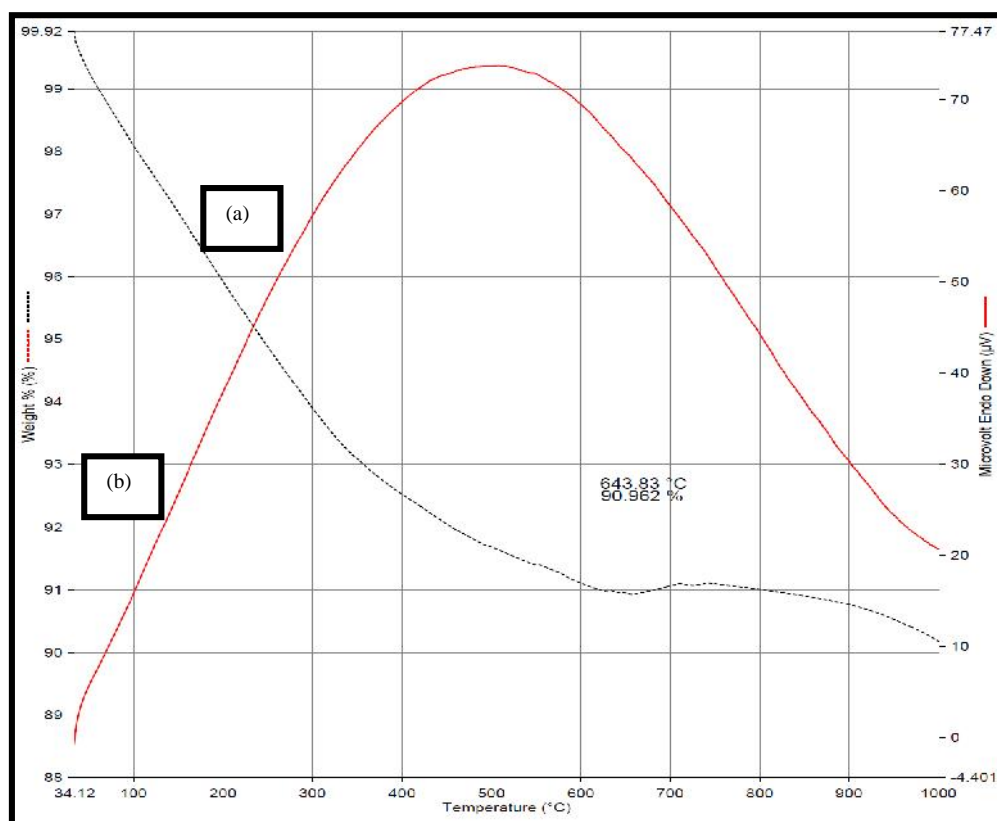
Figure 3.7: **(a) TGA and (b) DSC curves of NPC-15.**

3.3.7 *Ultra violet-Visible Diffuse Reflectance spectroscopy (UV-Vis analysis)*

UV–Vis DRS is a sensitive tool that has been widely used to detect the presence of framework or extra-framework active species that are incorporated into the mesoporous materials. Here, it is used to determine the state of nickel species incorporated into silica frameworks of perlite. During steps of synthesis, due to calcination of catalysts at 450°C for 4 h, the presence of $Ni(OH)_2$ can be ruled out. A broad band around 250 nm **(Figure 3.8)** which becomes more intense with increase in weight% of nickel loading suggests that Ni^{+2} ions are in octahedral local environment [53].
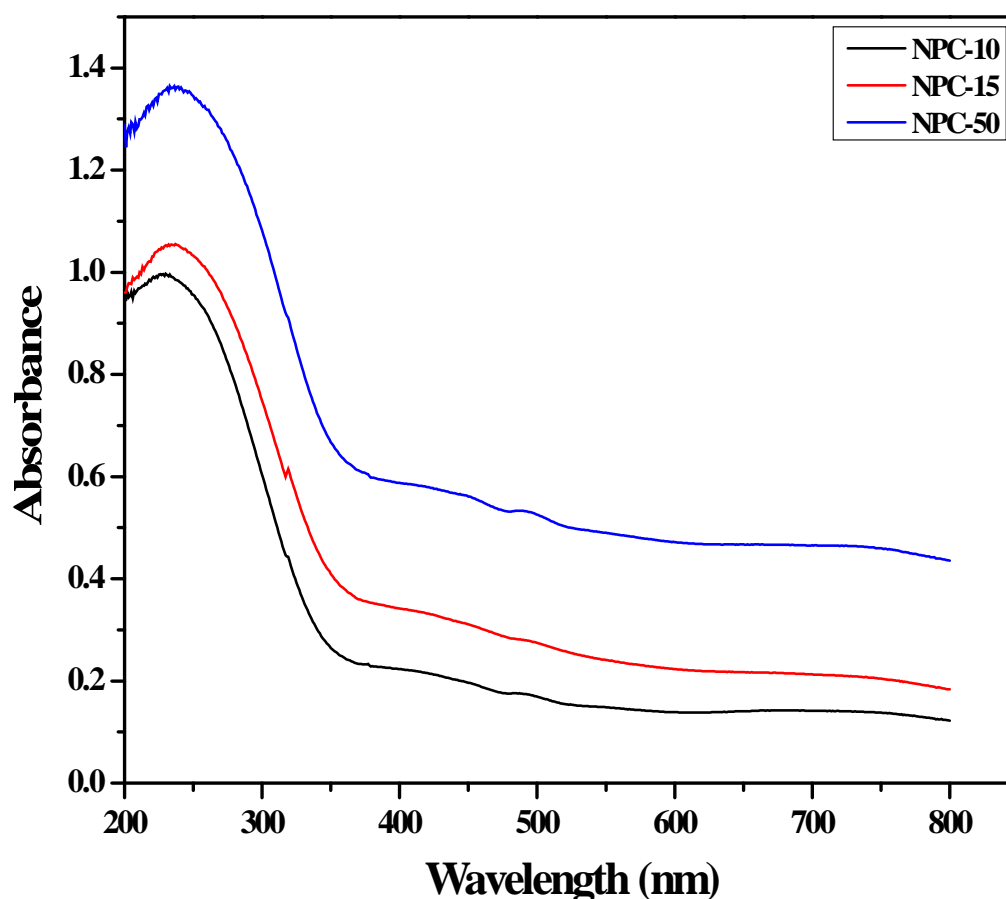
Figure 3.8: **UV-Vis DRS spectra of NPC-10, 15 and 50.**

3.4 Catalytic performance

The catalytic performance is tested by Claisen-Schmidt condensation reaction of cyclehexanone and benzaldehyde to give 2, 6- bis (benzylidene) cyclohexanone in single step, one-pot reaction conditions. Reaction is carried out at 120°C for 120 minutes, taking cyclohexanone/benzaldehyde molar ratio of 1:2 and cyclohexanone to catalyst weight ratio of 5:1. Results given in **Table 3.3** show that perlite, TAP and pure NiO do not possess any catalytic activity for this reaction. In case of NPC-10, less selectivity (56%) for desired product is obtained at lower conversion% (78%) due to presence of less Brønsted acid sites on catalytic surface while in the presence of NPC-15, the conversion, selectivity and yield% is highest due to significant increment of active sites. The conversion, selectivity and yield% are again decreased on using NPC-50 due to blockage of surface active Brønsted acidic sites by bulk deposition of NiO crystallites.

Table 3.3: **Catalytic activity of different catalysts for Claisen-Schmidt condensation reaction.**

Catalysts	Conversion% of cyclohexanone	Selectivity (%)	Yield (%)
Perlite	Nil	Nil	Nil
TAP	Nil	Nil	Nil
Pure NiO	Nil	Nil	Nil
NPC-10	78	56	58
NPC-15	88	95	80
NPC-50	72	42	48

Reaction conditions: Time = 120 minutes; Temperature = 120°C; molar ratio (cyclohexanone / benzaldehyde = 1:2); substrate/catalyst ratio = 5:1.

As suggested by these results, NPC-15 is chosen as the main catalyst for further optimization of reaction parameters such as effect of reaction temperature and time, molar ratio of reactants, substrate to catalyst ratio, in order to attain maximum conversion and yield% with better selectivity%.

3.4.1 Effect of reaction temperature

To optimize the reaction temperature giving maximum conversion, selectivity and yield%, reaction of cyclohexanone and benzaldehyde is studied at different temperatures ranging from 120 to 170°C for 150 minutes. The results illustrated that the conversion% of cyclehexanone gradually increases with increase in temperature as shown in **Figure 3.9**. The maximum conversion% of cyclohexanone (92%) is obtained at 150°C within 150 minutes along with higher selectivity (99%) and yield (90%) which get decreased on increasing temperature up to170°C due to formation of side products and at higher temperature, reactants remain in vapour phase, possessing less tendency to react with each other.
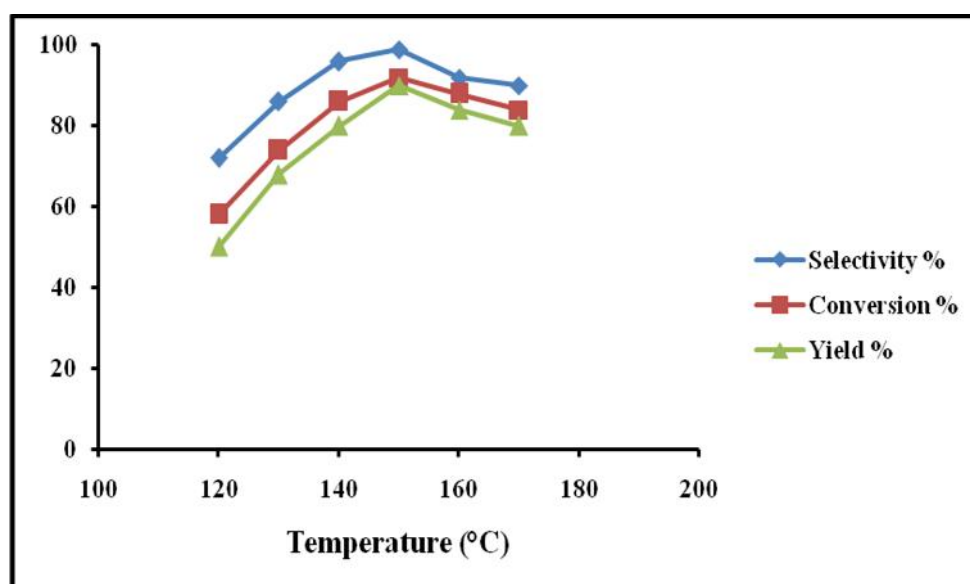
Figure 3.9:   Variation   of   conversion,   selectivity   and   yield%   of cyclohexanone over NPC-15 with temperature.

Reaction conditions: Time = 150 minutes; molar ratio (cyclohexanone / benzaldehyde = 1:2); substrate/catalyst ratio = 5:1.

3.4.2 Effect of reaction time

The optimization of reaction time is carried out at 150°C to achieve maximum conversion, selectivity and yield% of product in the range of 30 to 180 min as shown in **Figure 3.10**. It is found that in first 150 minutes, the conversion% increases linearly up to 92% which remained constant till 180 minutes giving highest selectivity (99%) of 2, 6- bis (benzylidene) cyclohexanone with 90% yield. On further increasing the reaction time, selectivity and yield%

decreases due to formation of side product, 2-benzylidene cyclohexanone because of enhancement of contact period of both reactants with each other.
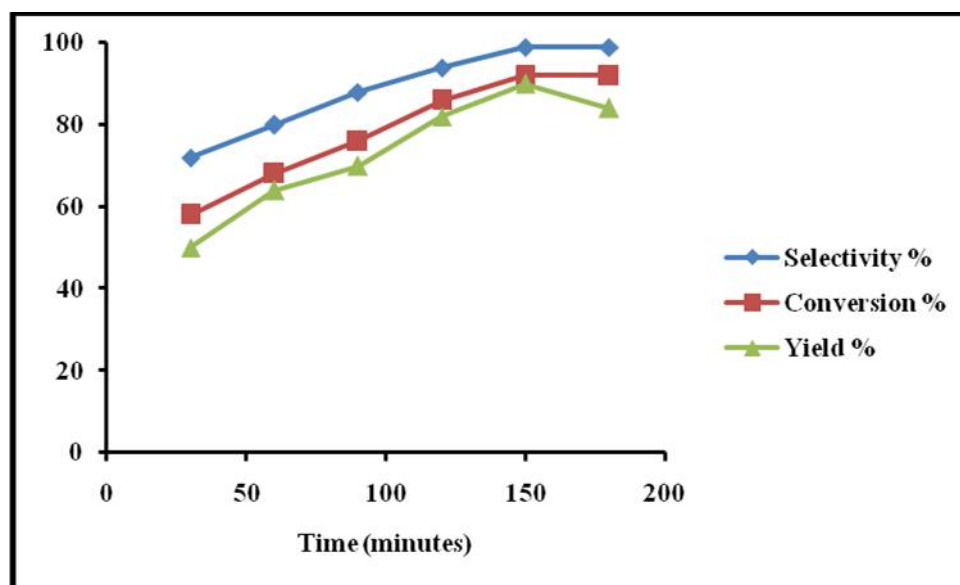
Figure 3.10: **Variation of conversion, selectivity and yield% of cyclohexanone over NPC-15 with time.**

Reaction conditions: Temperature = 150°C; molar ratio (cyclohexanone/ benzaldehyde = 1:2); substrate/catalyst ratio=5:1.

3.4.3 *Effect of molar ratio of reactants*

The effect of molar ratios of cyclohexanone and benzaldehyde on conversion and yield% is monitored at different molar ratios varying from 2:1 to 1:3 as given in **Table 3.4**. The conversion and yield% of cyclohexanone is found maximum (92 and 90%) respectively at 1:2 molar ratio as this could be the equilibrating of each reactant quantity on acidic sites of NPC. In case of other molar ratios, the amount of reactants was not sufficient to give higher conversion and yield%.

Table 3.4: **Effect of molar ratio of cyclohexanone/benzaldehyde on conversion and yield% over NPC-15.**

Molar ratio (cyclohexanone:benzaldehyde)	Conversion% of cyclohexanone	Yield%
2:1	58	48
1:1	76	62
1:2	92	90
1:3	66	62

Reaction conditions: Time = 150 minutes; Temperature = 150°C; substrate/catalyst ratio = 5:1.

3.4.4 Effect of substrate to catalyst weight ratio

The effect of substrate to catalyst weight ratio on conversion of cyclohexanone and yield% of product is studied by varying the amount of catalyst under optimized reaction conditions. As inferred from **Table 3.5**, it can be said that at on increasing catalytic amount, conversion and yield% increases. It can be attributed due to availability of enhanced number of catalytic active sites. On further increase in the amount of catalyst no significant change is observed.

Table 3.5: **Effect of substrate/catalyst weight ratio on conversion and yield% over NPC-15.**

Cyclohexanone/NPC weight ratio	Conversion% of cyclohexanone	Yield%
10:1	58	49
5:1	92	90
2.5:1	90	88

Reaction conditions: Time = 150 minutes; Temperature = 150°C; molar ratio (cyclohexanone/benzaldehyde = 1:2).

The maximum conversion (92%), selectivity (99%) and yield (90%) of product is found when reaction is carried out at 150°C for 150 minutes, taking cyclohexanone and benzaldehyde in 1:2 molar ratio and substrate to catalyst ratio of 5:1 over NPC-15.

3.4.5 Comparison with other reported catalysts

As depicted from **Table 3.6**, it can be said that NPC-15 gives higher yield% of 2, 6- bis (benzylidene) cyclohexanone than some previously reported catalysts.

Table 3.6: **A comparison of Claisen-Schmidt condensation reaction between cyclohexanone and benzaldehyde to give 2,6- bis (benzylidene) cyclohexanone over different types of solid acid catalysts.**

Catalysts	Yield %	References
SiO_2-R-SO_3H*	80	[54]
20% PW/N-SiO_2**	20	[55]
NPC-15***	90	This study

Reaction conditions:

* Time = 72 minutes; Temperature = 90°C; molar ratio (cyclohexanone/benzaldehyde = 1:2); catalyst weight =0.3g.

** Time = 30 minutes; Temperature = Room temperature; molar ratio (cyclohexanone/benzaldehyde = 1:2); catalyst weight =0.2g.

*** Time = 150 minutes; Temperature = 150°C; molar ratio (cyclohexanone/benzaldehyde = 1:2); catalyst weight =0.2g.

3.5 Mechanistic aspects

On the basis of results drawn from XRD, FT-IR, pyridine adsorbed FT-IR, UV-Vis DRS studies, models can be proposed for NPC-10, 15 and 50 catalysts **(Scheme 3.3)**. They show presence of Brønsted and Lewis acid sites on surface of catalysts. The possible pathway for the production of 2, 6- bis (benzylidene) cyclohexanone by condensation of cyclohexanone and benzaldehyde catalyzed by NPC is shown in **Scheme 3.4**. In first step, the surface Brønsted acidic sites of NPC-15 help in formation of intermediate from cyclohexanone. In next step, this intermediate in turn reacts with benzaldehyde to form desired condensation product and releases water as side product. In final step, proton is transferred to catalyst surface and the structure of catalyst remains intact.
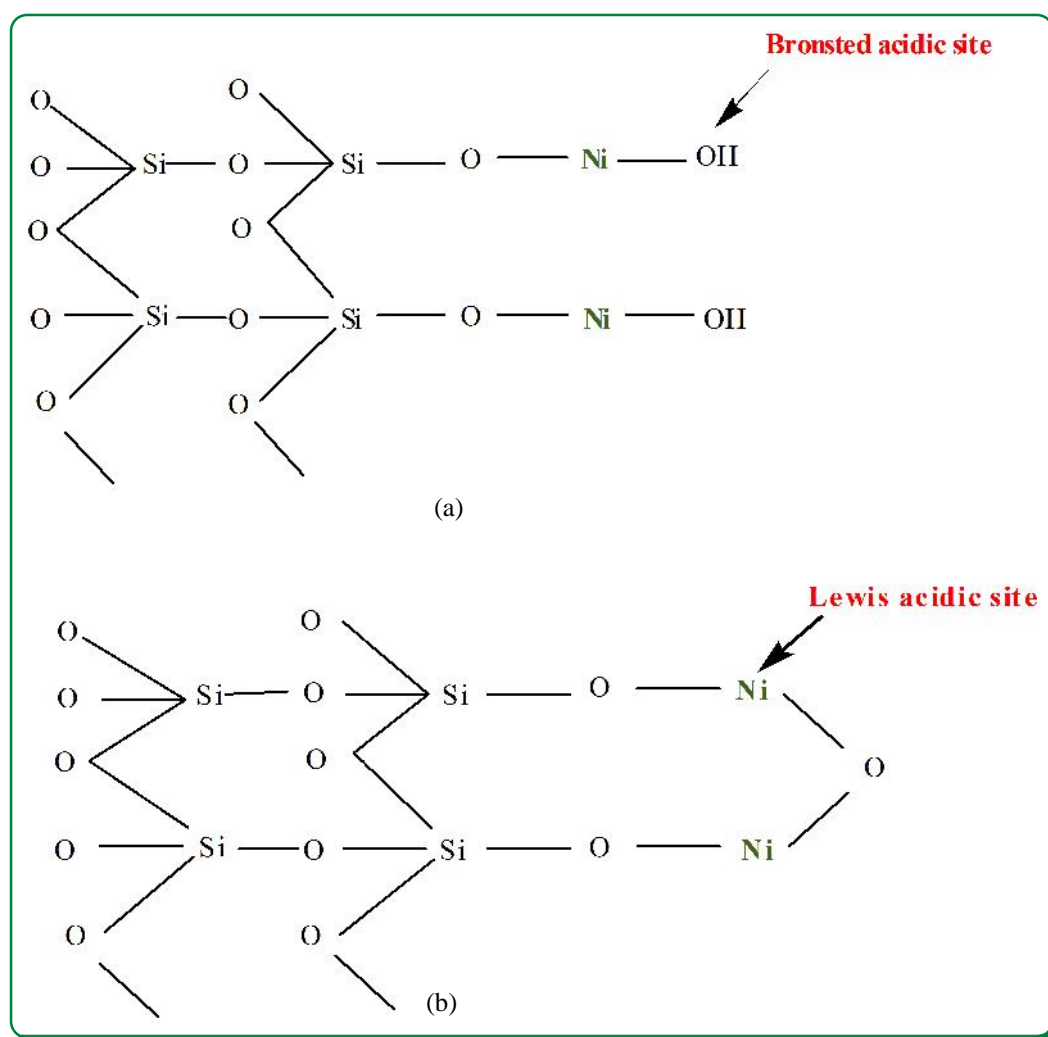
Scheme 3.3:   **Proposed models of (a) NPC-10, 15 and (b) NPC-50.**

Step- I
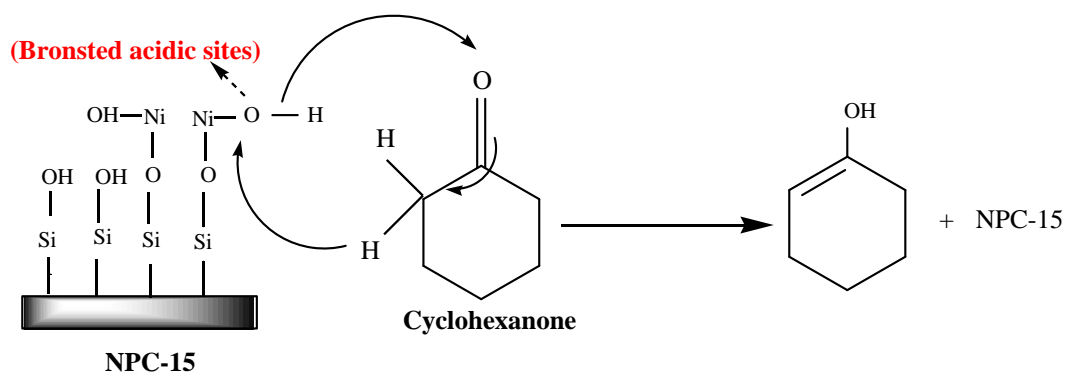
Step- II
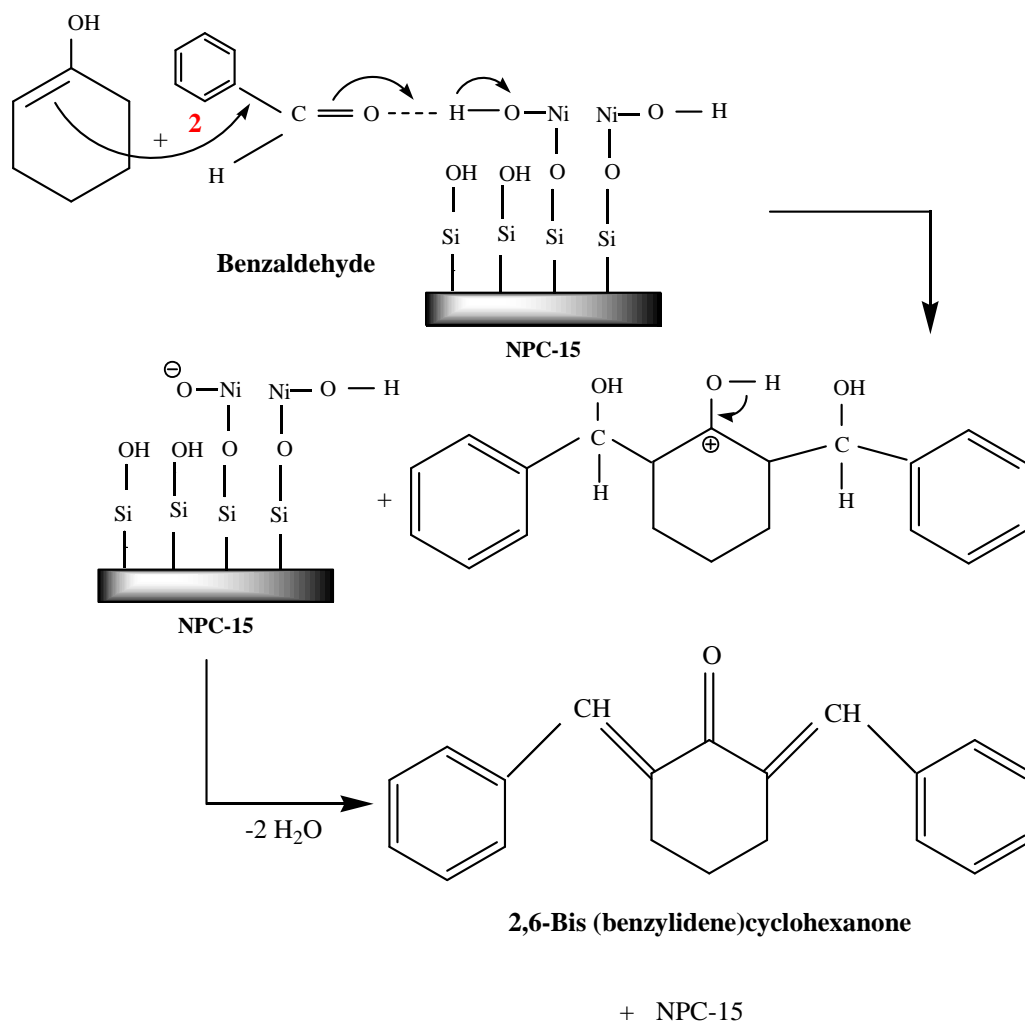
Scheme 3.4: **Proposed mechanism of condensation of cyclohexanone and benzaldehyde over NPC-15.**

3.6 Regeneration and reusability of catalyst

The catalyst is filtered, washed with acetone, dried in oven at 110°C/12 h and then calcined at 450°C/2h for its use in next reaction cycles. The regenerated NPC-15 show efficient catalytic activity up to consecutive 6 reaction cycles giving conversion% of cyclohexanone in the range of 92-83% and yield in the range of 90-81% as shown in **Figure 3.11**. The FT-IR spectrum **(Figure 3.12b)** of NPC regenerated after 6th reaction cycle resembles that of fresh NPC indicating the stability of nickel loading on perlite. On using catalyst many times, amorphous condensed polymer or   -carbon films are formed at lower temperature (<300 °C) get physically deposited on catalyst surface through fouling mechanism [56] and block the surface active sites of catalyst in such a way that access of reactants to the catalyst is denied [57]. This phenomenon is further proved by decrease in intensity of a broad band between 3600-3300 cm^{-1} **(Figure 3.12b)** attributed to surface hydroxyl groups responsible for catalytic activity. An intense peak at 1632 cm^{-1} characteristic of bending mode of –OH groups also decreases in FT-IR spectrum of regenerated catalyst. Due to plugging of active sites, conversion and yield% significantly decreases in sixth reaction cycle.
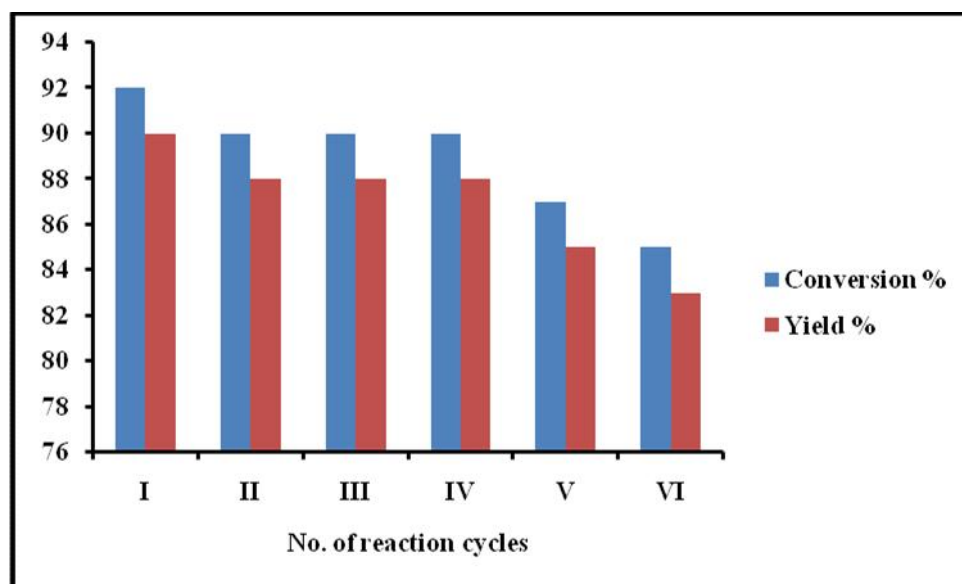
Figure 3.11:   The reusability of NPC-15 in Claisen-Scmidt condensation reaction.
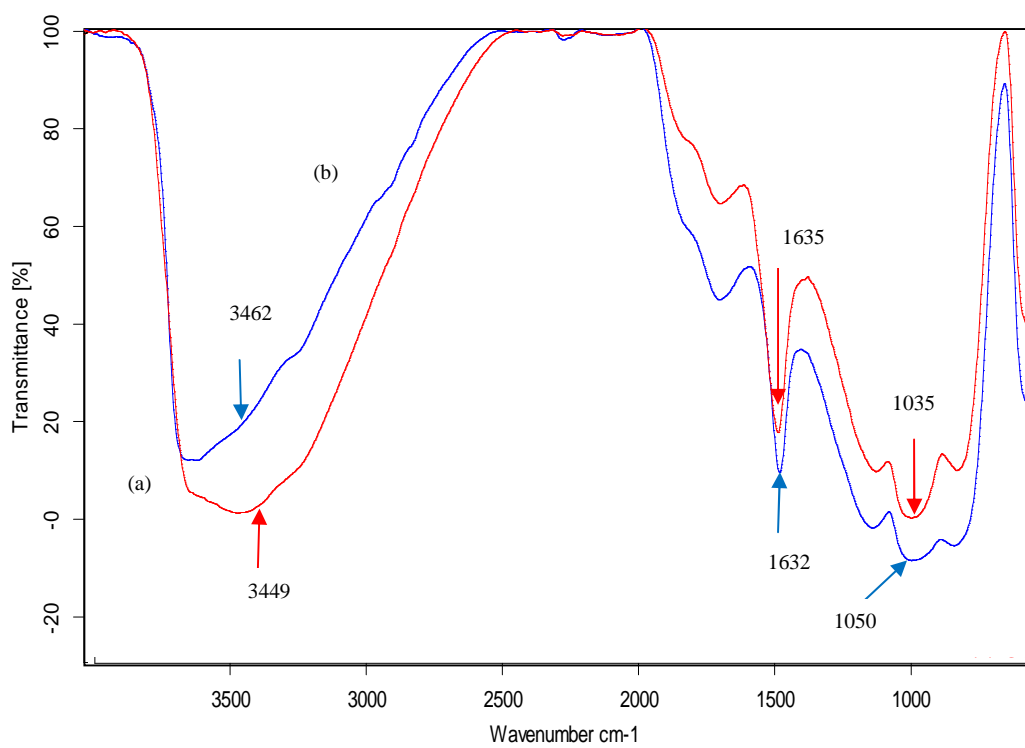
Figure 3.12:   FT-IR spectra of (a) NPC and (b) regenerated catalyst.

3.7 Identification of product

2, 6- bis (benzylidene) cyclohexanone - yellow crystals as shown in **Figure 3.13**, m.pt.- 119-120°C.

IR (KBr): 1664 cm-1($_{C=O}$); ^{1}H-NMR (CDCl$_3$): : 1.72-1.88 (m, 2H, 4-CH$_2$), 2.82 -2.98 (m, 4H, 3 & 5 -CH$_2$), 7.23-7.55 (m, 10H, Ar-H), 7.80 (s, 2H, 2 CH= CH).

Figure 3.13:   Crystals of 2, 6- bis (benzylidene) cyclohexanone.

3.8 Conclusion

The present study elaborates the synthesis of a new type of solid acid catalyst by loading of nickel on thermally activated perlite, possessing significant acidity to catalyze Claisen-Schmidt condensation of cyclohexanone and benzaldehyde with high conversion (92%), selectivity (99%) and yield (90%) of the desired product, 2,6- bis (benzylidene) cyclohexanone in one-pot, solvent free reaction conditions. The catalyst is easily filtered, regenerated and recycled several times with analogous efficiency, suggesting the stability of acidic sites of the catalyst during reaction. The results of various analyses recommend that the optimum catalytic activity of NPC-15 is due to presence of sufficient surface active Brønsted acidic sites. While, at higher nickel loading, NiO crystallites increases Lewis acidic sites and block the active Brønsted acidic sites hence, decrease in conversion, selectivity and yield% is observed. The novelty of this work is utilization of abundant natural waste, perlite as a solid support for the synthesis of highly efficient heterogeneous acid catalyst. This investigation suggests that perlite could be an alternative to commercial silica for synthesizing novel solid acid catalysts which can catalyze various industrially important reactions in a cost-effective manner.

3.9 References

[1]   J.K. Rajput, G. Kaur, Tet. Lett. 53 (2012) 646.

[2]   Y. Liu, E. Lotero, J.G. Goodwin Jr., J. Catal. 242 (2006) 278.

[3]   P.H. Lee, D. Kang, S. Choi, S. Kim, Org. Lett. 13 (2011) 3470.

[4]   L. Ronchin, A. Vavasori, L. Toniolo, J. Mol. Catal. A: Chem. 355 (2012) 134.

[5]   R. Sanz, D. Miguel, A. Martínez, J.M. Alvarez-Gutiérrez, F. Rodríguez, Org. Lett. 9 (2007) 2027.

[6]   M.T. Casale, A.R. Richman, M.J. Elrod, R.M. Garland, M.R. Beaver, M.A. Tolbert, Atmos. Environ. 41 (2007) 6212.

[7]   S. Bhagat, R. Sharma, A.K. Chakraborti, J. Mol. Catal. A: Chem. 260 (2006) 235.

[8]   A. Rostami, F. Ahmad-Jangi, Chin. Chem. Lett. 22 (2011) 1029.

[9]   P. Salehi, M. Dabiri, M.A. Zolfigol, M.A.B. Fard, Tet. Lett. 44 (2003)

2889.

[10]   N. Iranpoor, F. Kazemi, Tetrahedron 54 (1998) 9475.

[11]   M. A. Ermakova, D.Y. Ermakov, Appl. Catal. A: Gen. 245 (2003) 277.

[12]   I.E. Achouri, N. Abatzoglou, C. Fauteux-Lefebvre, N. Braidy, Catal. Today 207 (2013) 13.

[13]   W. Hally, J.H. Bitter, K. Seshan, J.A. Lercher, J.R.H. Ross, Catalyst Deactivation 1994, Proceedings of the 6th International Symposium, Elsevier (1994).

[14]   P. Frontera, A. Macario, A. Aloise, F. Crea, P.L. Antonucci, J.B. Nagy, F. Frusteri, G. Giordano, Catal. Today 179 (2012) 52.

[15]   S. Maddila, S.B. Jonnalagadda, J. Chil. Chem. Soc. 57 (2012) 1099.

[16]   L. Hermida, A.Z. Abdullah, A.R. Mohamed, Materials Sciences and Applications 4 (2013) 52.

[17]   C. Khatri, A. Rani, Fuel 87 (2008) 2886.

[18]   C. Khatri, D. Jain, A. Rani, Fuel 89 (2010) 3853.

[19]   C. Khatri, M.K. Mishra, A. Rani, Fuel Process. Technol. 91 (2010) 1288.

[20]   A. Rani, C. Khatri, R. Hada, Fuel Process. Technol. 116 (2013) 366.

[21]   C. Khatri, A. Rani, Indian Patent, 258334 (1980/DEL/2007), 2013.

[22]   S.N. Hosseini, S.M. Borghei, M. Vossoughi, N. Taghavinia, Appl. Catal. B: Environ. 74 (2007) 53.

[23]   M. Balat, Energy, Explor. Exploit. 26 (2008) 197.

[24]   J.R. Dimmock, N.W. Hamon, K.W. Hindmarsh, A.P. Sellar, W.A. Turner, G.H. Rank, A.J. Robertson, J. Pharm. Sci. 65 (1976) 538.

[25]   L.Q. Kang, G.H. Song, J.Y. Wang, B.G. Wei, J. Chin. Chem. Soc. 55 (2008) 1125.

[26]   A.F.M.M. Rahman, R. Ali, Y. Jahng, A.A. Kadi, Molecules 17 (2012) 571.

[27]   J.J. Shrikhande, M.B. Gawande, R. V. Jayaram, Catal. Comm. 9 (2008) 1010.

[28]   J. Temuujin, A. van Riessen, J. Hazard. Mater. 164 (2009) 634.

[29]   M. Salman, U. Shafique, R. Rehman, A. Yousaf,F. Azhar, J.M. Anzano, J. Mex. Chem. Soc. 55 (2011) 214.

[30]   A. Zhao, W. Ying, H. Zhang, H. Ma, D. Fang, Catal. Comm. 17 (2012) 34.

[31]   M. Zangouei, A.Z. Moghaddam, M. Arasteh, Chem. Eng. Res. Bull. 14

(2010) 97.

[32]   U. Kalapathy, A. Proctor, J. Shultz, Bioresour. Technol. 73 (2000) 257.

[33]   D. Jain, C. Khatri, A. Rani, Fuel 90 (2011) 2083.

[34]   S.H. Javed, S. Naveed, N. Feroze, M. Zafar, M. Shafaq, Journal of Quality and Technology Management 6 (2010) 81.

[35]   K. Amutha, R. Ravibaskar, G. Sivakumar, International Journal of Nanotechnology and Applications 4 (2010) 61.

[36]   R.S. Prakasham, G.S. Devi, C.S. Rao, V.S.S. Sivakumar, T. Sathish, P.N. Sarma, Appl. Biochem. Biotechnol. 160 (2010) 1888.

[37]   J.J. Gamman, G.J. Millar, G. Rose, J. Drennan, J. Chem. Soc., Faraday Trans. 94 (1998) 701.

[38]   M. He, A.I. Chernov, E.D. Obraztsova, J. Sainio, E. Rikkinen, H. Jiang, Z. Zhu, A. Kaskela, A.G. Nasibulin, E.I. Kauppinen, M. Niemelä, O. Krause, Nano Res. 4 (2010) 334.

[39]   S. Kabra, A. Sharma, S. Katara, R. Hada, A. Rani, Indian Journal of Applied Research 3 (2013) 40.

[40]   D. Jain, M. Mishra, A. Rani, Fuel Process. Technol. 95 (2012) 119.

[41]   F. Adam, S. Balakrishnan, P.L. Wong, Journal of Physical Science 17 (2006) 1.

[42]   B.J. Saikia, G. Parthasarathy, J. Mod. Phys. 1 (2010) 206.

[43]   S. Katara, S. Kabra, A. Sharma, R. Hada, A. Rani, International Research Journal of Pure and Applied Chemistry, 3 (2013) 299.

[44]   L. Aoudjit, A. Saadi, O. Cherifi, D. Halliche, Transitional Journal of Science and Technology 2 (2012) 79.

[45]   C.R. Reddy, Y.S. Bhat, G. Nagendrappa, B.S.J. Prakash, Catal. Today 141 (2009) 157.

[46]   M. Musthofa, A.H. Karim, N.A. Fadzlillaah, N. H.R. Annuar, A.A. Jalil, S. Triwahyono, J. Fundamental Science 6 (2010) 127.

[47]   Z. Wang, J. Navarette, World J. Nano Sci. Eng. 02 (2012) 134.

[48]   E.R. Vance, D.S. Perera, P. Imperia, D.J. Cassidy, J. Davis, J.T. Gourley, Journal of the Australian Ceramic Society 45 (2009) 44.

[49]   S. Kabra, S. Katara, A. Rani, International Journal of Innovative Research in Science, Engineering and Technology 2 (2013) 4319.

[50]   D. Bastani, A. A. Safekordi, A. Alihosseini, V. Taghikhani, Sep. Purif. Technol. 52 (2006) 295.

[51]   C. Lin, A. Shaheen, A. Al-muhtaseb, J.A. Ritter, J. Sol-gel Sci. Technol. 28 (2003) 133.

[52]   P.G. Savva, K. Goundani, J. Vakros, K. Bourikas, C. Fountzoula, D. Vattis, A. Lycourghiotis, C. Kourdulis, Appl. Catal. B Environ. 79 (2008) 199.

[53]   D. Liu, X.Y. Quek, W.N.E. Cheo, R. Lau, A. Borgna, Y. Yang, J. Catal. 266 (2009) 380.

[54]   A. Habibi, E. Sheikhhosseini, M. Bigdeli, S. Balalaie, E. Farrokhi, Int. J. Org. Chem. 01 (2011) 143.

[55]   E. Rafiee, S. Shahebrahimi, Chin. J. Catal. 33 (2012) 1326.

[56]   C.H. Bartholomew, Catal. Rev. 24 (2007) 67.

[57]   C.H. Bartholomew, Appl. Catal. A: Gen. 212 (2001) 17.

Synthesis of Fly Ash Supported Phosphomolybdic Acid: Green, Efficient and Recyclable Solid Acid Catalyst for a Series of Microwave Assisted Friedel- Crafts Acylation Reactions

Abstract

Fairly economic, potentially active, recyclable and microwave stable solid acid catalyst has been synthesized by loading varying weight% of phosphomolybdic acid on mechanically and thermally activated fly ash through incipient wetness impregnation method. As synthesized catalysts are analyzed by N_2 adsorption-desorption, X-ray diffraction, fourier transform infrared, scanning electron microscopy, transmission electron microscopy, thermo-gravimetric analysis, ultra-visible diffuse reflectance spectroscopy and solid state ^{31}P NMR techniques. The catalytic activity is evaluated by a series of microwave irradiated Friedel-Crafts acylation of various aliphatic alcohols and acetyl chloride under solvent-free reaction conditions. Lewis acidity of catalysts as inferred by pyridine adsorbed FT-IR studies initiates acylation reaction through generation of acylium ions by electrophillic attack at -electrons of the substrate. The effect of various reaction parameters like time, temperature, power output etc. on conversion% is also studied during this chapter. The catalyst could be recycled up to five reaction cycles giving analogous conversion% under similar microwave reaction conditions and the possibility of leaching of catalyst during reaction is analyzed by hot filtration test. Surface roughness, specific surface area and thus the capability of fly ash to serve as an effective catalyst support is increased by mechanical and thermal activation. This work paves a way for the development of a cost-effective, improved fly ash supported catalyst and its novel applications in industrially important microwave assisted acylation reactions.

4.1 Introduction

Use of MAOS (Microwave Assisted Organic Synthesis) and MARS (Microwave Assisted Reaction System) has been upsurge over last two decades. Microwave assisted reactions are green, clean, energy saving, reproducible, having fast reaction rates, suppress by-product and waste formation and hence enhances selectivity of desired products. Conventional heating is relatively inefficient and time consuming as it induces heating on walls of vessel while, microwaves produce in-core volumetric heating of reactants thus making the whole process efficient and fast up to 1000 folds. Microwave heating diminishes potential energy barrier and favours the easier and earlier formation of thermodynamic product depending upon the dipole moments of reactants and their interaction with microwave irradiation. Three different mechanisms, namely, dipolar polarization, conduction and interfacial polarization are responsible for microwave heating [1]. Easier post reaction processes, product purification and thus, low waste generation makes this process green and atom-efficient. Previous problems of lack of control and reproducibility in domestic microwave ovens have been overcome by use of dedicated microwave reactors with on-line accurate monitoring of both temperature and pressure. Microwave irradiations coupled with the use of inorganic mineral-supported catalysts under solvent-free conditions, provide clean chemical processes with the advantage of enhanced reaction rates, greater selectivity, higher yields and significant conversions.

Friedel-Crafts acylation reactions of aliphatic alcohols are of great industrial significance as they synthesize various esters having wide applications in pharmaceuticals [2], cosmetics [3], plasticizers through protection and deprotection reactions [4], multi-step synthesis of various organic compounds [5] etc. Acylations are commonly performed using carboxylic acids, acid anhydrides and acyl chlorides as acylating reagents. Acylations by acyl urea, acyl imidazoles [6] are also reported. However, higher yields and smooth rates of acylation of alcohols are seen on using aliphatic acyl chlorides [7]. Some microwave assisted acylation reactions of aromatic compounds are also well precedent in literature [8–11]. Numerous homogeneous catalysts like $AlCl_3$, $FeCl_3$, BF_3, $ZnCl_2$ etc. [12] are often used for acylation reactions, but most of them are harsh, non-recyclable,

moisture sensitive, require organic solvents and tedious reaction procedures. To avoid the problems associated with use of homogeneous catalysts, heterogeneous catalytic systems have been favoured. Commercial solid catalysts such as, clays, zeolites, silica sulfuric acid, ZnO, bismuth and scandium triflates, arenesulfonic acid functionalized SBA-15 [13–17] are employed in acylation reactions. However, such processes have some limitations viz. cost, stability, cumbersome methodologies, long reaction periods. Therefore, taking into account all above facts, there becomes an essential demand for the development of a green, solvent-free, economical protocol for acylation reactions especially for industrial uses.

Heteropolyacids like phosphomolybdic acids are non-polluting, promising, thermally and chemically stable Brønsted acids. Given that heteropolyacids are more efficient and acidic than conventional mineral acids like zeolites, mixed-oxides etc. [18], they have been widely used in various organic syntheses like methanol oxidation [19], glycerol esterification [20], acrolein production [21], transesterification [22] etc. However, bulk heteropoly acids are non-porous, having low surface area (5-8 m^2g^{-1}) with few acidic sites for acylation reactions, thus, they are generally supported on silica [23], silica-zirconia [24], zeolites in various Friedel-Crafts acylation reactions [11].

In this chapter, synthesis of a novel, extremely potential, cost-effective, recyclable fly ash supported phosphomolybdic acid catalyst (PMFA) has been reported as an alternative for highly expensive, commercial, supported and unsupported heteropoly acid catalysts. Mechanical and thermal activation increases surface area, surface silanol groups of fly ash and hence it can be utilized as a stable support for further loading of phosphomolybdic acid (PMA). The mineralogical, morphological, structural and surfacial properties of the prepared catalysts are analysed during the course of work. PMFA is found effectively stable and re-generable up to five reaction cycles over a series of microwave assisted Friedel-Crafts acylation reactions between various aliphatic alcohols and acetyl chloride under solvent-free atmosphere. The products of the test reactions are important as solvents in lacquer and enamel industries [25] as well as intermediates in perfumeries [26], thinner in paint formulations [3]. The reaction parameters such as time, temperature, microwave power output etc. are

further optimized for attaining maximum conversion% of reactants to desired products. Thus, the study provides the development of an innovative, stable catalytic system by utilizing a solid waste, fly ash for microwave irradiated industrially beneficial organic transformations.

4.2 Experimental

4.2.1 Materials

Fly ash is collected from Jamshedpur Thermal Power Plant, Jamshedpur (Jharkhand). Phosphomolybdic acid-PMA (99.99% purity) is purchased from Sigma Aldrich. Methanol, aliphatic alcohols, acetyl chloride are purchased from Merck.

4.2.2 Catalyst preparation

As received fly ash is mechanically activated in an agate jar of high energy planetary ball mill (Retsch PM-100, Germany) using agate balls of 5 mm size for 10, 20 and 30 h with 250 rpm rotation speed. The ball mill is loaded with ball to powder weight ratio (BPR) of 10:1. 30 h mechanically activated fly ash (MFA-30), having higher specific surface area (30.02 m^2/g) is selected for further study. MFA-30 is then thermally activated at 800°C for 3 h to remove excess water, carbon and other impurities [27] and gets converted to thermally activated MFA-30 (TMFA). PMFA catalysts are prepared using incipient wetness impregnation method. Therein, the requisite amounts (0.25 g for 5 wt. %, 0.50 g for 10 wt.%, 0.75 g for 15 wt.% and 1.25 g for 25 wt. %) of PMA dissolved in 20 ml methanol are added to 5 g of TMFA and stirred overnight in a closed vessel at room temperature. The impregnated samples are dried at 110°C for 12 h and then calcined in static air at 400°C for 3 h. As-synthesized catalysts are designated as PMFA-x, where x = 5, 10, 15 and 25 wt % of phosphomolybdic acid. The steps of synthesis of PMFA catalysts are summarized in **Scheme 4.1**.
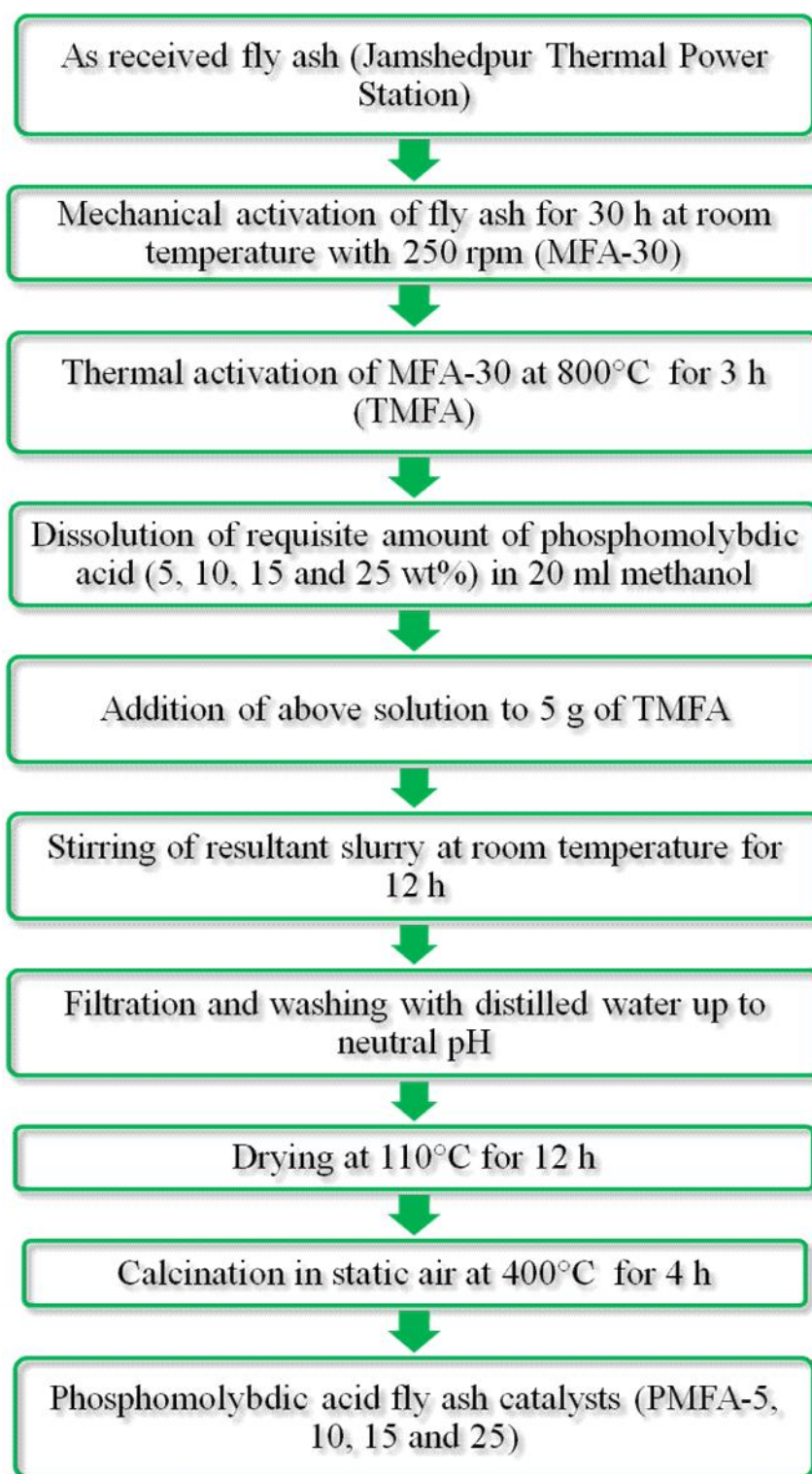
Scheme 4.1: **Synthesis of fly ash supported phosphomolybdic acid catalysts (PMFA).**

4.2.3 Equipment

The reactions are performed on single mode, PC operated, synergy.exe software based, microwave equipment (CEM Focused Microwave™ Synthesis System, Model Discover) shown in **Figure 4.1**, comprising of closed and open vessel systems, with a working frequency of 2.45 GHz, temperatures ranging from 25-250°C, pressure range from 0-300 Psi. An Infrared detector controls the temperature during the reactions and a Teflon spill cup protects the detector from exposure. An air compressor connected with the equipment is utilized for cooling of reactions. The reactions are preferred in Power$_{max}$ mode, using simultaneous heating and cooling method, under controlled conditions as maximum number of microwave radiations is utilized in this mode.

The Discover System used in this study consists of following options:

- **Infrared Temperature Control System-** The standard temperature control system consists of a non-contact infrared sensor which monitors and controls the temperature conditions of the reaction vessel located in the instrument cavity. The temperature sensor is centrally located beneath the cavity floor and "looks" up at the bottom of the vessel, shown in **Figure 4.2a**. A lens is positioned between the sensor and the cavity floor to protect the sensor. The temperature sensor data is set up in a feedback control loop with the magnetron to regulate the power output to maintain the temperature set-point through the onboard processor.

- **IntelliVent™ Pressure Control System-** This pressure control system as shown in **Figure 4.2b** consists of a load cell to enable pressure measurement and control of the reaction environment that senses changes in the external deflection of the septa on top of the sealed pressure vial. The sensor housing incorporates a capture and release mechanism that secures the reaction vessel in the cavity.with operator selectable power output from 0 - 300 watts (+/- 30 watts) programmable in 1-watt increments.

- A self-adjusting, single mode microwave cavity that is manually accessed via multiple attenuator ports (both ports are included).

- A 4-line x 20-character vacuum fluorescent display with alphanumeric keypad and on-board computer for programming and operational control of the system.

- 3 safety interlocks and an interlock monitoring system to prevent microwave emission when the attenuator port is not properly installed.

- **Stirring Option** - The stirring option consists of a rotating magnetic plate located below the floor of the microwave cavity. "Stirring" occurs when the rotating magnetic field couples with a stir bar in the vessel.

- **Cooling Option** – The cooling option consists of necessary valves and ports to direct a cooling gas (either nitrogen or "clean" air) onto the vessel in the system cavity. This option will decrease the temperature of a 2mL solution in a 10mL Pyrex reaction vessel from ~150 ºC to ~40 ºC in less than 120 seconds. The gas is user supplied at a minimum pressure level of 20 psi (~1.5 bar) and a flow rate of 25 liters/min.

4.2.4 Catalyst characterization

Physicochemical properties of all catalytic materials are studied by N_2 adsorption-desorption, XRD, FT-IR and pyridine adsorbed FT-IR, SEM, SEM-EDX, TEM, TGA, UV-Vis DRS, Solid State ^{31}P NMR techniques, as described in **Annexure-I**. Crystallite size of the crystalline phase is determined from the peak of maximum intensity by using Scherrer formula with a shape factor *(K)* of 0.9 as below:

Crystallite size = *K.   / W. Cos*

where, $W = W_b-W_s$; W_b is the broadened profile width of experimental sample and W_s is the standard profile width of reference sample.

4.2.5 Catalytic activity

Friedel-Crafts acylation reactions between aliphatic alcohols and acetyl chloride **(Scheme 4.2)** catalyzed by PMFA-5, 10, 15 and 25 to give corresponding esters are performed in a microwave reactor. In this procedure, a mixture of aliphatic alcohol and acetyl chloride (different molar ratios) is taken in a 10 ml microwave vial. The catalyst (substrate to catalyst weight ratio = 10:1) activated at 400°C for 1 h, is then added in the reaction mixture.

Figure 4.1: **CEM Focused Microwave^{TM} Synthesis System (Discover Model).**
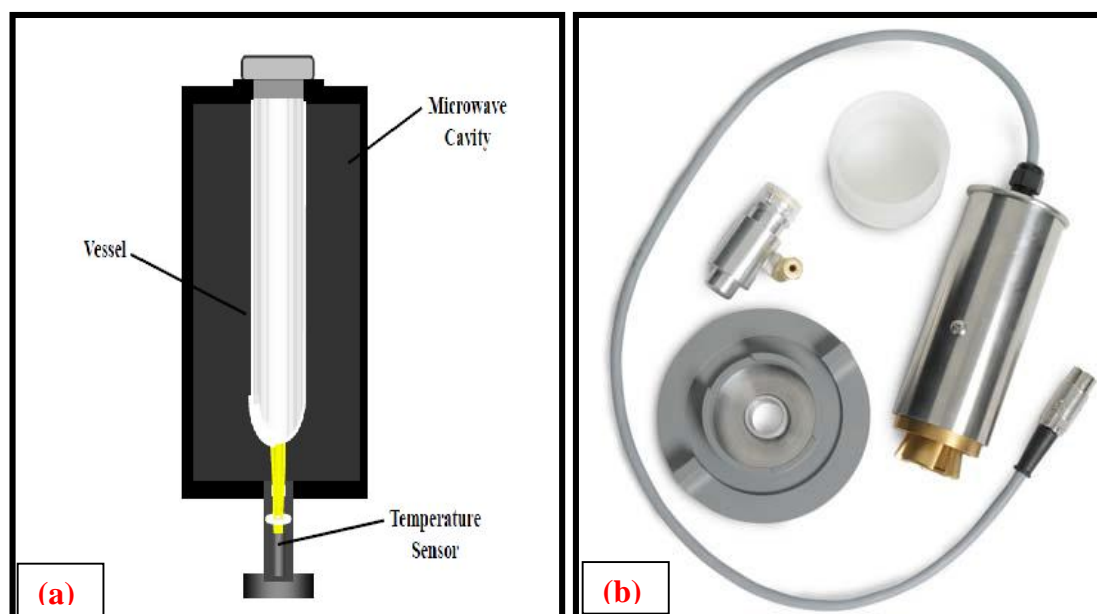
Figure 4.2: **(a) Infrared Temperature Sensor and (b) IntelliVent Pressure Sensor Assembly.**

The reaction is carried out in closed vessel system at 50 Psi pressure, by placing the vial on microwave cavity under constant stirring at different time periods, temperatures and power outputs. Then, the system is shut by an attenuator which prevents the passage of harmful microwaves into surroundings. After input of temperature, hold time, power and pressure parameters, the reaction is started by clicking on 'Play' button under Power$_{max}$-On conditions. Initially, a beep sound appears and reaction runs on 'Ramp time' mode. Therein, the equipment attains all the desired parameters and then mode changes to 'Hold time', where the reaction runs for the specified time period under simultaneous heating and cooling conditions. Usually, equipment takes 10-15 minutes to achieve all the set points, i.e., ramp time. After completion of holding time, the instrument is turned off and the reaction is cooled through air compressor. Then, the catalyst is separated, the product is filtered and analyzed by Gas Chromatograph. Some live graphs recorded by the instrument during reaction are shown in **Figure 4.3**.

The conversion% of alcohol is calculated by using following method –

$$\text{Conversion (\%)} = 100 \text{ X } \frac{(\text{Initial wt \% - Final wt \%})}{\text{Initial wt \%}}$$
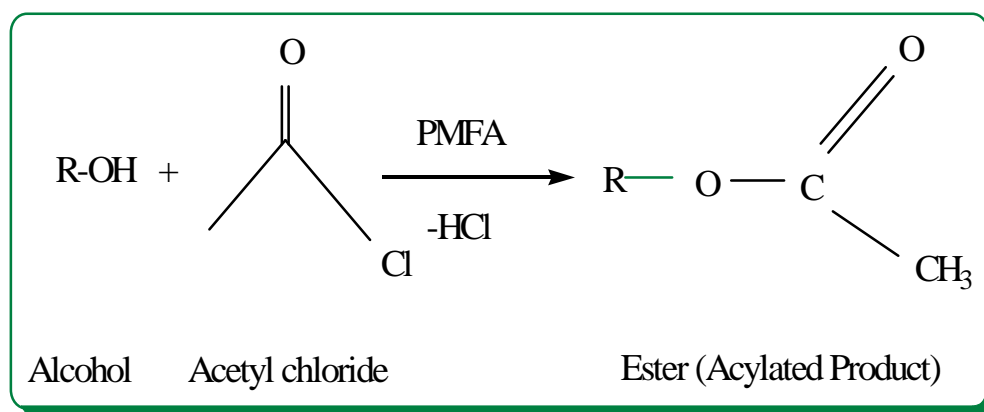
Scheme 4.2: **Simplified reaction pathway of Friedel-Crafts acylation of aliphatic alcohols and acetyl chloride over PMFA to give corresponding ester.**
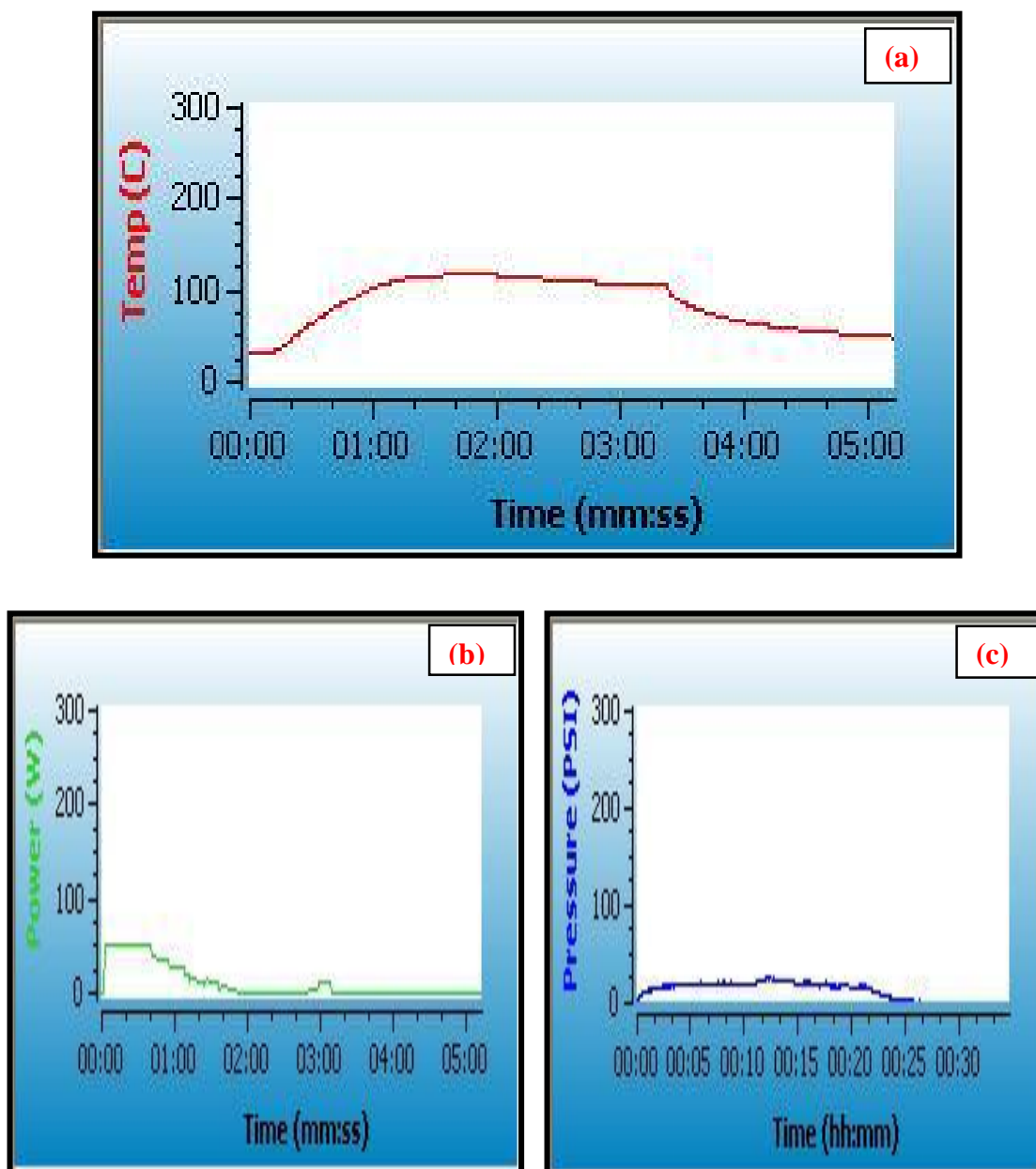
Figure 4.3:   **Graphs recorded by instrument showing progress of reaction (a) versus temperature, (b) versus power and (c) versus pressure.**

4.3 Results and discussion

4.3.1 BET analysis

BET specific surface area of fly ash samples as given in **Table 4.1** indicates that with enhancing milling time from 10 to 30 h, specific surface area of fly ash also increases from 9.18 to 30.02 m^2/g which later on decreases in TMFA due to thermal treatment. On increases loading of PMA content from 5 to 25 wt %, the specific surface area of catalysts decreases progressively [28], probably due to plugging of fly ash pores by PMA dispersion.

Table 4.1: **BET specific surface area data of samples.**

Samples	BET specific surface area (m^2/g)
Fly ash	9.18
MFA-10	15.14
MFA-20	22.54
MFA-30	30.02
TMFA	28.47
PMFA-5	26.62
PMFA-10	22.84
PMFA-15	19.64
PMFA-25	14.48

Figure 4.4a shows the distribution of pores in MFA-30 on the basis of their size. It can be clearly seen that majority of pores are mesoporous in nature and lie in the range of 10-100 nm. Average pore diameter of MFA-30 is calculated to be 4.76 nm depicting its mesoporous nature. B.E.T. adsorption isotherm for MFA-30 as shown in **Figure 4.4b**, shows resemblance with Type II and III adsorption isotherms, characteristic of a material, which is not porous, or possibly macroporous [29]. Although it also shows some deviations from Type II isotherm,

conferring the transition from macroporous to mesoporous behaviour as a consequence of mechanical activation. For fly ash, it is not possible to get any of the ideal types of isotherms due to availability of heterogeneous particles with large variations in size, shape and porosity arrangements. The BET plots are observed with linear range for saturation pressure range (0.05 to 0.28) i.e., the pressure observed over (P/Po value) for the BET equation which resembles to most of inorganic silica material [29]. High adsoprtion energy of fly ash is responsible for active dispersion of loading species on it and makes it a suitable catalyst support. While in case of B.E.T. adsorption isotherm of PMFA-15 catalyst **(Figure 4.4c)**, it is also showing deviations from Type II isotherm, so, it can be said that the catalyst is ensemble of all three types of porous particles, thus provide active sites for reactants to undergo various types of organic transformations.

4.3.2 X-ray diffraction analysis

The XRD patterns of the pure fly ash, MFA-30 and TMFA given in the **Figure 4.5** show decrement in the crystallinity of fly ash and increase in the amorphous nature as inferred with decrease in the crystallite size of fly ash from 33nm to 18 nm on milling. The peaks at 16.4° and 26.2° show mullite (alumino-silicate) phases while quartz (silica) exhibits strong peaks at 20.7°, 26.6°, 40.6° and 49.9° of 2 values [30]. As a result of ball milling, mostly quartz and mullite crystalline phases are reduced. After thermal activation, magnetite phase tends to disappear, while, peak responsible for haematite begins to appear [31] and intensities of crystalline phases (quartz and mullite) increases in TMFA.

In PMFA-5, 10, 15 and 25 catalysts **(Figure 4.6)** on impregnation of PMA, the crystalline phases of silico-aluminate species in fly ash reduce and consequently amorphous content increases because of interaction between anions of PMA and silanol groups present on fly ash surface [32,33]. No separate diffraction patterns corresponding to PMA or any molybdenum related phases are observed, even in 15 wt% composition [34].
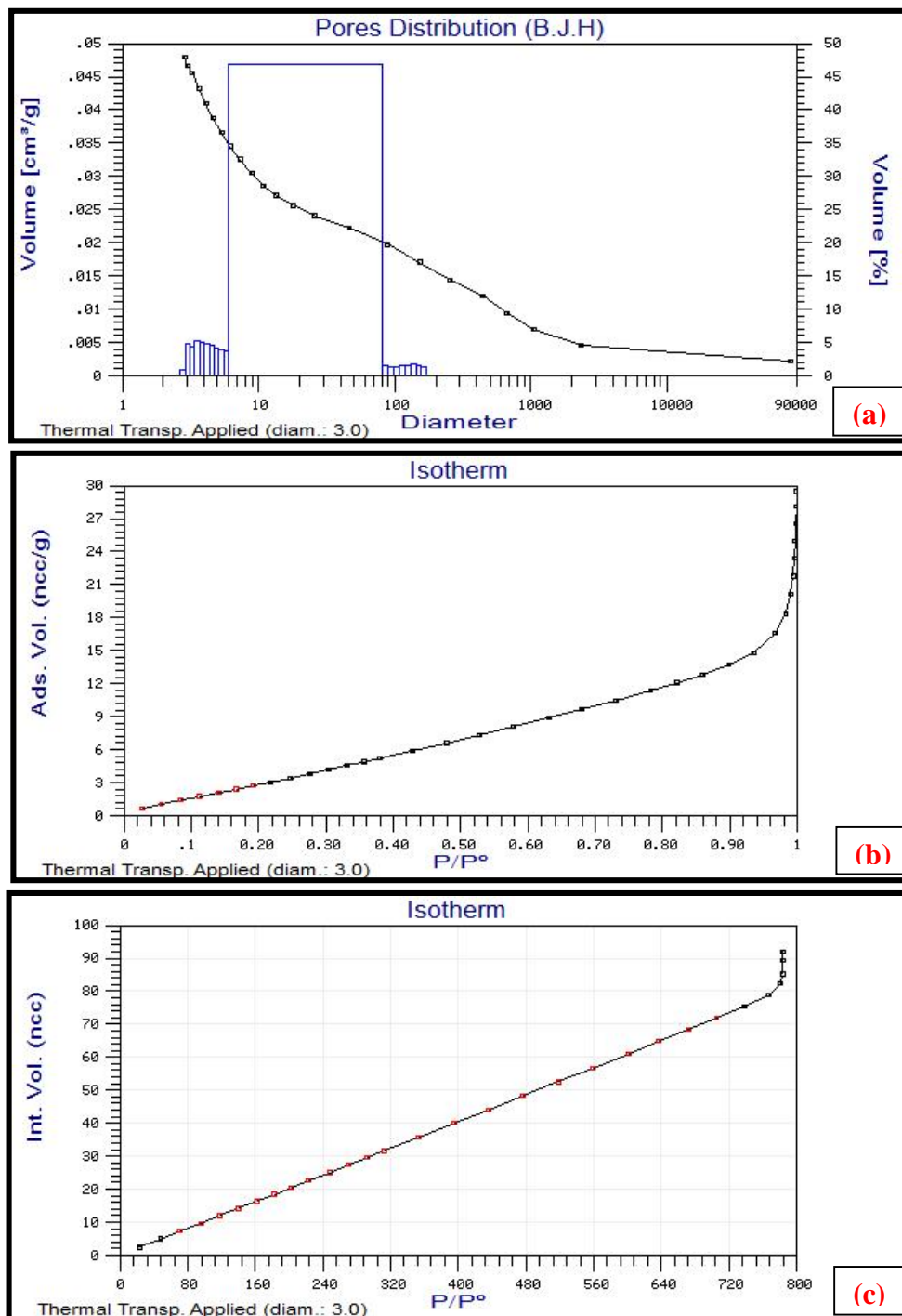
Figure 4. 4: **(a) Pore distribution curve of MFA-30, (b) B.E.T. Adsorption Isotherm of MFA-30 and (c) B.E.T. Adsorption Isotherm of PMFA-15.**
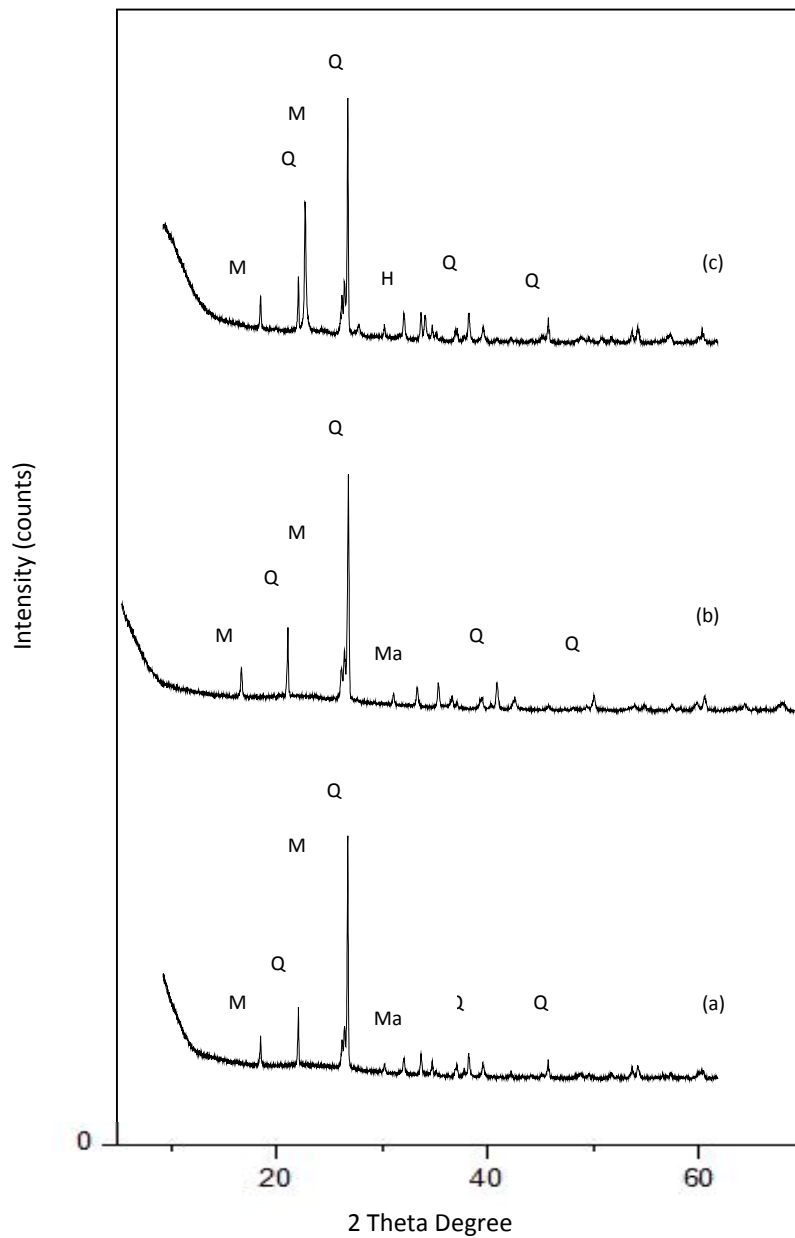
Figure 4.5: **X-ray diffraction pattern of (a) Pure fly ash, (b) MFA-30 and (c) TMFA.**

This fact indicates that PMA species are well dispersed on fly ash surface or present in non-crystalline phases [32,35–37]. It also shows the retention of characteristic Keggin structure of PMA as it did not decompose at 400°C (calcination temperature) thus, strong bonding between PMA species and fly ash is confirmed. PMFA-25 **(Figure 4.6d)** show some reflections of characteristic peaks of pure PMA at 2 = 24.7°, 28.6°, 32.4°and 58.2° confirming the aggregation of bulk PMA particles on fly ash surface [38].

4.3.3 *Fourier transform infra-red analysis (FT-IR)*

The FT-IR spectra of pure FA, MFA-30 and TMFA **(Figure 4.7)** show a broad band between 3500-3300cm^{-1}, attributed to surfacial Si-OH groups and adsorbed water molecules on the surface [39]. The broadness of this band indicates the presence of strong hydrogen bonding in the samples [40]. After milling, broadness of this peak increases, which is an evidence of breaking down of quartz structure and formation of more Si-OH groups [41]. On thermal activation, decrement in intensity and broadness of peak is observed which confirms the loss of water in TMFA. A peak around 1650 cm^{-1} present in all samples is attributed to bending mode ($_{O-H}$) of water molecules [42] which is decreased in TMFA. The broadening of peaks corresponding to Si-O-Si asymmetric vibrations (1000-1200 cm^{-1}) in MFA-30 shows structural rearrangement during mechanical activation. While, in TMFA, this peak gets shifted towards higher wave number because of transformation of Q_3 units [Si (OH) (SiO$_4$)$_3$] to Q4 units [Si (SiO$_4$)$_4$] [30]. As inferred from literature, pure PMA possesses four bands at 1065, 1000, 867 and 790 cm^{-1}, assigned to asymmetric stretching vibrations of $_{as}$ (P-O), $_{as}$ (Mo=O) and $_{as}$ (Mo-O-Mo) respectively [43–45]. These characteristic bands for Keggin structure are partially obscured in case of PMFA catalysts **(Figure 4.8)** as they overlap with the regions of Si-O-Si asymmetric (1000-1200 cm^{-1}) and symmetric stretching (800-1000 cm^{-1}) vibrations [46]. It is reasonable to mention here that the bands assigned at 1000 cm^{-1} and 867 cm^{-1} in case of pure PMA get shifted towards lower wave number, at 970 cm^{-1} and 825 cm^{-1} respectively in PMFA catalyst, confirming interaction between PMA and fly ash support [45]. These bands get enhanced with increase in wt % of PMA loading [33] as evidenced in **Figure 4.8**.
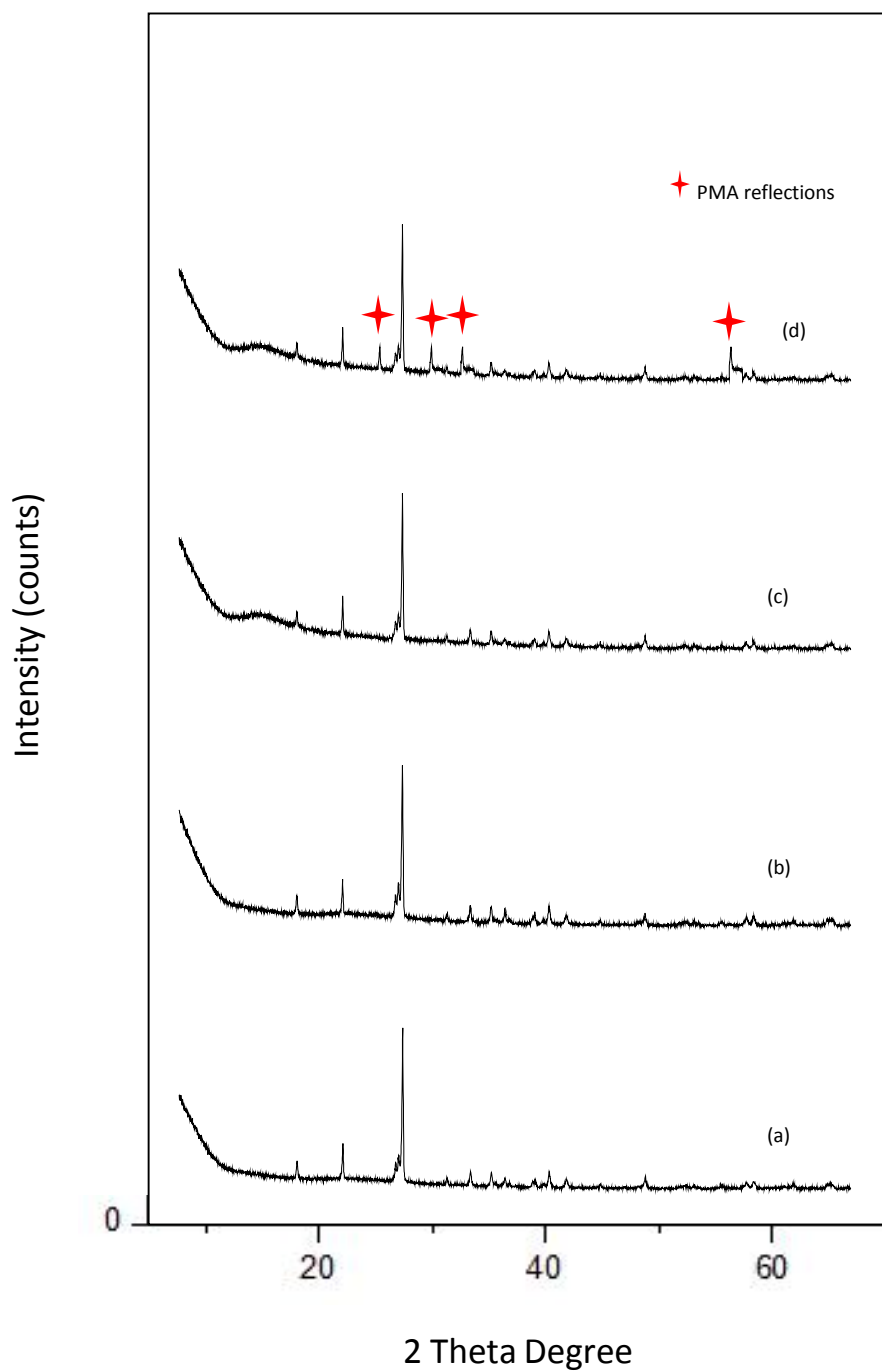
Figure 4.6: X-ray diffraction pattern of (a) PMFA-5, (b) PMFA-10, (c) PMFA-15 and (d) PMFA-25.
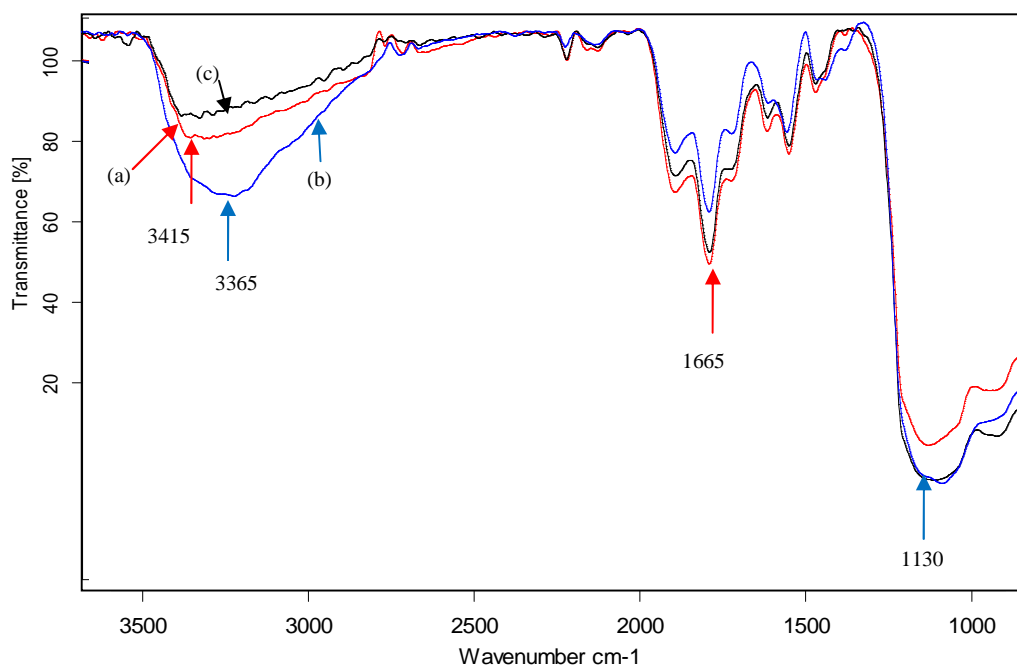
Figure 4.7: FT-IR spectra of (a) pure fly ash, (b) MFA-30 and (c) TMFA.
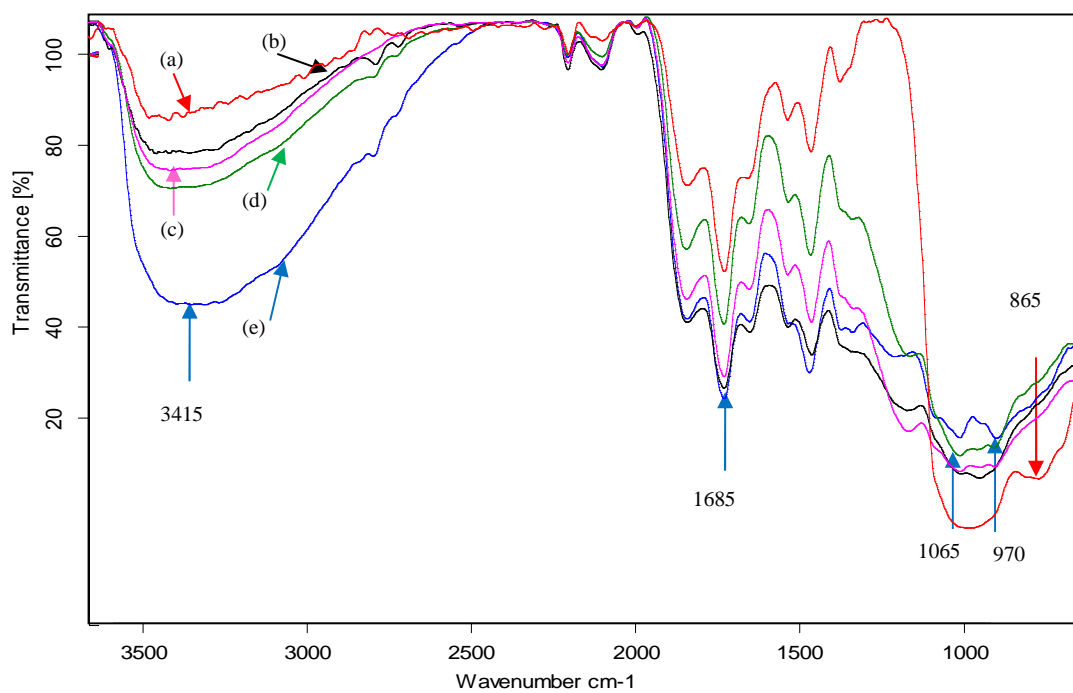
Figure 4.8: FT-IR spectra of (a) TMFA, (b) PMFA-5, (c) PMFA-10, (d) PMFA-15 and (e) PMFA-25.

4.3.4 Pyridine adsorbed FT-IR analysis of catalysts

The FT-IR spectra of PMFA-5, 10, 15 and 25, obtained after pyridine adsorption in the range of 1600-1400 cm^{-1} are shown in **Figure 4.9.** The bands appearing around 1538 cm^{-1} and 1443 cm^{-1} in all catalysts indicate the presence of Brønsted and Lewis acidic sites respectively [34,47]. On increasing the wt % of PMA loading from 5 to 15 %, the intensity of band responsible for Lewis acidity also increases. Mo^{6+} and Mo^{6+}- OH acidic sites of PMFA catalysts adsorb pyridine and show the existence of Lewis and Brønsted acidic sites in samples respectively [48]. In PMFA-25, intensity of band at 1443 cm^{-1} decreases. Pure PMA contains only Brønsted acidic sites [49], the appearance of Lewis acid sites on PMFA catalysts may be attributed due to loss of water/lattice oxygen during calcinations at higher temperature [50].

4.3.5 Scanning electron microscopy (SEM and SEM-EDX analysis)

The SEM photograph of pure fly ash **(Figure 4.10a)** is observed with hollow cenospheres and irregularly shaped amorphous particles, unburnt carbon, agglomerated particles minerals and mineral aggregates. As a result of mechanical activation, smooth, big, spherical cenospheres break down into irregular small particles **(Figure 4.10b)** resulting in increased surface roughness. [41]. Typical SEM image of PMFA-15 **(Figure 4.10c)** reveal that with the addition of PMA, small particles get agglomerated to form spherical or irregular large particles. Loading of PMA is further confirmed by the appearance of fine, shiny particles on fly ash cenospheres.

EDX analysis of FA **(Table 4.2)** shows the presence of Si, Al, K, Na, Fe, Ti and other minor metals. However, the presence of molybdenum and phosphorus in PMFA-15 confirms its loading on surface of fly ash.
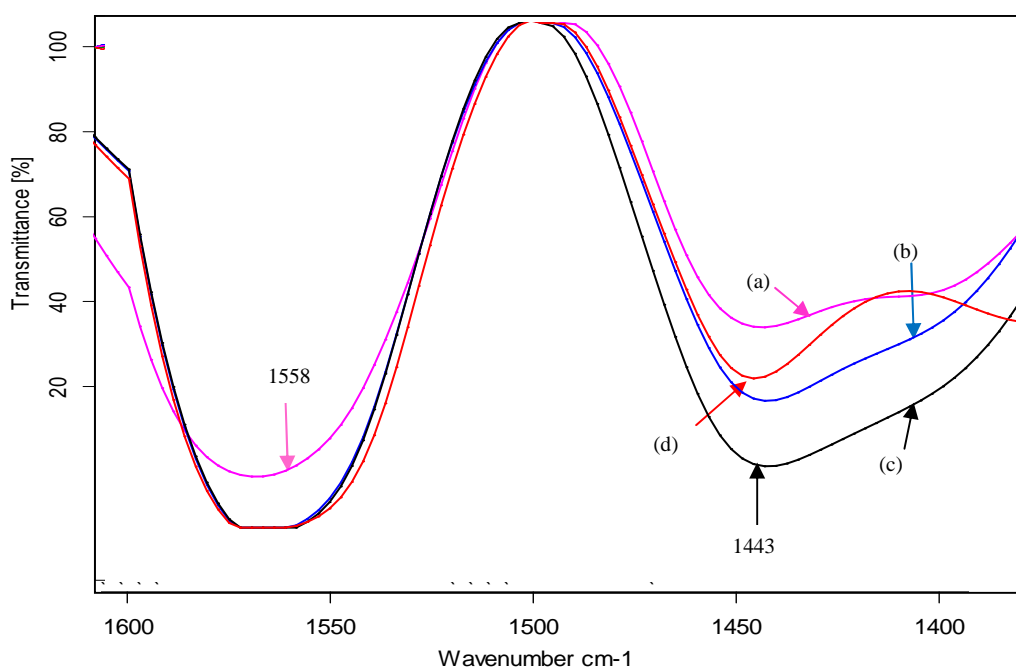
Figure 4.9: **Pyridine adsorbed FT-IR spectra of (a) PMFA-5, (b) PMFA-10, (c) PMFA-15 and (d) PMFA-25.**
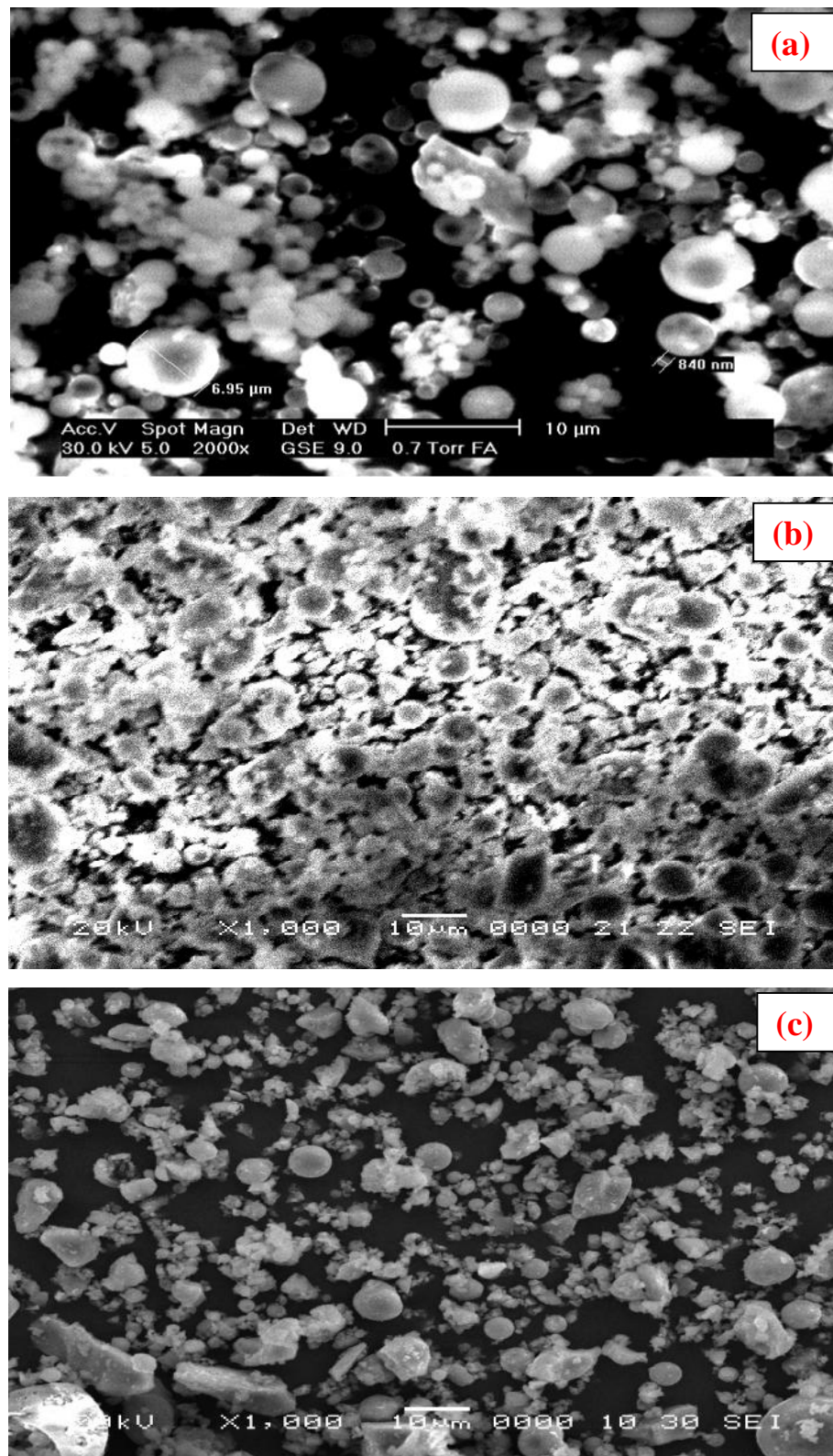
Figure 4.10: **SEM micrographs of (a) pure fly ash, (b) MFA-30 and (c) PMFA-15.**

Table 4.2:   EDX analysis of fly ash and PMFA-15.

Sample	O (wt %)	Si (wt %)	Al (wt %)	Ca (wt %)	Na (wt %)	Ti (wt %)	Fe (wt %)	Mg (wt %)	K (wt %)	Mo (wt %)	P (wt %)	LOI
Fly ash	55.45	25.88	16.11	0.68	0.19	0.45	0.79	0.8	0.28	-	-	2.2
PMFA-15	46.15	27.23	17.02	-	0.14	0.25	-	-	0.18	7.65	1.38	1.3

LOI- Loss on ignition

4.3.6 Transmission electron microscopy (TEM analysis)

The topography and surface dispersion of active PMA species is well understood by using TEM analysis. TEM image of fly ash **(Figure 4.11a)** reveals the appearance of smooth spherical particles. On mechanical activation, morphology of fly ash particles becomes irregular and surface roughness is also increased as seen in TEM image of MFA-30 **(Figure 4.11b)**. The micrograph of PMFA-15 **(Figure 4.11c)** shows fine dispersion of PMA particles on fly ash surface. The results are in agreement with SEM images. Particle size of loaded species could not be measured because of their greater dispersion in the support.
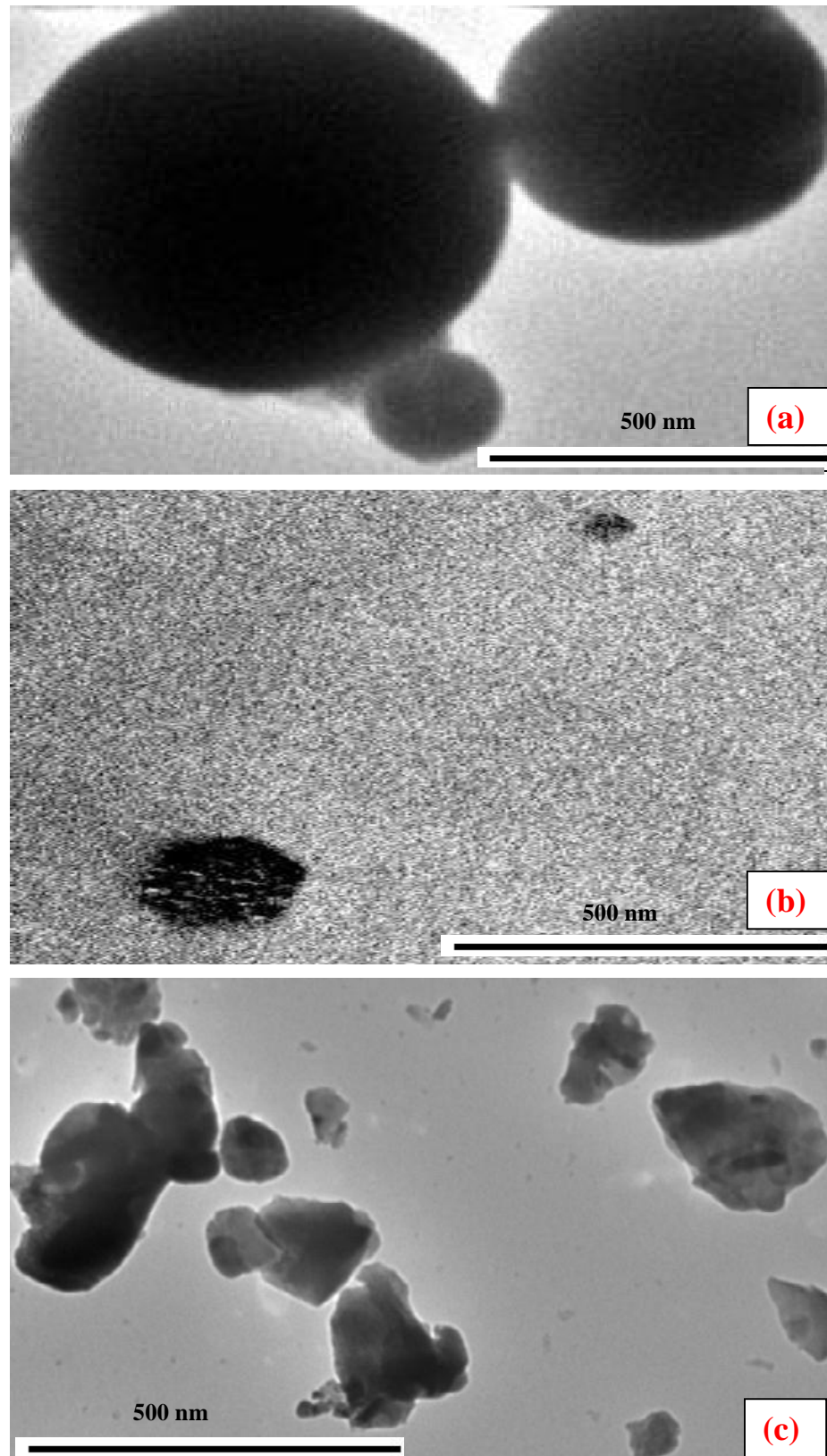
Figure 4.11: **TEM micrographs of (a) pure fly ash, (b) MFA-30 and (c) PMFA-15.**

4.3.7 Thermo-gravimmetric analysis (TGA)

The TGA analyses of both fly ash and PMFA-15 catalyst **(Figure 4.12)** comprises of two weight loss regions. In first region, sharp weight loss appears due to evolution of physically bonded water molecules at temperature up to 100 and 300°C respectively in FA and PMFA-15. As the temperature increases, above 400°C, chemisorbed water, usually called "constitutional water" is evolved. [28]. This water is formed by extraction of an oxygen atom from the Keggin anion by two protons [51]. As exemplified by these results, it can be concluded that both samples are thermally stable and do not decompose into their constituents even at higher temperatures. In PMFA-15, inherent Keggin structure embedded on fly ash surface remains preserved [45].
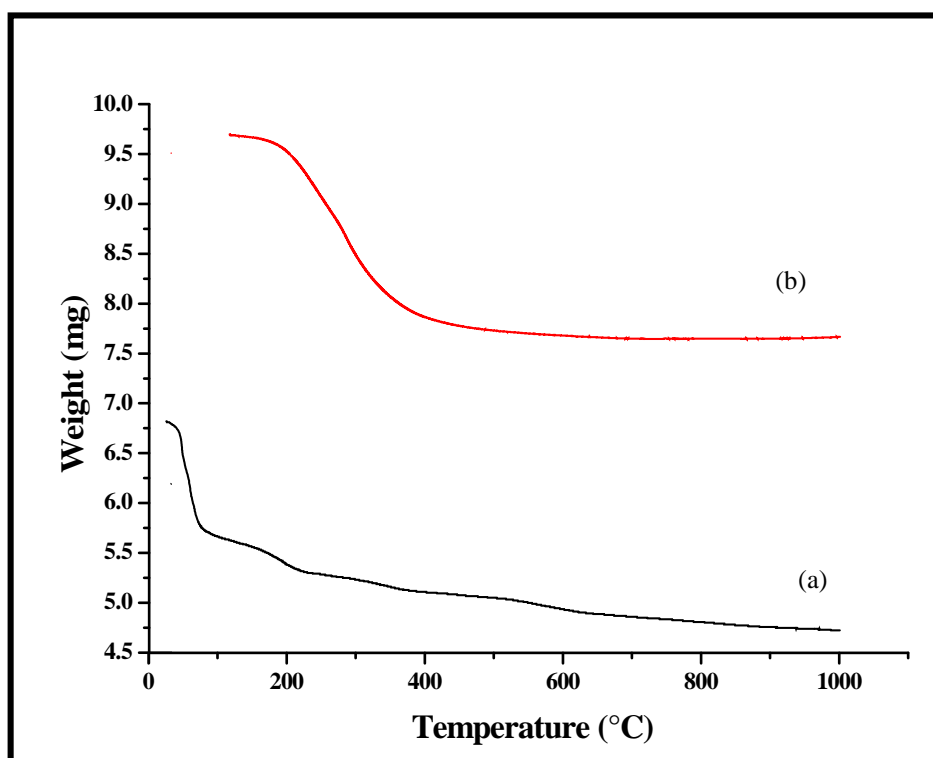
Figure 4.12:   TGA curves of (a) pure fly ash and (b) PMFA-15.

4.3.8 Ultra violet-Visible Diffuse Reflectance spectroscopy (UV-Vis DRS analysis)

By using UV–Vis DRS it is possible to probe the state of PMA species incorporated into silico-aluminate frameworks of fly ash. The absorption spectra appear in 200-500 nm region and the bands may be ascribed to oxygen to metal charge transfer. The tetrahedral Mo exhibits band centered at 220 nm which is shown in spectra of all catalysts **(Figure 4.13)** and become more intense on increasing weight % of PMA loading [52]. Whereas, another band appearing in region 450-560 nm in PMFA-10, 15 and 25, may be due to presence of Mo in octahedral environment also enhance on increasing PMA loading [53].
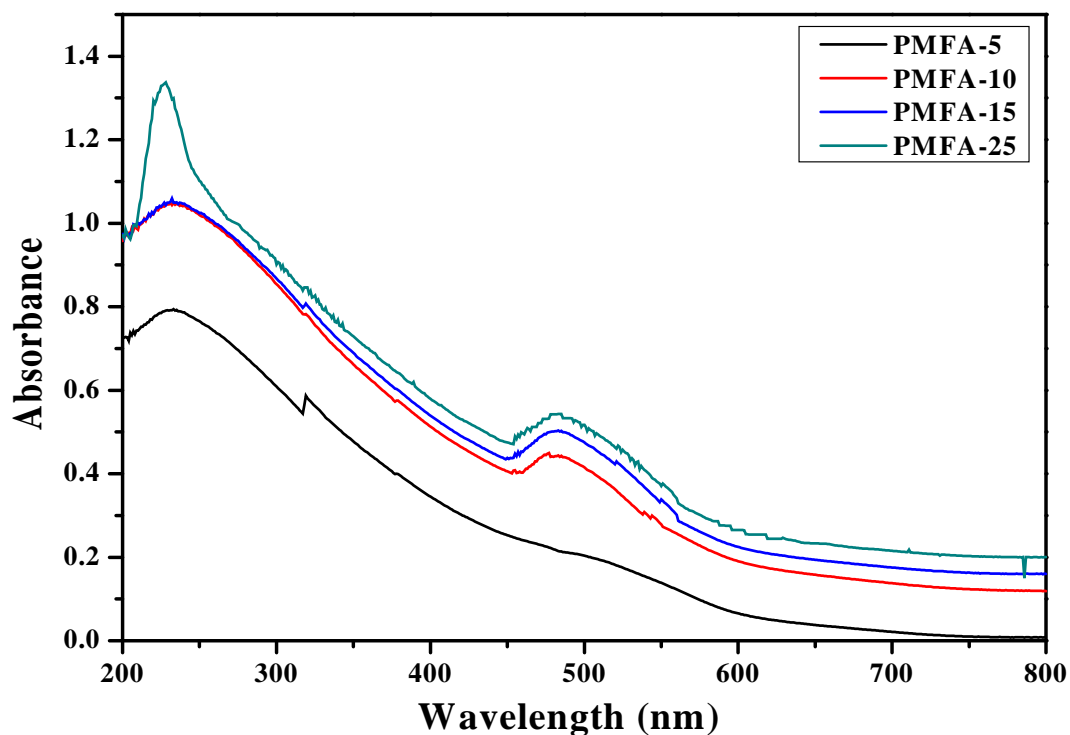
Figure 4.13:   UV-Vis DRS spectra of PMFA-5, 10, 15 and 25.

4.3.9 Solid state Phosphorus-31 NMR analysis

It is one of the main analytical techniques to study the state of phosphorous atom in heteropolyacids. The chemical shift seen in catalysts with respect to pure heteropolyacids depends upon surroundings of phosphorous or the factors like hydration number, nature of support, addenda metal ions etc. [54–58]. ^{31}P NMR spectrum of pure PMA (**Figure 4.14a**) shows a major peak at -0.088 ppm along with a small peak at 0.528 ppm reveals uniform phosphorous environment in highly hydrated structure of PMA. On calcining pure PMA at 400°C for 3 h, many small peaks or multiplet are obtained with a major peak at -2.300 ppm (**Figure 4.14b**) appears due to presence of microcrystalline PMA. A peak at -12.812 ppm could be assigned to phosphorous in Keggin unit of PMA [34]. Another sharp peak at 19.705 ppm can be ascribed to P_2O_5 (phosphorous oxide) resulting from decomposition of polyoxometallates [20]. On increasing calcinations temperature of PMA above 200°C, broadening of ^{31}P NMR signals is seen corresponding to formation of an anhydrous phase with preserved Keggin unit due to loss of hydrated water molecules [48]. Upfield and downfield shifts are seen in case of ^{31}P spectrum of PMFA-15 catalyst (**Figure 4.14c**), due to interaction of PMA with silica-alumina network of fly ash. The preservance of sharp signal at 0.283 ppm compared with that of pure PMA indicates that PMA Keggin units remain intact on the fly ash surface. When PMA Keggin units get interacted with support material, symmetry of central tetrahedral phosphorous atom is altered. Peaks around -30 and +30 ppm are due to formation of aluminophosphates mainly amorphous in nature [59,60]. ^{31}P NMR spectrum of PMFA-15 is more comparable to pure PMA rather calcined PMA suggesting the conservation of characteristic Keggin units of PMA during catalyst synthesis as interpreted by XRD and FT-IR results. All the samples showing more than one phosphorous resonance discloses the complicated structure of PMA.
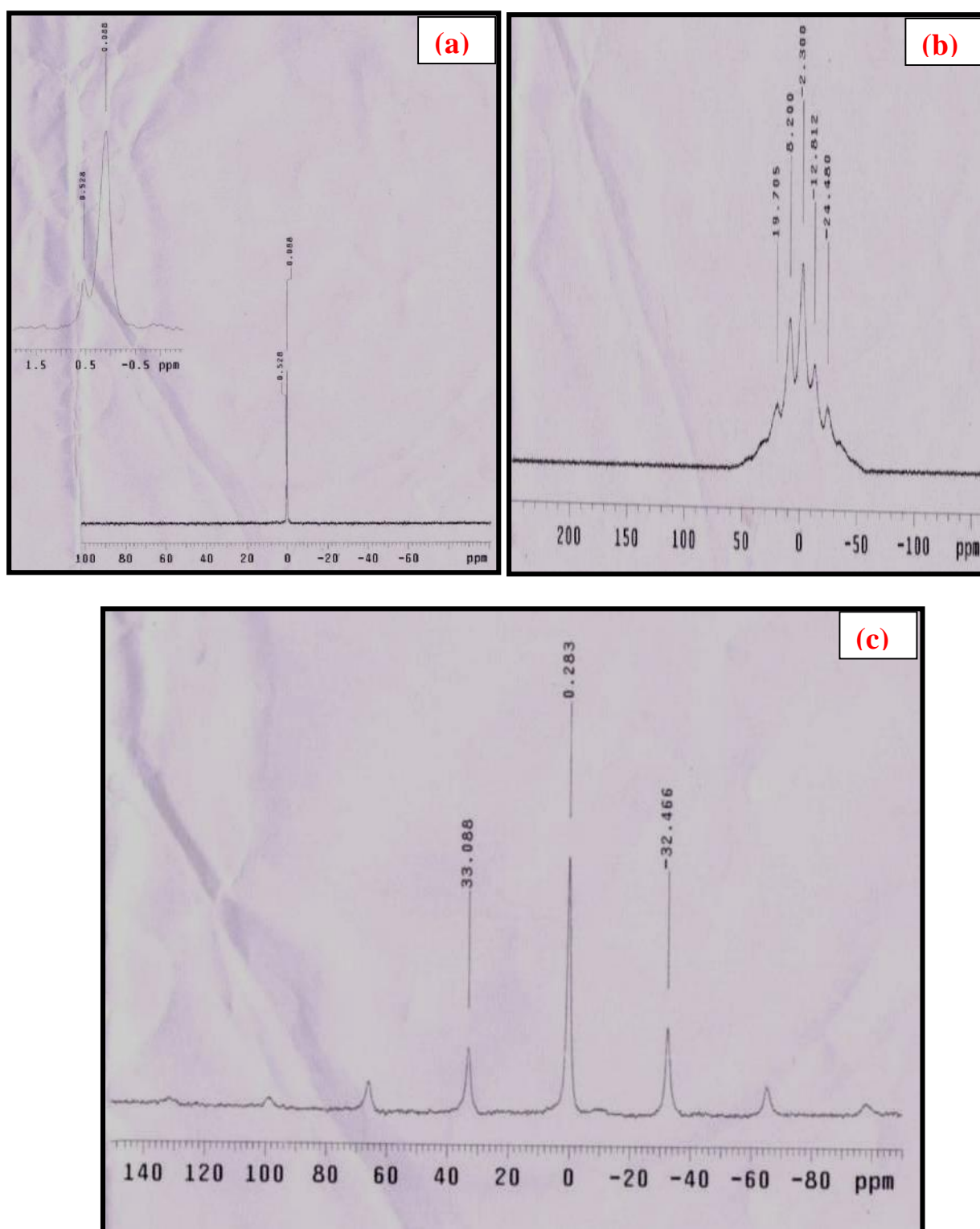
Figure 4.14: Solid state [31]Phosphorous NMR spectra of (a) PMA, (b) calcined PMA and (c) PMFA-15.

4.4 Catalytic behaviour

The catalytic performance is tested by Friedel-Crafts acylation reaction of isopropanol by acetyl chloride to give isopropyl acetate under microwave assisted, single step, solvent-free reaction conditions. Reaction is carried out at 100°C for 8 minutes, power output of 50 W, taking isopropanol/acetyl chloride molar ratio 1:1.5 and isopropanol to catalyst weight ratio of 10:1. Results given in **Table 4.3** show that fly ash, MFA-30 and TMFA do not possess any catalytic activity for this reaction. In case of PMFA-5 and 10, lower conversion% are obtained due to presence of less Lewis acid sites on catalytic surface while in PMFA-15, the conversion% is highest due to presence of sufficient active sites. The conversion% is again decreased on using PMFA-25 due to blockage of surface active Lewis acidic sites by bulk deposition of PMA crystallites as described earlier in pyridine FT-IR studies of PMFA-25.

Table 4.3: **Catalytic activity of different catalysts for Friedel-Crafts acylation reaction.**

Catalysts	Conversion (%)
Fly ash	Nil
MFA-30	Nil
TMFA	Nil
PMFA-5	68
PMFA-10	80
PMFA-15	88
PMFA-25	82

Reaction conditions: Time = 8 minutes; temperature = 100°C; power output = 50 W; molar ratio (isopropanol/acetyl chloride = 1:1.5); substrate/catalyst ratio = 10:1.

As suggested by these results, PMFA-15 is chosen as the main catalyst for catalyzing a series of Friedel-Crafts acylation reactions of various aliphatic alcohols by acetyl chloride. Further optimization of reaction parameters such as effect of reaction time and temperature, molar ratio of reactants, power output are also studied in order to attain maximum conversion%.

4.4.1 Influence of reaction temperature

To study the influence of reaction temperature on conversion%, acylation of aliphatic alcohols is conducted at different temperatures ranging from 70 to 140°C for 6-10 minutes. The results illustrated that the conversion% of alcohols gradually increases with increase in temperature as shown in **Figure 4.15**. The maximum conversion% is obtained at 90°C for isopropyl and t-butyl alcohols while, for iso butyl and iso amyl alcohols maximum conversion% is attained at 110 and 120°C respectively which get decreased on increasing temperature. Boiling points of most of reactants is less so at higher temperature reactants remain in gaseous phase and thus contact period between them decreases giving adverse effect on conversion%.
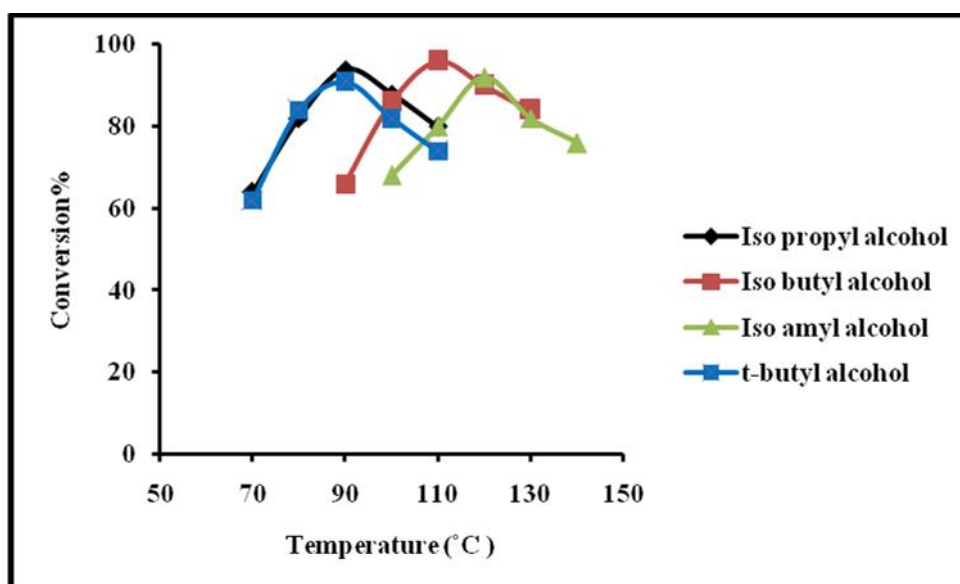
Figure 4.15: **Variation of conversion (%) of alcohols over PMFA-15 with temperature.**

Reaction conditions: Time = 6-10 minutes; molar ratio (alcohol/acetyl chloride = 1:1.5); power output = 60 W; substrate/catalyst ratio = 10:1.

4.4.2 Influence of reaction time

The variation of reaction time on conversion% is carried out in the range of 4 to 12 min at 90, 110 and 120°C for iso propyl, t-butyl, iso butyl and iso amyl alcohols respectively as shown in **Figure 4.16**. It is found that in first 10 minutes, the conversion% increases linearly giving highest conversion% at 6, 8 and 10

minutes which remained almost constant further. In this reaction, chances of formation of di or tri- acylated products is very less, so even if contact time between two reactants is increased, no significant effect is seen on conversion%.
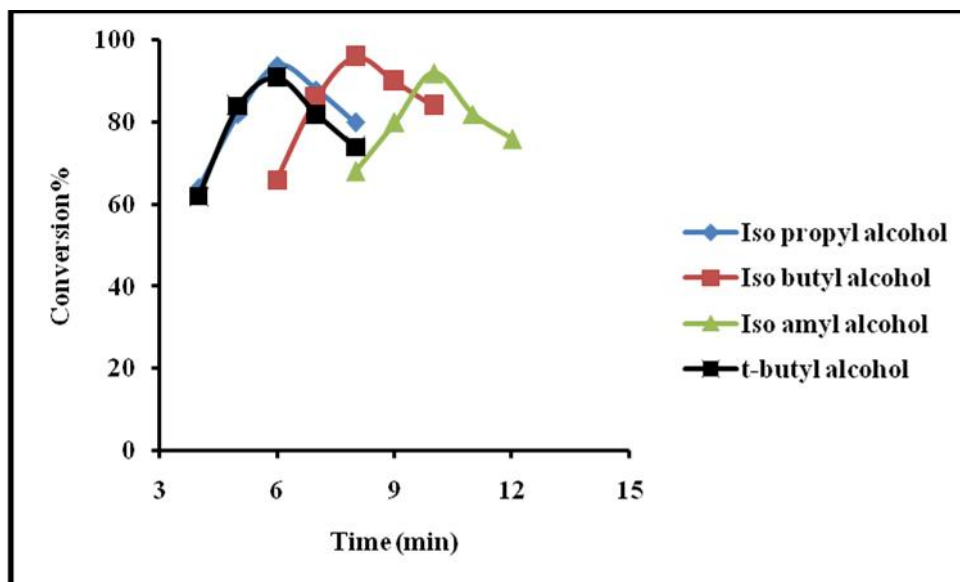
Figure 4.16: Variation of conversion (%) of alcohols over PMFA-15 with time.

Reaction conditions: Temperature = 90, 110 and 120°C for iso propyl, t-butyl, iso butyl and iso amyl alcohols respectively; molar ratio (alcohol/acetyl chloride = 1:1.5); power output = 60 W; substrate/catalyst ratio = 10:1.

4.4.3 Influence of molar ratio of reactants

The effect of molar ratios of alcohols and acetyl chloride on conversion% is monitored at different molar ratios varying from 1:1 to 2:1 as shown in **Figure 4.17**. Very less conversion% is observed at 1:1 molar ratio due to insufficient amount of both reactants to react with each other. In case of excess amount of any reactant, conversion% again decreases. If excess of acetyl chloride is taken, then chances of C-acylation increases which decreases selectivity of reaction towards ester formation. The conversion% of alcohols is found maximum at 1:1.5 molar ratio.
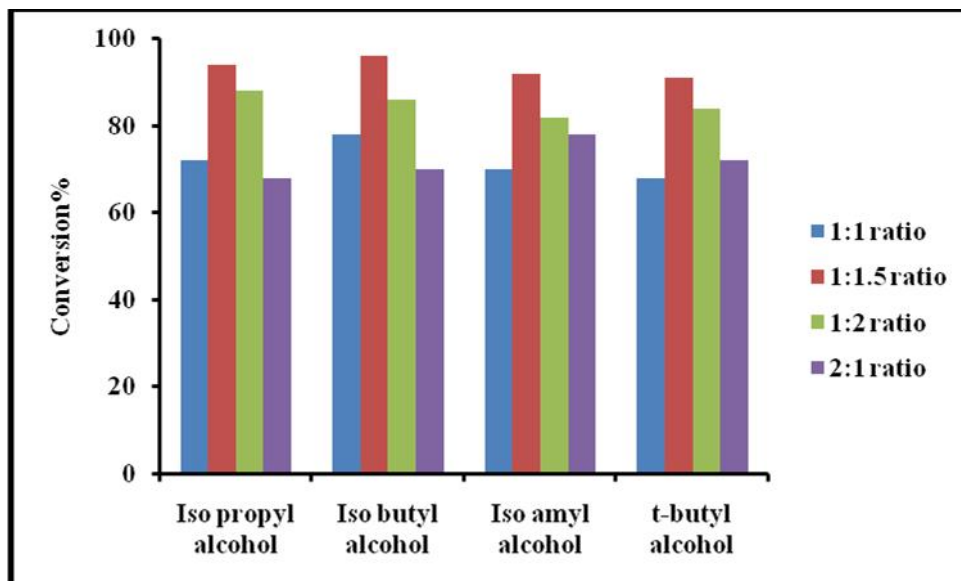
Figure 4.17: **Variation of conversion (%) of alcohols over PMFA-15 with molar ratio of reactants.**

Reaction conditions: Temperature = 90-120˚C; time = 6-10 min for iso propyl, t-butyl, iso butyl and iso amyl alcohols respectively; power output = 60 W; substrate/catalyst ratio = 10:1.

4.4.4 Influence of power output

The effect of power output of Microwave instrument on conversion% is studied at different power outputs ranging from 40 to 80 W as shown in **Figure 4.18**. The conversion% of alcohols is found maximum at 60 W suggesting that this much power of microwave irradiations are adequate for occurrence of acylation of alcohols with highest conversion%. On increasing power output from 60 to 80 W no sustainable change is seen in terms of conversion%.
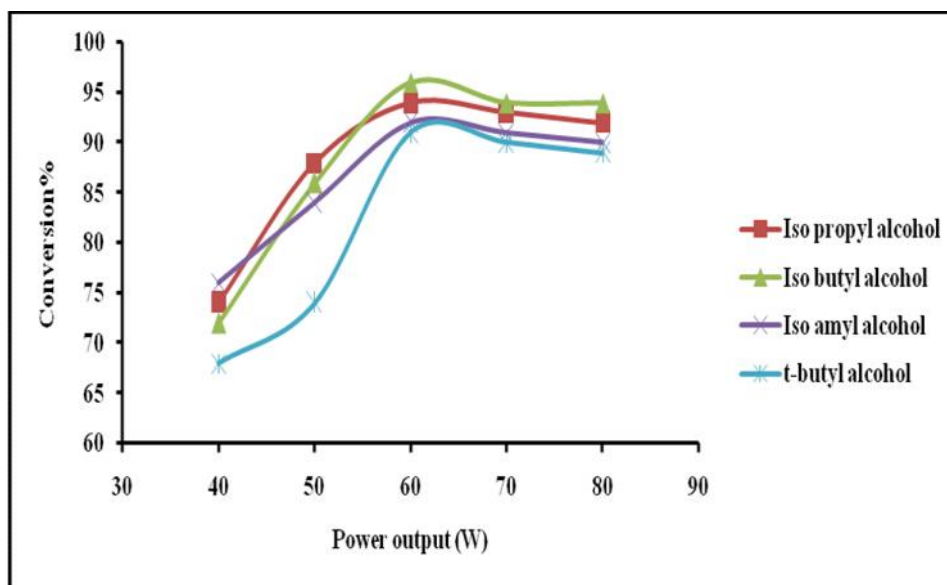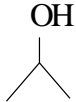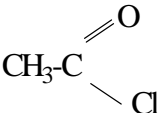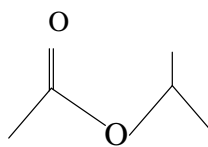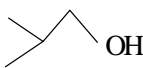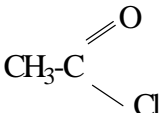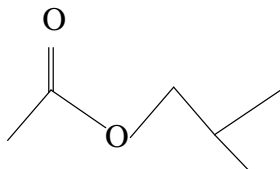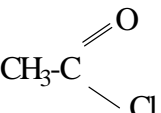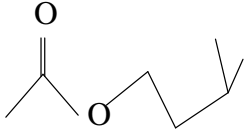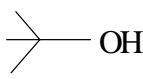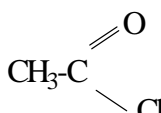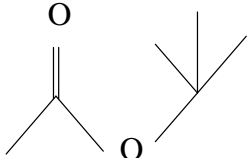
Figure 4.18: **Variation of conversion (%) of alcohols over PMFA-15 with power output.**

Reaction conditions: Temperature = 90-120°C; time = 6-10 min for iso propyl, t-butyl, iso butyl and iso amyl alcohols respectively; molar ratio (alcohols:acetyl chloride = 1:1.5; substrate/catalyst ratio = 10:1.

The maximum conversion% of products in a series of Friedel-Crafts acylation reactions **(Table 4.4)** is found when reaction is carried out at 90°C for 10 minutes, taking alcohols and acetyl chlotide in 1:1.5 molar ratio, power output of 60 W and substrate to catalyst ratio of 10:1 over PMFA-15. On increasing carbon chain, conversion% increases but in case of iso amyl alcohol, conversion% decreases. Same effect is also seen on taking branched aliphatic alcohol, t-butyl alcohol, because such alcohols obstruct entrance of acetyl chloride towards catalytic active sites, thus reducing the formation of acylium ions resulting in decrease of rate of reaction as well as converion% of reaction.

Table 4.4: Synthesis of various esters by PMFA-15 catalyzed Friedel-Crafts reaction between different aliphatic alcohols and acetyl chloride under microwave irradiated reaction conditions.

Entry	Alcohols	Acetyl chloride	Products	Conversion (%)
1				94
2				96
3				92
4				91

Reaction conditions:Temperature = 90°C; time = 10 min.; power output = 60 W; molar ratio (aliphatic alcohol/acetyl chloride = 1:1.5); substrate/catalyst ratio = 10:1.

4.5 Mechanistic aspects

The proposed structure for active sites of PMA-15 is given **Scheme 4.3.** Oxygen atoms attached with molybdenum attract electron density from the molybdenum making it electron deficient and generate Lewis acidity on the fly ash surface. The possible pathway for acylation of aliphatic alcohols by acetyl chloride catalyzed by PMFA-15 is shown in **Scheme 4.4**. The Lewis acidic sites of PMFA-15 help in formation of acylium ion from acetyl chloride. This intermediate in turn reacts with aliphatic alcohols to form desired acylated products (esters).
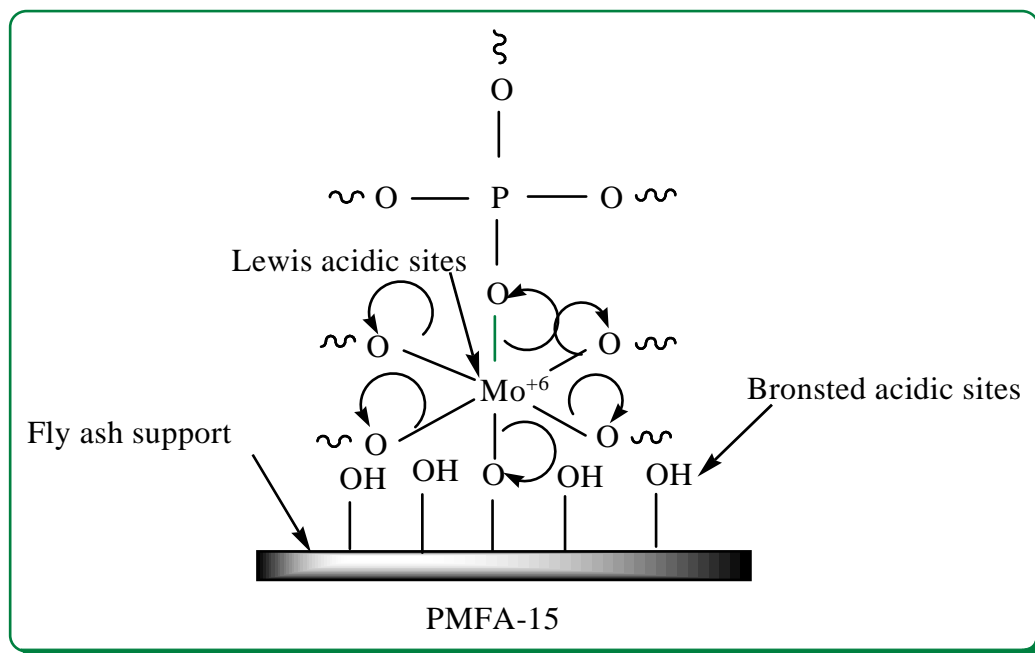
Scheme 4.3 : Proposed structure for active sites of PMFA-15.
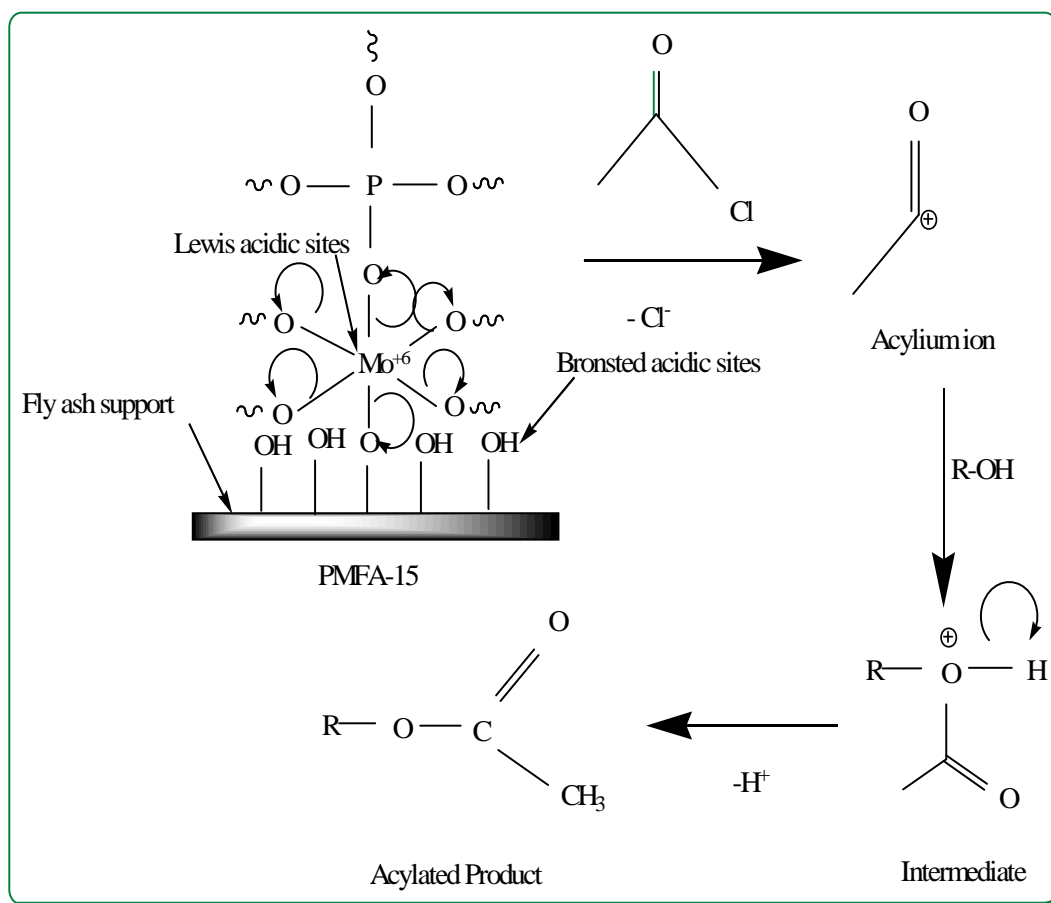
Scheme 4.4: Proposed mechanism of acylation of aliphatic alcohols by acetyl chloride over PMFA-15.

4.6 Regeneration and reusability of catalyst

The catalyst is filtered, washed with acetone, dried in oven at 110°C/12 h and then calcined at 400°C/2h for its use in next reaction cycles. The regenerated catalyst show efficient catalytic activity up to consecutive 5 reaction cycles giving similar conversion% of alcohols as shown in **Table 4.5**, which indicates that the acidic sites are not deactivated during regeneration. The conversion% is decreased after fifth reaction cycle, due to the deposition of carbonaceous materials on the surface of catalyst which could block the surface active sites of catalyst inferred by two peaks around 2850 cm^{-1} in FT-IR spectrum of PMFA-15 regenerated after fifth reaction cycle **(Figure 4.19b)** attributing to CH_2 symmetrical stretching vibrations of aliphatic hydrocarbons [61]. Loss in activity can also be further confirmed by decrease in intensity of band in the region of 3600-3300 cm$^-$1 in regenerated PMFA catalyst, responsible for catalytically active –OH groups. The stability, heterogeneous nature of PMFA-15 catalyst and possibility of leaching of highly soluble PMA species in reaction medium is further analyzed by Sheldon's hot filteration test [62] which involves filtration of catalyst from reaction mixture in between the reaction and further continuance of reaction in absence of catalyst. The results show that the reaction stops on filtering off the catalyst in mid of the reaction, hence it is confirmed that active PMA species responsible for catalytic activity do not get leached off during course of reaction.

Table 4.5: Friedel-Crafts acylation of alcohols by acetyl chloride over fresh and regenerated PMFA-15.

Reaction cycles	Conversion (%)
I	94
II	92
III	92
IV	90
V	87

Reaction conditions:Temperature = 90°C; time = 10 min.; power output = 60 W;
molar ratio (aliphatic alcohol/acetyl chloride = 1:1.5); substrate/catalyst ratio = 10:1.
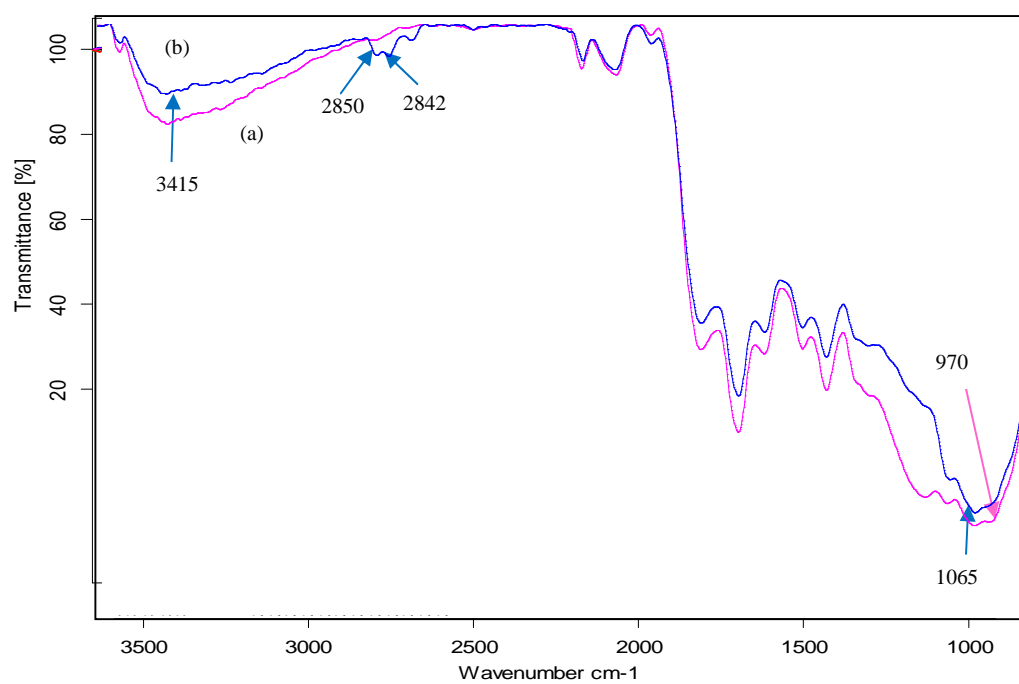
Figure 4.19:   FT-IR spectra of (a) PMFA-15 and (b) regenerated catalyst.

4.7 Conclusion

The present investigation elaborates the synthesis of a novel, efficient, economic, regenerable fly ash supported solid acid catalyst by loading of phosphomolybdic acid on mechanically and thermally activated fly ash. Surface roughness and stable silanol groups of fly ash increased by mechanical and thermal activations facilitates efficient loading of PMA. The prepared PMFA-15 catalyst having sufficient Lewis acidity successfully catalyze a series of microwave assisted Friedel-Crafts acylation reactions, giving excellent conversion%. Moreover, the catalyst is found to be extremely stable under microwave irradiations, suggesting a new greener area of time-saving catalysis for fly ash supported catalysts. The catalyst could be reused after thermal treatment up to five reaction cycles without significant loss in its activity. Furthermore, Sheldon's hot filtration test ascertains that the active PMA species of the catalyst do not get leached off while reaction and heterogenity of the catalyst remains intact. This comprehensive catalytic performance indicates that coal generated fly ash, an abundant industrial solid waste, can be succesfully utilized as an active silica support material for synthesis of a novel solid acid catalyst, PMFA-15 which has a promising future as an alternative for other commercial solid acid catalysts in area of microwave assisted Friedel-Crafts acylation reactions useful in pharmaceutical, fine chemical, cosmetic industrial applications etc.

## 4.8 References

[1]   A.S. Grewal, K. Kumar, S. Redhu, S. Bhardwaj, Int. Res. J. Pharm. Appl. Sci. 3 (2013) 278.

[2]   S.A.R. Mulla, S.M. Inamdar, M.Y. Pathan, S.S. Chavan, E.T. Al, Open J. Synth. Theory Appl. 2012 (2012) 31.

[3]   V. Umamaheshwari, M. Palanichamy, B. Arabindo, V. Murugesan, Indian J. Chem. 40 (2001) 704.

[4]   R. Ghosh, S. Maiti, A. Chakraborty, Tetrahedron Lett. 45 (2004) 6775.

[5]   R. Tayebee, F. Cheravi, Bull. Korean Chem. Soc. 30 (2009).

[6]   M.A. Pasha, M. Bhojegowd, M. Reddy, K. Manjula, Eur. J. Chem. 1 (2010) 385.

[7]   T.W. Green, P.G.M. Wuts, Protective Groups in Organic Synthesis, Third, Wiley, New York, 1999.

[8]   H. Yamashita, Y. Mitsukura, H. Kobashi, "Journal Mol. Catal. A, Chem. 327 (2010) 80.

[9]   M.A. Pasha, K. Manjula, V.P. Jayashankara, J. Saudi Chem. Soc. 11 (2007) 327.

[10]   G. Winé, E. Vanhaecke, S. Ivanova, R. Ziessel, C. Pham-huu, Catal. Commun. 10 (2009) 477.

[11]   G. Bai, T. Li, Y. Yang, H. Zhang, X. Lan, F. Li, J. Han, Z. Ma, Q. Chen, G. Chen, CATCOM 29 (2012) 114.

[12]   R. Luque, V. Budarin, J.H. Clark, P. Shuttleworth, R.J. White, CATCOM 12 (2011) 1471.

[13]   G.D. Yadav, M.S. Krishnan, Chem. Eng. Sci. 54 (1999) 4189.

[14]   J.A. Melero, R. Van Grieken, G. Morales, V. Nu, Catal. Commun. 5 (2004) 131.

[15]   F. Tamaddon, M.A. Amrollahi, L. Sharafat, Tetrahedron Lett. 46 (2005) 7841.

[16]   Y. Matsushita, K. Sugamoto, T. Matsui, Tetrahedron Lett. 45 (2004) 4723.

[17]   A. Alizadeh, M.M. Khodaei, E. Nazari, Bull. Korean Chem. Soc. 28 (2007) 1854.

[18]   I. V Kozhevnikov, Appl. Catal. A Gen. 256 (2003) 3.

[19]   P. Sharma, A. Patel, Indian J. Chem. 48 (2009) 964.

[20]   M.S. Khayoon, B.H. Hameed, "Applied Catal. A, Gen. 433-434 (2012) 152.

[21]   E. Tsukuda, S. Sato, R. Takahashi, T. Sodesawa, Catal. Commun. 8 (2007) 1349.

[22]   A.S. Badday, A.Z. Abdullah, K. Lee, Appl. Energy 105 (2013) 380.

[23]   L.A.M. Cardoso, W. Alves, A.R.E. Gonzaga, L.M.G. Aguiar, H.M.C. Andrade, J. Mol. Catal. A Chem. 209 (2004) 189.

[24]   B.B. Baeza, J.A. Anderson, J. Catal. 228 (2004) 225.

[25]   A.P. Toor, M. Sharma, G. Kumar, R.K. Wanchoo, Bull. Chem. React. Engg. Catal. 6 (2011) 23.

[26]   K. Ohyama, G. Shimada, Y. Tokumoto, Kazuo Sakamoto, Process for the Preparation of Isopropyl Acetate, 5384426, 1995.

[27]   J. Temuujin, A. van Riessen, J. Hazard. Mater. 164 (2009) 634.

[28]   D. Liu, X. Quek, S. Hu, L. Li, H.M. Lim, Y. Yang, Catal. Today (2009) 51.

[29]   J.B. Condon, Surface Area and Porosity Determinations By Physisorption, 2006.

[30]   S. Katara, S. Kabra, A. Sharma, R. Hada, A. Rani, Int. Res. J. Pure Appl. Chem. 3 (2013) 299.

[31]   J.M. Fox, in:, 2005 World Coal Ash, 2005.

[32]   C. Rocchiccioli-deltcheff, M. Amirouche, M. Fournier, J. Catal. 138 (1992) 445.

[33]   A.I. Ahmed, S.E. Samra, S.A. El-hakam, A.S. Khder, H.Z. El-shenawy, W.S.A. El-yazeed, Appl. Surf. Sci. 282 (2013) 217.

[34]   B.M. Devassy, F. Lefebvre, B. Walter, J. Fletcher, S.B. Halligudi, J. Mol. Catal. A Chem. 236 (2005) 162.

[35]   G. Shu-wen, L. Li-jun, Z. Qian, W. Liang-yin, Bull. Korean Chem. Soc. 33 (2012) 1279.

[36]   P. Vázquez, L. Pizzio, G. Romanelli, J. Autino, C. Cáceres, M. Blanco, Appl. Catal. A Gen. 235 (2002) 233.

[37]   H. Kim, J. Chul, D. Ryul, H. Lee, J. Lee, S. Hee, S. Baeck, K. Lee, J. Yi, I. Kyu, Catal. Today 132 (2008) 58.

[38]   S. Gong, L. Liu, Q. Cui, J. Ding, J. Hazard. Mater. 178 (2010) 404.

[39]   F. Adam, J.N. Appaturi, R. Thankappan, M. Asri, M. Nawi, Appl. Surf. Sci. 257 (2010) 811.

[40]   C. Khatri, A. Rani, Fuel 87 (2008) 2886.

[41]   A. Sharma, K. Srivastava, V. Devra, A. Rani, Am. Chem. Sci. J. 2 (2012) 177.

[42]   A. Palomo, M.W. Grutzeck, M.T. Blanco, Cem. Concr. Res. 29 (1999) 1323.

[43]   C. Rocchiccioli-deltcheff, A. Aouissi, S. Launay, M. Fournier, J. Mol. Catal. A Chem. 169 (1996).

[44]   M.R. El-Naggar, R.F. Aglan, M.S. Sayed, J. Environ. Chem. Eng. 1 (2013) 516.

[45]   M.M.M.A. El-wahab, A.A. Said, J. Mol. Catal. A Chem. 240 (2005) 109.

[46]   C. Chen, L.P. Zhou, Q.H. Zhang, H. Ma, H. Miao, J. Xu, Nanotechnology 18 (2007) 215603.

[47]   B.M. Devassy, G. V Shanbhag, S.B. Halligudi, J. Mol. Catal. A Chem. 247 (2006) 162.

[48]   B. Pawelec, S. Damyanova, R. Mariscal, J.L.G. Fierro, I. Sobrados, J. Sanz, L. Petrov, J. Catal. 223 (2004) 86.

[49]   M. Misono, Y. Konishi, M. Furuta, Y. Yoneda, Chem. Lett. (1978) 709.

[50]   M. Li, J. Shen, X. Ge, X. Chen, Appl. Catal. A Gen. 206 (2001) 161.

[51]   I.A. Laila, N.S. Abed-Elshafy, Hungarian J. Ind. Chem. 34 (2006) 55.

[52]   P. Vazquez, C. Caceres, M. Blanco, H. Thomas, E. Alesso, L. Finkielsztein, B. Lantano, J. Mol. Catal. A Chem. 161 (2000) 223.

[53]   G. Romanelli, P. Vázquez, L. Pizzio, N. Quaranta, J. Autino, M. Blanco, C. Cáceres, Appl. Catal. A Gen. 261 (2004) 163.

[54]   M. Misono, Chem. Commun. (2001) 1141.

[55]   C. Dillon, J. Catal. 218 (2003) 54.

[56]   M.W.A. A. Ghanbari-siahkali, A. Philippou, J. Dwyer, Appl. Catal. A Gen. 192 (2000) 57.

[57]   Á. Molnár, T. Beregszászi, Á. Fudala, P. Lentz, J.. Nagy, Z. Kónya, I. Kiricsi, J. Catal. 202 (2001) 379.

[58]   S. Uchida, K. Inumaru, M. Misono, J. Phys. Chem. B 104 (2000) 8108.

[59]   S. Nakata, S. Asoaka, H. Takahashi, K. Deguchi, Anal. Sci. 2 (1986) 91.

[60]   A. Corma, J. Catal. 145 (1994) 27.

[61]   L.J. Preston, M.R.M. Izawa, N.R. Banerjee, Astrobiology 11 (2011) 585.

[62]   A. Rani, C. Khatri, R. Hada, Fuel Process. Technol. 116 (2013) 366.

Synthesis of Acid Activated Catalysts from Perlite and their Application in a Series of Microwave Assisted Fischer Esterification Reactions

Abstract

This study investigates the structural, morphological, surfacial modifications of silica-alumina enriched, natural waste- perlite through thermal and chemical activations. Solid acid catalysts are synthesized by treatment of perlite with various mineral acids (H_2SO_4, HNO_3 and HCl). The catalytic performances of catalysts are evaluated for the series of microwave assisted Fischer esterification reactions of propionic acid and various aliphatic alcohols, producing esters widely used in pharmaceuticals, confectionaries, flavouring industries etc. Changes occur in surface area of perlite after activation is studied by N_2 adsorption-desorption. Structural modifications are determined by XRD and FT-IR techniques. Irregular morphology of perlite is revealed by SEM analysis. Presence of surface active acidic sites and their types are studied by pyridine adsorbed FT-IR. Various reaction parameters like time, temperature, molar ratio, power output are optimized for attaining highest conversion%. The catalyst could be recycled up to four reaction cycles without any significant loss in activity conferring its stability during course of reaction comparable with other commercial catalysts. The study focuses on conversion of silica-alumina rich perlite into potential heterogeneous acid catalysts for catalyzing industrially beneficial organic transformations, which is a promising and cost-effective route to utilize this abundant waste material.

5.1 Introduction

Fischer esterification also known as intermolecular dehydration reaction is an elementary yet important reaction, having wide applications in small and large scale industries, namely, fragrances, flavours, cosmetics, solvents, chiral auxiliaries, adhesives, lubricants, plasticizers, polymerization monomers etc. [1–5]. Esters also act as precursors of different pharmaceuticals, fine chemicals and agro-chemicals [6,7]. This reaction is significant in synthetic organic chemistry as it protects carboxyl acid group in various organic transformations [8]. Uncatalyzed esterification reaction is also possible [9]. However, in absence of catalyst, reaction is relatively slow, therefore presence of catalyst is essentially required. Catalyst helps in chemisorption of reactants on its surface, involves in carbocation formation and initiates esterification reactions. Commonly, liquid acid catalysts like H_2SO_4, HCl, HI, HNO_3, H_3PO_4, p-toluene sulfonic acid etc. [10–12] are extensively used in ester synthesis. Application of such catalysts encounter several inherent problems like instrumental corrosion, environmental hazards, difficult catalyst recovery and reuse, more by-product and waste formation etc. Moreover, homogeneous catalysts may also result in sulphur contamination of final product [3]. Thus, there is an urgent need to replace such unsafe catalysts by eco-friendly, less corrosive, green, efficient, long time persisting, sustainable heterogeneous acid catalysts which can be easily recovered from reaction mixture and recycled several times. Heterogeneous acid catalysts like ion-exchange resins, sulphated zirconia, zeolites, acidified silica, heteropoly acids, polymers with sulfonic acid group, H-ZSM-5, mesoporous Al-MCM-41 [13–19] constitute more eco-friendly substitutes in esterification reactions. Even though above-mentioned disadvantages can be resolved, these catalysts have their own short-comings, such as easy deactivation, high mass transfer resistance, adsorption of products, low densities of effective acid sites in zeolites [1], high cost of resins etc. Thus, the development of solid acid catalysts with higher product yield and selectivity, easy reusability and cost-effective features has become a sizzling topic in recent research endeavours.

Increasing environmental, economical and green chemistry concerns have pushed research interests to develop new, clean, eco-friendly technologies with

minimum waste generation. In this regard, microwave technology has gained much attention in organic synthesis. The use of microwave heating has noticeably reduced reaction times periods, leads to better conversion and yields of desired products with excellent purity as compared to conventional technique [20]. Microwave heating induces thermal or in situ heating resulting in uniform heating throughout the sample, thus enhances rate of reaction via superheating phenomenon. Polar molecules adsorbed on catalyst surface could facilitate superheating, leading to fast proton transfer to reactants and accordingly rate of esterification reaction increases under microwave irradiations.

The treatments which modify surface of support material are generally known as 'activation treatments'. Appropriate acid and thermal treatments enhances catalytic and adsorbing properties of supports. Perlite, being an ensemble of metal oxides in inert state exhibit very less or negligible catalytic activity. To prevail over such shortcomings, pre-treatment like thermal activation at higher temperature is necessary. It gives rise to a large number of interaction prospects among species present on surface of perlite at the time of further treatment. Perlite is thermally stable, rich in silica and alumina hence, it can incorporate large number of acidic sites and its surface can be activated. Acid activation is likely to improve surface area and porosity, silica/alumina ratio of perlite by leaching various minor metal oxides. Consequently, number of Si-OH groups and thus acidic sites increases on perlite surface up to a certain level. Development of acidic functional groups onto solid surfaces like silica, alumina, carbon based materials [21–23] has been investigated to produce promising heterogeneous catalysts. Acid treated clays have catalyzed many conventional and microwave assisted esterification reactions [8,24]. Nevertheless, no work has been reported to the best of our knowledge regarding use of solid acid catalysts for microwave irradiated esterification reactions using perlite, a natural waste as a catalyst support.

This chapter incorporates thermal followed by chemical activation of perlite, using mineral various acids and its conversion into heterogeneous catalyst having suitable acidic sites for undertaking a series of microwave assisted Fischer esterification reaction. Since esterification is a suitable test reaction for evaluation

of solid acid catalysts [25] and their products are of immense industrial significance in various areas such as pharmaceuticals, fine chemicals, flavouring industries, cosmetics etc., that's why we choose this reaction for determination of catalytic activity of our prepared catalysts. The work also shed the light on impact of different activation techniques on structure, morphology, chemical bonding of perlite. The reaction parameters are further optimized for maximum conversion%. The catalyst is found to be recyclable up to four consecutive runs with analogous efficiency. Use of less expensive support, recyclable catalyst, less time consuming microwave technique, solvent-less reaction conditions, green methodology, ease of product purification are the key features of this protocol and thus it may be considered as an efficient alternative to the existing, high-priced, less-effective procedures.

5.2   Experimental

5.2.1 Materials

Perlite is supplied by Indica Chem. Ind. Pvt. Ltd., India. Sulfuric acid, nitric acid and hydrochloric acids are purchased from Sigma Aldrich. Propionic acid, aliphatic alcohols are purchased from Merck.

5.2.2 Catalyst preparation

As received perlite is initially activated thermally at 800°C for 3 h and converted into thermally activated perlite (TAP). The chemical activation of TAP is performed in magnetic stirred reactor under constant stirring with concentrated sulphuric acid, nitric acid and hydrochloric acid in the ratio of 1:2 (TAP: Acid) for 4 days at 100°C. The slurries are washed with distilled water up to pH 7, to remove excess of acid and other soluble leached compounds. Some qualitative chemical tests are done on samples to detect presence of soluble ionic species (sulphate, nitrate, chloride ions). Then, the so-obtained pulps are dried at 110°C for 24 h. Sulfuic acid, nitric acid and hydrochloric acid activated perlite samples (SAPC, NAPC and HAPC) are then calcined at 550°C for 4 h in muffle furnace under static conditions. The steps of synthesis of acid activated perlite catalysts are summarized in **Scheme 5.1.**
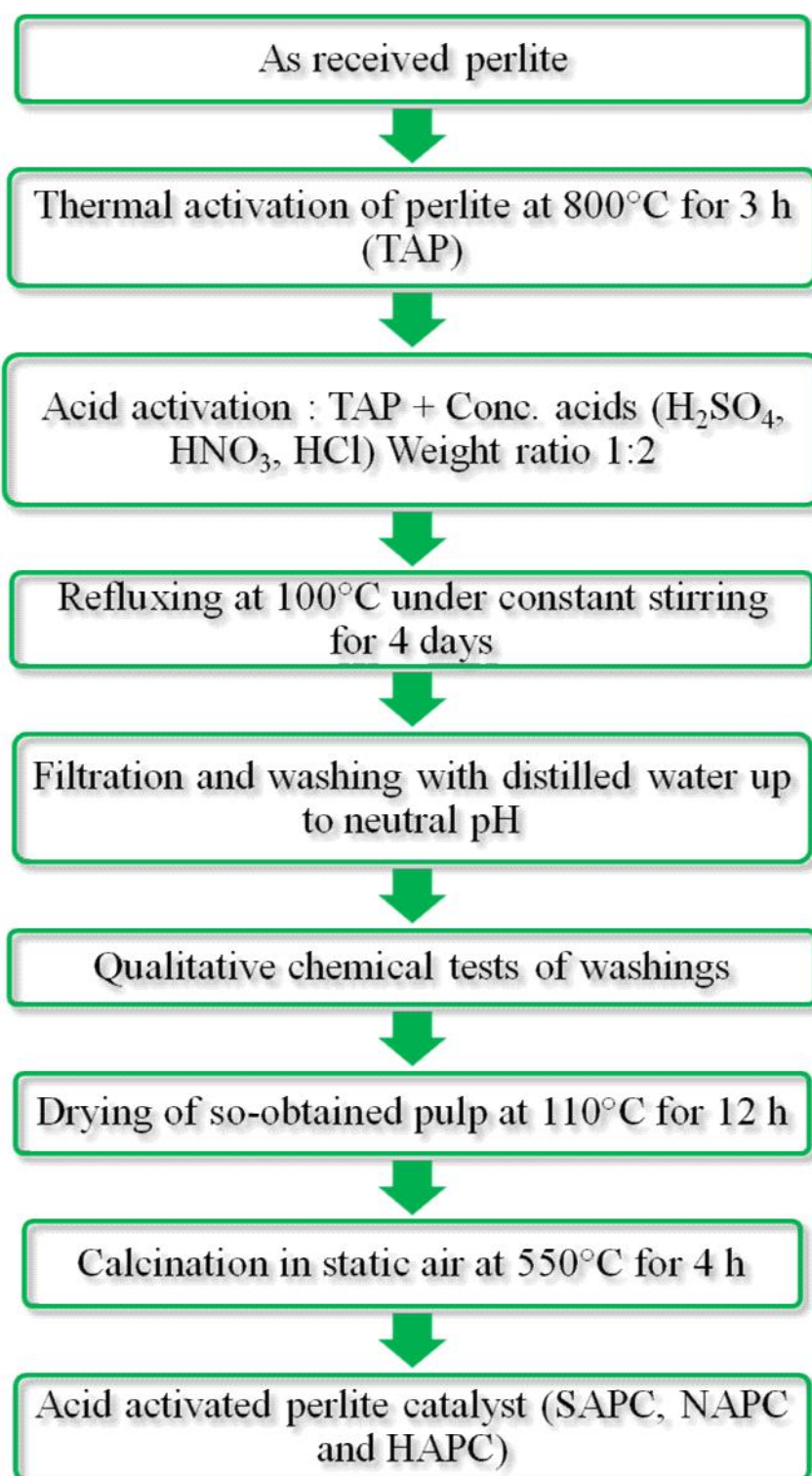
Scheme 5.1: **Synthesis of acid activated perlite catalysts.**

5.2.3 Instrument

The reactions are performed on single mode microwave cavity, PC operated, synergy.exe software based, microwave instrument (CEM-Discover) comprising of closed and open vessel systems, having an IntelliVent^{TM} Pressure Control System with a working frequency of 2.45 GHz, power output from 0 to 300 W, temperatures ranging from 25-300°C, pressure range from 0-300 Psi. The system comprises of vacuum fluorescent display with alphanumeric keypad and on-board computer for programming and operational control of the system. An Infrared detector and sensor controls and measures the temperature during the reactions respectively while, a Teflon spill cup protects the detector from exposure. An air compressor connected with the equipment is utilized for cooling of reactions. For sake of safety, an attenuator and three safety interlocks are provided in the system. The reactions are preferred in Power$_{max}$ mode, using simultaneous heating and cooling method.

5.2.4 Catalyst characterization

Physicochemical properties of all catalytic materials are studied by N$_2$ adsorption-desorption, XRD, FT-IR and pyridine adsorbed FT-IR and SEM, SEM-EDX techniques, as described in **Annexure-I**.

5.2.5 Catalytic activity

Fischer esterification reactions between aliphatic alcohols and propionic acid (**Scheme 5.2**) catalyzed by SAPC, NAPC and HAPC to give corresponding esters are performed in a microwave reactor. In this procedure, a mixture of aliphatic alcohol and propionic acid (different molar ratios) is taken in a 10 ml Pyrex microwave vial covered by intellivent septa cap. The varying amounts of catalyst activated at 400°C for 1 h, is then added in the reaction mixture. The reaction is carried out in closed vessel system at 50 Psi pressure, by placing the vial in microwave cavity under constant stirring at different time periods, molar ratios, temperatures and power outputs. After input of temperature, hold time, power and pressure parameters, the reaction is started by clicking on 'Play' button under Power$_{max}$- On conditions. After completion of holding time, the instrument

is turned off and the reaction is cooled through air compressor. Then, the catalyst is separated, product is filtered and analyzed by Gas Chromatograph.

The conversion% of alcohol is calculated by using following method:

$$\text{Conversion (\%)} = 100 \text{ X} \frac{(\text{Initial wt \% - Final wt \%})}{\text{Initial wt \%}}$$
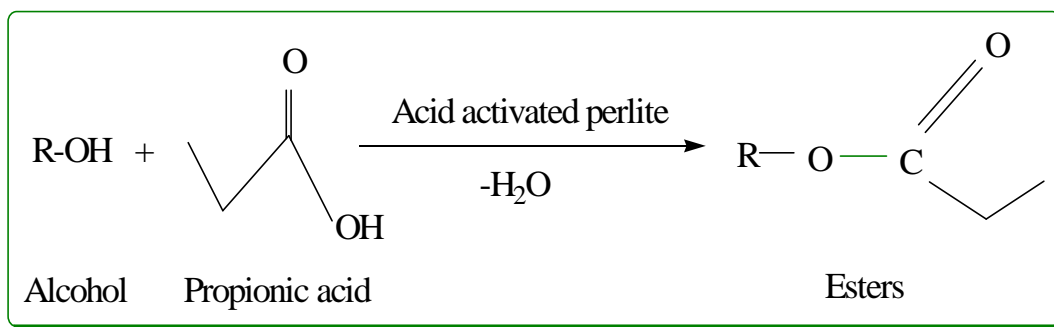
Scheme 5.2: **Simplified reaction pathway of Fischer esterification of aliphatic alcohols and propionic acid over acid activated perlite to give corresponding esters.**

5.3   Results and discussion

Thermal activation of perlite results in its colour change from light grey to light pink, due to removal of excess water and carbon. Loss on ignition (LOI) is determined experimentally by heating a certain weighed quantity of perlite in muffle furnace at 800°C for 3 h. The LOI amount is 4.1 wt % which corresponds to the removal of moisture and coexisting unburned carbon from sample [26].

5.3.1 BET analysis

BET specific surface area of samples as given in **Table 5.1** indicates that on thermal activation, specific surface area of perlite decreases from 2.6 to 2.2 m^2/g which increases on further activations by different acids, due to increase in amorphous silica content as a result of acid treatment [27]. Silica transformation becomes quite easier on using concentrated acids. On acid attack, even crystalline phases of impurities like Fe, Zn, Ti etc. also change into their amorphous forms respectively and get leached off easily [28].

Table 5.1:   **BET specific surface area data of samples.**

Samples	BET specific surface area (m^2/g)
Perlite	2.6
TAP	2.2
SAPC	10.6
NAPC	9.2
HAPC	7.4

5.3.2 X-ray diffraction analysis

The broad X-ray diffraction pattern of perlite **(Figure 5.1a)** confirmed the absence of crystalline structure [29] which is typical for amorphous solids. However, thermal treatment of perlite at higher temperature could convert less ordered structure to more ordered structure and a single, small crystalline peak appears in TAP at 2 = 27.642° **(Figure 5.1b)** which shows crystalline quartz formation in perlite [30] along with a broad hump at 2 = 22-23° confirming amorphous nature of silica [31]. It is well documented that at burning temperature higher than 973 K, production of crystalline structure is induced in silica [32]. On further chemical activation of TAP with concentrated acids **(Figure 5.1c-e)**, as developed crystalline component gets vanished, thus the associated crystalline peak disappears and amorphous nature of silica increases in catalysts [33]. A broad hump appearing in all samples confirms the presence of amorphous silica whose intensity increases with acid activation and is highest in case of SAPC. The results suggest that strongest chemical activation is done by sulphuric acid which completely destroy as developed crystalline structure and consequently highest amorphous silica content is present in SAPC also evident from SEM-EDX results later described in the chapter.
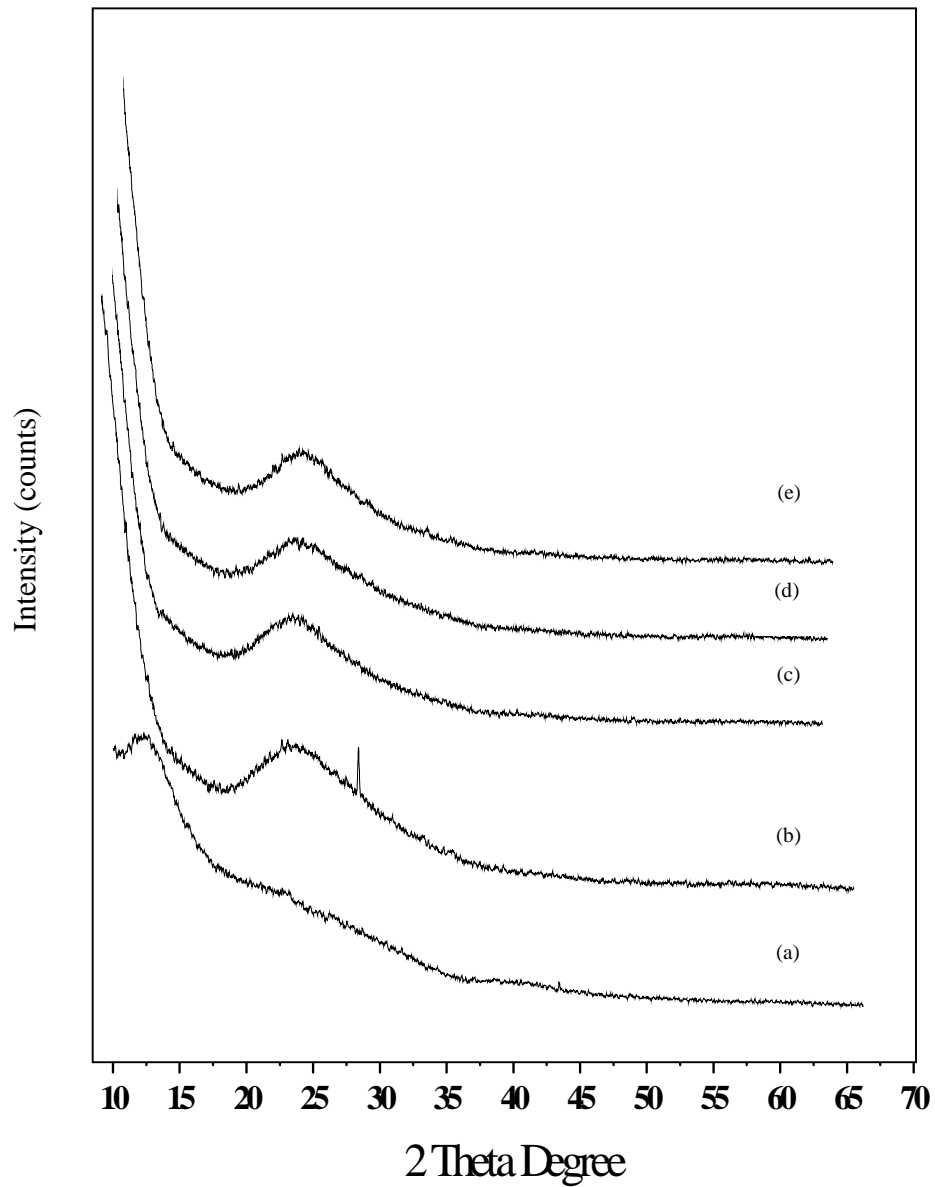
Figure 5.1: **X-ray diffraction pattern of (a) perlite, (b) TAP, (c) SAPC, (d) NAPC and (e) HAPC.**

5.3.2 *Fourier transform infra-red analysis (FT-IR)*

FT-IR spectra of perlite and TAP (**Figure 5.2**) shows a broad band between 3600-3300 cm^{-1}, which is attributed to surface hydroxyl groups of –Si-OH and water molecules adsorbed on the surface [34]. The broadness of band indicates the presence of strong hydrogen bonding in the sample [35]. In perlite, the hydroxyl groups exist in higher degree of association with each other which results in extensive hydrogen bonding, while in FT-IR spectrum of TAP, the intensity and broadness of band is decreased which confirms the loss of water. The strong band at 1178 cm^{-1} is due to the structural siloxane framework, which is the vibrational frequency of the Si-O-Si bond. The peak is shifted to higher wave number, i.e., 1227 cm^{-1} after thermal treatment, which is normally observed in amorphous silica samples [36]. An intense peak at 1632 cm^{-1} in the spectrum of perlite is attributed to bending mode ($_{O-H}$) of water molecule [37], which is again highly decreased in case of TAP.

Further chemical activation of TAP with different acids results in a significant increase in broadness and peak intensity of the band for –OH group which is highest in case of SAPC (**Figure 5.2c**). After acid treatment, the increase in silica content results in increase in surface hydroxyl groups, confirmed by broad and intense bands in the region of 3600-3300 and 1650 cm^{-1} responsible for stretching and bending vibrations of –OH group [38]. The shoulder at about 3200 cm^{-1} could be assigned to the stretching vibrations of Si-OH groups in the structure of amorphous SiO$_2$ [39]. An intense band in the range of 1300-1100 cm^{-1}, corresponding to valence vibrations of the silicate oxygen skeleton is usually assigned to the amorphous silica content which is increased after acid treatment of sample. The region around 805 cm^{-1} is characteristic of Si-O-Si symmetric stretching modes [31,40,41]. This increase in silica content, increased surface hydroxyl groups are responsible for generation of acidic sites on catalysts and enhance their catalytic activities.

5.3.3 *Pyridine adsorbed FT-IR analysis of catalysts*

For apparent vision about generation of surface acidic sites after chemical activation of TAP by different mineral acids and types of acidic sites, FT-IR

spectra, obtained after pyridine adsorption in the magnified range of 1600-1400 cm^{-1} are studied (**Figure 5.3**). The peaks observed in range of 1545-1530 cm^{-1} and 1480-1465 cm^{-1} in all demonstrated samples confirm the presence of sufficient Brønsted acidic sites on catalyst surface due to formation of co-ordinated pyridine and hydrogen bonded pyridine respectively with surface silanol groups [42]. The presence of Brønsted acidic sites in the catalysts confirms the effective acid activation on TAP which is later utilized as catalytic active sites for Fischer esterification reactions. The results indicate that maximum effective Brønsted acidic sites are available in SAPC as compared to other two catalysts. Increased amorphous silica content increases number of surface hydroxyl groups and thus Brønsted acidic sites raises in catalyst. Few Lewis acidic sites in case of HAPC are appeared around 1435 cm^{-1} because of rupture of Si-O-Al bond and arising of exposed Al^{+3} cations on edges of catalyst [43] or formation of Si^+ ions as a result of dehydroxylation [44].

5.3.4 *Scanning electron microscopy (SEM and SEM-EDX analysis)*

SEM micrograph of perlite (**Figure 5.4a**) revealed the irregular morphology of perlite particles. Similar pattern is observed in other reported micrographs of perlite [45]. SEM image of TAP (**Figure 5.4b**) is mainly fragmatic and random as a result of thermal activation [46]. But here, the morphology is less irregular which confirms the evaporation of water from the perlite sample on heating it at high temperature. After chemical activation, (**Figure 5.4c-e**) agglomeration occurs and particles tend to acquire spherical shape confering increase in amorphous silica content after acid leaching [31]. From the images it is cleared that fine agglomeration occurs in SAPC and the suitable acidic sites on SAPC provide enough space to reactant molecules for undergoing chemical reaction while due to formation of large clusters, catalytic activity is less in rest two catalysts.
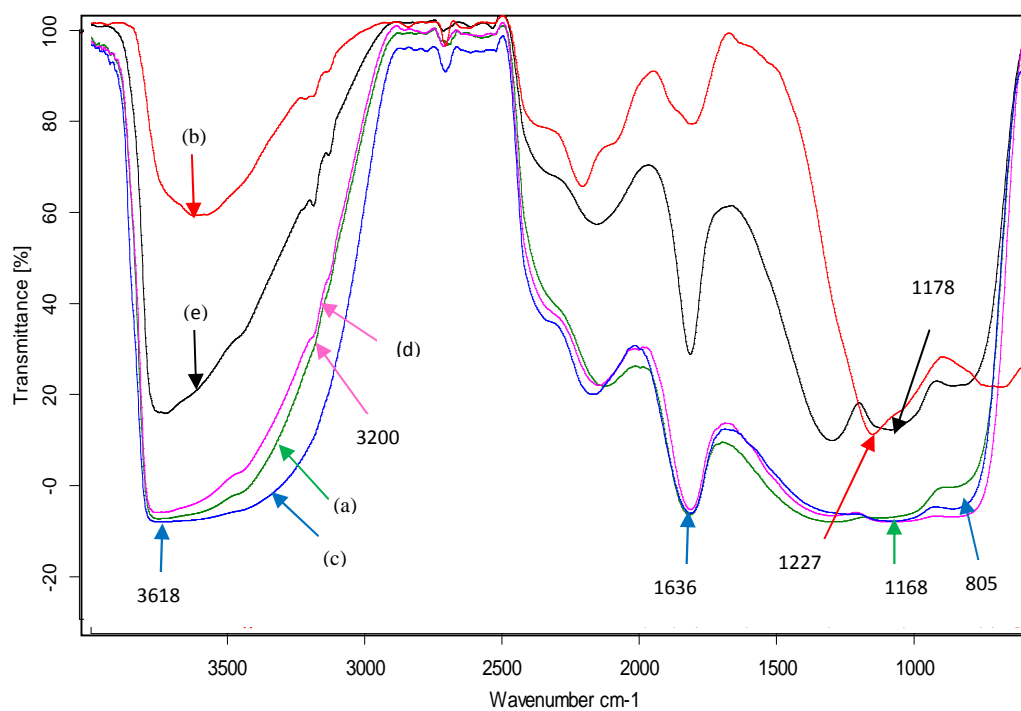
Figure 5.2: **FT-IR spectra of (a) perlite, (b) TAP, (c) SAPC, (d) NAPC and (e) HAPC.**
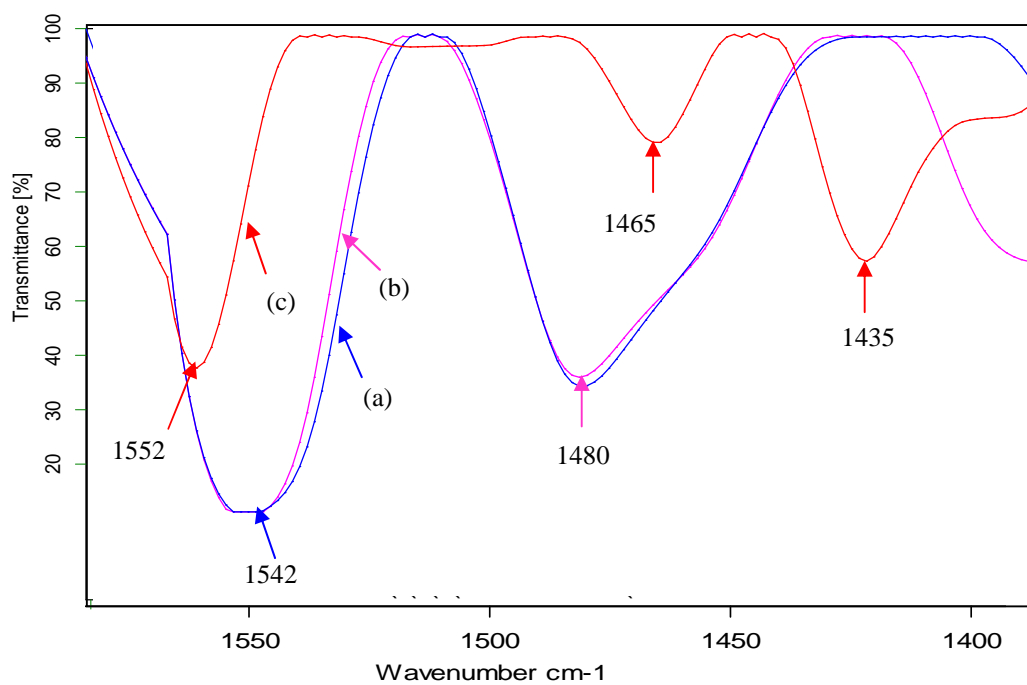
Figure 5.3: **Pyridine adsorbed FT-IR spectra of (a) SAPC, (b) NAPC and (c) HAPC.**
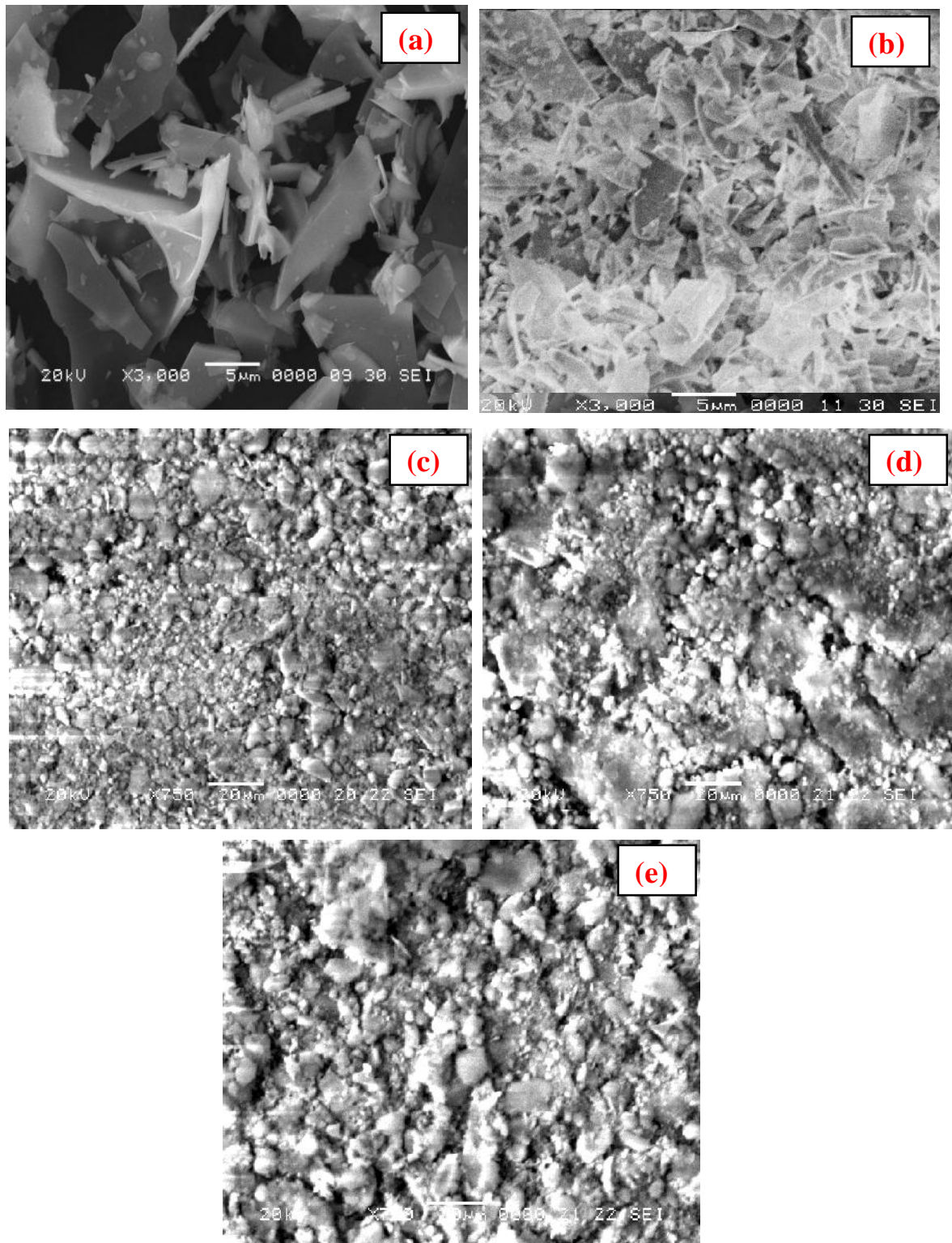
Figure 5.4: **SEM micrographs of (a) perlite, (b) TAP, (c) SAPC, (d) NAPC and (e) HAPC.**

EDX analysis of perlite, TAP and acid activated perlite samples **(Table 5.2)** showed that on acid activation, amount of silica increases while other minor metal oxides get removed from perlite. The increase in silica % is highest in case of SAPC while its minimum in HAPC.

Table 5.2:   EDX analysis of perlite, TAP, SAPC, NAPC and HAPC.

Samples	O (wt%)	Si (wt%)	Al (wt%)	K (wt%)	Na (wt%)	Zn (wt%)	Fe (wt%)	Ti (wt%)	LOI
Perlite	73.70	18.83	3.72	1.44	1.91	0.22	0.10	0.07	4.1
TAP	73.60	18.80	3.70	1.34	1.91	0.22	0.10	0.07	2.3
SAPC	74.82	21.62	2.74	0.23	0.47	-	-	-	1.5
NAPC	74.06	20.22	3.24	0.93	1.27	-	-	-	1.8
HAPC	73.98	19.76	3.56	1.02	1.57	-	-	-	1.8

LOI- Loss on ignition

5.4   Catalyst selection

The catalytic performance is tested by Fischer esterification reaction of methanol by propionic acid to give methyl propionate under microwave assisted, single step, solvent-free reaction conditions. Reaction is carried out at 70°C for 10 minutes, power output of 6s0 W, taking methanol/propionic acid molar ratio 1:1.5 and methanol to catalyst weight ratio of 5:1. Results given in **Table 5.3** show that perlite and TAP do not possess any catalytic activity for this reaction. NAPC and HAPC show less catalytic activity as compared to SAPC due to absence of sufficient number of acidic sites on their surface. It should be noted that modification of the perlite samples with sulphuric acid increased their textural parameters more effectively then modification with nitric and hydrochloric acids.

Table 5.3: **Catalytic activity of different catalysts for Fischer esterification reaction.**

Catalysts	Conversion%
Perlite	Nil
TAP	Nil
SAPC	88
NAPC	68
HAPC	80

Reaction conditions: Time = 10 minutes; temperature = 70°C; power output = 60 W; molar ratio (methanol/propionic acid = 1:1.5); substrate/catalyst ratio = 5:1.

As suggested by these results, SAPC is chosen as the main catalyst for catalyzing a series of Fischer esterification reactions of various aliphatic alcohols by propionic acid. Further optimization of reaction parameters such as effect of reaction time and temperature, molar ratio of reactants, power output are also studied over this catalyst in order to attain maximum conversion%.

5.5 Catalytic activity

5.5.1 Effect of reaction temperature

To optimize the reaction temperature for giving maximum conversion%, reactions are studied at different temperatures ranging from 60 to 100°C for 8 minutes. The results illustrated that the conversion% of alcohols gradually increases with increase in temperature from 60 to 80°C as shown in **Figure 5.5**, which confers endothermic nature of the reaction. The maximum conversion% is obtained at 80°C within 8 minutes which get decreased on increasing temperature up to 100°C. Given that boiling temperature of most of the reactants is very low, so above that temperature they become volatile, thus the contact time between the reactants reduces resulting in decrease in conversion%.
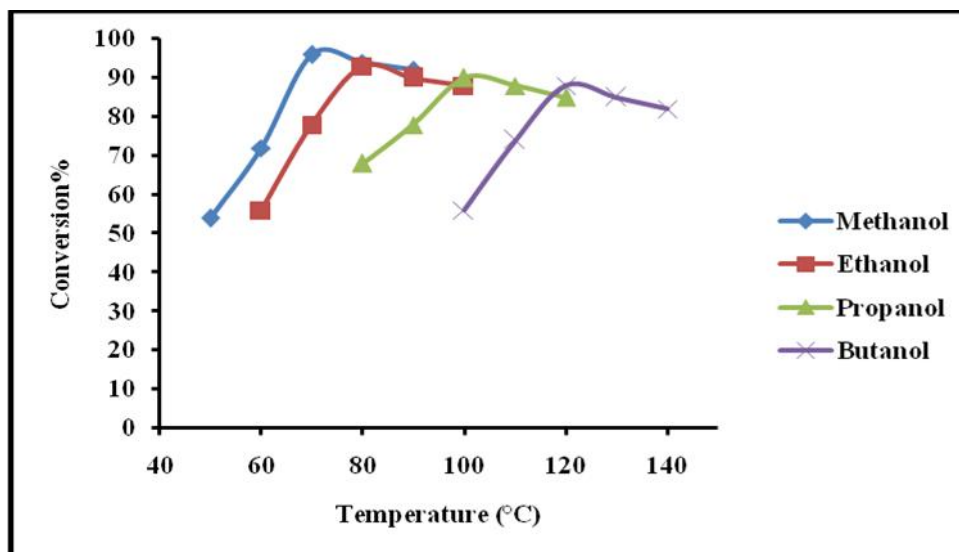
Figure 5.5: **Variation of conversion (%) of alcohols over SAPC with temperature.**

Reaction conditions: Time = 8 minutes; molar ratio (alcohol/propionic acid = 1:1.5); power output = 50 W; substrate/catalyst ratio = 5:1.

5.5.2 Effect of reaction time

The effect of reaction time on conversion% is investigated by carrying out reactions at 80°C to achieve maximum conversion% of product in the range of 4 to 12 min as shown in **Figure 5.6**. It is found that in first 8 minutes, the conversion% increases linearly which remained almost constant till 12 minutes.
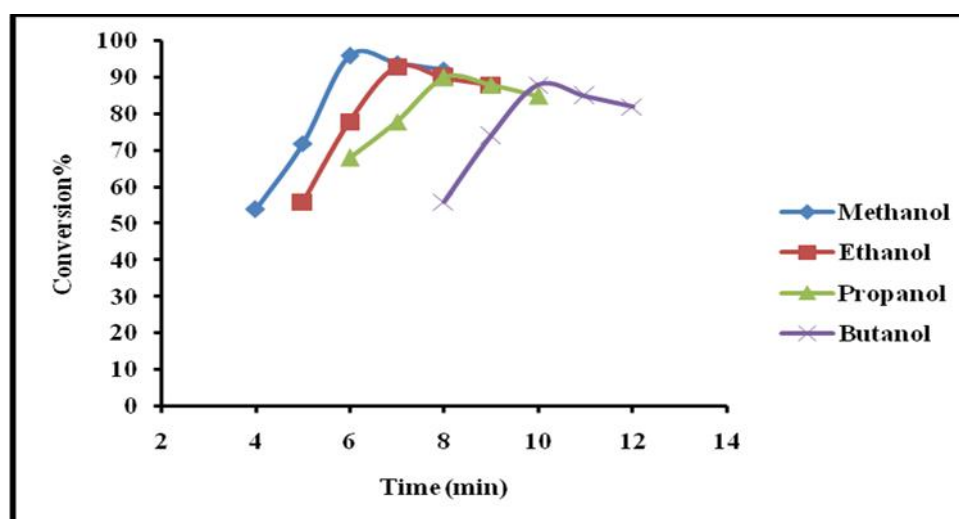
Figure 5.6: **Variation of conversion (%) of alcohols over SAPC with time.**

Reaction conditions: Temperature = 80°C; molar ratio (alcohol/propionic acid = 1:1.5); power output = 50 W; substrate/catalyst ratio = 5:1.

5.5.3 Effect of molar ratio

The effect of molar ratios of alcohols and propionic acid on conversion% is studied by employing different molar ratios varying from 1:1 to 2:1 as shown in **Figure 5.7.** The conversion% of alcohols is found maximum at 1:1.5 molar ratio. Conversion% is drastically very less when alcohol is either in excess or equimolar quantity as large amount of alcohol may prevent access of acid to the catalytic active sites, formation of carbocation decreases and thus ester production reduced.
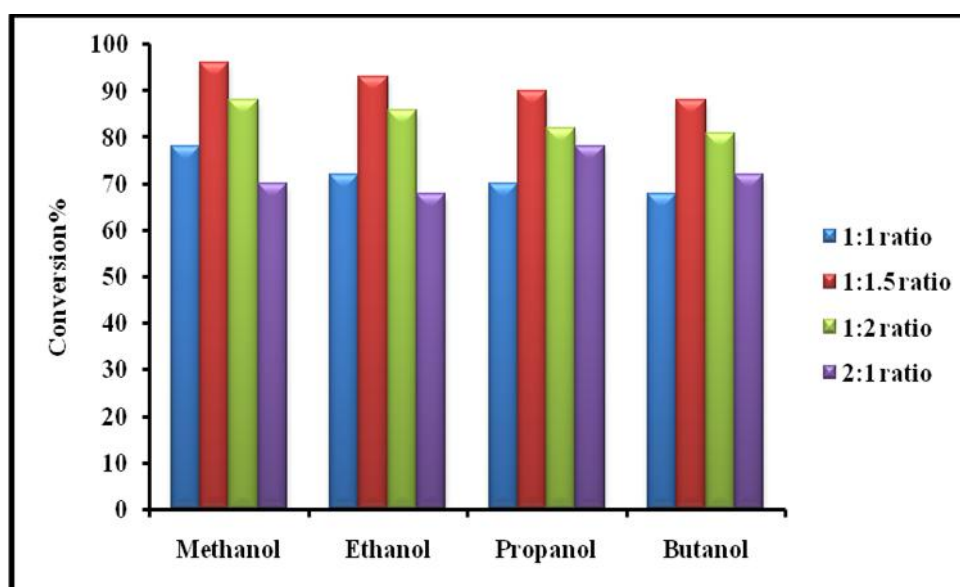
Figure 5.7:   **Variation of conversion (%) of alcohols over SAPC with molar ratio of reactants.**

Reaction conditions: Temperature = 80°C; time = 8 min; power output = 50 W; substrate/catalyst ratio = 5:1.

5.5.4 Effect of power output

The effect of power output of microwave instrument on conversion% is monitored at different power outputs ranging from 40 to 60 W as shown in **Figure 5.8.** The optimized power output is found to be 50 W where the conversion% of alcohols is maximum. On further increasing power output, no significant change in conversion% is seen.

5.5.5 Effect of substrate to catalyst weight ratio

The effect of substrate to catalyst weight ratio on conversion% of is examined by varying the amount of catalyst under optimized reaction conditions.

As inferred from **Figure 5.9**, it can be said that at on increasing catalytic amount from 10 to 5 weight%, conversion% increases. It can be attributed due to availability of sufficient number of catalytic active sites for the adsorption of the reactants. On further increase in the amount of catalyst no significant change is observed.
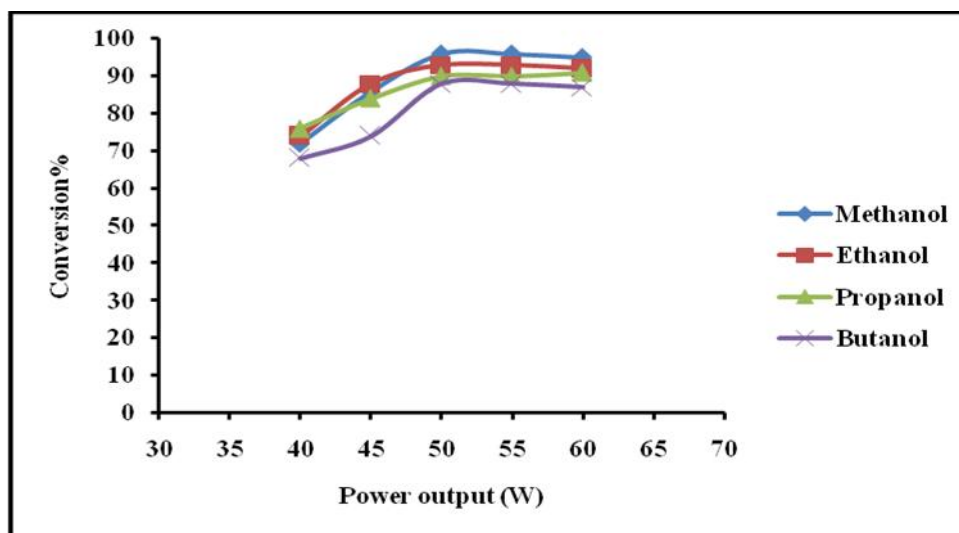
Figure 5.8: **Variation of conversion (%) of alcohols over SAPC with power output.**

Reaction conditions: Temperature = 80°C; time = 8 min; molar ratio (alcohols:propionic acid = 1:1.5; substrate/catalyst ratio = 5:1.
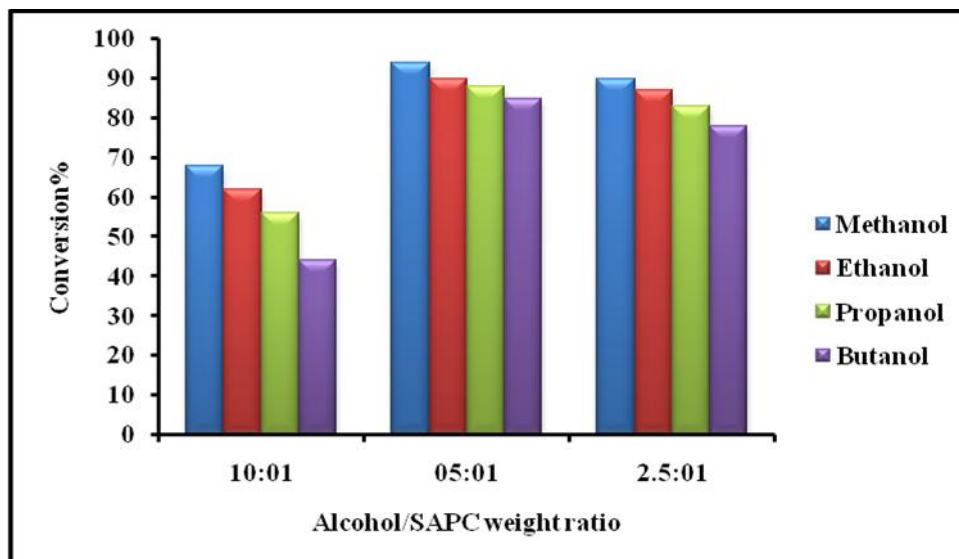
Figure 5.9: **Variation of conversion (%) of alcohols over SAPC with substrate to catalyst weight ratio.**

Reaction conditions: Temperature = 80°C; time = 8 min; molar ratio (alcohols:propionic acid = 1:1.5; power output = 50 W.

The maximum conversion% of products in a series of Fischer esterification reactions **(Table 5.4)** is found when reaction is carried out at 80°C for 8 minutes, taking alcohols and propionic acid in 1:1.5 molar ratio, power output of 50 W and substrate to catalyst ratio of 5:1 over SAPC. The percentage of conversion% decreases from 96 to 88% as chain of carbon atoms in alcohol becomes longer because long chain alcohols hinder access of acid to catalytic active sites due to sterric hindrance, thus, the formation of carbocation decreases and consequently rate of reaction as well as conversion% of reaction reduces.

Table 5.4 : **Synthesis of various esters by SAPC catalyzed Fischer esterification reaction between different aliphatic alcohols and propionic acid under microwave irradiated reaction conditions.**

Entry	Alcohols	Products	Conversion (%)
1	$CH_3\!-\!OH$	$CH_3\!-\!CH_2\!-\!\underset{\underset{O}{\|\|}}{C}\!-\!O\!-\!CH_3$	96
2	$CH_3\!-\!CH_2\!-\!OH$	$CH_3\!-\!CH_2\!-\!\underset{\underset{O}{\|\|}}{C}\!-\!O\!-\!CH_2\!-\!CH_3$	93
3	$CH_3\!-\!CH_2\!-\!CH_2\!-\!OH$	$CH_3\!-\!CH_2\!-\!\underset{\underset{O}{\|\|}}{C}\!-\!O\!-\!CH_2\!-\!CH_2\!-\!CH_3$	90
4	$CH_3\!-\!CH_2\!-\!CH_2\!-\!CH_2\!-\!OH$	$CH_3\!-\!CH_2\!-\!\underset{\underset{O}{\|\|}}{C}\!-\!O\!-\!CH_2\!-\!CH_2\!-\!CH_2\!-\!CH_3$	88

Reaction conditions:Temperature = 80°C; time = 8 min.; power output = 50 W; molar ratio (aliphatic alcohol/propionic acid =1:1.5); substrate/catalyst ratio = 5:1.

5.6   Mechanistic aspects

Heterogeneous acid catalyzed esterification reaction follows single site or Eley-Rideal meachanism as shown in **Scheme 5.3**. The reaction is initiated by protonation of propionic acid by Brønsted acidic sites of SAPC. The proton attaches with oxygen atom of carbonyl group and induces positive charge on the oxygen. Due to electronegativity difference, this positive charge gets transferred

to carbon atom of carbonyl group, thus making it more electrophillic which is attacked by hydroxyl group of alcohol molecule in next step to form a key intermediate of this reaction. Disproportionation of this intermediate results into final product- ester and releases water as side product. In the final step, the catalyst is recovered by transfer of proton to the catalyst surface.

5.7   Regeneration and reusability of catalyst

The catalyst is filtered from the reaction mixture, washed with acetone and regenerated at 450°C for use in subsequent reaction cycles. The regenerated catalyst show efficient catalytic activity up to 4 reaction cycles giving conversion% of aliphatic alcohol in the range of 94-88%, as shown in **Table 5.5**, which indicates that the acidic sites are not lexiviated during regeneration. The FT-IR spectrum **(Figure 5.10b)** of SAPC regenerated after 4th reaction run resembles with FT-IR spectrum of fresh SAPC **(Figure 5.10a)** indicating the stability of surface hydroxyl groups generated through chemical activation, responsible for catalytic activity [47]. The conversion% is decreased after fourth reaction cycle, which is assigned due to the physical adsorption of carbonaceous materials on the external surface of catalyst which could block the pores present on catalyst and causes poisoning of surface active sites [48]. This blocking phenomenon is further confirmed by decrease in intensity and broadness of band appearing between 3600-3300 cm^{-1} and peak around 1630 cm^{-1} attributing to –OH stretching and bending vibrations respectively in case of regenerated catalyst which are responsible for catalytic activity.

Table 5.5:   **Fischer esterification of alcohols by propionic acid over fresh and regenerated SAPC.**

Reaction cycle	Conversion (%)
I	94
II	91
III	91
IV	88

Reaction conditions:Temperature = 80°C; time = 8 min.; power output = 50 W; molar ratio (aliphatic alcohol/propionic acid = 1:1.5); substrate/catalyst ratio = 5:1.
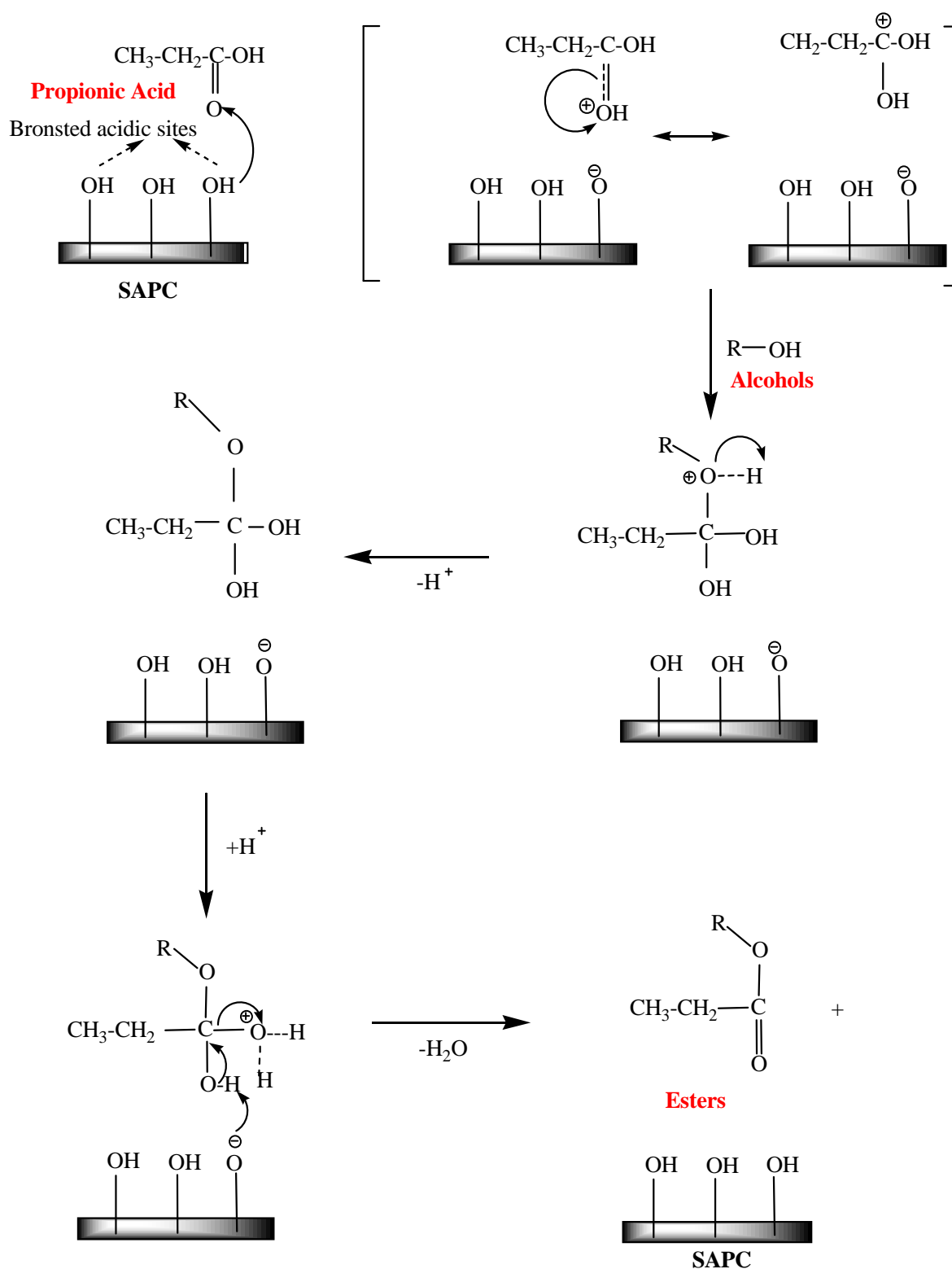
Scheme 5.3: **Mechanistic aspects of Fischer esterification of aliphatic alcohols and propionic acid over SAPC.**
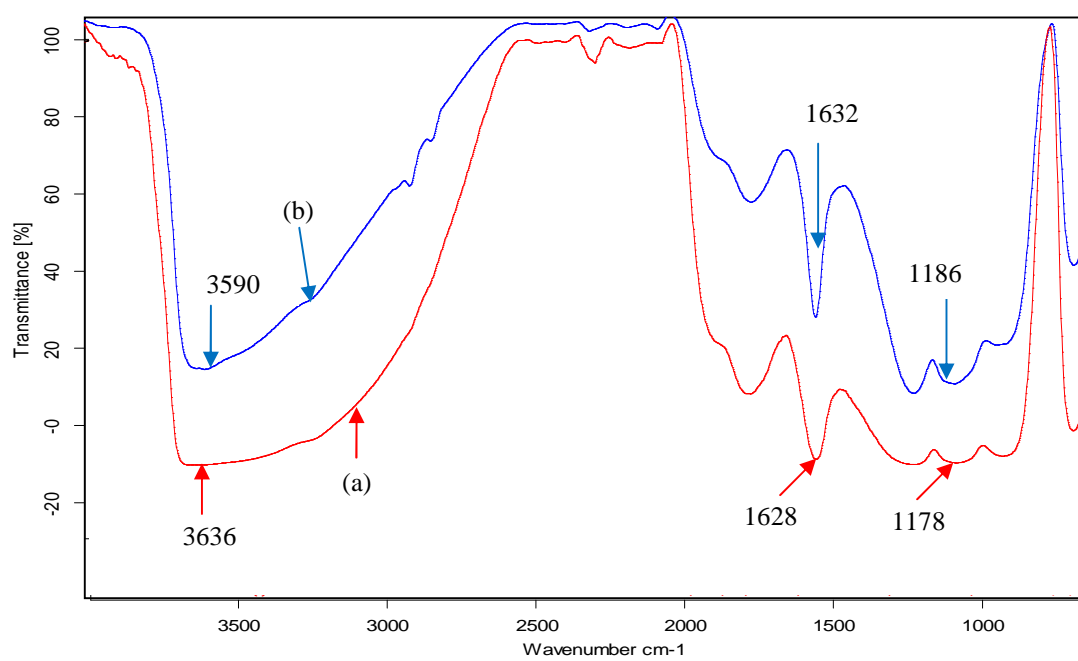
Figure 5.10: FT-IR spectra of (a) SAPC and (b) regenerated SAPC.

5.8   Conclusion

The present study provides a novel application of a waste siliceous material, perlite in preparing an effective heterogeneous acid catalyst through thermal followed by chemical activation with different mineral acids. Perlite enriched in several useful metal oxides has been reported very less in the field of heterogeneous catalysis and is yet to be utilized in comparable amount to its bulk production. The thermal as well as chemical activation of perlite consequences in increased amorphous silica content and surface hydroxyl groups, which ultimately results in enhanced surface acidity. Among all prepared catalysts, sulphuric acid treatment of TAP (SAPC) is found to be a potential heterogeneous acid catalyst having sufficient catalytic activity in series of microwave assisted Fischer esterification reaction, evident from higher conversion% of aliphatic alcohols to the desired products. The reactions are carried out in one-pot, single-step, green, solvent-free reaction conditions and the catalyst is easily filtered, regenerated and recycled 4 times with analogous efficiency, suggesting that acidic sites of the catalyst remain stable during the reaction. The novelty of the present work is the utilization of the abundant natural waste, perlite as a solid support for the synthesis of highly efficient heterogeneous acid catalyst. Moreover, this study also suggests that after proper thermal and chemical activation, perlite can replace pure, commercial silica as a solid support for synthesizing efficient heterogeneous catalyst useful in industrially significant esterification reaction having wide applications in flavouring industries, perfumeries, chemicals and pharmaceuticals.

5.9   References

[1]   H. Shi, W. Zhu, H. Li, H. Liu, M. Zhang, Y. Yan, Z. Wang, Catal. Commun. 11 (2010) 588.

[2]   H.C.B. K. Saravanan, Beena Tyagi, J Sol-Gel Sci. Technol. 62 (2012) 13.

[3]   J. Lilja, W. Johan, T. Salmi, L.J. Pettersson, J. Ahlkvist, H. Gr, Chem. Eng. J. 115 (2005) 1.

[4]   K.V.V.S.B.S.R.M. Sharath R Kirumakki, N. Nagaraju, N. Sankarasubbier, Appl. Catal. A Gen. 226 (2002) 175.

[5]   S.L. Barbosa, M.J. Dabdoub, G.R. Hurtado, S.I. Klein, A.C.M. Baroni, C. Cunha, Appl. Catal. A Gen. 313 (2006) 146.

[6]   K.G. Kabza, B.R. Chapados, J.E. Gestwicki, J.L. Mcgrath, J. Org. Chem. 65 (2000) 1210.

[7]   K.M. Amore, N.E. Leadbeater, Macromol. Rapid Commun. 28 (2007) 473.

[8]   D. Konwar, P.K. Gogoi, P. Gogoi, B. Geetika, B. Ruby, H. Neelakshi, B. Rituraj, Indian J. Chem. Technol. 15 (2008) 75.

[9]   P.M. Arvela, T. Salmi, M. Sundell, K. Ekman, R. Peltonen, J. Lehtonen, Appl. Catal. A Gen. 184 (1999) 25.

[10]   R. Ronnback, T. Salmi, A. Vuori, H.H. Juha, A. Sundqvist, E. Tirronen, Chem. Eng. Sci. 52 (1997) 3369.

[11]   Y. Liu, E. Lotero, J.G.G. Jr, J. Mol. Catal. A Chem. 245 (2006) 132.

[12]   Y. Liu, E. Lotero, J. Goodwinjr, J. Catal. 242 (2006) 278.

[13]   G. Kuriakose, N. Nagaraju, J. Mol. Catal. A Chem. 223 (2004) 155.

[14]   A. Kara, B. Erdem, J. Mol. Catal. A. Chem. 349 (2011) 42.

[15]   H.T.R. Teo, B. Saha, J. Catal. 228 (2004) 174.

[16]   A. Alsalme, E.F. Kozhevnikova, I. V Kozhevnikov, Appl. Catal. A Gen. 349 (2008) 170.

[17]   A. Rajendran, C. Karthikeyan, Am. Chem. Sci. J. 1 (2011) 28.

[18]   S.R. Kirumakki, N. Nagaraju, K.V.R. Chary, Appl. Catal. A Gen. 299 (2006) 185.

[19]   D.E. Lopez, J.G. Goodwin, D.A. Bruce, S. Furuta, Appl. Catal. A Gen. 339 (2008) 76.

[20]   P.C. Mazo, L.A. Rios, Lat. Am. Appl. Res. 349 (2010) 343.

[21]   R. Maggi, G. Martra, C. Giancarlo, G. Alberto, G. Sartori, J. Catal. 294 (2012) 19.

[22]   H.R. Shaterian, K. Azizi, N. Fahimi, Arab. J. Chem. (2012).

[23]   S.M. Yakout, G.S. El-deen, Arab. J. Chem. (2012).

[24]   S.R. Chitnis, M.M. Sharma, React. Funct. Polym. 32 (1997) 93.

[25]   H. Gurav, V. V Bokade, J. Nat. Gas Chem. 19 (2010) 161.

[26]   M.M. Abou-sekkina, Int. J. Chem. 2 (2010) 81.

[27]   L. Chmielarz, A. Kowalczyk, M. Michalik, B. Dudek, A. Matusiewicz, Appl. Clay Sci. 49 (2010) 156.

[28] M.A. Vicente, J.D.L. Gonzalez, M.A.B. Munoz, Clay Miner. 29 (1994) 361.

[29] U. Kalapathy, A. Proctor, J. Shultz, Bioresour. Technol. 73 (2000) 257.

[30] S. Kabra, S. Katara, A. Rani, Int. J. Innov. Res. Sci. Eng. Technol. 2 (2013) 4319.

[31] K. Amutha, R. Ravibaskar, G. Sivakumar, Int. J. Nanotechnol. Appl. 4 (2010) 61.

[32] C.M. Ana Maria de Sousa, Leila Visconte, and C. Furtado, Chem. Chem. Technol. 3 (2009).

[33] C. Khatri, A. Rani, Fuel 87 (2008) 2886.

[34] S. Kabra, A. Sharma, S. Katara, R. Hada, A. Rani, Indian J. Appl. Res. (2013) 2013.

[35] D. Jain, M. Mishra, A. Rani, Fuel Process. Technol. 95 (2012) 119.

[36] F. Adam, S. Balakrishnan, P. Wong, J. Phys. Sci. 17 (2006) 1.

[37] B.J. Saikia, J. Mod. Phys. 01 (2010) 206.

[38] A. Sharma, K. Srivastava, V. Devra, A. Rani, Am. Chem. Sci. J. 2 (2012) 177.

[39] S. Music, N.F. Vincekovic, L. Sekovanic, Brazilian J. Chem. Eng. 28 (2011) 89.

[40] S.H. Javed, S. Naveed, N. Feroze, M. Zafar, M. Shafaq, J. Qual. Technol. Manag. 6 (2010) 81.

[41] J.P. Nayak, J. Bera, Trans. Ind. Ceram. Soc. 68 (2009) 1.

[42] E.P. Parry, J. Catal. 2 (1963) 371.

[43] G. Jozefaciuk, G. Bowanko, Clay Clay Miner. 50 (2002) 771.

[44] S. Kumar, A.K. Panda, R.K. Singh, Bull. Chem. React. Engg. Catal. 8 (2013) 61.

[45] E.R. Vance, D.S. Perera, P. Imperia, D.J. Cassidy, J. Davis, J.T. Gourley, J. Aust. Ceram. Soc. 45 (2009) 44.

[46] D. Bastani, A.A. Safekordi, A. Alihosseini, V. Taghikhani, Sep. Purif. Technol. 52 (2006) 295.

[47] C. Khatri, D. Jain, A. Rani, Fuel 89 (2010) 3853.

[48] C.H. Bartholomew, Appl. Catal. A Gen. 212 (2001) 17.

Synthesis and Characterization of Perlite Supported Nano-crystalline Sulfated Zirconia Catalysts for a Series of Benzoylation Reactions

Abstract

A series of nano-crystalline, effective, recyclable and cost-efficient super solid acid catalysts has been prepared by loading varying amounts of sulfated zirconia (9, 12 and 15 weight%) on thermally activated perlite by adopting two step sol-gel procedure. Presence of crystalline phases is confirmed by XRD and FT-IR studies. TEM images reveal nano size of catalyst. Loading and stabilisation of sulfated zirconia on perlite is further proved by N_2 adsorption-desorption, SEM, SEM-EDX, TGA and UV-Vis DRS techniques. The catalytic activity of as prepared catalysts is measured through a series of liquid phase benzoylation reactions of different aromatic substrates using benzoyl chloride as benzoylating agent under solvent-free, one pot reaction conditions. The desired products are extremely beneficial in production of pharmaceuticals, agro and fine chemicals, petroleum products, perfumes etc. The FT-IR study of pyridine adsorbed samples reflects the presence of both Brønsted as well as Lewis acidic sites as catalytic active centres on the surface of catalyst. Regeneration and reusability of catalyst up to five reaction cycles without any considerable loss in catalytic activity confer the stability of catalyst. The possibility of leaching of loaded species of catalyst is analysed by Sheldon's hot filtration test. The catalytic activity of catalysts thus formed is compara ble to the results of earlier reported sulfated zirconia catalysts. This comprehensive study states that a natural abundant solid waste, perlite can be utilised as a support for generation of nano-crystalline, super solid acid catalyst and has a promising future in providing environmentally clean processes for the industrial sector.

6.1   Introduction

Sulphated zirconia has been claimed to be a super acid possessing acidity in range of H_o -16.04 and pK_a -14.52 measured by Hammett indicator method [1]. The acidity of sulphated zirconia is believed to be 10,000 times stronger than 100% H_2SO_4 or $HClO_4$ [2]. The amorphous zirconia cannot be utilized as a catalytic material as it has low thermal stability and degrades at $> 400°C$. On some modifications like incorporation of sulphates, thermal and hydrothermal stability of zirconia enhances [3]. ZrO_2 itself possess low acidic properties, but on sulfation super acidity is generated [4]. The nature of acidity of sulfated zirconia depends on its pre*para* tion methods. Super acidity is developed because of generation of ionic S-O-Zr bond along with co-ordination S-O-Zr bonds [5]. Use of zirconia in area of ceramics, flexible capacitors, solid oxide fuel cells, metal oxide semiconductor devices, heat resistant, protective and highly reflective optical coatings [6–8] is common.

Over the last three decades, catalytic use of anion modified metal oxides in organic transformations has been received greater attention. Among them, higher thermal stability, super acidity, resistance to thermal extrusion, strength, toughness, high activity, selectivity and stability in acidic and alkaline environment, easy and low cost synthesis of sulfated zirconia offer several advantages over other solid acid catalysts. Catalytic applications of sulfated zirconia include alkylation, light alkane isomerisation, cracking reaction, skeletal etherification of alcohols, acylation, esterification, benzylation, nitration [9–12] etc. The acidity as well as catalytic activity of sulfated zirconia mainly depends on some important factors viz. method adopted for synthesis, surface area, zirconia precursor, precipitating agent, sulphating agent, pH during synthesis, temperature of synthesis, ageing time, calcination temperature and also on environment of storage [13]. $Zr(OH)_4$ is amorphous at room temperature, calcination at 550°C results in formation of ZrO_2 with co-existing tetragonal and monoclinic phases. On increasing calcination temperature, tetragonal phase diminishes gradually and above 650°C, only monoclinic phase is observed. Sulfation retards the conversion of tetragonal phase into thermodynamically stable monoclinic phase which is vital for organic transformations [14]. Need for supported sulfated zirconia catalyst

arises because of their lower cost, probability to enhance relatively lower surface area of sulfated zirconia and it also stabilise sulfated zirconia against sintering at higher temperature. Normally, silica based supports like MCM-41, SBA-15, HMS, UDCaT-5, zeolites, Al_2O_3 [14–17] etc. are utilized for this purpose. Commonly used methods for pre*para* tion of sulfated zirconia are two step sol-gel, one step sol-gel, precipitation, co-precipitation, liquid crystal templating, one step incipient wetness impregnation, hydrothermal, ball milling technique, one step crystallization methods [6,18–21]. While, generally used starting materials or precursors are zirconium acetate, zirconium hydroxide, zirconium oxychloride, zirconium sulphate, zirconium n-propoxide, zirconium nitrate, zirconium chloride [6,20,22,23]. Precipitating or sulphating agents usually used in sol-gel method are H_2SO_4, $(NH_4)_2SO_4$, $(NH_4)_2S_2O_8$, chlorosulphonic acid, H_2S and SO_2, $(NH_4)_2SO_3$, $(NH_4)_2S$ [1,4,24]. Relatively lower surface area and small pore size of conventionally prepared sulfated zirconia limit its potential catalytic applications.

Metal alkoxides undergo hydrolysis and subsequent condensation or gelation in alcoholic solvent forms a macro-polymeric oxide network known as alcogel. During drying and calcination, a number of chemical and physical changes occur in gel which finally results to a highly mesoporous material [25]. Sol-gel procedure is preferred over other procedures like precipitation and co-precipitation as it produces oxides with uniform textural and surfacial properties [18]. The whole procedure depends on different pre*para* tion *para* meters like concentration of metal alkoxide, pH, type of complexing agent, amount of hydrolyzing water, water to alkoxide molar ratio. The catalytic activity of sulfated zirconia catalyst depends on pre*para* tion procedure, crystalline phase of zirconia, sulphur species, calcination temperature and textural properties [26].

Benzoylation of aromatic substrates is a key reaction of organic chemistry as it produces diaryl ketones like Ibrupofen, S-naproxen, musk fragrance useful in production of various pharmaceuticals, agro chemicals, perfumeries [27] etc. It is an important C-C bond formation reaction in organic synthesis. Benzoylation is an aromatic electrophillic substitution reaction in which the carbocation intermediate is produced by complexation between benzoyl halide and catalyst. Substituted benzophenones are final products or intermediates of UV adsorbents, plastics,

printing ink, varnishes, cosmetics, dyes, medicines [28,29] etc. The *para* product of benzoylation of toluene, 4-methyl benzophenone (4-MBP) is useful intermediate in synthesis of pharmaceuticals, fine chemicals, petroleum products, dielectric fluids [30] etc. While, benzoylated product of anisole, 4-methoxy benzophenone is also an important intermediate for fine chemical production [31]. Over past few decades, benzoylation reaction has been carried out extensively using molar quantities of Lewis acids such as $AlCl_3$, BF_3, $FeCl_3$, HF, $TiCl_4$, $ZnCl_2$, triflic acid and Brønsted acids like H_2SO_4, polyphosphoric acid [29–33] etc. as catalysts. Lewis acid catalysts form complexes with product ketone molecules which are to be cleaved by hydrolysis and neutralization steps. Taking into consideration growing environmental concerns, high amount of toxic effluents generated in neutralisation process is unbearable and thus, replacement of homogeneous Lewis acids is essential. Heterogeneous acids used in this protocol are $Fe_2(SO_4)_3$, methane sulfonic acid, palladium trimethyl poly phosphate, nafion-H/silica, bismuth (III) trifluoro methane sulfonate, montmorillonite, hetero poly acids, zeolites, clay supported catalysts, microencapsulated scandium (III) triflate, metal organic framework (MOF) or mesoporous molecular sieves [34–39] etc. Besides homogeneous and heterogeneous acid catalysts, some bases like pyridine, triethyl amine are also employed in benzoylation reactions [40]. Numerous benzoylating reagents are employed for carrying out benzoylation reactions, such as, benzoyl chloride, benzoic anhydride, benzoyl tetrazole, 2-benzoyl-1-methyl pyridinium chloride, S-benzoic-o, o-diethyl phosphodithoic anhydride, benzoyl chloride [40–42] etc. Benzoyl chloride is widely used benzoylating agent because of its readily availability and lower cost. Conventional solid acid catalysts efficiently catalyze benzoylation reactions but they require solvent system, nitromethane and lithium perchlorate [43] which is inconvenient for industrial applications, hence, it has become crucial to develop an alternative solid acid catalytic system which should be eco- benevolent, industrially applicable, regenerable and cost-effective. This progressing apprehension for greener and safer environment has drawn our attention to explore the capabilities of thermally stable silica-alumina enriched

natural waste, perlite to serve as a support material for loading of a super acid, sulfated zirconia for catalyzing industrially beneficial benzoylation reactions.

The work described in this chapter reports synthesis of innovative, highly efficient, environment friendly, cost-effective, reusable perlite supported varying amounts of sulfated zirconia catalysts (SZP). Different weight% of sulfated zirconia is loaded on thermally activated perlite through two step sol-gel methodology. The catalytic activity of as prepared catalysts is tested through liquid phase series of benzoylation reactions of arenes having wide applications in pharmaceuticals, perfumeries, fine chemicals etc. Higher conversion and selectivity% of products reflects the stability of sulfated zirconia on perlite surface responsible for generation of significant acidity and excellent catalytic activity. The chapter also includes analytical study of structural, surfacial, morphological and chemical aspects of all prepared materials though several characterization techniques. Effect of various reaction variables on conversion and selectivity% is studied during the course of reactions. The reusability of SZP up to five consecutive runs with analogous efficiency and its better catalytic activity as compared to other reported catalysts provide as a possible solution to overcome the use of harmful liquid acid and costly commercial solid acid catalysts for industrially significant benzoylation reactions. Moreover, this work also imparts a key to control disposal problem of huge deposits of natural waste, perlite by utilizing it as an innovative support material in heterogeneous catalysis.

6.2   Experimental

6.2.1 Materials

Zirconium propoxide is purcahsed from Sigma Aldrich, while concentrated H_2SO_4, n-Propanol, benzene, toluene, anisole and benzoyl chloride are purchased from Merck and used as such. Perlite is supplied by Indica Chem. Ind. Pvt. Ltd., India.

6.2.2 Catalyst preparation

As received perlite is initially activated thermally at 800°C for 3 h to remove excess water, carbon and other impurities and converted into thermally

activated perlite (TAP). All the catalysts investigated in this study (SZP-9, 12 and 15) are synthesized by loading 9, 12 and 15 wt% of sulfated zirconia on TAP by two step sol-gel methodology. The requisite amount of zirconium propoxide (1.44 g for 9 wt%, 1.92 g for 12 wt% and 2.39 g for 15 wt%) is taken in a 100 ml beaker and diluted with 15 ml of n-propanol. 6 gm of TAP is then added in the mixture and kept under constant stirring for 15 minutes. Water is added drop-wise in the TAP-zirconium propoxide mixture under constant magnetic stirring at room temperature (water: zirconium propoxide molar ratio = 4:1) for hydrolysis and polycondensation. The resultant gel is aged for 24 h and dried at room temperature followed by drying at 110°C for 24 h in oven to remove excess of solvent from the pores of the gel. In the second step, the dried gel is powdered and sulfated with 1 N solution of concentrated H_2SO_4 under stirring for 1 h (15 ml H_2SO_4 solution is taken for sulfation of 1 g powdered dried gel). The sulfated gel was filtered and dried at room temperature and then at 110°C for 24 h for complete evaporation of water from gel. The porous structure of dried gel can be seen in **Figures 6.1**. All the samples are then calcined at 550°C for 2 h in a muffle furnace under static conditions. The steps of SZP catalysts synthesis are summarized in **Scheme 6.1**.

Figure 6.1: **Gel obtained after drying at 110°C for 24 h.**

As received perlirte → Thermal activation of perlite at 800°C for 3 h (TAP)

Two step sol-gel methodology

Dissolution of requisite amonut of Zirconium propoxide (9, 12 and 15 wt%) in 15 ml of propanol

Constant stirring for 15 minutes

Addition of above solution to 6 g of TAP

Magnetic bar

Drop-wise addition of water in TAP-Zirconium propoxide mixture under constant stirring at room temperature (water : zirconium propoxide molar ratio = 4 : 1

Ageing of resultant gel for 24 h

Sulfation of powdered gel with 1 N H_2SO_4 solution under stirring for 1 h (15 ml H_2SO_4 solution is taken per 1 g of powdered gel)

Powdering of dried gel

Drying at room temperature followed by drying at 110°C for 12 h

Filtration and drying of gel at 110°C for 12 h

Calcination under static conditions at 550°C for 2 h

Nano crystalline sulfated zirconia perlite catalyst (SZP-9, 12 and 15)

Scheme 6.1:   Synthesis of sulfated zirconia perlite catalysts (SZP).

6.2.3 Catalyst characterization

Physicochemical properties of all catalytic materials are studied by N_2 adsorption-desorption, XRD, FT-IR and pyridine adsorbed FT-IR, SEM, SEM-EDX, TEM, TGA and UV-Vis DRS techniques, as described in **Annexure-I**.

6.2.4 Catalytic activity

The catalytic activity of SZP catalysts is tested by benzoylation of various arenes by benzoyl chloride in solvent-free, liquid phase reaction conditions under atmospheric pressure as shown in **Scheme 6.2**. The whole reaction is performed in a liquid phase batch reactor equipped with 250 ml double necked round bottom flask, digital magnetic stirrer and spiral glass condenser immersed in a constant temperature oil bath. A mixture of arenes and benzoyl chloride (different molar ratios) is taken in round bottom flask. Before introduction in reaction medium, the varying amounts of catalyst are activated at 450°C under inert conditions for 1 h. The reaction is carried out at different molar ratio of reactants at different temperatures ranging from 50-170°C for time in the range of 2-5 h. After completion of the reaction the catalyst is se*para*ted and the product is analyzed by Gas Chromatograph (Agilent Technologies 7820A) having FID and Agilent J&W Advanced Capillary HP 5 GC Columns and N_2 (1.5 ml/min) as a carrier gas.

The conversion% of arenes is calculated by using weight percent method given below-

$$\text{Conversion } (\%) = 100 \text{ X } \frac{(\text{Initial wt \% - Final wt \%})}{\text{Initial wt \%}}$$

The selectivity % of desired products is determined through GC by following method-

$$\text{Selectivity } (\%) \text{ of desired product} = 100 \text{ X } \frac{(\text{GC peak area \% of desired product})}{\text{Sum of total peak area \% for all products}}$$
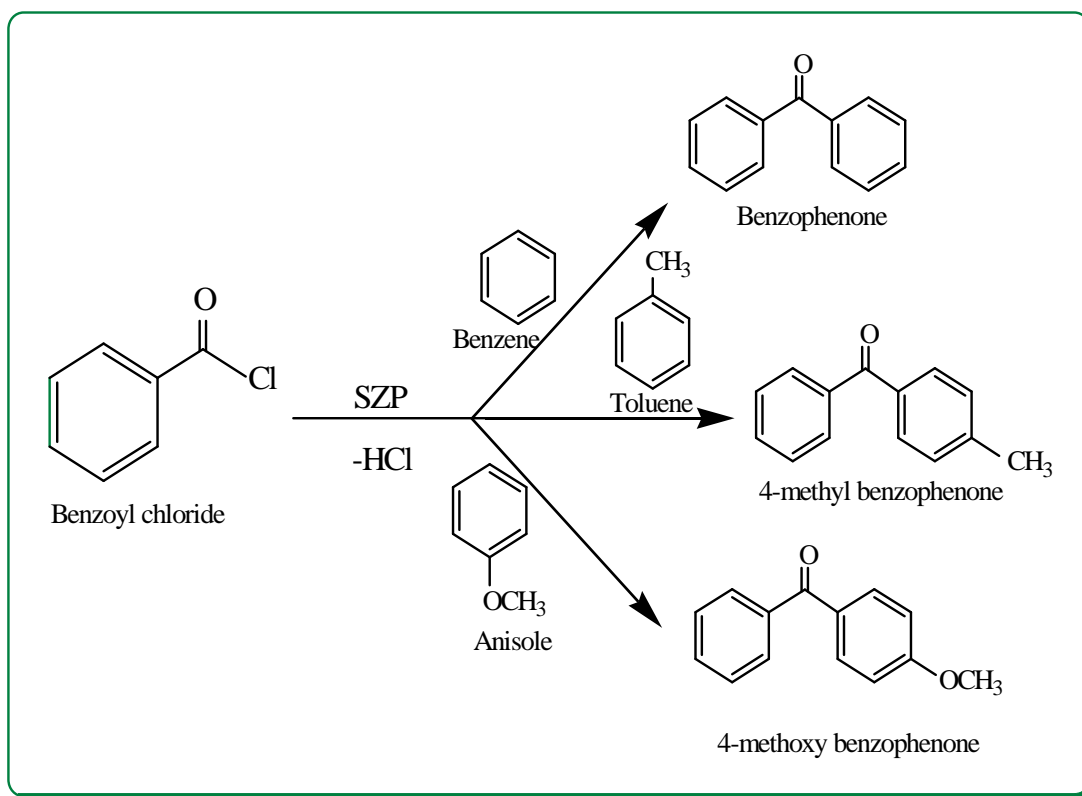
Scheme 6.2: **Simplified reaction pathway of benzoylation of aromatic substrates by benzoyl chloride over SZP catalysts to give corresponding benzophenones and its substitutions.**

6.3 Results and discussion

6.3.1 BET analysis

BET specific surface area of samples as given in **Table 6.1** indicates that on loading sulfated zirconia, specific surface area increases. As precedent in literature, zirconia itself possesses lower specific surface area [26], which increases on sulfation due to interaction between sulphate and zirconium ions. This enhancement can be explained on the basis of higher resistance to sintering acquires through sulfation [44]. It can also be related to the changes occur in crystallization process of zirconia when sulphate groups are introduced in it. On calcination, sulphates decompose into SO_3 which remains present on catalyst surface, suppresses particle growth and thus induced formation of nanoparticles having average pore diameter of about 4.7 nm calculated by N_2 adsorption-desorption analysis. They in turn stabilize thermodynamically stable tetragonal zirconia phase on catalyst which is responsible for catalytic activity, later

explained in this chapter. The suppression of particle growth increases specific surface area of catalysts.

Table 6.1:   BET specific surface area data of samples.

Samples	BET specific surface area (m^2/g)
Perlite	2.6
TAP	2.2
SZP-9	48.84
SZP-12	65.58
SZP-15	80.45

6.3.2 X-ray diffraction analysis

The X-ray diffraction pattern of perlite **(Figure 6.2a)** shows a broad band centred at 2θ = 12-13° confirming the presence of amorphous silica. In TAP, a small crystalline peak appearing at 2θ = 27.642° **(Figure 6.2b)** shows the formation of quartz crystalline phase as a result of thermal activation at higher temperature [45]. Here, a broad hump at 2θ = 22-23° confirms the co-existence of amorphous silica [46]. In case of SZP-9, 12 and 15 catalysts, as shown in **Figure 6.2c, d and e**, a two phase mixture of monoclinic and tetragonal phases of zirconia is present (ICSD collection code 066787). The peaks located in all catalysts at 2θ = 25-27° are characteristic monoclinic phases [24] while peaks at 2θ = 30, 41, 50 and 60° are characteristic for predominant tetragonal phases [1]. On increasing loading of zirconia from 9 to 15 weight %, intensity for monoclinic phases also get increased. Though, number of peaks and the intensity of catalytic efficient tetragonal phase are found to be highest in SZP-15 catalyst. Pure zirconia mainly consists of monoclinic, tetragonal and cubic phases [44]. In pure ZrO_2, monoclinic phase is stable up to 1100°C and transforms into tetragonal phase above 1200°C [44]. On introducing sulphate ions, metastable tetragonal phase stabilizes at relatively lower temperature, i.e., up to 600°C. On increasing calcination temperature above 600°C, tetragonal phase transforms into

thermodynamically stable monoclinic phase [47]. The phenomenon involving in this transformation is sintering in which, the surface sites adsorb oxygen and helps in conversion of tetragonal to monoclinic phase. At lower temperature, as incorporated sulphate ions cover these sites and stabilize acidic tetragonal phase [48]. In SZP-9 and 12, sulphate content is relatively lower, so these monoclinic phases are stronger and more in number than tetragonal phases. Due to sulphate ion introduction, crystallite size of zirconia decreases in catalysts and thus size determination of such peaks is not feasible. A hump centred at $2\theta = 12\text{-}13°$ characteristic of support material (perlite) is retained in XRD patterns of all samples. Few previous reports stated that when zirconium content is < 30 weight %, then it is also present in amorphous form along with its crystalline phases. Amorphous zirconium atoms get incorporated into amorphous silica skeleton of perlite [49] and reacts with silica to form zircon ($ZrSiO_4$) as a major component [50].

6.3.3 *Fourier transform infra-red analysis (FT-IR)*

FT-IR spectrum of perlite (**Figure 6.a**) shows a broad band between 3600-3300 cm^{-1} which is attributed to surface hydroxyl groups of Si-OH and water molecules adsorbed on the surface [51]. The intensity and broadness of this band decreases in TAP (**Figure 6.3b**) conferring loss of water during thermal activation. The strong band at 1178 cm^{-1} in perlite due to asymmetric vibration frequency of Si-O-Si bond also gets shifted at 1227 cm^{-1} in TAP after thermal activation, which is a common feature of amorphous silica samples [52]. The FT-IR spectra of SZP-9, 12 and 15 catalysts as displayed in **Figure 6.3c, d and e** also show a broad band characteristic of surface –OH groups whose intensity increases with increase in loading of sulfated zirconia due to incorporation of zirconia and sulphate content. In all catalysts, this band shifts at lower frequency (3575 cm^{-1}) as compared to support material suggesting the enhancement in acid strength due to generation of S-OH groups as a result of sulfation [44]. Peaks around 1630 cm^{-1} are also observed in all samples corroborating to bending mode ($\delta_{O\text{-}H}$) of –OH groups and water molecules [53]. The persistence of above bands in catalysts even after calcination at 550°C points to the stability of their Brønsted acid.
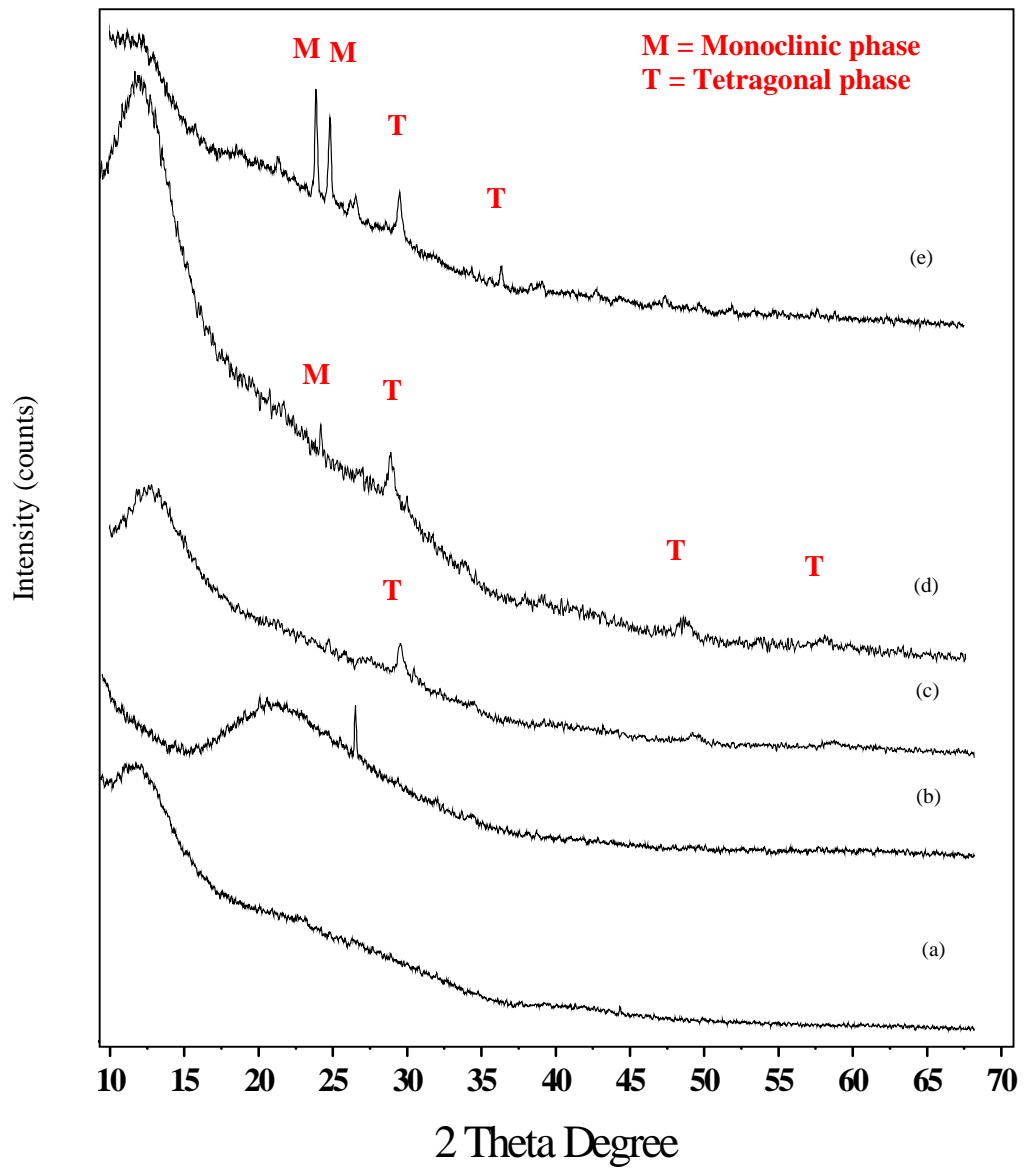
Figure 6.2: **X-ray diffraction pattern of (a) Perlite, (b) TAP, (c) SZP-9, (d) SZP-12 and (e) SZP-15.**

In all SZP catalysts (**Figure 6.4a, b and c**), FT-IR bands at 1153 and 1207 cm^{-1} are assigned to S-O asymmetric stretching mode of vibration of an inorganic chelating bidentate ion co-ordinated to a metal cation like Zr^{+4} [54]. The partial ionic character of S-O band is responsible for Brønsted acidity in SZP catalysts [55]. Literature accounts for the presence of an intense band at 1382-1391 cm^{-1} due to S=O asymmetric stretching vibration in sulphur complexes formed by interaction of metal oxides with sulphate ions [56] which is a characteristic band of sulfated zirconia and its analogues [19]. On adsorbing water molecules, a red shift in wavenumber (1344 cm^{-1}) is seen here. This wavenumber shift corresponds to a decrease in bond order of S=O covalent bond and an increase in partial charge of oxygen atom [1] resulting in increase in acid strength of catalysts. This is a common phenomenon for sulfated zirconia loaded silica samples [57]. On increasing sulphate content in SZP-9, 12 and 15 catalysts, this wavenumber shift occurs in same fashion. But the intensity of this band is less in SZP-9 and 12 indicating the migration of sulphur into bulk phase of zirconia and existence of less sulphur content on surface [24]. The absence of band around 1400 cm^{-1} in all samples denotes that there is no formation of polynuclear sulphates, $S_2O_7^{-2}$ on surface of catalysts [58].

On addition of zirconium, the Si-O-Si lattice stretching vibration appearing in 1300-1100 cm^{-1} region shifts to lower wavenumbers, i.e., 953 and 898 cm^{-1} probably due to incorporation of zirconium into silica network of perlite [59] and formation of Zr-O-Si linkage [60]. The intensity of these bands increases progressively with increase in zirconium content from SZP-9 to SZP-15 catalysts. Some bands in the region of 700-550 cm^{-1} can be attributed to Zr-O stretching vibrations which are still less resolved due to their superimposition with Si-O-Si deformation bands [61]. These bands appear due to presence of dispersed ZrO_2 clusters on TAP surface.
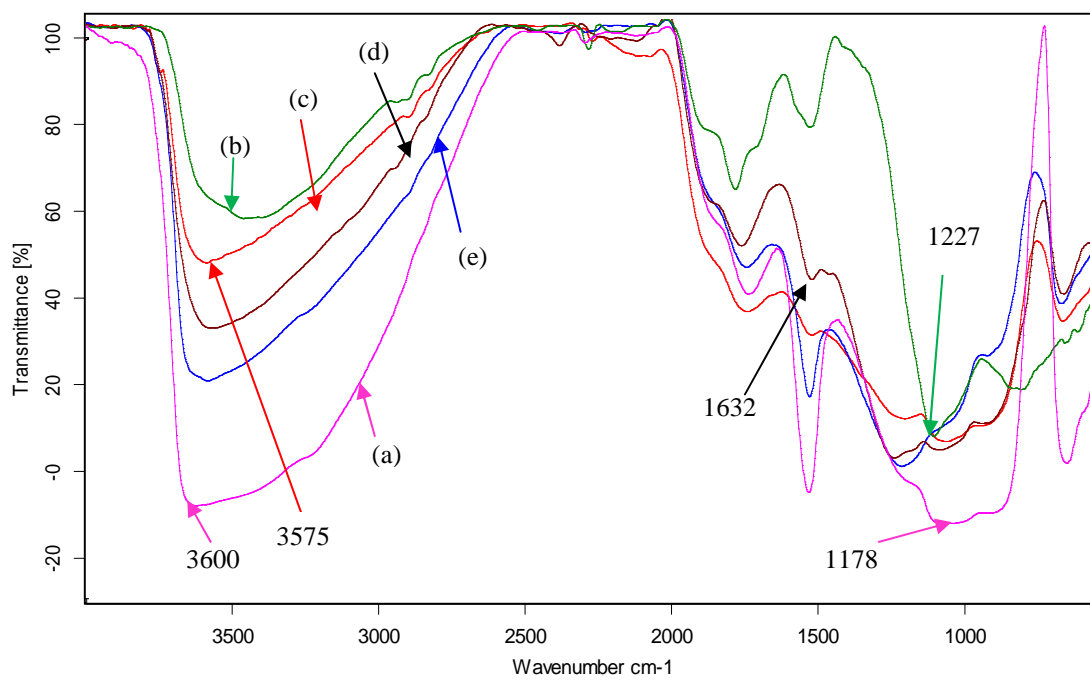
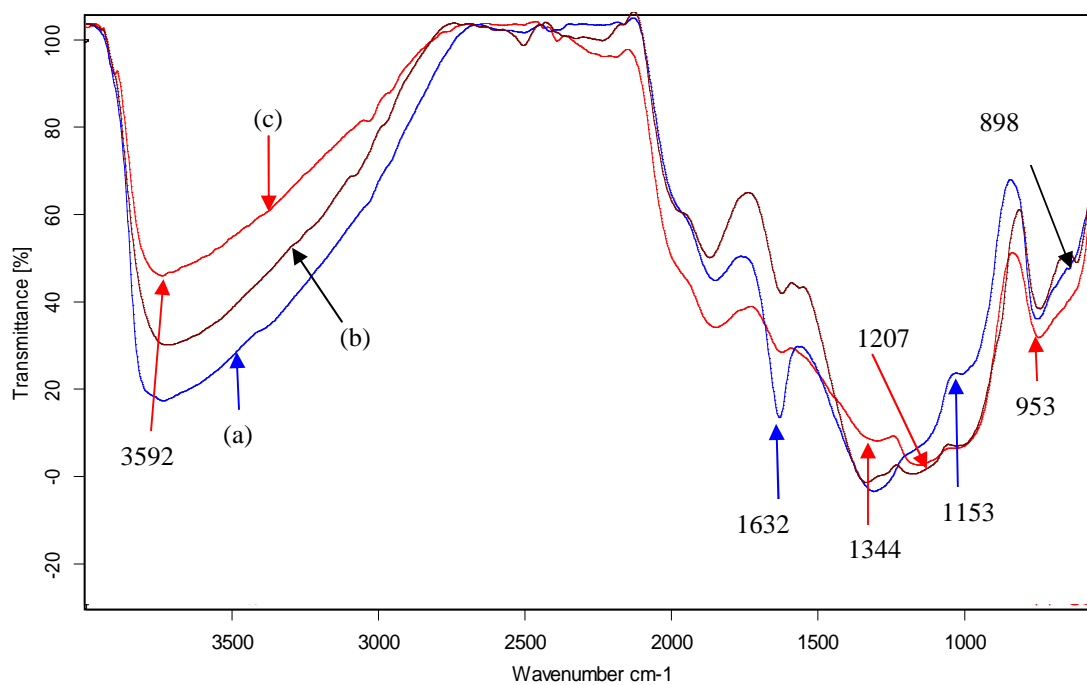**Figure 6.3:** **FT-IR spectra of (a) Perlite, (b) TAP, (c) SZP-9, (d) SZP-12 and (e) SZP-15.**

Figure 6.4: **FT-IR spectra of (a) SZP-9, (b) SZP-12 and (c) SZP-15.**

6.3.4 Pyridine adsorbed FT-IR analysis of catalysts

The types and strengths of acid sites on solid catalyst can be determined by using pyridine adsorption in conjunction with FT-IR spectroscopy. In case of sulfated zirconia loaded catalysts, acidity is more likely due to presence of sulphate ions as ZrO_2 possess low acidic properties [4]. The superacidic character arises because of double bond nature of S=O complex formed as a result of interaction between ZrO_2 and sulphates. In **Figure 6.5**, the spectra show intense bands at 1545 and 1445 cm^{-1} attributing to Brønsted and Lewis acid sites respectively [62–64]. Pyridine interacts with Brønsted acid sites to form pyridinium ion, as a result, N-H bending of pyridinium ion gives its characteristic band at 1545 cm^{-1} while, pyridine co-ordinatively bonded to Lewis acid sites and give band at 1445 cm^{-1} [65]. Sulphate groups are itself Lewis acidic and when they withdraw electron density from zirconia through bridging oxygen, Lewis acid sites generated on zirconia, while Brønsted acid centres in catalysts are due to protons generated by sulphate groups. Interchange of Lewis and Brønsted acidic sites in these catalysts is an important concept for catalysis which is also described in catalyst model, later explained in this chapter. During water vapour adsorption or hydration, presence of H_3O^+ and HSO_4^{-} converts Lewis acidic sites to Brønsted acidic sites with high protonic strength [66]. On increase in sulphur content, number of Lewis and Brønsted acid sites also increases [67]. Stability of tetragonal phase also plays an important role in increase in Brønsted acid sites as it produces most stable structure during hydration [68]. Thus Brønsted bands are less intense in SZP-9 and 12, most intense in SZP-15 while more intense and broad Lewis bands are found in case of SZP-9 and 12 as compared to SZP-15. A band present at 1485 cm^{-1} in all samples is ascribed to presence of both Brønsted and Lewis sites in the samples [69].
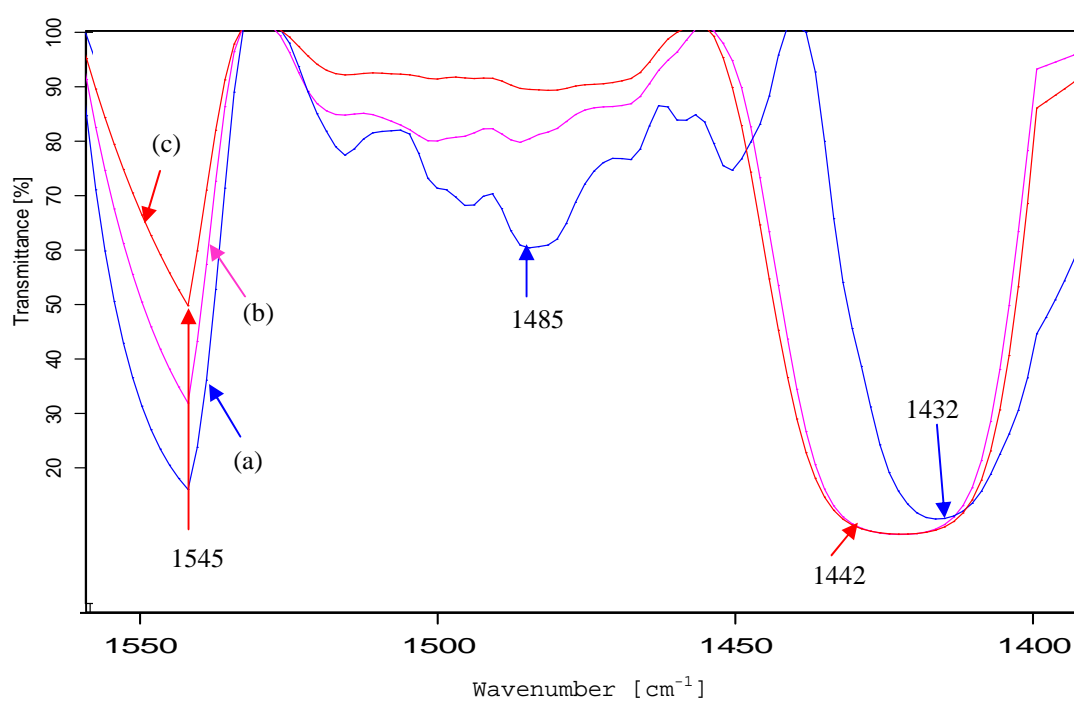
Figure 6.5: **Pyridine adsorbed FT-IR spectra of (a) SZP-9, (b) SZP-12 and (c) SZP-15.**

6.3.5 Scanning electron microscopy (SEM and SEM-EDX analysis)

The SEM micrograph of perlite **(Figure 6.6a)** clearly reveals the irregular morphology of perlite particles. SEM image of TAP **(Figure 6.6b)** is mainly fragmatic and less irregular. While SEM images of SZP-9, 12 and 15 **(Figure 6.6c, d and e)** depict the agglomeration of particles after chemical treatment with H_2SO_4. Loading of sulfated zirconia is further confirmed by appearance of shiny particles finely dispersed on perlite surface.

SEM-EDX analysis as given in **Table 6.2** illustrates the silica and alumina to be the major constituents of perlite. While presence of S and Zr in all catalysts confirm the loading of sulfated zirconia which increases on increasing S and Zr content in SZP-9, 12 and 15 catalysts.

Table 6.2:   **EDX analysis of perlite, TAP, SZP-9, SZP-12 and SZP-15.**

Samples	O (wt%)	Si (wt%)	Al (wt%)	K (wt%)	Na (wt%)	Zn (wt%)	Fe (wt%)	Ti (wt%)	S (wt%)	Zr (wt%)
Perlite	73.70	18.83	3.72	1.44	1.91	0.22	0.10	0.07	-	-
SZP-9	72.82	20.62	2.74	0.23	0.47	-	-	-	2.18	0.94
SZP-12	72.43	19.22	2.54	0.23	0.47	-	-	-	3.68	1.43
SZP-15	71.94	17.76	2.26	0.23	0.37	-	-	-	5.46	1.98

6.3.6 Transmission electron microscopy (TEM analysis)

TEM image of perlite **(Figure 6.7a)** also exhibits its irregular morphology. Dark field image of SZP-15 catalyst **(Figure 6.7b)** shows small dots indicating the presence of nanocrystalline, finely dispersed tetragonal zirconia on perlite surface [70]. With the help of another TEM image **(Figure 6.7c)** particle size of catalyst can be determined which is found to be in the range of 9-25 nm. Thus, it can be said that two step sol-gel method adopted for catalyst synthesis is suitable enough to obtain stable, adherent loading of nanocrystalline sulfated zirconia particles on perlite surface which increases surface area of catalyst, thus, number of catalytic sites also increases and ultimately catalytic efficiency of SZP-15 increases.
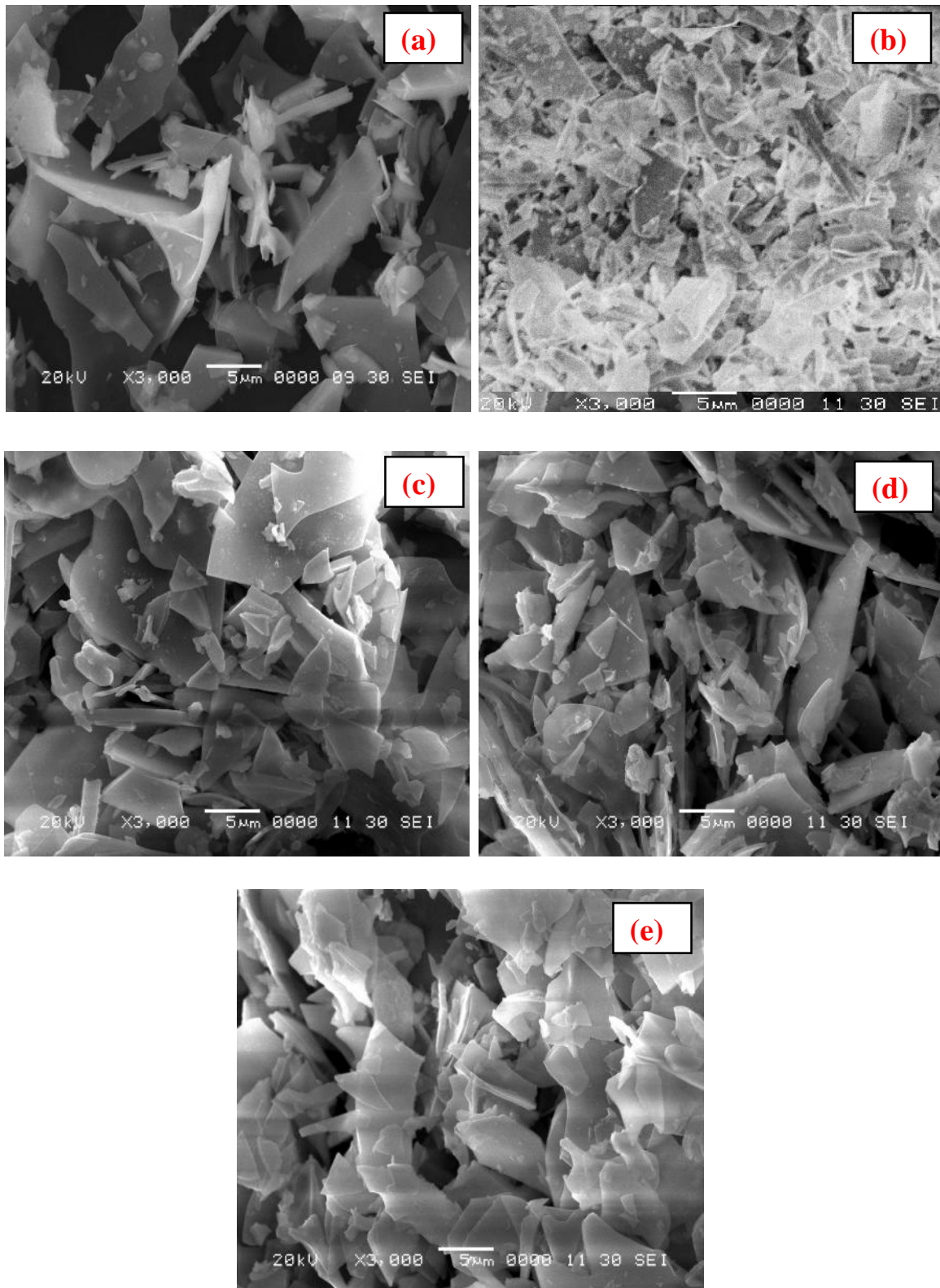
Figure 6.6: **SEM micrographs of (a) perlite, (b) TAP, (c) SZP-9, (d) SZP-12 and (e) SZP-15.**
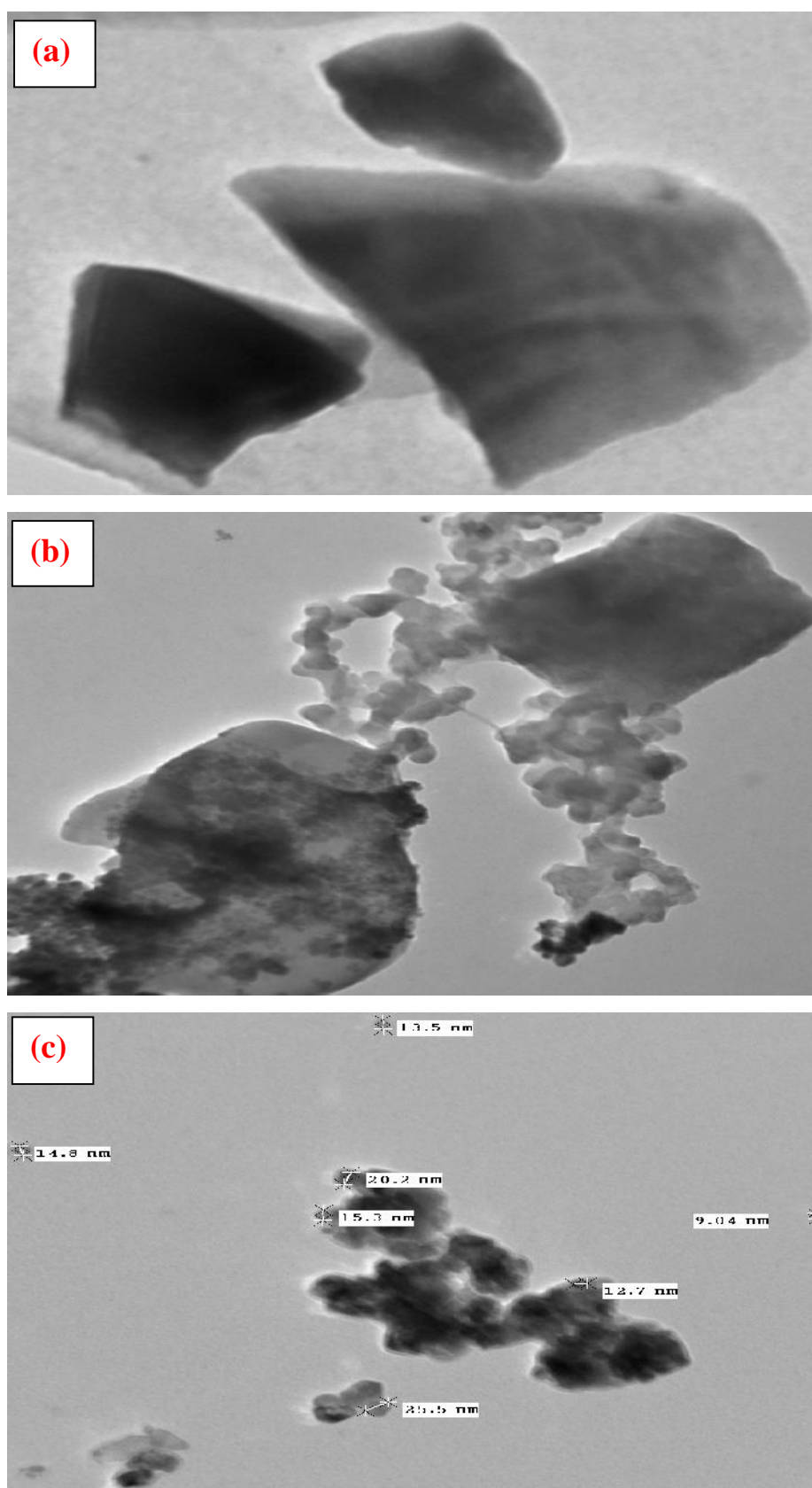
Figure 6.7: **TEM micrographs of (a) perlite, (b) and (c) SZP-15.**

6.3.7 Thermo-gravimmetric analysis (TGA)

TGA curve of perlite **(Figure 6.8a)** portrays that there is a sharp decrease in weight in region between 100-400°C due to removal of moisture adsorbed on surface. While, at higher temperature, a gradual weight loss is seen which can be due to decomposition of volatile metal oxides or carbonaceous materials present in perlite. In TGA pattern of SZP-15 catalyst as displayed in **Figure 6.8b**, the initial sharp weight loss up to 400°C could be assigned to removal of physically adsorbed water of hydration. In unsulfated zirconia systems, a prominent weight loss is observed between 420-470°C, which is attributed to the phase transformation of zirconium from amorphous to crystalline phases [71]. However, the absence of such weight loss in our catalyst reveals that sulphate incorporation increases stability of metastable tetragonal zirconia phase which is essential for efficient catalytic activity and is also in well agreement with XRD results. A gradual weight loss in higher temperature range, i.e., 600-900°C can be due to decomposition of sulphate ions and transformation of tetragonal to monoclinic phase of zirconia. The overall weight loss of sulfated zirconia sample is much less than unsulfated materials suggesting that sulphate species has displaced some loosely bonded surface hydroxyl groups [72].
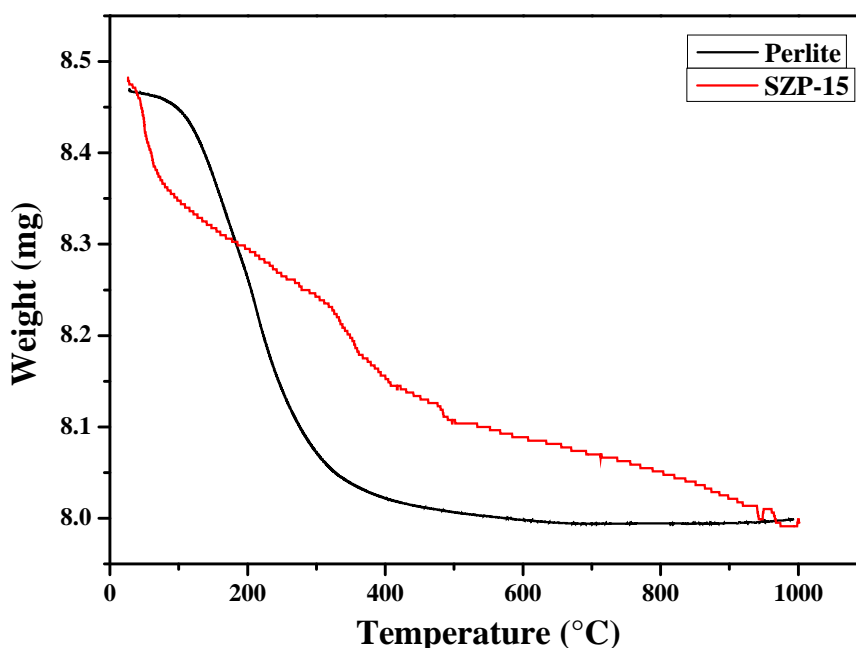
Figure 6.8: TGA curves of perlite and SZP-15.

6.3.8 Ultra violet-Visible Diffuse Reflectance spectroscopy (UV-Vis analysis)

UV-Vis spectroscopy has been used to determine molecular structure of zirconium species after incorporation into silica based support materials. In UV-Vis spectra of all catalysts as shown in **Figure 6.9**, a band near 210 nm is seen which can be assigned to oxygen-zirconium charge transfer [14]. It also suggests the presence of tetragonal phase of ZrO_2 in tetrahedral environment [19]. Such bands are seen when zirconium species are successfully incorporated into mesoporous silica skeleton of support. Absence of band at 230 nm in all catalysts reveals non-dominance of monoclinic phase of ZrO_2 [59]. For nano sulfated zirconia particles, an additional band at 298 nm attributing to oxygen-zirconium charge transfer also appears, which is present in all catalysts [73]. A band between 375-400 nm characteristic of rich zirconium content is also present in all catalysts.
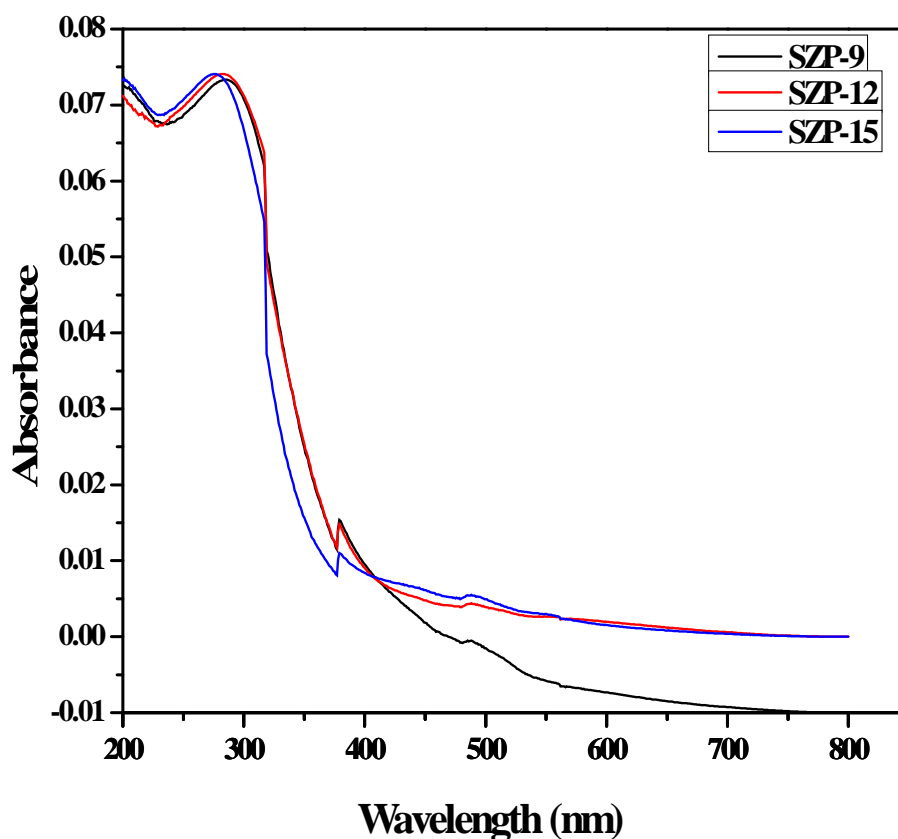
Figure 6.9:   UV-Vis DRS spectra of SZP-9, 12 and 15.

6.4   Catalyst selection

The catalytic activity of all samples is evaluated by benzoylation reaction of benzene by benzoyl chloride to give benzophenone under single step, one pot, solvent-free, liquid phase reaction conditions. Reaction is carried out at 90°C for 2.5 h, taking benzene/benzoyl chloride molar ratio 1:2 and benzene to catalyst weight ratio of 5:1. Results depicted in **Table 6.3** show that no reaction occurs in absence of catalyst, as well as, perlite and TAP do not possess any catalytic activity towards this reaction. SZP-9 and 12 show less catalytic activity towards the reaction because of lower presence of catalytic active Brønsted acidic sites also confirmed by pyridine adsorbed FT-IR studies given before in the chapter. As benzoylation reactions are Brønsted acid catalyzed reactions, SZP-15 show maximum conversion% owing to presence of sufficient catalytic active Brønsted acidic sites.

Table 6.3:   **Catalytic activity of different catalysts for benzoylation reaction of benzene by benzoyl chloride.**

Catalysts	Conversion (%)
Without catalyst	Nil
Perlite	Nil
TAP	Nil
SZP-9	54
SZP-12	78
SZP-15	86

Reaction conditions: Time = 2.5 h; Temperature = 90°C; molar ratio (benzene/benzoyl chloride = 1:2); substrate/catalyst weight ratio = 5:1.

In light of above inferences, effect of various reaction variables like reaction temperature and time, molar ratio of reactants, substrate/catalyst ratio, and nature of substrate for a series of benzoylation reactions of different arenes by benzoyl chloride are studied in detail using SZP-15 catalyst. Consequently, optimized

reaction conditions are determined to achieve maximum conversion% and selectivity of desired products.

6.5   Catalytic activity

6.5.1 *Influence of reaction temperature*

The effect of reaction temperature on conversion and selectivity% is studied to optimize the reaction temperature. For this purpose, benzoylation of benzene, toluene and anisole is carried out at different temperatures ranging from 50-170°C for 3, 3.5 and 4 h. **Figure 6.10** indicates that conversion% of benzene increases linearly up to 80°C with 100% selectivity of benzophenone. However, on further increasing reaction temperature up to 90°C, the conversion remains constant with decrease in selectivity from 100% to 78%. Similarly, on increasing reaction temperature above optimized temperature in case of toluene and anisole i.e., 110 and 150°C respectively, the conversion% remains almost constant while desired product selectivity% decrease abruptly as shown in **Figure 6.11** and **Figure 6.12**. At higher temperature, possibility of consecutive benzoylation reactions between thus formed benzoylated products and benzoyl chloride increases forming di or tri benzoylated products and consequently selectivity% of desired products. Moreover, benzoylation is a C-C bond forming reaction, but at higher temperature, O-benzoylation can also occur producing esters as minor products thus decreasing the overall desired product selectivity% of the reaction. In case of toluene, at higher temperature, selectivity towards thermodynamically stable product, 3-methyl benzophenone also increases [30] and thus selectivity of desired product, 4-methyl benzophenone decreases.
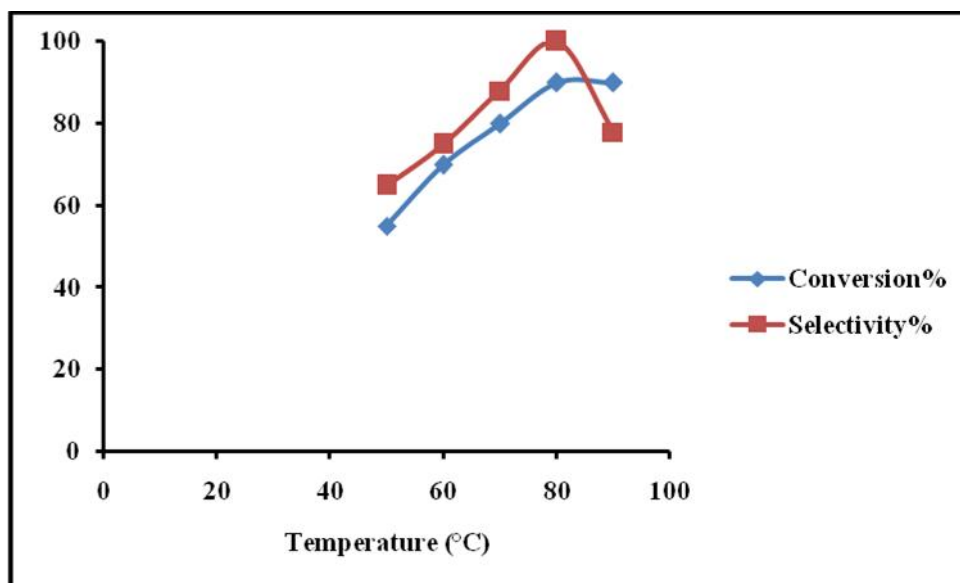
Figure 6.10: Variation of conversion and selectivity (%) of benzene over SZP-15 with temperature.

Reaction conditions: Time = 3 h; molar ratio (benzene/benzoyl chloride = 1:2); substrate/catalyst weight ratio = 5:1.
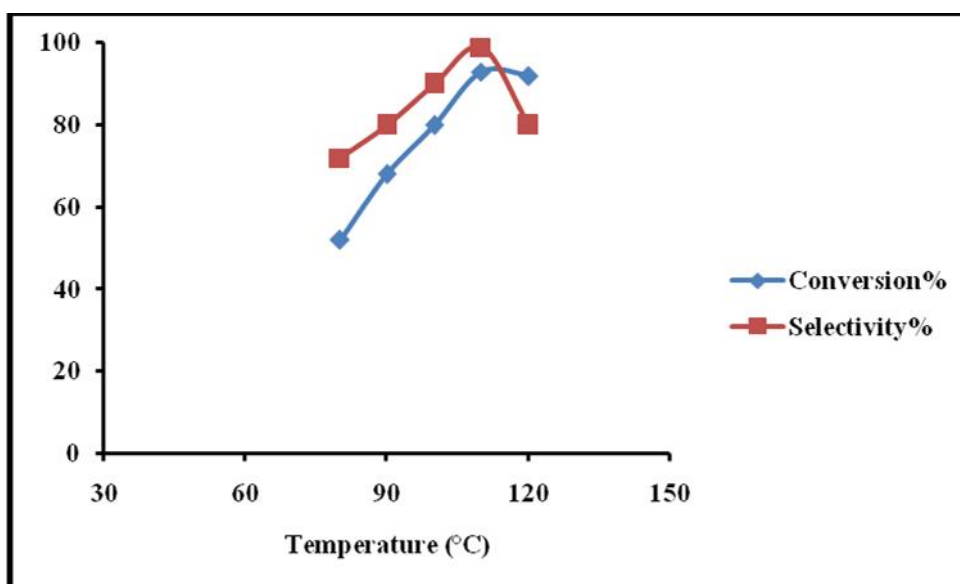
Figure 6.11: Variation of conversion and selectivity (%) of toluene over SZP-15 with temperature.

Reaction conditions: Time = 3.5 h; molar ratio (toluene/benzoyl chloride = 1:2); substrate/catalyst weight ratio = 5:1.
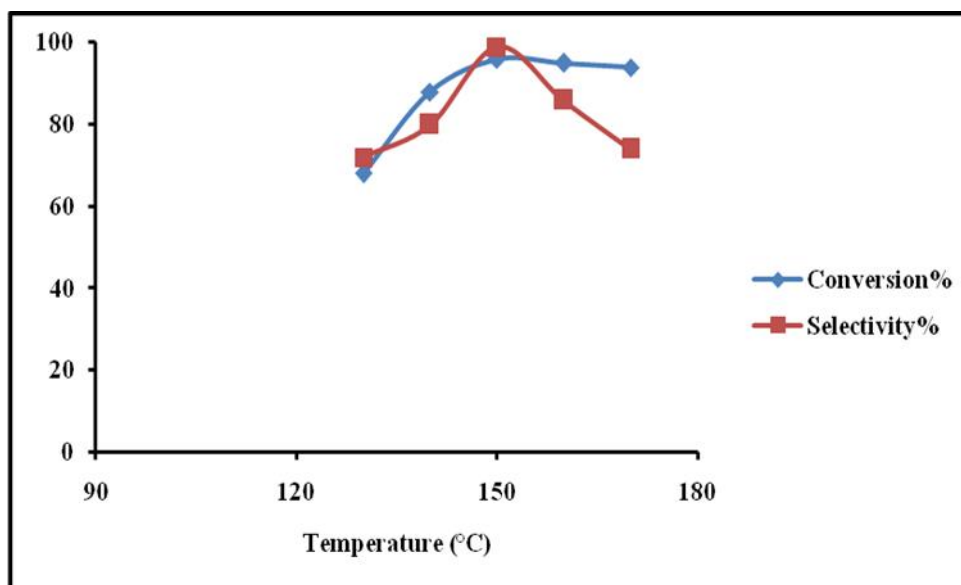
Figure 6.12: **Variation of conversion and selectivity (%) of anisole over SZP-15 with temperature.**

Reaction conditions: Time = 4 h; molar ratio (anisole/benzoyl chloride = 1:2); substrate/catalyst weight ratio = 5:1.

6.5.2 Influence of reaction time

To study the influence of reaction time periods on conversion and selectivity%, benzoylation of benzene, toluene and anisole are carried out for different time intervals ranging from 2-5 h at 80, 110 and 150°C respectively. As shown in **Figure 6.13**, conversion% of benzene increases up to 3 h and remains constant till 4 h. Likewise, conversion% of toluene and anisole also increase up to 3.5 and 4 h respectively and remains constant at higher time periods as inferred from **Figure 6.14** and **Figure 6.15**. Whereas, on increasing time period, selectivity% decreases in all reactions, because on providing more contact time to reactants, chances of continuous benzoylation reaction increases and thus, di or tri benzoylated products formed more decreasing the total selectivity% of reactions.
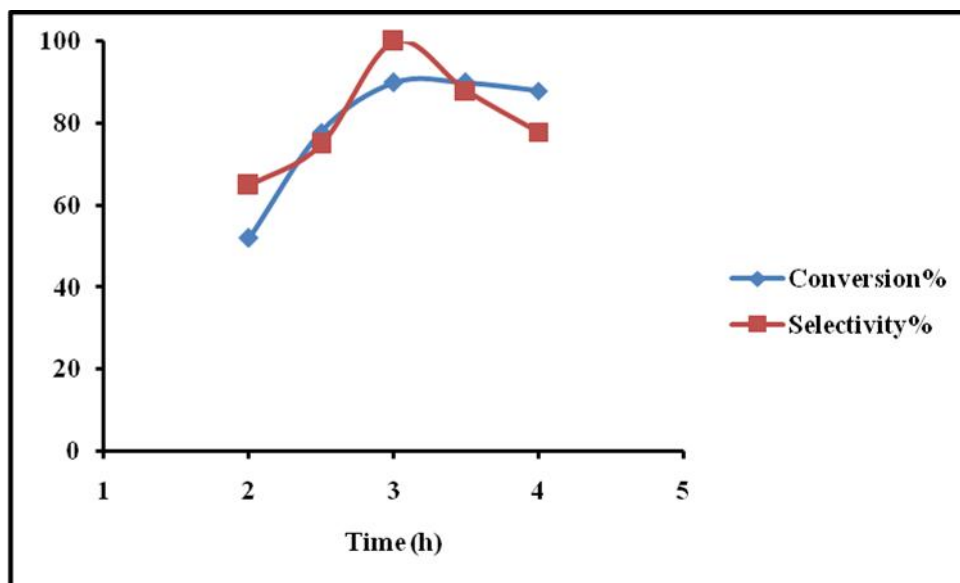
Figure 6.13: **Variation of conversion and selectivity (%) of benzene over SZP-15 with time.**

Reaction conditions: Temperature = 80°C; molar ratio (benzene/benzoyl chloride = 1:2); substrate/catalyst weight ratio = 5:1.
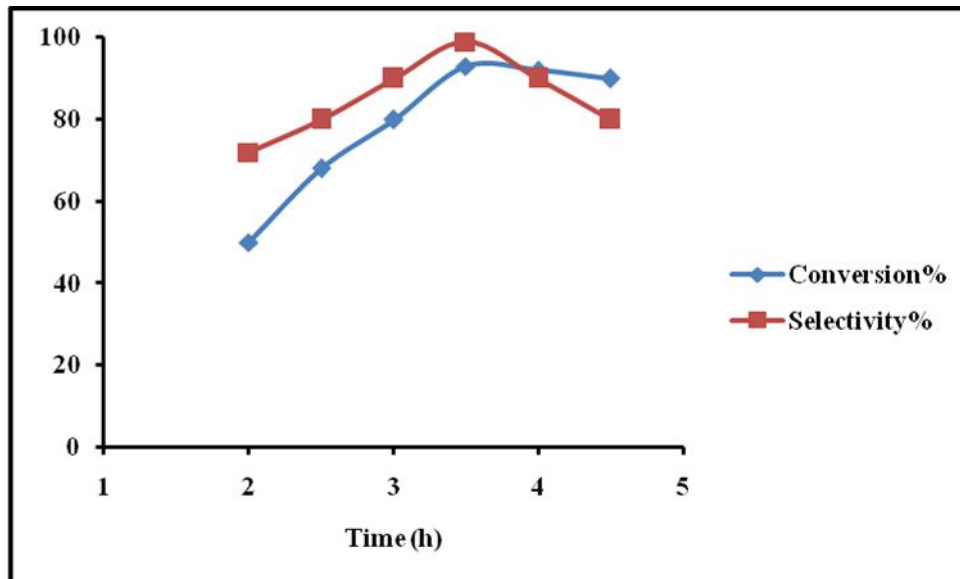
Figure 6.14: **Variation of conversion and selectivity (%) of toluene over SZP-15 with time.**

Reaction conditions: Temperature = 110°C; molar ratio (toluene/benzoyl chloride = 1:2); substrate/catalyst weight ratio = 5:1.
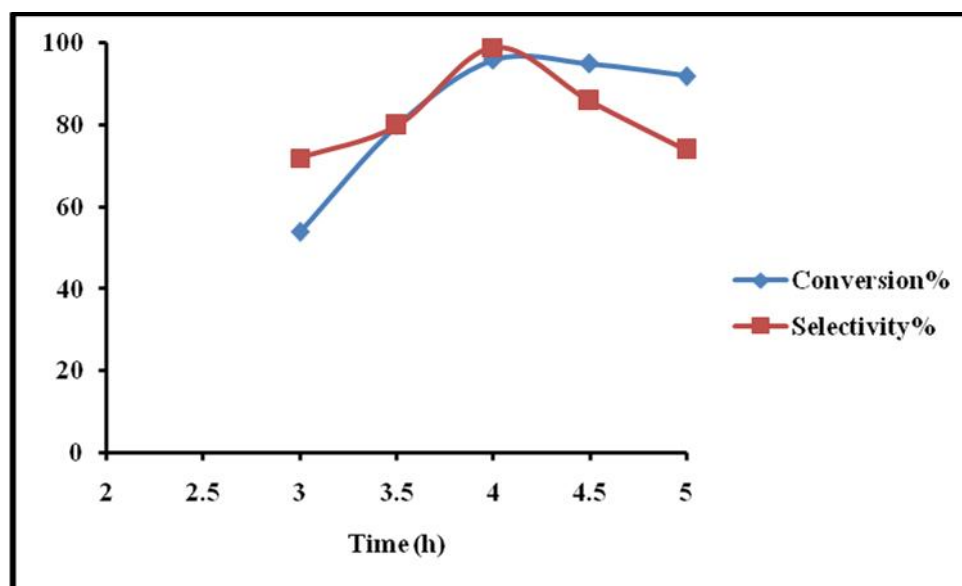
Figure 6.15: **Variation of conversion and selectivity (%) of anisole over SZP-15 with time.**

Reaction conditions: Temperature = 150°C; molar ratio (anisole/benzoyl chloride = 1:2); substrate/catalyst weight ratio = 5:1.

6.5.3 Influence of molar ratio of reactants

The effect of molar ratio of benzene, toluene and anisole to benzoyl chloride on conversion and selectivity% of desired products is also studied over SZP-15 catalyst under optimized reaction conditions. According to data provided in **Table 6.4**, it is found that at molar ratio 1:2, maximum conversion% of benzene, toluene and anisole with highest selectivity of their respective products (benzophenone, 4-methyl benzophenone and 4-methoxy benzophenone) is obtained. At 2:1 molar ratio, less conversion% is observed due to inadequate quantity of benzoyl chloride and thus most of arenes remain unreacted in reaction medium. When toluene is taken in higher amount, possibility of formation of 3-methyl benzophenone increases thus whole selectivity% of reaction decreases. In case of excess amount of benzoyl chloride the selectivity% decreases which can be attributed to formation of di or tri benzoylated products by repeated benzoylation reactions between excessive benzoyl chloride and as formed benzoylated products. In addition to, polycondensation products of benzoyl chloride may also form in case of excess benzoyl chloride.

Table 6.4: **Effect of molar ratio of arenes/benzoyl chloride on conversion and selectivity % over SZP-15.**

Molar ratio	Conversion % of benzene	Selectivity % of benzophe-none	Conversion % of toluene	Selectivity % of 4-methyl benzophe-none	Conversion % of anisole	Selectivity % of 4-methoxy benzophe-none
2:1	62	68	58	70	60	70
1:1	78	82	83	80	81	82
1:2	90	100	93	99	96	99
1:5	85	78	82	76	84	78

Reaction conditions: Time = 3, 3.5 and 4 h; Temperature = 80, 110 and 150°C for benzoylation of benzene, toluene and anisole respectively; substrate/catalyst weight ratio = 5:1.

6.5.4 *Influence of substrate to catalyst weight ratio*

The effect of substrate to catalyst weight ratio on conversion% of desired products is studied by varying the amount of catalyst under optimized reaction conditions. As inferred from **Figure 6.16**, it can be said that at on increasing catalytic amount, conversion% increases in all reactions. It can be ascribed to availability of enhanced number of catalytic active sites. On further increase in the amount of catalyst no significant change is observed.
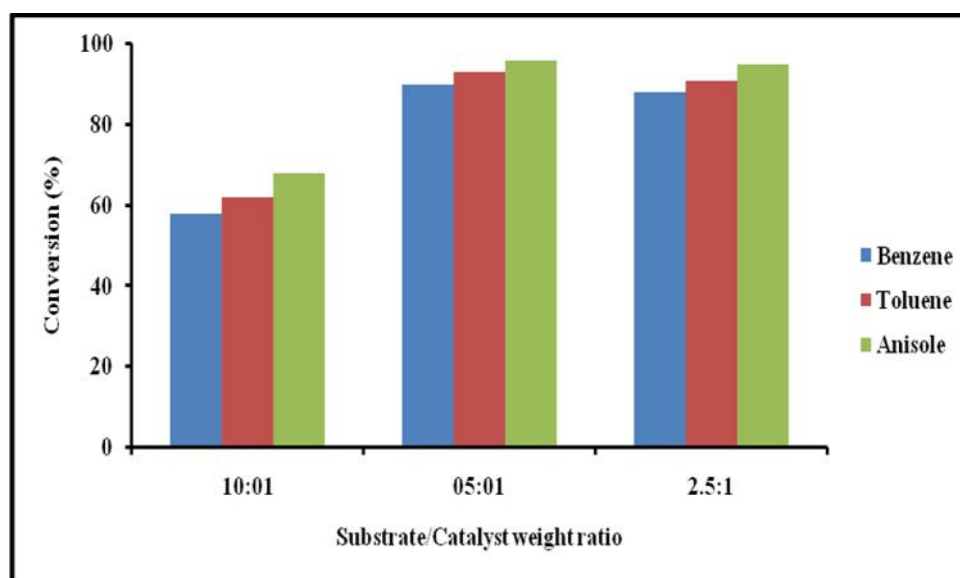
Figure 6.16: **Variation of conversion % of benzene, toluene and anisole over SZP-15 with substrate/catalyst weight ratio.**

Reaction conditions: Time = 3, 3.5 and 4 h; Temperature = 80, 110 and 150°C for benzoylation of benzene, toluene and anisole respectively; molar ratio (arenes/benzoyl chloride = 1:2.

6.5.5 Influence of aromatic substrate

The reactivity of aromatic substrates are in order – benzene (90% conversion) < toluene (93% conversion) < anisole (96% conversion). This can be explained on the basis of *ortho-para* directing effect of alkyl substituent present on aromatic ring. The electron releasing nature of –CH$_3$ and –OCH$_3$ groups present in toluene and anisole respectively favour electrophillic substitution at aromatic nucleus. Hence, electrophillic attack of benzoyl carbocation on substituted aromatic ring is favoured, leading to formation of benzoylated aromatic compounds at higher rate than that expected in absence of any electron donating group.

The optimized reaction parameters for a series of benzoylation reactions over SZP-15 in order to achieve maximum conversion and selectivity% are listed below in **Table 6.5**.

Table 6.5: **Optimized reaction *para* meters for a series of benzoylation reactions of aromatic substrates by benzoyl chloride over SZP-15 with maximum conversion and selectivity % of major products.**

S. No.	Aromatic substrates	Reaction temperature (°C)	Reaction time (h)	Conversion %	Major products with selectivity %
1.	Benzene	80	3	90	Benzophenone (100%)
2.	Toluene	110	3.5	93	4-methyl benzophenone (99%)
3.	Anisole	150	4	96	4-methoxy benzophenone (99%)

Reaction conditions: Molar ratio (arenes/benzoyl chloride = 1:2); substrate/catalyst weight ratio = 5:1.

Due to bulky nature of benzoyl group, *para* - substitution predominates. Owing to deactivating character of –ArCO group of benzoyl chloride, chances of formation of dibenzoylated products is very less under optimized reaction conditions. The predominance of *para* product can be correlated with sigma ( ) value of substituents. As per Hammett equation, negative sigma value indicates electron releasing nature of substituents. Since, $_p$ value of –CH$_3$ and –OCH$_3$

groups is greater than ₘ and ₒ values, thus, formation of *para* products is favoured.

6.5.6 Comparison with other reported catalysts

As depicted from **Table 6.6**, it can be said that SZP-15 gives higher conversion% of desired products for a series of benzoylation reactions than some previously documented commercial catalysts.

Table 6.6: **A comparison of benzoylation reaction of benzene, toluene and anisole by benzoyl chloride to give corresponding benzophenones over different types of solid catalysts.**

Catalysts	Benzene conversion%	Toluene conversion%	Anisole conversion%	References
PIZP*	87	90	94	[74]
In$_2$O$_3$/Si-MCM-41**	54	85	86	[39]
SZP-15***	90	93	96	This study

Reaction conditions:

* Time = 3.5, 3 and 1; Temperature = 80, 100 and 100°C for benzoylation of benzene, toluene and anisole respectively; molar ratio (arenes/benzoyl chloride = 0.1:0.02).

** Time = 5.8, 2.5 and 4.9 h; Temperature = 80, 110, 80°C for benzoylation of benzene, toluene and anisole respectively; catalyst/benzoyl chloride weight ratio =0.33.

*** Time = 3, 3.5 and 4 h; Temperature = 80, 110 and 150°C for benzoylation of benzene, toluene and anisole respectively; molar ratio (arenes/benzoyl chloride = 1:2); catalyst weight =0.2g.

6.6 Mechanical aspects

The proposed model structure of SZP-15 catalyst is shown in **Scheme 6.3 (a) and (b)**. The zirconia clusters are supported on surface of perlite by Si–O–Zr linkages. The sulfate species are bonded with zirconium atom as bidentate chelating ligand. The catalyst exhibit both types of acid sites, Brønsted as well as Lewis sites, on its surface, as confirmed by pyridine FT-IR spectrum described earlier in this chapter. The sulfate group in association of water molecules behaves like ionic sulfate and generates Brønsted acid sites on the surface. The desorption of water molecule can convert the ionic sulfate to covalently linked sulfate with zirconium atom and generate Lewis acid sites [50]. However inter-conversion of Lewis sites to Brønsted sites may occur during our reaction system which is represented in **Scheme 6.3a**. Other acid sites arise on the surface are due to Si–OH or Si–O–Zr–OH groups.

Electrophillic substitution reaction follows Eley-Rideal type mechanism. Benzoyl chloride is polarised over surface Brønsted acid sites of the catalyst and produces carbocation which acts as surface electrophile as shown in **Scheme 6.4**, then attacks on the aromatic substrate present in liquid phase and form benzoylated product by simple electrophilic substitution reaction. Thus, in reaction mechanism, formation of carbocation is an important step. $-CH_3$ and $-OCH_3$ being electron releasing groups, increase electron density on aromatic ring and make it more vulnerable towards electrophillic attack of benzoyl carbocations. Therefore, conversion% is higher for anisole and toluene as compared to benzene for benzoylation.
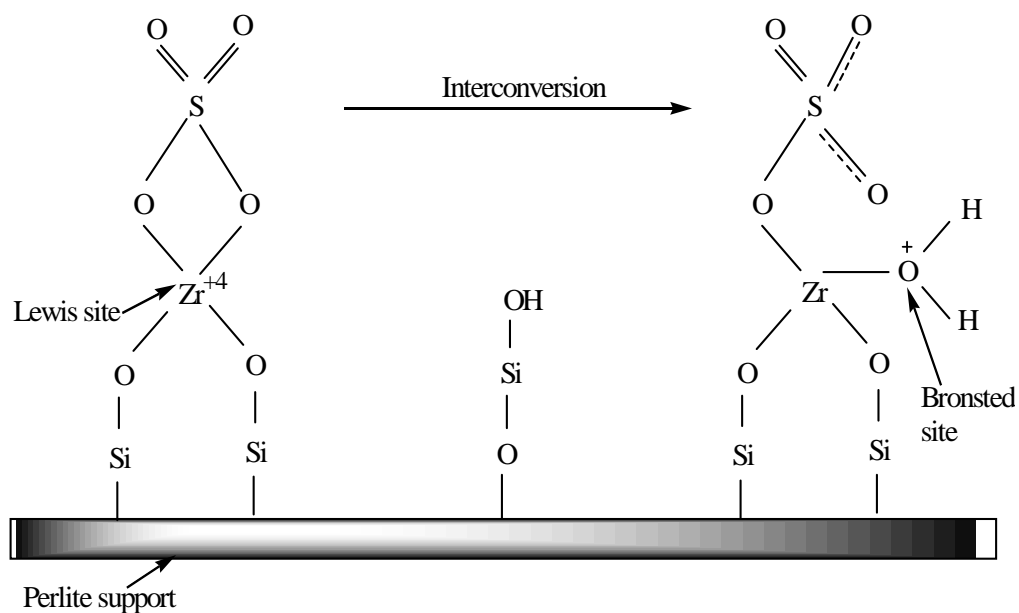
(a)
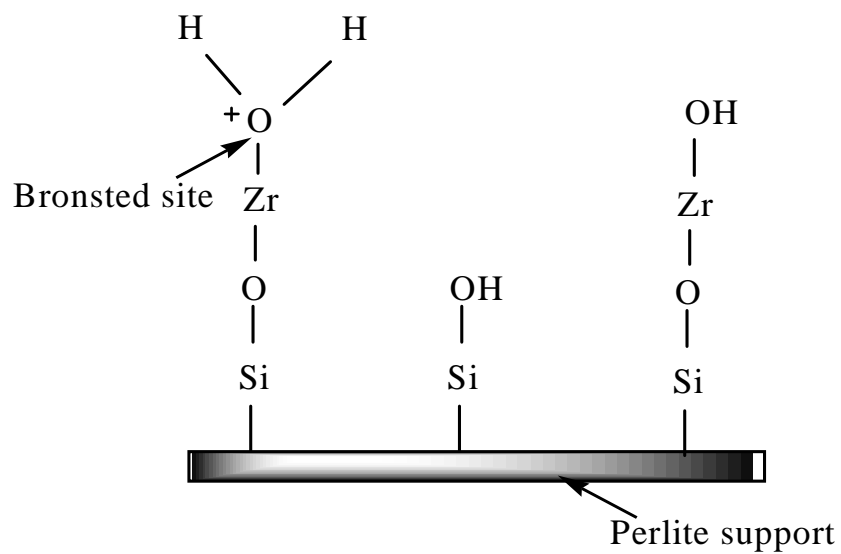
(b)

Scheme 6.3: Proposed structure for active sites of SZP-15 (a) Generation of Brønsted and Lewis acidic sites and their interconversion, (b) Generation of Brønsted acidic sites due to Si-Zr-OH group.

Scheme 6.4: **Proposed mechanism of benzoylation of aromatic substrates by benzoyl chloride over SZP-15.**

6.7 Catalyst reusability

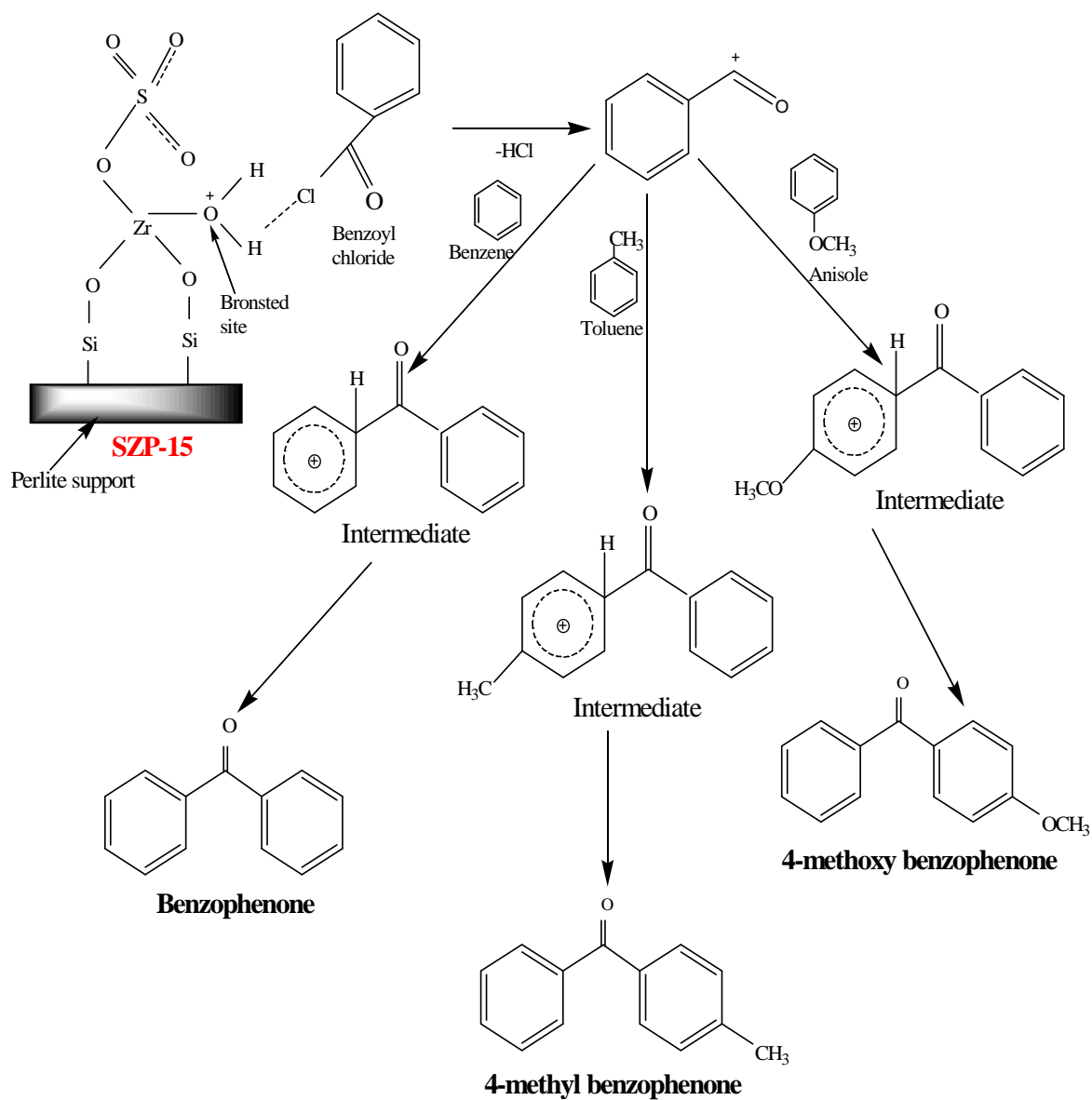The catalyst from all reaction mixtures are filtered, washed with acetone and regenerated by thermal treatment at 450°C for 2 h for their use in next reaction runs under similar reaction conditions. The regenerated catalyst is found to be equally efficient up to 5 reaction cycles for all reactions giving conversion in range of 90-85%, 93-88% and 96-90% for benzoylation of benzene, toluene and anisole respectively as shown in **Table 6.7**. The FT-IR spectrum **(Figure 6.17b)** of SZP-15 regenerated after 5th reaction cycle resembles with the FT-IR spectrum of fresh SZP-15 catalyst **(Figure 6.17a)** indicating the intact chemical composition and stability of active sites of catalyst. The results interpret that the catalyst can be easily regenerated by simple filtration and thermal treatment without any considerable loss of activity of catalytic sites. The conversion% is decreased after fifth reaction cycle, attributed to the physical adsorption of carbonaceous materials on surface of catalyst which blocks the pores of catalyst, restricts access of reactants on catalytic active sites [75], limits their reaction with each other and thus decreases the overall conversion% of the reaction. This phenomenon is also confirmed by decrease in broadness and intensity of band appearing between 3600-3300 cm^{-1} and a peak around 1630 cm^{-1} attributing to stretching and bending –OH vibrations respectively in case of regenerated catalyst which plays an important role in catalysing benzoylation reactions. HCl produced during reaction also deactivates catalytic sites. The stability, heterogenity of SZP-15 catalyst and possibility of leaching of active sulphur and zirconia content by HCl, formed as by-product in reaction medium is further analyzed by Sheldon's hot filteration test [76] which involves filtration of catalyst from reaction mixture in middle of the reaction and further continuance of reaction in absence of catalyst. The results show that the reaction queches on filtering off the catalyst, hence it is confirmed that active sulfated zirconia species responsible for catalytic activity do not get leached off during course of reaction.
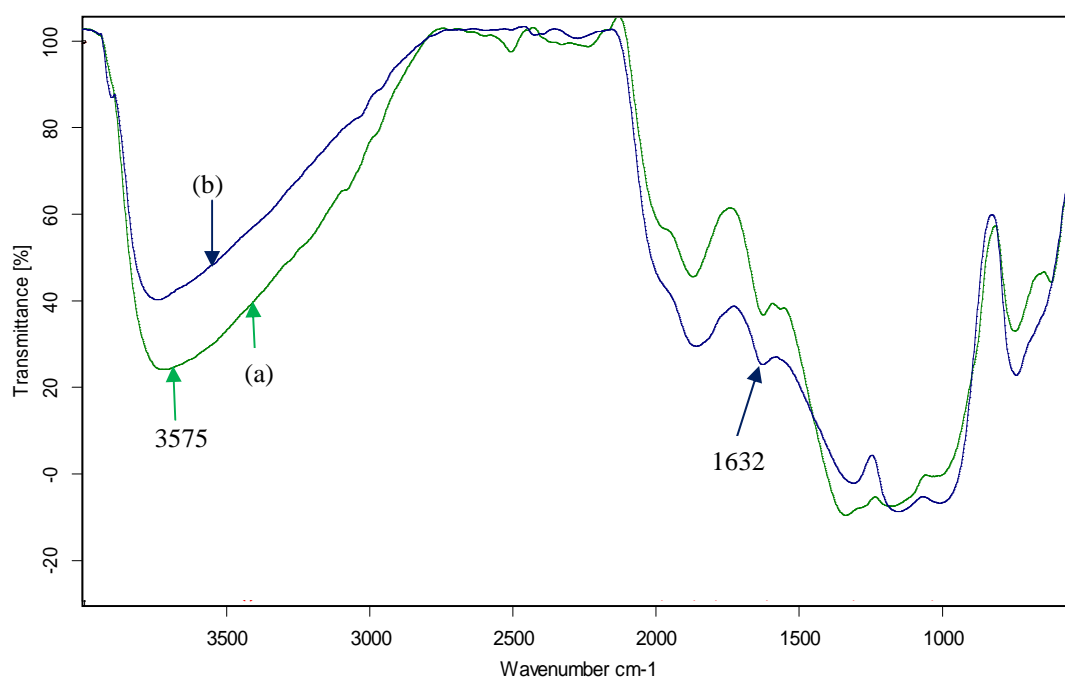
Figure 6.17:   FT-IR spectra of (a) SZP-15 and (b) regenerated catalyst.

Table 6.7: **Benzoylation of benzene, toluene and anisole by benzoyl chloride over fresh and regenerated SZP-15.**

Reaction cycle	Conversion (%) of benzene	Conversion (%) of toluene	Conversion (%) of anisole
I	90	93	96
II	90	92	95
III	89	91	93
IV	87	90	92
V	85	88	90

Reaction conditions: Time = 3, 3.5 and 4 h; Temperature = 80, 110 and 150°C for benzoylation of benzene, toluene and anisole respectively; molar ratio (arenes/benzoyl chloride = 1:2); substrate/catalyst weight ratio = 5:1.

6.8   Identification of products

Product confirmation is done by melting point analysis, ^{1}H NMR and ^{13}C NMR techniques by comparison with standard products.

Benzophenone – Melting point - 49°C; ^{1}H NMR: 7.77–7.74 (d, 4H, J = 7 Hz), 7.55–7.50 (t, 2H, J = 7 Hz), 7.45–7.40 (t, 2H, J = 7 Hz); ^{13}C NMR: 196.61 (CO), 137.49, 132.33, 128.19.

4-Methylbenzophenone – Melting point - 57°C; ^{1}H NMR: 7.79–7.76 (d, 2H, J = 7 Hz), 7.73–7.70 (d, 2H, J = 8 Hz), 7.59–7.54 (t, 1H, J = 6 Hz), 7.48–7.43 (t, 2H, J = 7 Hz), 7.29–7.26 (d, 2H, J = 8 Hz), 2.42 (s, 3H); ^{13}C NMR: 196.35 (CO), 134.14, 137.86, 134.79, 132.08, 130.22, 129.85, 128.90, 128.13, 21.63 (Me).

4-Methoxybenzophenone – Melting point - 62°C; ^{1}H NMR: 7.82–7.79 (d, 2H, J = 9 Hz), 7.74–7.71 (d, 2H, J = 8 Hz), 7.60–7.53 (t, 1H, J = 7 Hz), 7.46–7.41(t, 2H, J = 7 Hz), 6.95–6.92 (d, 2H, J = 9 Hz), 3.87 (s, 3H); ^{13}C NMR: 197.17 (CO), 163.18, 138.24, 132.55, 131.86, 130.10, 129.70, 128.16, 113.52, 55.48 (OMe).

6.9 Conclusion

The present investigation discusses the synthesis of a novel, highly potential, nano-crystalline, recyclable super solid acid catalyst, sulfated zirconia supported on thermally activated perlite (SZP). Thermal activation of perlite stabilizes its rich silica-alumina content and provides an excellent support material for further loading of sulfated zirconia in varying amounts through two step sol-gel methodology. SZP-15 catalyst possessing optimum Brønsted acidic sites, as determined by pyridine adsorbed FT-IR spectroscopy efficiently catalyze a series of liquid phase benzoylation reactions of arenes utilizing benzoyl chloride as benzoylating agent. XRD studies reveal the existence of catalytic active tetragonal phase of zirconia in SZP-15. The efficiency of catalyst is further confirmed by higher conversion% obtained in all reactions. In addition to, catalyst can also be reutilized up to five consecutive reaction runs with analogous potency after simple filtration and thermal treatment. Sheldon's hot filtration find out that the active sulfated zirconia species is firmly stabilized on perlite and do not get leached off during the reaction conserving the heterogeneous nature of catalyst during whole procedure. Influence of various reaction variables are studied during the reactions which helps in determining optimized reaction conditions to obtain maximum conversion and selectivity%. Catalytic activity of SZP-15 has been proved better than some previously reported solid acid catalysts establishing the stability of super acidic sites in catalyst. Hence, the novelty of this work is that perlite after its appropriate activation can replace other conventional supports for loading of sulfated zirconia and can be utilized in catalyzing benzoylation reactions having wide applications in pharmaceutical, fine chemical, perfumeries sectors.

6.10 References

[1]   E. Liu, A.J. Locke, R.L. Frost, W.N. Martens, "Journal Mol. Catal. A, Chem. 353-354 (2012) 95.

[2]   M. Hino, S. Kobayashi, K. Arata, J. Am. Chem. Soc. 101 (1979) 6439.

[3]   Y. Zhang, W. Wong, K. Yung, Bioresour. Technol. 147 (2013) 59.

[4]   G.D. Yadav, A.D. Murkute, 224 (2004) 218.

[5]   S. Garg, K. Soni, G.M. Kumaran, R. Bal, K. Gora-marek, J.K. Gupta, L.D. Sharma, G.M. Dhar, 141 (2009) 125.

[6]   U.K.H. Bangi, C. Park, S. Baek, H. Park, Powder Technol. 239 (2013) 314.

[7]   S.K. Bhattacharya, R.R. Tummala, J. Mater. Sci. Mater. Electron. 11 (2000) 253.

[8]   G.D. Wilk, R.M. Wallace, J.M. Anthony, J. Appl. Phys. 89 (2001) 5243.

[9]   D. Yunchen, L. Sen, Z. Yonglai, J. Yanyan, X. Feng-shou, Paper.edu.cn (n.d.) 1.

[10]   N. Lohitharn, E. Lotero, J.G.G. Jr, J. Catal. 241 (2006) 328.

[11]   S. Wang, J.A. Guin, Fuel Process. Technol. 84 (2003) 135.

[12]   K.R.S. Devi, S. Jayashree, Bull. Chem. React. Engg. Catal. 7 (2013) 205.

[13]   A. Sinhamahapatra, N. Sutradhar, M. Ghosh, H.C. Bajaj, A.B. Panda, "Applied Catal. A, Gen. 402 (2011) 87.

[14]   G. Negrón-silva, C.X. Hernández-reyes, D. Angeles-beltrán, L. Lomas-romero, E. González-zamora, J. Méndez-vivar, Molecules (2007) 2515.

[15]   A.R.M. L. Hermida, A.Z. Abdullah, J. Appl. Sci. 10 (2010) 3199.

[16]   G.D. Yadav, S.R. More, "Applied Catal. A, Gen. 411-412 (2012) 123.

[17]   X. Yang, R.E. Jentoft, F.C. Jentoft, I. Chemistry, F. Mpg, Catal. Letters 106 (2006) 195.

[18]   M.K. Mishra, B. Tyagi, R. V Jasra, J. Mol. Catal. A Chem. 223 (2004) 61.

[19]   J. Zhao, Y. Yue, W. Hua, H. He, Z. Gao, Appl. Catal. A Gen. 336 (2008) 133.

[20]   G. Chen, C. Guo, H. Qiao, M. Ye, X. Qiu, C. Yue, CATCOM 41 (2013) 70.

[21]   E. Ghedini, M. Signoretto, F. Pinna, G. Cerrato, C. Morterra, Appl. Catal. B Environ. 67 (2006) 24.

[22]   M.H.A.Y. Choi, A.W. Apblett, Catal. Letters (2013) 705.

[23]   V. Ganpat, Y. Gbadebo, "Applied Catal. A, Gen. 462-463 (2013) 196.

[24]   V.S. Marakatti, G. V Shanbhag, A.B. Halgeri, "Applied Catal. A, Gen. 451 (2013) 71.

[25]   Q. Zhuang, J.M. Miller, Appl. Catal. A Gen. 209 (2001) 1.

[26]   R. Akkari, A. Ghorbel, N. Essayem, F. Figueras, Appl. Catal. A Gen. 328 (2007) 43.

[27]   P. Laidlaw, D. Bethell, S.M. Brown, G.J. Hutchings, J. Mol. Catal. A Chem. 174 (2001) 187.

[28]   F. Adam, I.A. Hassan, R. Thankappan, Open Colloid Sci. J. 3 (2010) 15.

[29]   Y. Bing, Y. Bing, L.I. Zong-shi, Q. Wei-hong, W. Gui-ru, C. Lu-bai, in:, Proc. 3rd Int. Conf. Funct. Mol., 2003, pp. 278–283.

[30]   F. Adam, K.L. Sek, Chinese J. Catal. 33 (2012) 1802.

[31] P.T. Patil, K.M. Malshe, P. Kumar, M.K. Dongare, E. Kemnitz, Catal. Commun. 3 (2002) 411.

[32] D.P. Sawant, B.M. Devassy, S.B. Halligudi, J. Mol. Catal. A Chem. 217 (2004) 211.

[33] F. Effenberger, E. Sohn, G. Epple, Chem. Ber. 116 (1983) 1195.

[34] G.D. Yadav, N.S. Asthana, V.S. Kamble, Appl. Catal. A Gen. 240 (2003) 53.

[35] M. Bolognini, F. Cavani, M. Cimini, L. Dal, L. Maselli, D. Venerito, F. Pizzoli, G. Veronesi, C.R. Chim. 7 (2004) 143.

[36] R. Fang, R. Prins, Stud. Surf. Sci. Catal. 84 (1994) 1441.

[37] P.H. Tran, N. Bich, L. Do, T.N. Le, Tetrahedron Lett. 55 (2014) 205.

[38] F.Z. El Berrichi, C. Pham-huu, L. Cherif, B. Louis, M.J. Ledoux, CATCOM 12 (2011) 790.

[39] V.R. Choudhary, S.K. Jana, Appl. Catal. A Gen. 184 (2002) 247.

[40] S. Paul, P. Nanda, R. Gupta, Molecules 8 (2003) 374.

[41] H. Suja, C.S. Deepa, K.S. Rani, S. Sugunan, Appl. Catal. A Gen. 230 (2002) 233.

[42] D. Bhattacharya, S. Sharma, A.P. Singh, Appl. Catal. A Gen. 150 (1997) 53.

[43] S. Kobayashi, S. Nagayama, J. Am. Chem. Soc. 120 (1998) 2985.

[44] K.R.S. Devi, S. Jayashree, 7 (2013) 205.

[45] S. Kabra, S. Katara, A. Rani, Int. J. Innov. Res. Sci. Eng. Technol. 2 (2013) 4319.

[46] K. Amutha, R. Ravibaskar, G. Sivakumar, Int. J. Nanotechnol. Appl. 4 (2010) 61.

[47] A.I. Ahmed, S.E. Samra, A.S. Khder, Colloids Surfaces A Physicochem. Eng. Asp. 317 (2008) 62.

[48] X. Wang, H. Wang, Y. Liu, F. Liu, Y. Yu, H. He, J. Catal. 279 (2011) 301.

[49] Z. Wu, Y. Zhao, D. Liu, Microporous Mesoporous Mater. 68 (2004) 127.

[50] C. Khatri, M.K. Mishra, A. Rani, Fuel Process. Technol. 91 (2010) 1288.

[51] S. Kabra, A. Sharma, S. Katara, R. Hada, A. Rani, Indian J. Appl. Res. (2013) 2013.

[52] F. Adam, S. Balakrishnan, P. Wong, J. Phys. Sci. 17 (2006) 1.

[53] B.J. Saikia, G. Parthasarathy, J. Mod. Phys. 1 (2010) 206.

[54] J.R. Sohn, T. Kwon, S. Kim, Bull. Korean Chem. Soc. 22 (2001) 1309.

[55] S.D. Sharma, S. Singh, Am. J. Chem. 3 (2013) 96.

[56] E.A.E.S. S, Al-shihry, Montash Chem (2010) 259.

[57]   S.K. Q.H. Xia, K. Hidajat, J. Catal. 205 (2002) 318.

[58]   G.D. Yadav, N.P. Ajgaonkar, A. Varma, J. Catal. 292 (2012) 99.

[59]   A. Jime, D.J. Jones, E. Rodrı, M. Trombetta, G. Busca, M. Lenarda, L. Storaro, J. Solid State Chem. 175 (2003) 159.

[60]   H. Sepehrian, A.R. Khanchi, M.K. Rofouei, S.W. Husain, J. Iran. Chem. Soc. 3 (2006) 253.

[61]   B. Tyagi, M.K. Mishra, R.V. Jasra, J. Mol. Catal. A Chem. 317 (2010) 41.

[62]   C.R. Reddy, Y.S. Bhat, G. Nagendrappa, B.S. Jai Prakash, Catal. Today 141 (2009) 157.

[63]   M. Musthofa, A.H. Karim, N.A. Fadzlillaah, N. Hazirah, R. Annuar, A.A. Jalil, S. Triwahyono, J. Fundam. Sci. 6 (2010) 127.

[64]   Z. Wang, World J. Nano Sci. Eng. 02 (2012) 134.

[65]   H. Yang, H. Song, H. Zhang, P. Chen, Z. Zhao, "Journal Mol. Catal. A, Chem. 381 (2014) 54.

[66]   L.O. Alemán-vázquez, J.L. Cano-domínguez, E. Torres-garcía, J.R. Villagómez-ibarra, (2011) 5916.

[67]   S.T. Hussain, M. Mazhar, S. Gul, Chinese J. Catal. 28 (2007) 622.

[68]   M.A. Ahmed, Fuel Process. Technol. 92 (2011) 1121.

[69]   E.P. Parry, J. Catal. 2 (1963) 371.

[70]   Y. Sun, L. Yuan, S. Ma, Y. Han, L. Zhao, W. Wang, C. Chen, F. Xiao, Appl. Catal. A Gen. 268 (2004) 17.

[71]   S. Gao, X. Chen, H. Wang, J. Mo, Z. Wu, Y. Liu, X. Weng, J. Colloid Interface Sci. 394 (2013) 515.

[72]   A.B. P. Bautista, M. Faraldos, M. Yates, Appl. Catal. B Environ. 71 (2007) 254.

[73]   J.A. Wang, L.F. Chen, L.E. Norena, J. Navarrete, M.E. Llanos, J.L. Contreras, O. Novaro, Microporous Mesoporous Mater. 112 (2008) 61.

[74]   M.B. Gawande, S.S. Deshpande, S.U. Sonavane, R. V Jayaram, J. Mol. Catal. A Chem. 241 (2005) 151.

[75]   C.H. Bartholomew, Appl. Catal. A Gen. 212 (2001) 17.

[76]   A. Rani, C. Khatri, R. Hada, Fuel Process. Technol. 116 (2013) 366.

Annexure – I and II

CHARACTERIZATION TECHNIQUES

Physicochemical properties of all catalytic materials are studied by N_2 adsorption-desorption, XRD, FT-IR and pyridine adsorbed FT-IR, SEM, SEM-EDX, TEM, TGA, UV-Vis DRS, Solid state ^{31}P NMR techniques. The reaction products are analyzed by ^{1}H, ^{13}C NMR and gas chromatography.

1. BET analysis

Specific surface area and average pore diameter of samples are determined from N_2 adsorption-desorption, done by using Thermo Scientific^{TM} Surfer surface area analyzer. The samples are degassed under vacuum at 120°C for 4 h, prior to adsorption in order to evacuate the physisorbed moisture. BET analysis is done at **University of Pune, Pune.**

2. X-ray diffraction analysis

The structural features of samples are analyzed by X-ray diffraction studies. X-ray diffraction (XRD) patterns are recorded by Bruker D8 Advance diffractometer, using Ni-filter and Cu K radiation (E = 8047.8 eV, = 1.5406A˚). The samples are scanned in 2 range of 5-75˚ at a scanning rate of $0.04˚s^{-1}$. XRD analysis has been done at **UGC-DAE CSR, Indore.**

3. Fourier transform infra-red analysis (FT-IR)

FT-IR study is executed on Bruker FT-IR Spectrophotometer (TENSOR 27) in DRS (Diffuse Reflectance System) mode by mixing samples with KBr in 1:20 weight ratio. The acidity of the catalysts is measured by pyridine adsorbed FT-IR. The samples (0.2 g) were activated at 450 °C for 2 h and exposed to pyridine (25 ml) for 24 h. The spectra were recorded in the range of 550-4000 cm^{-1} with a resolution of 4 cm^{-1}. FT-IR analysis is conducted at **Department of Pure and Applied Chemistry, University of Kota, Kota.**

4. Scanning electron microscopy (SEM and SEM-EDX analysis)

The detailed imaging information about the morphology and surface topography is studied by Scanning electron microscope (Model-JEOL-JSM 5600 and LEO 435VP). SEM analysis is done at **UGC-DAE CSR Indore, University of Pune, Pune and IIT-Roorkee.**

5. *Transmission electron microscopy (TEM analysis)*

The surface morphology and texture of samples is further confirmed by TEM analysis, Model: H-7500 (Hitachi Make). TEM analysis is done at **SAIF-Chandigarh.**

6. *Thermo-gravimmetric analysis (TGA)*

Thermo gravimetric analysis (TGA) of the samples is carried out using DTG-60-H- Shimadzu thermal analyzer (C-30574400175), by heating the samples in the range of 50–1000 °C with a heating rate of 10°C/min under nitrogen flow (50 cm^3/min). TGA analysis of samples is done at **University of Pune, Pune and IIT-Roorkee.**

7. *Ultra violet-Visible Diffuse Reflectance spectroscopy (UV-Vis analysis)*

UV–Vis spectra in the range of 200–800 nm were measured with a Perkin Elmer Lambda 950 UV–Vis spectrophotometer equipped with Harrick DRS assembly at ambient temperature. UV-Vis DRS analysis is done at **UGC-DAE CSR Indore.**

8. *Solid state ^{31}Phosphorus NMR analysis*

Solid state ^{31}P MAS NMR spectra (Mercury Plus-300 spectrometer. Make: Varian) are recorded at 121.5MHz with high power decoupling with a Bruker 4mmprobe head. The spinning ratewas 10 kHz and the delay between two pulses was varied between 1 and 30 s to ensure that complete relaxation of the ^{31}P nuclei occurred. The chemical shifts are given relative to external 85% H_3PO_4.This analysis is done at **SAIF-IIT Bombay.**

9. *^{1}H and ^{13}C NMR analysis*

^{1}H and ^{13}C NMR analysis of reaction products is carried out on Bruker AvIII HD-300 NMR spectrometer. The analysis is done at **CDRI Lucknow.**

10. *Mechanical activation*

Mechanical activation of fly ash is carried out in a high energy planetary ball mill (Retsch PM-100, Germany). As received fly ash is mechanically activated in an agate jar using 5 mm agate balls with 10:1 ball to powder weight ratio (BPR). The mechanical activation was done at 250 rpm rotation speed for specified time period. Mechanical activation is carried out at **Department of Pure and Applied Chemistry, University of Kota, Kota.**

11. *Gas Chromatography*

The products are analyzed by Gas Chromatograph (Agilent Technologies 7820A) having FID and Agilent J&W Advanced Capillary HP 5 GC Columns of 30 m length and 0.320 mm diameter, programmed oven temperature of 60–325ºC and N_2 (1.5 ml/min) as a carrier gas. GC analysis is conducted at **Department of Pure and Applied Chemistry, University of Kota, Kota.**

12. *Melting point detection*

Melting points of products are detected by using Xd-6 microscope melting apparatus. Melting point determination is done at **Department of Pure and Applied Chemistry, University of Kota, Kota.**

LIST OF PUBLICATIONS

In International and National Journals-

1. DRIFT- Spectroscopic Study of Modification of Surface Morphology of Perlite During Thermal Activation**,** *Sakshi Kabra*, Anita Sharma, Stuti Katara, Renu Hada and Ashu Rani, Ind. J. Appl. Res., 3 (4), April 2013.

2. Synthesis of Nanosized Titania by sol-gel route, Renu Hada, *Sakshi Kabra*, Stuti Katara, Ashu Rani, Vijay Devra and S.S. Amritphale, Ind. J. Appl. Res., 3 (4), April 2013.

3. Acid Activated fly Ash, as a Novel Solid Acid Catalyst for Esterification of Acetic Acid, Anita Sharma, Stuti Katara, *Sakshi Kabra* and Ashu Rani, Ind. J. Appl. Res., 3 (4), April 2013.

4. Surface modification of fly ash by thermal activation: A DR/FTIR study, Stuti Katara, *Sakshi Kabra*, Anita Sharma, Renu Hada and Ashu Rani, Int. Res. J. Pure App. Chem. 2013, 3 (4), 299-307.

5. Characterization and study of Turkish perlite, *Sakshi Kabra*, Stuti Katara and Ashu Rani, Int. J. Innov. Res. Sci. Engg. Technol. 2013, 2 (9), 4319-26.

6. Perlite supported nickel catalyst: synthesis, characterization and catalytic activity in Claisen-Schmidt condensation reactions, *Sakshi Kabra*, Stuti Katara, Renu Hada and Ashu Rani, Catalysis Communications (Communicated).

7. Fly ash supported phosphomolybdic acid as a highly efficient solid Lewis acid catalyst for microwave assisted Friedel- Crafts acylation reactions, *Sakshi Kabra*, Renu Hada, Stuti Katara and Ashu Rani, Fuel (Communicated).

8. An Efficient and Cost-Effective Solid Base Catalyst for Cross-Aldol Condensation of Ketones with Aromatic Aldehydes under Solvent Free Condition. Stuti Katara, *Sakshi Kabra*, Renu Hada, Ashu Rani, Catalysis Communications (Communicated).

9. Fly ash supported solid base catalyst for microwave assisted Michael addition reaction. Stuti Katara, Renu Hada**,** *Sakshi Kabra*, Ashu Rani, Fuel Processing Technology (Communicated).

10. Non Aqueous Synthesis of Fly Ash Supported TiO_2 Nanoparticles for Enhanced Photo-Oxidation of Congo Red Dye, Renu Hada, *Sakshi Kabra*,

Stuti Katara, Vijay Devra, Ashu Rani, Fuel Processing Technology (Communicated).

11. Microwave Assisted Solution Combustion Synthesis of Activated Fly Ash Supported NiO Nanoparticles for Hydrogen Peroxide Decomposition, Renu Hada, Stuti Katara, *Sakshi Kabra*, Vijay Devra, Ashu Rani, Fuel (Communicated).

In International Conferences/Workshop/Symposium-

1. Participated in an Indo-Swedish Symposium, **Strategic Knowledge on Climate Change** held on 9 October 2012 at University of Kota, Kota.

2. Poster presentation in International Conference on **Waste, Wealth and Health (ICWWH-2013)** held on 15-17 February 2013 at MPCST, Bhopal.

3. Poster presentation in International Conference on **New Emerging Trends in Chemistry** held on 3-4 March 2013 at IIS University, Jaipur.

4. Poster presentation in International Workshop on **Green Initiatives in Energy, Environment & Health** held on 2-3 December 2013, organized by Green Chemistry Centre of Excellence, The Energy and Resources Institute, Green Chemistry Network Centre, DU, Gautam Buddha University, Green Chemistry Network and sponsored by Royal Society of Chemistry London (North India Section) at Delhi.

5. Paper presentation as first author in International Conference on **Advanced Trends in Engineering and Technology (ICATET) 2013** on 19-20 December 2013 at Arya College of Engineering & I.T., Jaipur.

6. Paper presentation as co-author in International Conference on **Advanced Trends in Engineering and Technology (ICATET) 2013** on 19-20 December 2013 at Arya College of Engineering & I.T., Jaipur.

7. Paper presentation as first author and won **"Best Presentation Award"** in 3rd International Conference on **Advance Trends in Engineering, Technology and Research (ICATET-2014)** on 23-24 December 2014 at Bal Krishna Institute of Technology, Kota.

8. Paper presentation as co-author in International Conference on **Advanced Trends in Engineering, Technology and Research (ICATET-2014)** on 23-24 December 2014 at Bal Krishna Institute of Technology, Kota.

9. An Abstract accepted for Oral Presentation and three other abstracts accepted for Poster Presentations at **World of Coal Ash Conference-2015** to be held in May at Nashville, Tennessee (U.S.).

In National Conferences/School-

1. Participated in a National Conference, **New Strategies for Reducing Carbon Foot Prints and Its Impact on Global Warming,** held on 20-21 August 2010 at RCEW, Jaipur.

2. Paper presentation in a National Conference, **Emerging Views In Advanced Chemistry** held on 17-19 December 2010 at Govt. College, Bhilwara.

3. Poster presentation in a National Conference, **National Symposium on Recent Advances in Chemical Sciences** held on 7-8 January 2011 at University of Kota, Kota.

4. Participated in **School on Analytical Chemistry-6** held on 13-20 May 2013 at BARC, Mumbai.

5. Participated in **National Seminar on Chemistry for Economic Growth and Human Comforts** held on 31 August 2013 at Department of Chemistry, University of Rajasthan, Jaipur.

6. Poster presentation in **National Conference on Frontiers in Physical, Chemical and Biological Sciences** held on 4-6 October 2013 at Department of Chemistry, University of Pune.

7. Participated **National Seminar on Socio Legal Issues and Challenges of Female Foeticide and Infanticide in India** on 4-5 October 2013 at University of Kota.

8. Participated in **5th National Academic Workshop on Organic Reaction Mechanisms & Analytical Techniques used in Chemical Sciences** held on 21-25 October 2013 at Department of Pure & Applied Chemistry, University of Kota, Kota.

9. Participated in **Symposium of E-Resources** on 16-17 December 2013 at Department of Library and Information Science, University of Kota.

10. Participated in **National Seminar on Environmental Issues and Social Concerns** held on 21-22 March at Department of Social Sciences, University of Kota, Kota.

DRIFT- Spectroscopic Study of Modification of Surface Morphology of Perlite During Thermal Activation

KEYWORDS | perlite, DRIFT, thermal activation.

Sakshi Kabra	Anita Sharma	Stuti Katara
Department of Pure and Applied Chemistry, University of Kota, Kota 324005, Rajasthan, India	Department of Pure and Applied Chemistry, University of Kota, Kota 324005, Rajasthan, India	Department of Pure and Applied Chemistry, University of Kota, Kota 324005, Rajasthan, India

Renu Hada	Ashu Rani
Department of Pure and Applied Chemistry, University of Kota, Kota 324005, Rajasthan, India	Department of Pure and Applied Chemistry, University of Kota, Kota 324005, Rajasthan, India

ABSTRACT *This article presents the use of diffuse reflectance infrared Fourier transform (DRIFT) spectroscopic technique in investigation of the effect of thermal activation on morphology of perlite. Perlite, a naturally occurring waste siliceous material formed by rapid cooling of volcanic eruptions was thermally treated over a range of temperatures. This study focuses on changes in both structure and chemical bonding of perlite due to thermal activation at different temperatures viz., 400, 600, 800, 1000°C for certain time period. The results reveal that on increasing temperature of thermal activation, loss of water occurs which is confirmed by decrease in intensity and broadness of the band, appears between 3600-3300 cm^{-1}, attributing to surface –OH groups. Other bands present in the DRIFT spectra shows the presence of Si-O-Si network and amorphous nature of silica in perlite.*

Introduction

Infrared spectroscopy is a well established technique for the identification of chemical compounds and/or specific functional groups in compounds. An alternative is the use of Fourier Transform Infrared Spectroscopy (FTIR), which is both rapid, non-destructive and requires small, <1 mg, sized samples. Chemical bonds vibrate at a characteristic frequency representative of their structure, bond angle and length. Accordingly, individual molecules have the ability to interact with incident radiation by absorbing the radiation at specific wavelengths. FTIR spectroscopy takes advantage of this by recording the energy absorption of a sample over a range of frequencies. Diffuse reflectance infrared Fourier transform (DRIFT) spectroscopy in conjunction with other analytical techniques has been extensively applied over the years to explore the structure and bonding in amorphous siliceous materials [1]. This technique has proved to be a powerful method to identify the isolated and H-bonded hydroxyl groups on surface of silica [2,3].

R.L. Frost et al. [4] proposed that DRIFT spectroscopy is more applicable than transmission infrared spectroscopy for powdered samples because it provides a rapid technique for analyzing samples without any interference through sample preparation, suitable for the study on the hydroxyl stretching region of silicate minerals. DRIFT has several other advantages including ease of sample preparation, greater number of useful bands and the ability to detect both major and minor components from the same spectra.

Perlite is a hydrated, naturally occurring amorphous volcanic glass formed by cooling of volcanic eruptions, estimating about 700 million tonnes worldwide reserves. Its unique structure consists of numerous concentric layers having SiO_2, Al_2O_3, K_2O and Na_2O as major constituents while TiO_2, CaO, MgO, Fe_2O_3 and hydrated water as well as unburned carbon remain present in varying quantities [5]. On heating the perlite to its softening range, i.e., above 850°C, water molecules vaporize and escape resulting in unusual expansion of perlite up to 7-16 times of its original volume,

creating inert, non-toxic, lightweight particles with specific surface area of about 1.22 m^2g^{-1} [6], density in the range of 0.6 - 2.30 gml^{-1} [7] and particle size in range of 0.2-4 mm. [8]. As far as applications of perlite are concerned, it is mainly consumed as fillers, filter aids, in producing building construction materials [9,10].

In the current work, perlite was thermally treated at different temperatures viz., 400, 600, 800 and 1000°C for 3 h and then analyzed by DRIFT spectroscopy. The purpose of this investigation is to use DRIFT spectroscopy to characterize the structure and determine the chemical bonding of silica with other species present in the perlite, so that it can be further utilized for various applications in future.

Material

Perlite sample was supplied by Indica Chem. Ind. Pvt. Ltd., India.

Experimental

Perlite sample was thermally treated in a muffle furnace under static conditions over a range of temperatures, 400, 600, 800 and 1000°C for 3h and abbreviated as TAP-400, TAP-600, TAP-800 and TAP-1000 respectively. The DRIFT spectroscopic study of the samples was done by Bruker FT-IR Spectrophotometer (TENSOR 27) in DRS (diffuse reflectance system) mode by homogenizing samples thoroughly with spectroscopic grade KBr in 1:20 weight ratio. The samples were crushed in an agate mortar. The spectra were recorded in the range 550-4000 cm^{-1} with a resolution of 4 cm^{-1}.

Results and discussion

The colour change is seen in perlite from light grey to white-light pink on thermal treatment at higher temperature. The chemical composition of perlite was determined by EDX analysis which is shown in Table 1. Loss on ignition (LOI) was determined by heating a certain weighed quantity of perlite in muffle furnace at 1000°C for 3 h. The LOI amount was 4.4 wt % which corresponds to the removal of moisture and coexisting unburned carbon from sample [11].

Table 1. EDX analysis of perlite.

Samples	O(wt%)	Si(wt%)	Al(wt%)	K(wt%)	Na(wt%)	Zn(wt%)	Fe(wt%)	Ti(wt%)	S(wt%)	LOI
Perlite	73.70	18.83	3.72	1.44	1.91	0.22	0.10	0.07	-	4.4

LOI- Loss on ignition

The FT-IR spectra of perlite and thermally activated perlite at different temperatures confirmed that the calcination at any conditions in this experiment produced dehydroxylation in the perlite samples i.e. elimination of the -OH stretching from Si-OH [12,13]. In this fig., a broad band between 3600-3300 cm^{-1} is shown, which is attributed to surface –OH groups of –Si-OH and water molecules adsorbed on the surface. The broadness of band indicates the existence of hydroxyl groups in higher degree of association with each other which results in extensive hydrogen bonding [14], while in FT-IR spectra of thermally activated perlite samples, the intensity and broadness of band is decreased, confirming the loss of water, which is highest in case of TAP-1000 (Fig. 1e). The strong band at 1030 cm^{-1} is due to the structural siloxane framework, which is the vibrational frequency of the Si-O-Si bond. The peak gets shifted to higher wave number, i.e., 1227 cm^{-1} after thermal treatment in TAP-1000 (fig. 1e), normally observed in amorphous silica samples [15]. An intense peak at 1632 cm^{-1} in the spectrum of perlite is attributed to bending mode (δ_{O-H}) of water molecule, which is again highly decreased in case of TAP-1000. The shoulder at about 3200 cm^{-1} (fig. 1a) could be assigned to the stretching vibrations of Si-OH groups in the structure of amorphous SiO$_2$ [16]. An intense band in the range of 1300-1100 cm^{-1}, corresponding to valence vibrations of the silicate oxygen skeleton is usually assigned to the amorphous silica content. The region around 805 cm^{-1} is characteristic of Si-O-Si symmetric stretching modes [17,18,19]. In the Si–O stretching vibration region (800–1195 cm^{-1}), the bands at 802, 808, 812, 942, 1050 cm^{-1} are identical to the bands at 800, 958, 1088 cm–1 due to amorphous silica [20]. Amorphous silica exhibited a relatively strong peak at about 800 cm^{-1} and it can be distinguished from the band of crystalline silicate [20]. The structure of most SiO$_2$ is polymorphous, both crystalline and amorphous, based on tetrahedral unit of silicon coordinated to four oxygen atoms. In the Si–O–Si bending vibration region (400–700 cm^{-1}) of quartz, the band at 695 cm^{-1} is determinative whether it is crystalline or amorphous [21]. The band at 695 cm^{-1} appears due to the vibrations in octahedral site symmetry [22]. In the amorphous state this band will be missing. In the perlite samples, we did not get this band which indicates that the silica mineral in this sample is in amorphous form. Another evidence of the presence of amorphous silica in perlite sample is the appearance of a peak at about 1100 cm^{-1}, which is normally assumed to be formed by continuous network of Q^4 species, characteristic in case of amorphous silica [23].

The major component of perlite is silica and untreated silica is totally hydroxylated and the hydroxyl layer is covered with physically adsorbed water. Thermal treatment of the support leads first to removal of water (dehydration) and then to combination of adjacent hydroxyl groups to form water (dehydroxylation) [24].

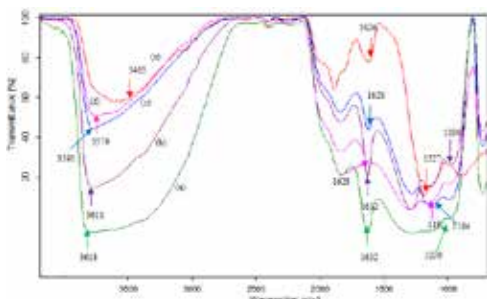Fig. 2 shows the magnified FT-IR spectra of all studied samples in the range between 550-1750 cm^{-1}.

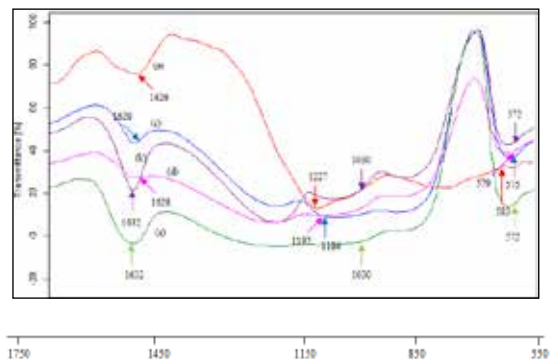**Fig 1. FT-IR spectrum of (a) perlite, (b) TAP-400, (c) TAP-600, (d) TAP-800 and (e) TAP-1000.**

Fig 2. Magnified FT-IR spectrum of (a) perlite (b) TAP-400 (c) TAP-600 (d) TAP-800 and (e) TAP-1000

The observed frequencies of IR bands of all samples and their possible assignments are summarized in Table 2.

Table 2. The observed frequencies of IR Bands of all samples and their possible assignments

Assignments	Perlite	Wave number (cm^{-1}) TAP-400	TAP-600	TAP-800	TAP-1000
Si-O-Si symm. stretching vib.	802	802	808	812	942
Si-O-Si asymm. stretching vib.	1030	1030	1184	1192 1192	1227
Si-O-Si bending vib.	572	572	575	579	583
-O-H bending vib.	1632	1632	1628	1628	1626 1626
-O-H stretching vib.	3618	3611	3591	3579	3465

Conclusions

Results found in this paper showed that DRIFT can be successfully employed in investigation of the effect of thermal treatment on perlite morphology. After calcination, physically adsorbed water gets driven away from the surface, so intensity of –OH stretching and bending bands decreases. The present spectroscopic study could be useful in understanding characteristic features of perlite, changes occurred in its structure and chemical bonding because of thermal treatment. This knowledge may be employed in further utilization of perlite for several applications.

REFERENCE 1. A. Hamoudi, L. Khouchaf, C. Depecker, B. Revel, L. Montagne and P. Cordier, J. Non-crystalline Solids, 354 (2008) 5074–78. | 2. R K.Iller, The Chemistry of Silica, John Wiley & Sons, New York, 1979. | 3. H. E. Bergna. In the colloid chemistry of silica (ed. H.E. Bergna), American Chemical Society, 1994. | 4. R. L. Frost, U. Johansson, Clays and Clay Minerals 46 (1998) 466. | 5. M. Dogan, M. Alkan, U. Cakir, J. Colloid Interface Sci. 192 (1997)114-118. | 6. M. Dogan, M. Alkan, Chemosphere, 50 (2003) 517-528. | 7. M. Roulia, K. Chassapis, J. A. Kapoutsis, E. I. Kamitsos, T. Savvidis, J. Mater. Sci., 41 (2006) 5870-81. | 8. D. Bastani, A.A. Safekordi, A. Alihosseini, V. Taghikhani, Sep. Purif. Technol., 52 (2006) 295-300. | 9. M.S. Morsy , S.S. Shebl, M. Abd El Gawad Saif, Building Research Journal, 56 (2008) 49-58. | 10. H. Aglan , M. Morsy, A. Allie, F. Fouad, Construction and Building Materials, 23(1) (2009) 138-145. | 11. K. Kordatos, S. Gavela, A. Ntziouni, K.N. Pistiolas, A. Kyritsi, V. Kasselouri-Rigopoulou, Microporous Mesoporous Mater., 115(1-2) (2008) 189-196. | 12. C. Belver, M.A.B Munoz and M.A.Vicente. Chem. Mater., 14 (2002) 2,033-43. | 13. R.A. Shawabkeh and M.F. Tutunji. Clay. Sci., 24 (2003) 111-120. | 14. R.M. Silverstein, F.X. Webster, Spectrometric Identification of Organic Compounds, Sixth ed., John Wiley Pub., 2006, pp. 88. | 15. F. Adam, S. Balakrishnan, P.L. Wong, Journal of Physical Science, 17(2) (2006) 1–13. | 16. S. Music, N.F. Vincekovic, L. Sekovanic, Brazilian Journal of Chemical Engineering, 28(1) (2011) 89-94. | 17. S.H. Javed, S. Naveed, N. Feroze, M. Zafar, M. Shafaq, Journal of Quality and Technology Management, 6(1) (2010) 81-90. | 18. K. Amutha, R. Ravibaskar, G. Sivakumar, International Journal of Nanotechnology and Applications, 4(1) (2010) 61-66. | 19. J.P. Nayak, J. Bera, Trans. Indian Ceram. Soc., 68 (2) (2009) 1-4. | 20. J. Ojima, J. Occup. Health 45 (2003) 94-103. | 21. G. Parthasarathy, A.C. Kunwar and R. Srinivasan, Eur. J. Mineral. 13 (2001) 127. | 22. H. Schneider, Contrib. Miner. Petr. 43 (1974) 233. | 23. F.I. Hurwitz, D.V. Aranda and M.E. Gallagher, Presented at the 236th National Meeting, American Chemical Society, Philadelphia, PA (2008) | 24. B.M. Reddy, G.K. Reddy, K.N. Rao, A. Khan, I. Ganesh, J. Mol. Catal. A: Chem., 265 (2007) 276-82.

Synthesis of Nanosized Titania by sol Gel Route

Renu Hada	Sakshi Kabra	Stuti Katara
Department of Pure and applied Chemistry, University of Kota, Kota (Raj), India	Department of Pure and applied Chemistry, University of Kota, Kota (Raj), India	Department of Pure and applied Chemistry, University of Kota, Kota (Raj), India
Ashu Rani	**Vijay Devra**	**S. S. Amritphale**
Department of Pure and applied Chemistry, University of Kota, Kota (Raj), India	Jankidevi Bajaj Government Girls College, Kota (Raj), India.	Advanced Materials & Processes Research Institute (CSIR), Hoshangabad Road, Bhopal (M.P), India.

ABSTRACT *The main objective of this work was to prepare anti-pollutant and photocatalyst. Titanium dioxide nanoparticles by simple ethylene glycol route to synthesize titanium dioxide nanoparticles at industrial level. In this work TiO2 was prepared by sol-gel route in presence of titanium n-butoxide (TNBT) as TiO2 precursor, n-butanol as dilutant and EG as solvent and chelating agent. The X-ray diffraction and scanning electron microscopy studies show that the product has anatase crystal structure with average particle size 20-50 nm. The nanoparticles thus prepared can be used for gas sensing and biological applications, also as photo-electrodes for dye-sensitized solar cells and in removing the organic chemicals which occur as pollutants in wastewater effluents from industrial and domestic sources.*

Introduction

Nanosized titania has been the subject of a great deal of research because of their unique physicochemical properties and applications in the areas of pigments, catalysts and supports, cosmetics, gas sensors, inorganic membranes, environmental purification, and dielectric materials [1-9]. Much interest has been shown in photochemical reactions on nanosized titania particles due to their potential application in the conversion of solar energy into chemical energy [10-13] and electric energy [14, 15]. When titania powder is irradiated with photon energy larger than the band-gap energy, electrons (e-) and holes (h+) are generated in the conduction band and the valence band, respectively. These electrons and holes are thought to have the respective abilities to reduce and oxidize chemical species adsorbed on the surfaces of titania particles [16]. The uses and performance for a given application are, however, strongly influenced by the crystalline structure, the morphology, and the size of the particles. It is well known that titania exists in three kinds of crystal structures namely anatase, rutile and brookite. Anatase and brookite phases are thermodynamically metastable and can be transformed exothermally and irreversibly to the rutile phase at higher temperatures. The transition temperatures reported in the literature ranges from 450 to 1200 0C. The transformation temperature depends on the nature and structure of the precursor and the preparation conditions [17, 18]. Among the three kinds of crystal structures of Titania, anatase TiO2 has been widely used as a well known catalyst, because of its various merits, such as electronic and optical properties, non-toxicity, high photocatalytic activity, low cost, and chemical stability [19-23]. A number of methods for the synthesis of TiO2 nanoparticle have been reported, such as chemical precipitation [24], microemulsion [25], hydrothermal crystallization [26] and sol-gel [27]. The sol-gel process is the most successful for preparing nanosized metal oxide semiconductors. For example, sol-gel derived TiO2 powders have been reported to show high catalytic activity due to their fine structure, wide surface area and high porosity. Thus in this research work we have prepared titania by sol gel route using ethylene glycol as gelling agent and titanium n-butoxide as titania precursor.

Experimental Work

Titanium (IV)-n-butoxide (TNBT) (20 g) was added to n-butanol (16 g) and the mixture was stirred for 5 min using a magnetic stirrer operating at 2000 rpm. After stirring, above mixture was added to Ethylene glycol (100 ml) and mixture was stirred with heating at 850 C till sol converted to gel then gel was dried in oven at 500 C. Dried sample was calcined at 5000 C for 3 h.

Results and discussion

The XRD pattern and SEM image of nanosized Titanium Oxide particles, prepared by EG route is shown in figure 1 and 2.
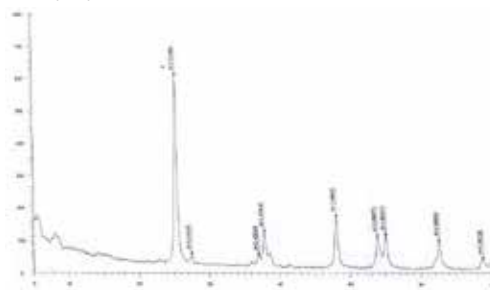

Figure 1. XRD patterns of nanosized titania obtained from sol gel route at 500 0C
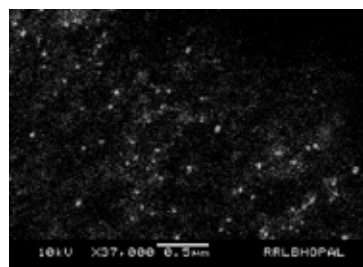

Figure 2. SEM photograph of nanosized titania obtained from sol gel route at 500 0C

The XRD patterns of the calcined sample of nanosized titania powder prepared using sol gel route is given in Figure 1. The presence of peaks of anatase titania at 'd' values 3.49, 1.88, 2.35 have been observed in XRD pattern. The d-values of the pattern recorded were compared and matched with the standard d-values along with the intensity given in JCPDS manuals. The average crystalline size of nanosized titania has been calculated by applying Scherrer's equation (d = k / cos) to the 100 % intensity peak and is found 19 nm. The prepared nanosized powder of TiO2 was fired at 500 0C, leads to its conversion from amorphous phase to anatase phase.

The crystal size of the powder sample of TiO2 is of 19 nm size as estimated by Scherrer equation. SEM photograph shows that particles are strongly aggregated which is typical for particles with a size less than 50 nm, so the particle size was estimated to be 20-50 nm.

Conclusion

We synthesized TiO2 nanoparticles by sol gel route using ethylene glycol as geling agent. The physical properties, such as crystallite size and crystallinity were investigated by XRD, and SEM. X-ray diffraction pattern shows that TiO2 particles calcined at 500°C have a stable anatase phase with 19 nm average crystallite size, determined according to the Scherrer equation. The SEM image shows that particles have spherical shape. The yield of the prepared photocatalyst was comparatively higher than other methods used for nanoparticles preparation i.e. microemulsion route.

Acknowledgement

REFERENCE 1. T. Moritz, J. Reiss, K. Diesner, D. Su and A. Chemseddine, J. Phys. Chem. B, 1997 101, 8052-8053. | 2. J. Karch, R. Birriger and H. Gleiter, Nature, 1987, 330, 556-558. | 3. M. R. Hoffmann, S. T. Martin, W. Choi and D. W. Bahnemann, Chem. Rev., 1995, 95, 69-96. | 4. A. Fujishima and K. Honda, Nature, 1972, 238, 37-38. | 5. M. A. Fox and M. T. Dulay, Chem. Rev., 1993, 93, 341-357. | 6. R. J. Gonzalez, R. Zallen and H. Berger, Phys. Rev. B, 1997, 55, 7014-7017. | 7. K.-N. P. Kumar, K. Keizer and A. J. Burggraaf, J. Mater. Chem., 1993, 3, 1141 - 1149. | 8. R.Wang, K. Hashimoto, A. Fujishima, M. Chikuni, E. Kojima, A. Kitamura, M. Shimohigoshi and T. Watanabe, Nature, 1997, 388, 431-443. | 9. P. A.Mandelbaum, A. E. Regazzoni, M. A. Blesa and S. A. Bilmes, J. Phys. Chem. B, 1999, 103, 5505-5511. | 10. K. Fujiwara, T. Ohno, M. Matsumura, J. Chem. Soc., Faraday Trans., 1998, 94, 3705- 3709. | 11. T. Ohno, K. Fujihara, K. Sarukawa, F. Tanigawa, M. Matsumura, Z. Phys. Chem., 1999, 213, 165-174. | 12. Z.G. Zou, H. Arakawa, J. Photochem. Photobiol. A: Chem., 2003, 158, 145-162. | 13. R. Abe, K. Sayama, H. Arakawa, Chem. Phys. Lett., 2003, 371, 360-364. | 14. J. Ye, Z. Zou, H. Arakawa, M. Oshikiri, M. Shimoda, A. Matsushita, T. Shishido, J. Photochem. Photobiol. A: Chem., 2002, 148, 79-83. | 15. B. O'Regan, M. Gr̈atzel, Nature, 1991, 353, 737-740. | 16. S. Kambe, S. Nakade, T. Kitamura, Y. Wada, S. Yanagida, J. Phys. Chem. B, 2002, 106, 2967- 2972. | 17. H. Goto, Y. Hanada, T. Ohno, M. Matshmura, J. Catal., 2004, 225, 223-229. | 18. V. Chhabra, V. Pillai, B.K. Mishra, A. Morrone, D.O. Shah, Langmuir, 1995, 11, 3307- 3311. | 19. A. Rammal, F. Brisach and M. Henry, C. R. Chimie, 2002, 5, 59-66. | 20. P.V. Kamat, Chem. Rev., 1999, 93, 267-300. | 21. A. Mills, G. Hill, S. Bhopal, I.P.Parkin and S.A. O'Neill, J. Photochem. Photobiol. A: | Chemistry, 2003, 160, 185-194. | 22. P.S. Awati, S.V. Awate, P.P. Shah and V. Ramaswamy, Catal. Comm, 2003, 4, 393-400. | 23. R. Zhang, L. Gao and Q. Zhang, Chemosphere,2004, 54, 405-411. | 24. S. Jeon and P.V. Braun, Chem. Mater., 2003, 15, 1256-1263. | 25. Y. Bessekhouad, D. Robert and J.W. Veber, J. Photochem. Photobiol. A: Chemistry, 2003, 157, 47- 53. | 26. M.M. Yusuf, H. Imai and H. Hirashima, J. Sol-Gel Sci. Technol., 2002, 25, 65-74. | 27. Y. Diaoued, S. Badilescu, P.V. Ashirt, D. Bersani, P.P. Lottici and J. Robichaud, J. Sol- | Gel Sci.Technol., 2002, 24, 255-264.

Acid Activated fly Ash, as a Novel Solid Acid Catalyst for Esterification of Acetic Acid

Anita Sharma	Stuti Katara
Department of Pure and Applied Chemistry, University of Kota-324005, Rajasthan, India	Department of Pure and Applied Chemistry, University of Kota-324005, Rajasthan, India
Sakshi Kabra	**Ashu Rani**
Department of Pure and Applied Chemistry, University of Kota-324005, Rajasthan, India	Department of Pure and Applied Chemistry, University of Kota-324005, Rajasthan, India

ABSTRACT *An efficient solid acid catalyst (AAFA) has been synthesized by mechanical and thermal activation of F-type fly ash (SiO_2 and Al_2O_3 >70%) followed by chemical activation using concentrated HCl at 110°C. The activation of fly ash resulted in increased silica content (79%) and surface area (5.42 m^2/g) having sufficient silanol activity for esterification of n-butanol and acetic acid. The catalyst was characterized by XRD, FT-IR, and SEM techniques. The product n-butyl acetate is an important fine chemical intermediate, widely used in pharmaceutical and as flavoring agent in confectionary. The catalyst was completely recyclable without significant loss in activity up to five reaction cycles, which confers its stability during reaction. The work reports an innovative use of solid waste fly ash as an effective solid acid catalyst.*

1. Introduction

Acid catalyzed esterification is one of the most important industrial reactions, which are widely employed in synthetic organic process industries. Generally n-butyl esters of acetic acid are prepared under liquid phase, refluxing the reactant in the presence of small amount of concentrated H_2SO_4, HCl, HI, $AlCl_3$, BF_3, $ZnCl_2$, SbF_5 phosphoric acid and p-toluenesulfonic acid as the catalyst in homogenous systems [1]. The use of the above mentioned catalysts is undesirable from the environmental point of view as these chemicals are corrosive and generally encounter the problems of handling and transportation. Moreover reusability of the catalysts cannot be expected. For this purpose, the solid acid catalysts are employed as safe alternatives for conventional liquid acid catalysts in synthetic organic chemistry. Solid acids such as zeolites (ZSM-5), Metal oxides viz. Al_2O_3, SiO_2, ZrO_2 ZrO_2–Al_2O_3, ZrO_2–SiO_2 and their sulphated forms have been extensively studied as possible alternatives to conventional Lewis/Bronsted acid catalysts for esterification reaction [2,3].

A number of solid acids such as ion exchange resin eg. Amberlyst 15, smopex-101 [4,5] , mesoporous molecular sieves like mesoporous Al-MCM-41, H-Mordenite [6] , H-beta [7] , H-ZSM-5 and HY zeolites [8,9] , solid super acids [10] and heteropolyacids (salts), lipase, sulfonic acids supported on molecular sieves, active carbon [11-13] , niobic acid and supported heteropoly acids (eg. $H_4SiW_{12}O_{40}$/ $ZrO2$), -alumina-supported vanadium oxide catalysts, sulfated zirconia and tetravalent metals acid salts [14] , hafnium (IV) and zirconium (IV) salts [15] , $Zr(SO_4)_2.4H_2$[16] and modified zirconia catalyst have also been found to be acidic in nature and catalyze esterification, alkylation and condensation reactions [17,18]. In our previous work, fly ash has been used for developing several solid acid catalysts by loading cerium triflate, sulphated zirconia and used for the synthesis of aspirin, oil of wintergreen, 3, 4-dimethoxyacetophenone (anti neoplastic) and diphenylmethane [19-21].

The present work elaborates the synthesis of AAFA catalyst to have high acidity and catalytic activity for esterification reaction to produce n-butyl acetate with high yield and purity up to five reaction cycles. This investigation brings into light the structural aspects of a solid acid which exhibit good conversion and yield of an industrially important chemical "n-butyl acetate" an important chemical intermediate, widely used in pharmaceutical and as flavoring agent in confectionary, under solvent free conditions and in low cost route.

2. Experimental methods
2.1 Materials

Class-F type fly ash was collected from Kota Thermal Power Plant, Kota (Rajasthan) HCl (98%); Acetic acid (98%) and n-butanol (99%) were purchased from S. D. Fine Chem. Ltd. and used as such.

2.2 Catalyst Synthesis

As received fly ash was ball milled (1h at room temperature) followed by thermal activation at 900°C for 4h .The chemical activation of mechanically activated fly ash (MFA) was carried out in a stirred reactor by stirring 5M aqueous solution of mineral acid (HCl) in the ratio of 1:2 (FA: HCl) for 5 days at 110°C temperature followed by washing till pH 7.0 with complete removal of soluble ionic species (Cl^-, NO_3^-, SO_4^{2-}, ClO^{4-} etc.) and drying at 110°C for 24h. The obtained solid acid catalyst (AAFA) was calcined at 500°C for 4h under static conditions in a muffle furnace.

2.3 Characterization Techniques
2.3.1. Physicochemical properties of AAFA

The silica content of the fly ash samples after mechano-chemical activations were analyzed by X-ray fluorescence spectrometer (Philips PW1606). Powder X-ray diffraction studies were carried out by using (Philips X'pert) analytical diffractometer with monochromatic CuKα radiation (k = 1.54056 Å) in a 2θ range of 0-80°. The FT-IR study of the samples was done using FT-IR spectrophotometer (Tensor-27, Bruker, Germany) in DRS (Diffuse Reflectance Spectroscopy) system. The detailed imaging information about the morphology and surface texture of the sample was provided by SEM-EDAX (Philips XL30 ESEM TMP).

2.3.2. Catalytic activity

The esterification of n-butanol with acetic acid was performed in liquid phase batch reactor consisting of 50 ml round bottom flask with condenser in a constant temperature oil bath with magnetic stirring. A mixture of acetic acid and n-butanol (molar ratio of n-butanol and acetic acid is = 1:2) was taken in a 50 ml round bottom flask. The catalyst (sub-

strate to catalyst ratio = 10), activated at 500°C for 2h was added in the reaction mixture. After completion of the reaction the catalyst was filtered and the product was analyzed by Gas Chromatograph.

2.3.3 Catalyst regeneration

The spent catalyst was washed with acetone, dried in oven at 110°C for 12h followed by calcinations at 500°C for 2 h and reused for next reaction cycle under similar reaction conditions as earlier.

3. Results and Discussion
3.1 Catalyst Characterization

A comparison of FA, MFA, TFA and AAFA catalyst is given in Table 1, which shows that after mechanical activation BET surface area is increased from 0.97 m^2/g to 2.57 m^2/g, which is further increased to 5.42 m^2/g after chemical activation. This result confirms that the AAFA catalyst has a higher specific surface area of 5.42 m /g than the heat-treated fly ash with 2.99 m^2/g [22, 23]. The particle diameter is reduced from 37.7 µm to 3.12 µm during milling, increased slightly (3.71 µm) after chemical activation [24]. The mechanical activation did not indicate any perceptible change in silica content of fly ash but the chemical activation increased the silica amount greatly (58% to 79%) [25].

Table 1: Physico-chemical properties of FA, MFA, TFA and AAFA catalyst.

Catalyst	Silica (Wt %)	Crystallite size (nm)	BET surface area (m²/g)	Particle diameter (µm)
FA	58	33	0.97	37.7
MFA	59	21	2.57	3.12
TFA	70	18	2.99	3.10
AAFA	79	16	5.42	3.71

FA (Fly ash); MFA (mechanically activated fly ash); TAFA (thermally activated fly ash) and AAFA (chemically activated fly ash).

The XRD pattern of the FA showed (figure 1a) the presences of quartz, mullite, iron oxide, hematite, sulfur oxide, small amounts of magnetite [26], CaO and amorphous phases. The XRD studies of milled fly ash (figure 1b) indicate that decrease in crystallite size from 33 to 21 nm results in increased amorphous content in it but after thermal activation the crystallinity is increased slightly as indicated by higher peak intensities in Figure 1b and c. [27]. After chemical activation of thermally activated fly ash, the crystallinity is further decreased due to removal of most of the crystalline components present in FA, thus increasing the amorphous nature [28, 29].
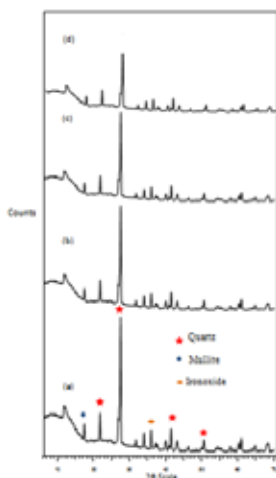

Figure 1: X-ray diffraction pattern of (a) FA (b) MFA (c) TFA and (d) AAFA catalyst.
The FT-IR spectra of FA, MFA, TFA and AAFA in Figure2a-d

show broad band between 3500-3000 cm^{-1}, which is attributed to surface -OH groups of Si-OH and adsorbed water molecules on the surface. The increment in broadness after ball milling is an evidence for the breaking down of the quartz structure and formation of Si-OH groups [30]. However, FT-IR studies clearly show changes in the broadening of IR peaks corresponding to Si-O-Si asymmetric stretching vibrations indicating structural rearrangement during mechanical milling.

The FT-IR spectra of AAFA shows the tremendous increment in broadness at 3500-3000 cm^{-1} region as compared with FA, MFA and TFA which reflects strong hydrogen bonding between the hydroxyl groups due to increase in silica content and loss of significant amount of other components (Figure 2d). The increased amorphous silica in the activated fly ash can be characterized by an intense band in the range 1000-1300 cm^{-1} corresponding to the valence vibrations of the silicate oxygen skeleton. The main absorption band of the valence oscillations of the groups Si-O-Si in quartz appears with a main absorption maximum at 1162 cm^{-1} [20].
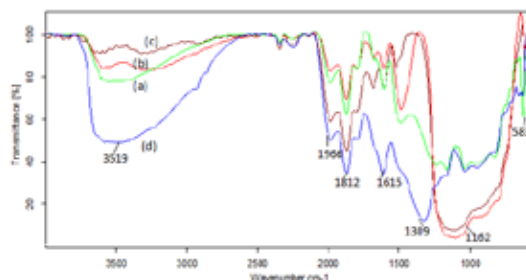

Figure 2: FT-IR of (a) FA (b) MFA (c) TFA and (d) AAFA catalyst.

SEM micrograph of the FA (Figure 3a) indicates that the most of the particles present in the fly ash are micro-particles in the shape of smooth balls (microspheres) with a relatively smooth surface grain. SEM image of MFA (Figure 3b) shows the structural break down of larger particles and increased surface roughness. The smooth spherical cenospheres are affected most resulting remarkable changes in morphology. After chemical activation with acid, rough cenospheres are transformed into agglomerations of more amorphous undefined shapes with no observation of crystal formation as seen in SEM micrographs presented in Figure 3a-d [31].
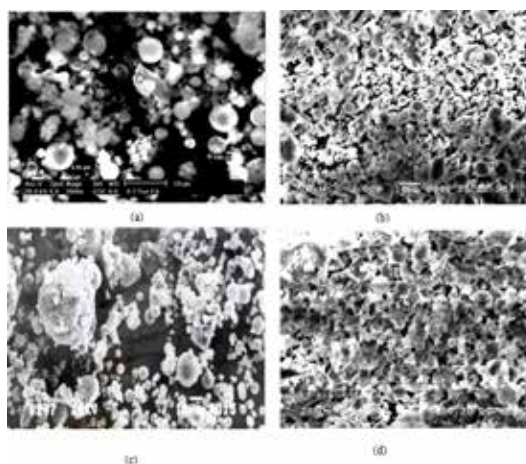

Figure 3: SEM images of (a) FA (b) MFA (c) TFA (d) AAFA.

4. Catalytic performance

To measure the catalytic performance of catalyst, esterification of acetic acid with n-butanol over AAFA was carried out at 110°C for 4h, taking n-butanol/acetic acid molar ratio 1:2 and n-butanol to catalyst weight ratio of 10. The catalyst AAFA was found highly active for esterification of acetic acid

with n-butanol giving high selectivity (99.6%) and yield of n-butyl acetate after 4h under optimized conditions, whereas both FA as well as MFA did not possess any catalytic activity.

The esterification of acetic acid with n-butanol was also carried out at different temperature ranging from 90°C to 130°C for 4h to optimize the reaction temperature giving maximum conversion of n-butanol to n-butyl acetate. The result shows that the maximum conversion (87.3%) of n-butanol to n-butyl acetate is found at 110°C, which remains almost, steady till 130°C.The spent catalyst from the reaction mixture was filtered, washed with acetone and regenerated at 450°C to use for the next reaction cycles. The catalyst was equally efficient up to five reaction cycles.

5. Conclusion
The study provides fly ash supported AAFA as an efficient solid acid catalyst possessing significant amount of acidity. The specific surface area of FA (0.97 m²/g) was greatly enhanced after mechanical, thermal and chemical activation using HCl. AAFA catalyst possessed surface area upto 5.42 m²/g with greater number of surface silanols responsible for surface acidity as evident by comparatively broad band at 3500-3000 cm⁻¹ in FT-IR spectra.

AAFA catalyst catalyzed the esterification of acetic acid with n-butanol giving high yield of the product n-butyl acetate in heterogeneous, solvent free optimized reaction conditions. It is concluded that the mechno-chemical activation can generate sufficient activity on fly ash surface rendering its potential application in heterogeneous catalysis.

REFERENCE 1. Igbokwe,P.K., Ugonabo, V.I., Iwegbu, N.A., Akachukwu, P.C. and Olisa C.J., Journal of university of chemical technology and metallurgy, 43(3) (2008) 345-348. | 2. Kuriakose, G., Nagaraju, N., J. Mol. Cat. A: Chem. 223 (2004) 155-159. | 3. Mohamed Shamshuddin, S.Z., Nagaraju, N., Cat. Comm., 7(2006) 593-599. | 4. Blagova, S., Paradaa, S., Bailerb, O., Moritzb, P., Lamc, D., Weinandd, R., Hassea, H., Chem. Eng. Sci. 61 (2006) 753-765. | 5. Zhang, Y., Ma L., Yang J., React. Funct. Polym. 6 (2004) 101-114. | 6. Mbaraka, I.K., Shanks, B.H J., Cat., 229 (2005) 365-373. | 7. Alvaro, M., Corma, A., Das D., Fornés, V, Garcia, H., J. Cat., 231 (2005) 48-55. | 8. Kirumakki, S.R., Nagaraju, N., Narayanan, S., Appl.Catal. A. 273 (2004)1-9. | 9. Rabindran,B., Jermy,A., Journal of Molecular Catalysis A: Chemical 237 (2005) 146–154. | 10. Jiang, Y.X., Chen, X.M., Mo Y.F., Tong, Z.F., J. Mol. Cat. A. Chem., 213 (2004) 231-234. | 11. Abd, E.l.,_Wahab ,M.M.M., Said A.A., J. Mol. Catal. A. Chem, 240 (2005) 109-118. | 12. Sepulveda, J.H., Yori J.C., Vera C.R., Appl. Catal. A, 288 (2005)18-24. | 13. Peres, C., Harper, N., Marco, D.R., da Silva, G., Bar reiros, S., Enz. Micro. Tech. 37(1) (2005) 145-149. | 14. Mitran, G., Makó ,E., Redey, A., Marcu, I. C .,Comptes Rendus Chimie, 15(9) (2012) 793–798. | 15. Ishihara, K., Nakayama, M., Ohara, S., Yamamoto, H., Tetrahedron, 58 (2002) 8179-8188. | 16. Juan, J.C., Zhang, J.C., Yarmo, M.A., Cat. Lett. 117 (2007)153-158. | 17. Patel, H.K., Joshi, R.S., Chudasama, U.V., Indian J. Chem. 47 (2008) 348-352. | 18. Dora, E., James, G., Goodwin, Jr., David, A., Appl. Catal. A: Gen. 339 (2008) 76-83. | 19. Khatri, C., Jain, D., Rani, A., Fuel, 89(2012)3853-3859. | 20. Khatri, C., Mishra M., Rani, A., Fuel Process. Technol., 91(10) (2010) 1288-1295. | 21. Khatri, C., Rani, A., Fuel 87 (2008)2886-2892. | 22. Sarbak Z., Kramer-Wachowiak M., Powder Technol, 123 (2002)53–8. | 23. Penilla PR, Bustos AG, Elizalde SG. Fuel 85 (2006) 823–32. | 24. Kumar S., Kumar R., (2010) The University of Wisconsin Milwaukee Centre for By-products Utilisation, Second International Conference on Sustainable Construction Materials and Technologies. June 28- June 30. | 25. Blanco F, Garcia MP, Ayala J., Fuel 84 (2005) 89-96. | 26. Bada S.O., Potgieter-Vermaak S,. J. Prac. Technol. 12 (2008) 37-48. | 27. John M.F., (2005), Changes in fly ash with thermal treatment. World of Coal Ash (WOCA), April 11-15; Kentucky, USA. | 28. Blanco F., Garcia M.P., Ayala J.,Mayoral G.,Garcia M.A.,Fuel, 85 (2006)2018-2026. | 29. Pengthamkeerati P., Satapanajaru T., Chularuengoaksorn P., Fuel, 87 (2008) 2469–2476. | 30. Patil, G.A., Anandhan, S., International. J. Energy Eng., 2 (2012) 57-62. | 31. Woolard, C.D., Petrus, K., van der Horst, M. Water SA, 26 (2002)531–6. |

Surface Modification of Fly Ash by Thermal Activation: A DR/FTIR Study

Stuti Katara[1], Sakshi Kabra[1], Anita Sharma[1], Renu Hada[1]
and Ashu Rani[1*]

[1]*Department of Pure and Applied Chemistry, University of Kota, Kota, Rajasthan, India.*

Authors' contributions

This work was carried out in collaboration between all authors. Authors SK and AR supervised and designed the study. Author SK (Stuti Katara) performed the experimental and analytical study, wrote the protocol, and wrote the first draft of the manuscript. Authors SK, AS and RH managed the literature searches and helped in analytical study. All authors read and approved the final manuscript.

Research Article

ABSTRACT

To acquire a deeper understanding of surface chemistry of fly ash along with thermal activation, the states of mineral phases, water and –OH groups on silica are studied in fly ash at different calcination temperatures by DR/FTIR spectroscopic technique. DR/FTIR spectroscopy allows differentiation of various types of bonds in a material on a molecular level. The spectroscopic results are also supported by XRF, XRD and SEM analysis. Studied fly ash was collected from Jamshedpur Thermal Power Station as an extremely fine ash, formed from the inorganic components of the coal, mainly silica and alumina which remain after combustion of the carbonaceous part of the coal. Distinguish changes were observed in fly ash IR bands regarding absorbed water, -OH group and Si-O-Si group with thermal activation. This investigation reveals that as the temperature increases, the physically adsorbed water begins to remove first, then silanol groups on surface is dehydrated. Increased temperature causes formation of different crystalline phases like quartz, mullite and hematite etc. and increased the crystallinity of the calcined samples.

---

*Corresponding author: Email: ashu.uok@gmail.com;

1. INTRODUCTION

The coal fired power plant which consumes pulverized solid fuels composed of combustible organic matter with varying amount of inorganic mineral parts produce large amount of solid waste fly ash. Every year a crude estimation of 600 million tons of fly ash generated worldwide [1] and about 110 million tons only in India [2]. The combustible gasification takes place in coal fired boiler at an operative temperature 1450ºC under reducing atmosphere. The mixture of effluent gases is cooled and fly ash gets solidify at temperature from 950ºC to 400ºC. In the form of spherical particles consisting of SiO_2 , Al_2O_3, Fe_2O_3, CaO, MgO and alkali in varying amounts with some unburned activated carbon [3]. As per the ASTM C618-12a guideline [4] the fly ash containing >70% SiO_2, Al_2O_3 and Fe_2O_3 is classified as Class F type fly ash and those consists mainly of silica, alumina and calcium containing SiO_2, Al_2O_3 and Fe_2O_3 minimum upto 50 % are referred to as Class C fly ash. Class F type fly ash is used in agriculture, metal recovery, water and atmospheric pollution control [5] while class C type fly ash is used in cement production [6], steam cured bricks manufacturing [7] etc. Calcination temperature of fly ash before using as source material for synthesis of concrete material and geopolymer etc. is reported to be crucial for the end product [8]. Fly ash has a complex microstructure comprising of mixture of amorphous and crystalline components. The chemical and mineralogical compositions of fly ash vary with coal source as well as calcination temperature [9]. Fly ash also contains different amount of unburned carbon which may reach upto 17% [10] responsible for high ignition loss and undesirable constituents for geopolymerisation and concrete formation. Fly ash is also being used as heterogeneous catalytic support material due to high silica, surface mineralogy, morphology and surface silanol groups [11, 12]. Both the adsorbed water and silanol groups on surface may affect the surface modification process thus play important roles in catalytic application on silica surface. It is difficult to distinguish between the adsorbed moisture and actual surface hydroxyl groups in a form of crystalline water or amorphous silanol (Si-OH) [13]. Literature reports that high temperature calcination forms new crystalline phases on fly ash surface modifying siloxane groups (Si-O-Si) and different forms of silanol groups [8]. Therefore it is of interest to understand the modification of fly ash mineralogy and morphology with thermal activation by using Diffuse Reflectance Fourier Transform Infrared (DR\FTIR) spectroscopic technique, which is one of the advance techniques to illustrate the chemical structure of the bonding materials. The results of the DR\FTIR study are supported by other characterization tools such as X-ray Fluorescence (XRF), X-ray Diffraction (XRD) and Scanning Electron Microscopy (SEM).

2. EXPERIMENTAL DETAILS

2.1 Materials

The coal fly ash (Class F type with SiO_2 and Al_2O_3 > 70%) used in this study was collected from Jamshedpur Thermal Power Station (Jamshedpur, Jharkhand, India). Fly ash (FA) was thermally activated by calcining in muffle furnace at 400, 600, 800 and 1000ºC for 3h and abbreviated as TFA-400, TFA-600, TFA-800 and TFA-1000 respectively (TFA –Thermally activated fly ash).

2.2 Sample Preparation and Characterization

DR/FTIR analysis of fly ash samples were carried out by diluting fly ash samples with KBr in 1:20 weight ratio and mixed gently with the help of mortar and pestle, being careful about atmospheric moisture absorption. In this study, FTIR spectra of the materials were recorded using FTIR Tensor 27 Brucker with DR (Diffuse Reflectance) accessory. The spectra were recorded in the range 550 – 4000 cm^{-1} with a resolution of 4 cm^{-1}. The chemical composition was determined by wavelength dispersive X-ray fluorescence (WD-XRF) model Bruker S8 Tiger. The detailed imaging information about the morphology and surface texture of the sample was provided by SEM (Philips XL30 ESEM TMP). The XRD measurements were carried out using Bruker D8 Advance X-ray diffractometer with monochromatic CuKα radiation (λ = 1.54056 Å) in a 2θ range of 5-70º.

3. RESULTS AND DISCUSSION

The chemical composition of FA and all TFA samples reveals that major components of fly ash are SiO_2 and Al_2O_3. Some minor components like Fe_2O_3, CaO, MgO, TiO_2, Na_2O, K_2O and trace elements around 1.5 wt% are also present in FA and all TFA samples (Table 1). The thermal activation of fly ash removes C, S, moisture and other adsorbed gases. The removal of moisture and co-existing unburned carbon increases with increasing temperature [14]. It can be concluded that all the compounds remained almost constant after thermal treatment, besides a reduction in Na_2O, K_2O and other elements in all TFA samples.

Table 1. Chemical composition of FA and all TFA samples

Sample	SiO_2 (wt%)	Al_2O_3 (wt%)	Fe_2O_3 (wt%)	CaO (wt%)	MgO (wt%)	TiO_2 (wt%)	Na_2O (wt%)	K_2O (wt%)	Other elements (wt%)
FA	62	30	3.0	0.4	0.3	1.4	0.4	0.8	1.7
TFA-400	62.3	30	3.2	0.4	0.3	1.4	0.3	0.5	1.6
TFA-600	62.5	30.1	3.2	0.3	0.3	1.4	0.3	0.3	1.6
TFA-800	62.8	30.3	3.2	0.3	0.2	1.3	0.2	0.2	1.5
TFA-1000	63	30.5	3.2	0.3	0.2	1.3	0.2	0.1	1.2

The FTIR spectra in Fig. 1 shows a broad band between 3400-3000 cm^{-1}, which is attributed to surface –OH groups of silanol groups (-Si-OH) and adsorbed water molecules on the surface. The broadness of band indicates the presence of strong hydrogen bonding [11]. The gradual decrement in the intensity and broadness in this band, as shown in Fig. 1 confirms loss of water in all TFA samples during thermal activation. Most of the molecular water gets removed from the sample by heating up to 250ºC, while crystalline –OH remains in the sample till 700ºC [15]. A peak around 1607 cm^{-1} (Fig. 1) is attributed to bending mode (δO-H) of water molecule [16] which is shown in all fly ash samples. A broad band ranging from 1070 cm^{-1} to 1170 cm^{-1} due to Si–O–Si asymmetric stretching vibrations [17] of silica is present in FA and all TFA samples. FA shows Si–O–Si asymmetric stretching vibration centered at 1100 cm^{-1} which get shifted towards higher wave number at 1162 cm^{-1} in case of TFA-1000. This high wave number shift is the result of loss of water thus transformation of Q^3 units [Si (OH) $(SiO_4)_3$]   to Q^4 units [Si $(SiO_4)_4$] thus decrease in silanol groups (-Si-OH). This phenomenon shows reverse accordance with the statement that an increase in the hydroxide concentration shifts the position of the maximum absorbance of Si-O bands toward lower number, indicating the transformation of Q^4 units [Si $(SiO_4)_4$] to Q^3 units [Si(OH)

$(SiO_4)_3$] [18]. Peak at 2887 cm^{-1} could be assigned to C-H stretching vibration of organic contaminants which may be introduced during sample handling or some hydrocarbon present in fly ash [17.] This peak shows high intensity in FA while on thermal activation organic contaminants get removed from FA and show low intense peak in all TFA samples as compared to FA. Peaks appeared around 2343 cm^{-1} attributed to v O-H stretching [19], 2241 cm^{-1} responsible for H-SiO$_3$ [20], 1984 cm^{-1} due to =Si-H monohydride [21], 1872 cm^{-1} due to calcium carbonate [22] present in FA and all TFA samples (Table 2). Peaks centered at 1521 cm^{-1} [23] and 1681 cm^{-1} [17] are due to $(CO_3)^{2-}$ stretching vibration show highest intensity in FA, which is reduced on thermal activation in all TFA samples conferring that during thermal activation C and C associated impurities like CO$_2$ are removed with increased temperature. A peak related to Al-O-Si stretching vibration appears around 600 cm^{-1} [24] and is present in FA and all TFA samples (Table 2) conferring that Si and Al are present in silico aluminate phase not affected by thermal activation [25].
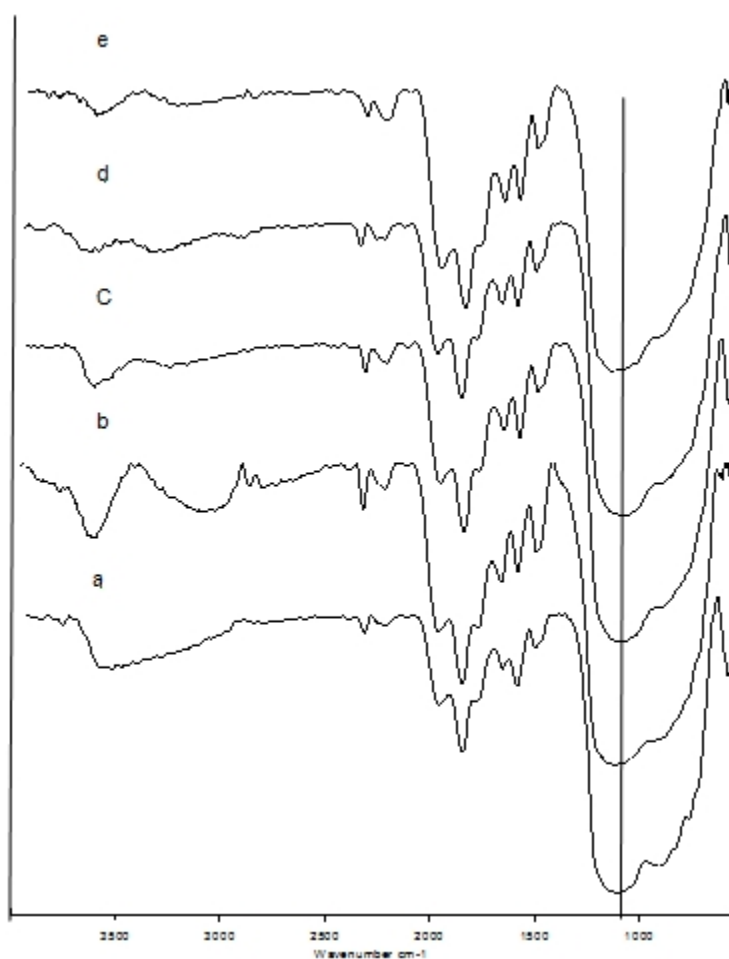

**Fig. 1. DR/FTIR spectra of (a) FA (b) TFA-400 (c) TFA-600 (d) TFA-800 (e) TFA-1000
Table 2. Different DR/FTIR observed frequencies of (1.) FA (2.) TFA-400 (3.) TFA-600
(4.) TFA-800 (5.) TFA-1000 and their possible assignments**

Assignments	FA	TFA-400	TFA-600	TFA-800	TFA-1000	Reference no.
Si-O-Al stretching vibration	600	611	589	592	603	24
Si-O-Si asymm. Stretching Vibration	1100	1102	1113	1148	1162	17
$(CO_3)^{2-}$ –stretching vibration	1521, 1679	1519, 1686	1519, 1680	1519, 1683	1521, 1681	23, 17
H-O-H bending Vibration	1608	1606	1606	1607	1607	16
Calcium Carbonate	1872	1872	1872	1872	1873	22
=Si-H (monohydride)	1984	1984	1986	1984	1987	21
$H-SiO_3$	2241	2240	2244	2236	2250	20
v -O-H stretching vibration	2343	2344	2341	2347	2345	19
-C–H stretching vibration	2827	2887	2886	2890	2895	17
-O-H stretching vibration	3553	3096	3276	3327	3260	11

The SEM image (Fig. 2) of FA demonstrates particles of different shapes and sizes, hollow cenospheres, irregularly shaped unburned carbon particles, miner aggregates and agglomerated particles whereas the typical SEM image of TFA-1000 shows different shape and size particles while irregular shaped unburned carbon is not seen. Some fused silica particles are showing which has been formed during thermal activation [11].
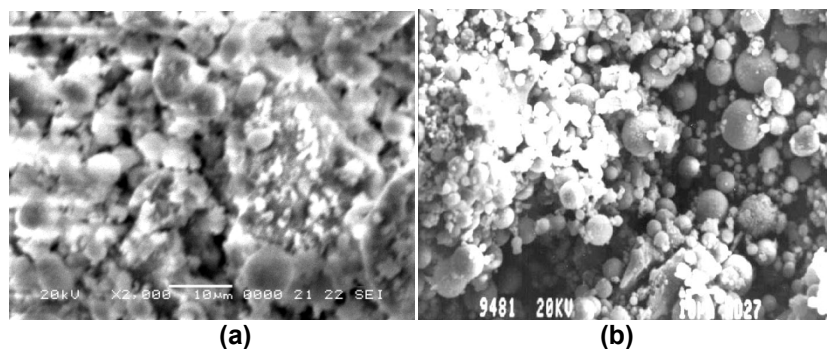

(a) **(b)**

Fig. 2. SEM images of (a) FA (b) TFA-1000

The XRD patterns of FA and TFA-1000 are shown in Fig. 3. In both FA and TFA-1000, peaks at 2θ values of 16.4º, 25.9º and 26.2º show presence of mullite (alumino-silicate)

phases and quartz (silica) exhibits strong peaks at 20.7º, 26.5º, 26.66º, 40.66º and 49.96º of 2θ values [26] while calcite shows peaks at 33.4º of 2θ values [11]. TFA-1000 shows number of crystalline phases like quartz, hematite, mullite, calcite in higher intensities than FA, due to high temperature calcination. With thermal activation magnetite peak tends to disappear while a peak responsible for hematite begins to appear (Table 3) [27].
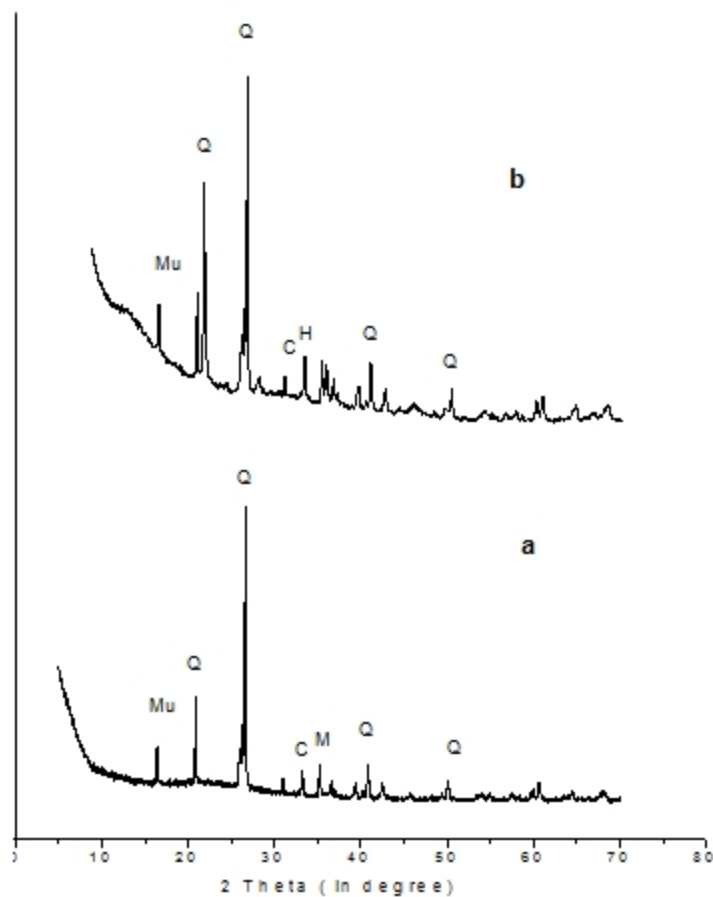

Fig. 3. XRD pattern of (a) FA (b) TFA-1000; (Q- Quartz, Mu- Mullite, M- Magnetite, H-Hematite, C- Calcite)

Table 3. Color and crystalline phases of FA and TFA samples

Sample	Color	Quartz	Magnetite	Hematite	Mullite	Calcite
FA	Grey	√	√	---	√	√
TFA-400	Light grey	√	√	---	√	√
TFA-600	Yellowish brown	√	√	---	√	√
TFA-800	Yellowish brown	√	---	√	√	---
TFA-1000	Reddish brown	√	---	√	√	---

(√ = Present, --- = Absent)

Variation of colors and crystalline phases of FA and TFA calcined at different temperatures is shown in Table 3. Initially fly ash was of grey color due to presence of unburned carbon content with increase in thermal activation temperature grey color of fly ash changes to yellowish brown and then finally red brown possibly due to hematite crystallization [8].

4. CONCLUSION

In each DR/FTIR spectrum broad band ranging from 3000-3400 cm^{-1} is showing a successive decrement in the intensity with increasing thermal activation temperature. It is thus revealed that as the temperature increases, physically adsorbed water is removed first, then silanol groups on surface is dehydrated resulting in transformation of Q^3 units [Si(OH)(SiO$_4$)$_3$] to Q^4 units [Si (SiO$_4$)$_4$]. Due to thermal activation of fly ash, SiO$_2$, Al$_2$O$_3$ are increased which is also evidenced by increased intensity of quartz and mullite phases, the magnetite phases are converted into hematite phase at higher temperature. It can be concluded that modification in properties of fly ash with reference to Si-OH, intensity and crystallinity of crystalline phases can be achieved by thermal activation method to generate a solid support material for catalytic applications.

ACKNOWLEDGEMENT

COMPETING INTERESTS

Authors have declared that no competing interests exist.

REFERENCES

1. Yao ZT, Xia MS, Ye Y, Zhang L. Synthesis of zeolite Li-ABW from fly ash by fusion method. J Hazard Mater. 2009;170(2):639-44. doi:10.1016/j.bbr.2011.03.031.
2. Senapati MR. Fly ash from thermal power plants - waste management and overview. Curr Sci. 2011;100(12).
3. Kutchko BG, Kim AG. Fly ash characterization by SEM–EDS. Fuel. 2006;85(17):2537-44. doi:10.1016/j.fuel.2006.05.016.
4. American Society for Testing and Materials (ASTM), ASTM C618 – 12a,"Standard specification for coal fly ash and raw or calcined natural pozzolan for use in concrete", Annual book of ASTM standards, Vol.04.02, Philadelphia, Pennsylvania,1994.
5. Blanco F, Garcia MP, Ayala J. The effect of mechanically and chemically activated fly ashes on mortar properties. Fuel. 2006;85(14):2018–26. doi:10.1016/j.fuel.2006.03.031.
6. Sahu S, Majling J. Preparation of sulphoaluminate belite cement from fly ash. Cem Concr Res. 1994;24(6):1065-72. doi:10.1016/0008-8846(94)90030-2.
7. Scheetz BE, Earle R. Utilization of fly ash. Curr Opin Solid State Mater Sci.1998;3(5):510-20. doi:10.1016/S1359-0286(98)80017-X.

8. Temuujin J, Riessen AV. Effect of fly ash preliminary calcination on the properties of geopolymer. J Hazard Mater. 2009;164:634–39. doi:10.1016/j.jhazmat.2008.08.065.

9. Van Jaarsveld JSG, Van Deventer JSJ, Lukey GC. The characterisation of source materials in fly ash-based geopolymers. Mater Lett. 2003;57(7):1272–80. doi: 10.1016/S0167-577X(02)00971-0.

10. Gray ML, Champagne KJ, Soong Y, Killmeyer RP, Maroto-Valer MM, Andresen JM et al. Physical cleaning of high carbon fly ash. Fuel Process Technol. 2002;76(1):11–21. doi:10.1016/S0378-3820(02)00006-1.

11. Khatri C, Rani A. Synthesis of a nano-crystalline solid acid catalyst from fly ash and its catalytic performance. Fuel. 2008;87(13):2886–92. doi:10.1016/j.fuel.2008.04.011.

12. Jain D, Rani A. MgO enriched coal fly ash as highly active heterogeneous base catalyst for Claisen-Schmidt condensation reaction. Am Chem Sci J. 2011;1(2):37-49.

13. Peng L, Qisui W, Xi L, Chaocan Z. Investigation of the states of water and OH groups on the surface of silica. Colloids and Surfaces A: Physicochem Eng Aspects. 2009;334:112–15. doi:10.1016/j.colsurfa.2008.10.028.

14. Kordatos K, Gavela S, Ntziouni A, Pistiolas KN, Kyritsi A, Rigopoulou VK. Synthesis of highly siliceous ZSM-5 zeolite using silica from rice husk ash. Micropor Mesopor Mater. 2008;115(1-2):189-96. doi:10.1016/S0167-577X(02)00971-0.

15. Richardson IG. The calcium silicate hydrates. Cem Concr Res. 2008;38:137–58.

16. Palomo A, Grutzeck MW, Blanco MT. Alkali-activated fly ashes a cement for the future. Cem Concr Res. 1999;29:1323-29.

17. Saikia BJ, Parthasarthy G, Sarmah NC, Baruah GD. Fourier-transform infrared spectroscopic characterization of naturally occurring glassy fulgurites. Bull Mater Sci. 2008;31(2):155–58.

18. Morten ES, Camilla S, Li Z, Sogaard EG. Xps and Ft-Ir Investigation of Silicate Polymers. J Mater Sci. 2009;44:2079–88. doi:10.1007/s10853-009-3270-9.

19. Zaki MI, Knozinger H, Tese B, Mekhemer GAH. Influence of phosphonation and phosphation on surface acid–base and morphological properties of CaO as investigated by in situ FTIR spectroscopy and electron microscopy. J colloid Interface Sci. 2006;303(1):9-17. doi: 10.1016/j.jcis.2006.07.011.

20. Sun XH, Wang SD, Wong NB, Ma DDD, Lee ST, Teo BK. FTIR spectroscopic studies of the stabilities and reactivities of hydrogen-terminated surfaces of silicon nanowires. Inorg Chem. 2003;42(7):2398-404. doi:10.1021/ic020723e.

21. Blanco F, Garcia MP, Ayala J. Variation in fly ash properties with milling and acid leaching. Fuel. 2005;84(1):89-96. doi:10.1016/j.fuel.2004.05.010.

22. Jacox EM. Vibrational and Electronic Energy Levels of Polyatomic Transient Molecules Supplement B. J Phys Chem Ref Data. 2003;32(1). doi: 10.1063/1.1497629.

23. Handa H, Baba T, Sugisawa H, Ono Y. Highly efficient self-condensation of benzaldehyde to benzyl benzoate over KF-loaded alumina. J Mol Catal A Chem. 1998;134(1):171-77. doi:10.1016/S1381-1169(98)00033-8.

24. Frances IH, Denisse VA, Meghan EG. High temperature aerogels in the Al_2O_3-SiO_2 system. Presented at the American chemical society 236th national meeting Philadelphia, Pa, August 20, 2008. Accessed 24 May 2013.
Available: http://usrp.usra.edu/technicalPapers/glenn/arrandaAug08.pdf.

25. Temuujin J, Okada K, Kenneth JDM. Preparation and properties of potassium aluminosilicate prepared from the waste solution of selectively leached calcined kaolinite. Appl Clay Sci. 2002;21:125–31. doi:10.1016/S0169-1317(01)00082-5.

26. Sharma A, Srivastava K, Devra V, Rani A. Modification in Properties of Fly Ash through Mechanical and Chemical Activation. Am Chem Sci J. 2012;2(4):177-87.

27.   Fox JM. Changes in fly ash with thermal treatment. Presented in 2005 World of Coal Ash (WOCA), April 11-15,2005, Lexington, Kentucky, USA. Accessed 24 May 2013. Available: http://www.flyash.info/2005/132fox.pdf.

_____

Characterization and Study of Turkish Perlite

Sakshi Kabra[1], Stuti Katara [2], Ashu Rani[3]∗

Research Scholar, Department of Pure and Applied Chemistry, University of Kota, Kota, Rajasthan, India[1]

Research Scholar, Department of Pure and Applied Chemistry, University of Kota, Kota, Rajasthan, India[2]

Head, Department of Pure and Applied Chemistry, University of Kota, Kota, Rajasthan, India[3∗]

Abstract: An examination of the structural, morphological and mineralogical features of Turkish perlite sample was carried out by FT-IR, SEM, SEM-EDX, XRD, TGA and N_2-adsorption-desorption analytical techniques. Perlite is a natural, silica enriched igneous rock. This article features the primary step of study of basic characterization of perlite to investigate its utilization in different areas. Higher silica and alumina content was shown by EDX analysis. Both XRD and FT-IR studies reveal the presence of amorphous silica in perlite. TGA and LOI analysis illustrate the presence of water in the sample. The irregular morphology was exposed through SEM images. It was evident from the results that silica-enriched perlite could be developed further into a potential material in several area including catalyst synthesis by using various activation techniques.

Keywords: perlite, characterization, XRD, FT-IR.

I. INTRODUCTION

The basic objective of this paper is to provide the comprehensive characterization of Turkish perlite and suggest its suitability towards several fields of utilization. Perlite is a hydrated, widely occurring amorphous igneous rock formed by cooling of volcanic eruptions. Its unique structure consists of numerous concentric layers having SiO_2, Al_2O_3, K_2O and Na_2O as major constituents while TiO_2, CaO, MgO, Fe_2O_3 and hydrated water as well as unburned carbon remain present in varying quantities [1]. On heating the perlite to its softening range, i.e., above 850°C, crystalline water molecules vaporize and escape resulting in unusual expansion of perlite up to 7-16 times of its original volume, creating inert, non-toxic, lightweight particles with specific surface area of about 1.22 m^2g^{-1} [2], density in the range of 0.6 - 2.30 gml^{-1} [3] and particle size in range of 0.2-4 mm. [4]. Physio-chemical properties of perlite need to be examined prior to evaluation of its possible utilization in various fields. As far as applications of perlite are concerned, it is mainly consumed as fillers, filter aids, in producing building construction materials [5], [6], adsorptive materials, precursor for geo-polymer formation [7], removal of heavy metal ions and other pollutants from atmosphere [8], in thermal insulation [9], removal of dyes [10], [11], in horticulture [12], sorption of oil [4] etc. Perlite is a naturally occurring waste, estimating about 700 million tons worldwide reserves. Turkey has rich resources of perlite, approximately 160 tons [13], since, domestic demand is very limited, so, most of the produced perlite is exported to various countries including India. Thus its effective, conducive and eco-friendly utilization has always been a challenge for scientific community. Above applications could thrive up to only some level in utilizing the huge reserves of perlite. However, the search of new applications of the perlite as either catalyst or catalyst support material is still enduring. Literature accounts only for the few applications of perlite as photo catalyst [14], pyrolysis catalyst [15] and catalyst used for different chemical reactions such as, immobilization [16], methacrolein production [17], zeolite synthesis [18], [19] etc.

The objective of the present work is to characterize perlite, in terms of structure, mineralogical composition, chemical behaviour, colour and morphology. This is the foundation stone in our research work to investigate the physio-chemical properties of perlite for its utilization in different fields. This paper mainly deals with identification of

characteristics of perlite and their study using spectroscopic and microscopic analysis through FT-IR, SEM, SEM-EDX, XRD, TGA and N_2-adsorption-desorption techniques.

II.   EXPERIMENTAL

A.   Materials
Perlite sample was imported from Turkey and supplied to us by Indica Chem. Ind. Pvt. Ltd., India.
B.   Procedure

Perlite sample was taken as such and thermally treated in a muffle furnace under static conditions at 800°C for 3 h and named as TAP.

C.   Characterization
Physiochemical properties of perlite and TAP were studied by FT-IR, SEM and SEM-EDX, XRD, TGA, and N_2 adsorption-desorption studies.
The FT-IR study of the sample was done by Bruker FT-IR Spectrophotometer (TENSOR 27) in DRS mode by mixing samples with KBr in 1:20 weight ratio. The spectra were recorded in the range 550-4000 cm^{-1} with a resolution of 4 cm^{-1}. SEM (Model-JEOL-JSM 5600) was used to investigate morphology and surface texture of the sample while elemental analysis was studied by SEM-EDX analysis (Model-INCA Oxford). X-ray diffraction study was done by X-ray powder diffractometer (Bruker D8 Advance) using Cu K_α radiation (λ = 1.5406A˚). The samples were scanned in 2θ range of 5-65˚ at a scanning rate of 0.04˚s^{-1}. TGA of the sample was carried out using Mettler Toledo thermal analyser (TGA/DSC1 SF/752), by heating the sample in the range of 50–850 °C with a heating rate of 10 °C/min under nitrogen flow (50 cm^3/min). BET surface area of the samples was measured at liquid nitrogen temperature (77 K) using Quantachrome NOVA 1000e surface area analyser. The samples were degassed under vacuum at 120 °C for 2 h, prior to measurement.

III.   RESULTS AND DISCUSSION
Perlite is white or light-gray coloured material which turns to light pinkish on thermal treatment. FT-IR spectrum of perlite and TAP (Fig. 1) shows a broad band between 3600-3300 cm^{-1}, which is attributed to surface –OH groups of –Si-OH and water molecules adsorbed on the surface. The broadness of band indicates the presence of strong hydrogen bonding in the sample [20]. The hydroxyl groups exist in higher degree of association with each other which results in extensive hydrogen bonding, while in FT-IR spectrum of TAP, the intensity and broadness of band is decreased which confirms the loss of water (Fig. 1b). The strong band at 1178 cm^{-1} is due to the structural siloxane framework, which is the vibrational frequency of the Si-O-Si bond. The peak is shifted to higher wave number, i.e., 1192 cm^{-1} after thermal treatment, which is normally observed in amorphous silica samples [21]. An intense peak at 1633 cm^{-1} in the spectrum of perlite is attributed to bending mode (δ_{O-H}) of water molecule [22], which is again highly decreased in case of TAP. The region around 805 cm^{-1} is characteristic of Si-O-Si symmetric stretching modes [23], [24]. Amorphous silica exhibited a relatively strong peak at about 800 cm^{-1} and it can be distinguished from the band of crystalline silicate [25]. The observed frequencies of IR bands of perlite and their possible assignments are summarized in Table 1.
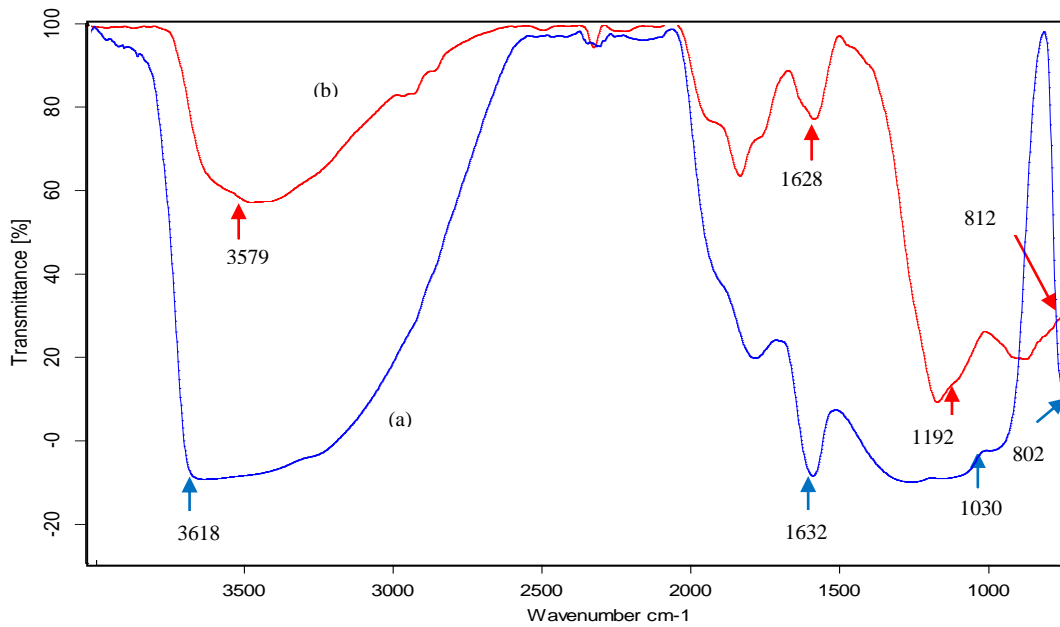
Fig 1. FT-IR spectrum of (a) perlite and (b) TAP

Table I. The Observed Frequencies of IR Bands of Perlite, TAP and their Possible Assignments

Assignments	Wave number(cm^{-1})	
	Perlite	TAP
Si-O-Si symm. stretching vib.	802	812
Si-O-Si asymm. stretching vib.	1030	1192
-O-H bending vib.	1632	1628
-O-H stretching vib.	3618	3579

SEM micrograph of perlite and its magnified view (Fig. 2 a and b) revealed the irregular morphology of perlite particles with broken or ragged edges. Similar pattern was observed in other reported micrographs of perlite [7]. SEM images of TAP and its magnified view (Fig. 3 a and b) are mainly fragmatic and random as a result of thermal activation [4]. But here, the morphology is less irregular which confirms the evaporation of water from the perlite sample on heating at high temperature.
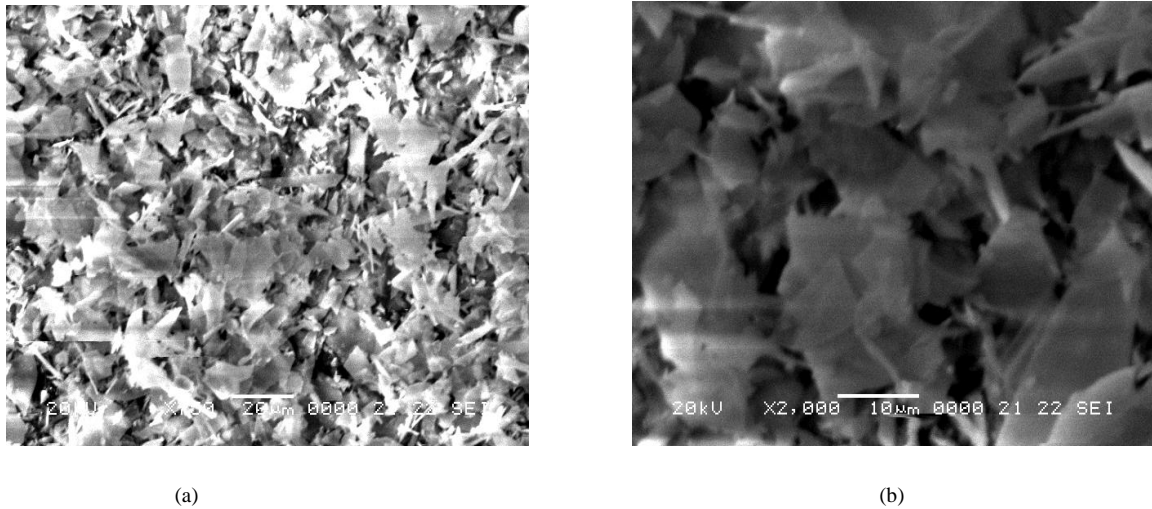
(a)

(b)

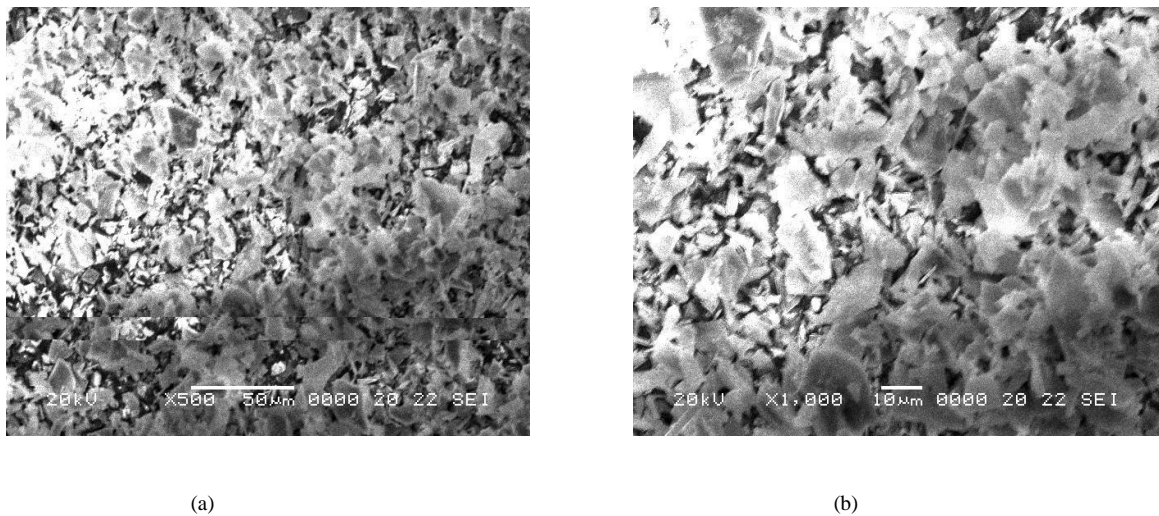Fig 2. SEM micrograph of (a) perlite and (b) its magnified view

(a)

(b)

Fig 3. SEM micrograph of (a) TAP and (b) its magnified view

The chemical composition of perlite and TAP were determined by SEM-EDX technique which is shown in Table 2.

Table II. EDX Analysis of Perlite and TAP

Samples	O(wt%)	Si(wt%)	Al(wt%)	K(wt%)	Na(wt%)	Zn(wt%)	Fe(wt%)	Ti(wt%)	S(wt%)	LOI
Perlite	73.70	18.83	3.72	1.44	1.91	0.22	0.10	0.07	-	4.1
TAP	73.60	18.80	3.70	1.34	1.91	0.22	0.10	0.07	-	-

Loss on ignition (LOI) was determined by heating a certain weighed quantity of perlite in muffle furnace at 800˚C for 3 h. The LOI amount was 4.1 wt % which corresponds to the removal of moisture and coexisting unburned carbon from sample [26]. The TGA curve of perlite, as shown in Fig. 4, shows continuous decrease in weight of sample from 50-

900°C. Weight loss in lower temperature range relates to the removal of moisture content of the sample together with some volatile materials. While, the weight loss of sample within range of 550-900˚C would correspond to the burning of carbonaceous materials that were firmly adsorbed on the surface of the solid materials remaining or volatilization of some trace metal oxides [27].
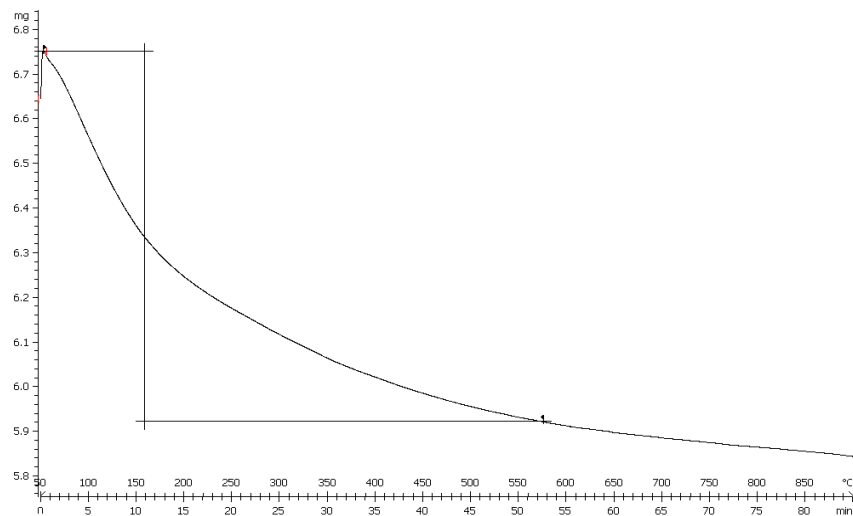

Fig 4. TGA curve of perlite

BET surface area of perlite and TAP samples were found to be 2.6 and 2.3 m^2/g respectively.

The broad powder X-ray diffraction pattern of perlite (Fig. 5a), confirmed the absence of any ordered crystalline structure [28] which is typical for amorphous solids. However, heating of perlite at temperature over 800˚C for 3 h could convert less ordered structure to a more highly ordered structure and a single crystalline peak appears at $2\theta =$ 27.642˚ (Fig. 5b) which shows presence of quartz in the sample [29], along with a broad peak at $2\theta = 22$-23˚ confirming amorphous nature of silica [24], [30].
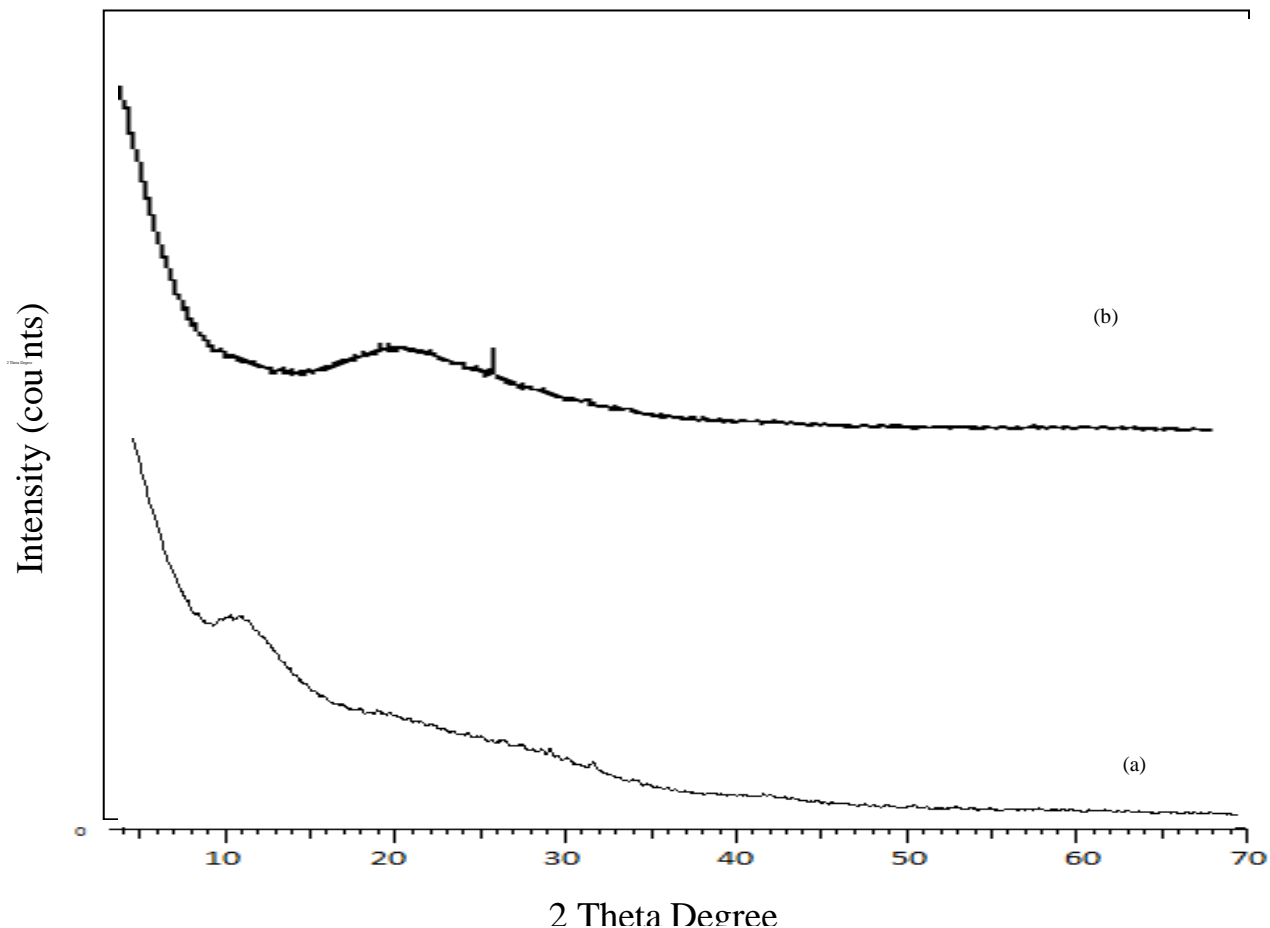
Fig 5. X-ray diffraction pattern of (a) Perlite and (b) TAP

IV. CONCLUSIONS

Results obtained in the present investigation confirm silica and alumina as major constituents of perlite. It is also observed that the nature of silica in perlite is mainly amorphous with irregular morphology and only a single crystalline peak appears on thermal treatment. On the basis of analysis, it can also be said that high number of hydroxyl groups and Si-O-Si network is also present in perlite. Moreover, comparison of perlite with TAP shows the effects of thermal treatment on structure, mineralogy, colour, surface area and morphology of perlite. The contemporary report aims at study of fundamental characteristics of perlite for its further applications in novel fields. The results like presence of amorphous silica network and surface hydroxyl groups in perlite indicate towards the potential capability of perlite as a support material in catalyst synthesis.

ACKNOWLEDGEMENT

REFERENCES

[1] Dogan, M., Alkan, M., Cakir, U., "Electrokinetic Properties of Perlite", *J. Colloid Interface Sci*. Vol. 192, pp.114-18, 1997.

[2] Dogan, M., Alkan, M., "Adsorption kinetics of methyl violet onto perlite*", Chemosphere*, Vol.50, pp.517-28, 2003.

[3] Roulia, M., Chassapis, K., Kapoutsis, J.A.., Kamitsos, E.I., Savvidis, T., "Influence of thermal treatment on the water release and the glassy structure of perlite",*J. Mater. Sci.*, Vol.41, pp.5870-81, 2006.

[4] Bastani, D., Safekordi, A.A., Alihosseini, A., Taghikhani, V., "Study of oil sorption by expanded perlite at 298.15 K*", Sep. Purif. Technol.*, Vol.52, pp.295-300, 2006.

[5] Morsy, M.S., Shebl, S.S., Abd El Gawad Saif, M., "Development of perlite-gypsum-slag-Lime sludge-composite system for building application*",Building Research Journal*, Vol.56, pp.49-58, 2008.

[6] Aglan, H., Morsy, M., Allie, A., Fouad, F., "Evaluation of fiber reinforced nanostuctured perlite-cementitious surface compounds for building skin applications*", Construction and Building Materials*, Vol.23 (1), pp.138-45, 2009.

[7] Vance, E.R., Perera, D.S., Imperia, P., Cassidy, D.J., Davis, J., Gourley, J.T., "Perlite Waste as a Precursor for Geopolymer Formation*", Journal of the Australian Ceramic Society*, Vol.45 (1), pp.44-49, 2009.

[8] Mostaedi, M.T., Ghassabzadeh, H., Maragheh, M.G., Ahmadi, S.J., Taheri, H., "Removal of cadmium and nickel from aqueous solution using expanded perlite*", Brazilian Journal of Chemical Engineering*, Vol.27 (2), pp. 299-308, 2010.

[9] Vaou, V., Panias, D., "Thermal insulating foamy geopolymers from perlite*", Miner. Eng.*, Vol.23 (14), pp.1146-51, 2010.

[10] Vijaykumar, G., Dharmendirakumar, M., Renganathan, S., Sivanesan, S., Baskar, G., Elango, K.P., "Removal of Congo Red from Aqueous Solutions by Perlite*", Clean- Soil, Air, Water*, Vol.37 (4-5), pp.355-64, 2009.

[11] Dogan, M., Alkan, M., "Removal of methyl violet from aqueous solution by perlite*", J. Colloid Interface Sci.*, Vol.267 (1), pp. 32-41, 2003.

[12] Silber, A., Bar-Yosef, B., Levkovitch, I., Kautzky, L., Minz, D., "Kinetics and mechanisms of pH-dependent Mn (II) reactions in plant-growth medium*", Soil Biol. Biochem.*, Vol. 40, pp. 2787-95, 2008.

[13] Celik, A.G., Kilic, A.M., Cakal, G.O., "Expanded perlite aggregate characterization for use as a lightweight construction raw material", *Physicochem. Probl. Miner. Process.* Vol. 49 (2), pp. 689-700, 2013.

[14] Hosseini, S.N., Borghei, S.M., Vossoughi, M., Taghavinia, N., "Immobilization of TiO_2 on perlite granules for photocatalytic degradation of phenol", *Appl. Catal., B*, Vol. 74 (1-2), pp. 53-62, 2007.

[15] Balat, M., "Diesel-like Fuel Obtained by Catalytic Pyrolysis of Waste Engine Oil", Energy, Exploration and Exploitation, Vol. 26 (3), pp. 197-208, 2008.

[16] Jafarzadeh, N.K., Sharifnia, S., Hosseini, S.N., Rahimpour, F., "Statistical optimization of process conditions for photocatalytic degradation of phenol with immobilization of nano TiO_2 on perlite granules*", Korean J. Chem. Eng.*, Vol. 28 (2), pp. 531-38, 2011.

[17] Schlaefer, Francis, W., Hansen, A., "Methacrolein production utilizing novel Catalyst", George, *US Patent*, 05/428, pp. 150, 1978.

[18] Kongkachuichay, P., Lohsoontorn, P., "Phase Diagram of Zeolite Synthesized from Perlite and Rice Husk Ash", *Science Asia*, Vol. 32, pp. 13-16, 2006.

[19] Wang, P., Shen, B., Shen, D., Peng, T., Gao, "Synthesis of ZSM-5 zeolite from expanded perlite/kaolin and its catalytic performance for FCC naphtha aromatization", J. *Catal. Commun.*, Vol. 8 (10), pp. 1452-56, 2007.

[20] Silverstein, R.M., Webster, F.X. *Spectrometric Identification of Organic Compounds*, Sixth ed., John Wiley Pub., Wiley India Pvt. Ltd., pp. 88., 2006.

[21] Adam, F., Balakrishnan, S., Wong, P.L., "Rice Husk Ash Silica as a Support Material for Ruthenium based Heterogenous Catalyst*", Journal of Physical Science*, Vol. 17 (2), pp. 1-13, 2006.

[22] Khatri, C., Rani, A., "Synthesis of a nano-crystalline solid acid catalyst from fly ash and its catalytic performance*", Fuel*, Vol. 87, pp. 2886-92, 2008.

[23] Kabra, S., Sharma, A., Katara, S., Hada, R., Rani, A., 'DRIFT- spectroscopic study of modification of surface morphology of perlite during thermal activation", *Indian Journal of Applied Research*, Vol. 3 (4), pp. 40-42, 2013.

[24] Javed, S.H., Naveed, S., Feroze, N., Zafar, M., Shafaq, M., *"*Crystal and Amorphous Silica from $KMnO_4$ treated and untreated Rice Husk Ash*", Journal of Quality and Technology Management*, Vol. 6 (1), pp. 81-90, 2010.

[25] Ojima, J., "Determining of Crystalline Silica in Respirable Dust Samples by Infrared Spectrophotometry in the Presence of Interferences", *J. Occup. Health*, Vol. 45, pp. 94-103, 2003.

[26] Kordatos, K., Gavela, S., Ntziouni, A., Pistiolas, K.N., Kyritsi, A., Kasselouri-Rigopoulou, V., "Synthesis of highly siliceous ZSM-5 zeolite using silica from rice husk ash*", Microporous Mesoporous Mater.*, Vol. 115 (1-2), pp. 189-96, 2008.

[27] Sekkina, M.M.A., Issa, R.M., El-Deen, A., Bastawisy, M., El-Helece, W.A., "Characterization and Evaluation of Thermodynamic Parameters for Egyptian Heap Fired Rice Straw Ash (RSA)", *Int. J. Chem.*, Vol. 2 (1), pp. 81-88, 2010.

[28] Kalapathy, U., Proctor, A., Shultz, J., "A simple method for production of pure silica from rice hull ash", *Bioresour. Technol.*, Vol. 73, pp. 257-62, 2000.

[29] Jain, D., Khatri, C., Rani, A., "Synthesis and characterization of novel solid base catalyst from fly ash*", Fuel*, Vol. 90, pp.2083-88, 2011.

[30] Amutha, K., Ravibaskar, R., Sivakumar, G., "Extraction, Synthesis and Characterization of Nanosilica from Rice Husk Ash*", International Journal of Nanotechnology and Applications*, Vol. 4 (1), pp. 61-66, 2010.

BIOGRAPHY

Mrs. Sakshi Kabra is pursuing Ph.D. from Department of Pure and Applied Chemistry, University of Kota, Kota (Rajasthan). She secured All India Rank 385 in National Eligibility Test (June-2009) and acquired UGC-JRF. She is currently working as UGC-SRF in the department. Her research interests mainly include synthesis of heterogeneous acid catalysts and their various applications, solid waste management, material synthesis etc.

Ms. Stuti Katara is doing Ph.D. from Department of Pure and Applied Chemistry, University of Kota, Kota (Rajasthan). She got all India Rank 353 in National Eligibility Test (June-2009) and attained UGC-JRF. She is associated with solid base catalysis, green catalysis etc. and presently working as UGC-SRF in the department.

Prof. Ashu Rani is Head, Department of Pure and Applied Chemistry, Dean of post graduate departments and Convenor of various boards at University of Kota, Kota (Rajasthan). Several research scholars are pursuing M. Phil and Ph. D. under her guidance. Her wide research interests involve Heterogeneous Catalysis, Waste management, climate change, Lithospheric salt transport kinetics, Nanotechnology, Material Synthesis. She is associated with several National and International Collaborations and is a Principle Investigator of several projects funded by central and state governments.